Microwave-Assisted Production of Aggregates from Demolition Debris

Ali Akbarnezhad

(B.Eng, Amirkabir University of Technology)

A THESIS SUBMITTED

FOR THE DEGREE OF DOCTOR OF PHILOSOPHY

DEPARTMENT OF CIVIL ENGINEERING

NATIONAL UNIVERSITY OF SINGAPORE

2010

ACKNOWLEDGEMENT

I would like to expresses my sincere gratitude to a number of people who have supported and encouraged me during my graduate studies. I hope that the pages of this thesis can serve as letters of "thanks" to the many individuals who have helped me bring it to completion.

I am deeply indebted to my supervisor, A/Prof. Gary Ong Khim Chye whom his wealth of knowledge and his attitude towards graduate student supervision contributed immensely to my research efforts. Without his guidance, persistent help, and encouragement this thesis would not have been possible.

I also wish to express my deepest gratitude and appreciation to A/Prof. Tam Chat Tim, A/Prof. Zhang Min Hong and Mr. Timothy Wan Juang Foo for their invaluable advice and guidance throughout the course of this research.

I would like to express my special thanks to all the staffs of the concrete and structural laboratory of NUS, especially Mr. Ang Beng Oon, Ms. Annie Tan, Mr. Lim Huay Bak, Mr. Kamsan Bin Rasman, Mr. Koh Yian Kheng and Mr. Choo Peng Kin for their kind assistant and support during the experimental stage of this study.

I am also extremely thankful to my lovely wife whom meeting her was my most significant achievement during my stay in Singapore.

Finally, this undertaking could never have been achieved without the encouragement and love of my wonderful father, mother and sisters who have encouraged me and believed in me from the earliest time I can remember.

And above all, I thank God for everything that I have experienced and achieved. I believe that He always provides me the best of all things.

TABLE OF CONTENTS

ABSTRACT

Concrete recycling is an increasingly common method of disposing of demolition rubble and can provide a sustainable source of concrete aggregates. However, Recycled Concrete Aggregates (RCA) currently produced are usually of low quality and generally considered not suitable for use in ready mix concrete. The presence of the contaminants (impurities) in the concrete debris and the presence of the mortar adhered to the RCA particles have been identified as the main causes lowering the quality of RCA compared to Natural Aggregates (NA). The current study was aimed to investigate the possible methods to eliminate the abovementioned causes and thereby increase the quality of RCA. Based on a comprehensive literature review conducted to investigate the capability of different surface removal techniques for removal of the contaminants from the concrete surface, the focus was placed on the microwave decontamination technique that had been reported to have a relatively better removal speed and performance. A comprehensive numerical study was conducted to examine the phenomenon leading to delamination of the concrete surface when exposed to microwaves and to develop an easy-to-use simulation technique to be used in practical predictions and control of the microwave decontamination of concrete. In addition, besides the concrete surface decontamination, a novel microwave-assisted technique to remove the adhering mortar from RCA was developed during the current study. The capability of this method to remove the adhering mortar from RCA was numerically and experimentally investigated and compared with the other RCA beneficiation methods proposed in available literature. Moreover, an industrial microwave heating system that can be used in concrete surface decontamination and RCA beneficiation methods was designed and installed during the current study. The results of

this study demonstrated that incorporating the microwave-assisted decontamination and RCA beneficiation techniques into the conventional concrete recycling procedure may significantly increase the quality of RCA.

LIST OF FIGURES

LIST OF TABLES

LIST OF SYMBOLS

a	=	Permeability (m^2)
a_0	=	Reference permeability at 25 °C (m^2)
B	=	Magnetic flux density (Tesla)
B_i	=	Biot number
B_w	=	Moisture transfer coefficient
c	=	Transmissivity
C_w	=	Specific heat of water ($kJ \cdot kg^{-1} \cdot K^{-1}$)
dp	=	Microwave dissipation depth (m)
D	=	Electric displacement (C/m^2)
E	=	Electric field intensity (V/m)
f	=	Frequency (Hz)
f_c	=	Waveguide cutoff frequency (Hz)
g	=	Earth gravity (=9.81 m/s^2)
H	=	Magnetic field intensity (A/m)
HD (w)	=	Change in water content because of hydration and dehydration
I(x)	=	Transmitted power flux at distance x from the incident surface (W)
I_0	=	Incident power (W)
J	=	Current density (A/m^2)
k	=	Propagation constant
M_c	=	Adhering mortar content of RCA (%)
n	=	Effective refractive index
P	=	Pore water pressure (Pa)

P_a = Ambient pressure (Pa)

P_e = Electric power (W)

P_{eo} = Effective elastic-optic coefficient

P_m = Magnetic power (W)

$P_s(T)$ = Saturation pore pressure at temperature T (Pa)

$PL(x)$ = Microwave power dissipated at distance x from the incident surface of the medium (W)

Q = Activation energy for water migration (J)

$Q_{emw}(x)$ = Microwave power dissipated at distance x from the incident surface of concrete as predicted by Maxwell's equations (W)

$Q_{lambert}(x)$ = Microwave power dissipated at distance x from the incident surface of concrete as predicted by Lambert's law (W)

q = Total flux vector (W/m^2)

q_{cd} = Conductive heat flux (W/m^2)

q_{cv} = Convective heat flux (W/m^2)

r = Reflectivity

R = Reflection coefficient

R_g = Gas constant

S = Poynting vector

S_r = Radiation number

t = Time (s)

T = Temperature (°C)

T_a = Ambient temperature (°C)

$\bar{T}$ = Absolute temperature (=-273.15 °C)

U_x	=	Displacement in x direction (m)
U_y	=	Displacement in y direction (m)
U_z	=	Displacement in z direction (m)
w	=	Water content of concrete
w_{s1}	=	Saturation water content at 25 °C
W_e	=	Electric energy (J)
W_i	=	Initial weight of the oven dried RCA sample prior to beneficiation (kg)
W_m	=	Magnetic energy (J)
W_r	=	Weight of the oven dried RCA samples retained on a 4 mm sieve after beneficiation (kg)
Z	=	Impedance (Ω)
α	=	Thermal expansion coefficient (1/°C)
β	=	Attenuation factor (Np/m)
Tan δ	=	Loss tangent
λ	=	Wavelength (m)
$λ_B$	=	Bragg wavelength (m)
Λ	=	Grating period (m)
ε	=	Complex permittivity of a material (F/m)
ε′	=	The real part of complex permittivity (F/m)
ε″	=	The imaginary part of complex permittivity (F/m)
$ε_0$	=	Permittivity of free space (=8.86×10^{-12} F/m)
$ε_r$	=	Relative permittivity
$ε_r$′	=	Dielectric constant

$\varepsilon_r°$	=	Loss factor
ξ	=	Thermo-optic coefficient (1/°C)
θ_i	=	Angle of incidence (rad)
θ_B	=	Brewester angle (rad)
θ_t	=	Angle of transmission (rad)
μ	=	Complex Permeability (H/m)
μ_0	=	Permeability of vacuum ($4\pi\times10^{-7}$ H/m)
ρ_q	=	Charge density (C/m^3)
σ	=	Electrical conductivity (S/m^{-1})
ω	=	Angular frequency (rad/s)

Chapter 1 : INTRODUCTION

1.1 Background

Singapore has to import materials, including aggregates, for the production of ready-mix concrete for use in its construction industry. This reliance on imported aggregates is unhealthy and recent developments have shown that there is a need for alternative supplies of aggregates to meet Singapore's needs for the next decade or so.

The aggregates used in Singapore's construction are mainly granite. Till 2004, almost 94% of Singapore's granite had been imported from a single country, Indonesia (Table 1.1). In 2007, the Indonesian government imposed an export ban on granite which led to a dramatic increase in the price of aggregates in Singapore (Figure 1.1). The resulting turmoil in construction industry following the ban highlighted the necessity of seeking alternative domestic sources of aggregate to militate against such events.

A ready source would become available if use can be made of aggregates recycled from Singapore's construction debris. Concrete recycling is an increasingly common method of disposing of demolition rubble and can provide a sustainable source of concrete

aggregates. Results of a previous study (Table 1.3) shows that up to 90% of structural concrete debris may be used to produce recycled aggregates of an acceptable quality (EnviroCentre, 2005).

Besides serving as an alternative source of aggregate, considering Singapore's limited land space to dispose of construction debris, recycling of concrete may be used to reduce landfill spaces needed. In addition, lower transportation cost and reduced environmental impact are among other advantages of concrete recycling.

The use of recycled concrete aggregate (RCA) in construction works is a subject of high priority in the building industry throughout the world (De Vries, 1996). In 2000, 96% of demolished concrete was recycled in Japan and mostly used as sub-base material for road carriageways.

In Germany, recycling is a normal practice. This is due to the strict limitations on the extraction of natural aggregates and restrictions on the use of landfills imposed by the German government. In Germany, since 1996, the disposal through landfills is under strict control and the landfill owners are not allowed to accept unsorted Construction and Demolition (C&D) materials (Budelmann and Dora, 1999). Moreover, extraction of gravel from river beds is no longer permitted and aggregates obtained by quarrying are subject to severe restrictions imposed to prevent disturbing the landscape.

Recycling is also very well developed in the Netherlands because of its stringent environmental regulations together with the non-availability of natural aggregates in the vicinity of centers of construction. According to the Dutch government, 90% of recycling of C&D materials is now being achieved. The C&D dumping ban, effective since 1997, requires the Netherland's dumping site owners to accept residual materials only from

certified sorting companies who have to make sure that the amount of the re-usable material contained therein does not exceed 12%. In 1994, 78000 tons of RCA has been used in Holland as the Dutch standard NEN 5950 permitted up to 20% replacement of natural aggregate with recycled concrete aggregate, for concrete produced with a characteristic strength of up to 65 MPa (De Vries, 1996).

In contrast to the promising success achieved by many European countries, to date, considerably less attention has been paid to advance concrete recycling technology in Singapore. Although there have been a few attempts in the past to recycle concrete waste in Singapore, a major stumbling block is the cost and productivity of recycling compared to the cost of direct imports. In the light of current projected demands and the potential for future disruption in supplies of imports, use of recycled aggregates makes more economic sense.

1.2 Recycled Concrete Aggregate (RCA) vs. Recycled Aggregate (RA)

Construction and demolition (C&D) debris normally include non-concrete impurities such as bricks, tiles, sand, dust, timber, plastics, cardboard, paper, and metals. Based on the source of the debris and the recycling procedure used in the recycling of the C&D debris, the aggregates produced may be divided into two categories:

- Recycled Concrete Aggregate (RCA): When measures are taken to reduce the amount of impurities during demolition and production procedures so that the recycled aggregates produced consist mainly of crushed concrete with insignificant amount of impurities.

- Recycled Aggregate (RA): when the recycled aggregates produced contain a significant proportion of waste materials other than concrete such as bricks and tiles.

In the current study, focus is placed on the aggregates belonging to the first category. The amount of the impurities recommended for differentiating between RA and RCA differs as specified in different standards. For example, BS 8500-2 defines RCA as recycled aggregate composed predominantly of concrete (at least 83.5% by mass) with no more than 5% masonry (BS 8500-2, 2006). If the recycled aggregate does not meet this criterion, it is considered as RA. Due to the difficulties encountered by many producers to meet such masonry proportion limits, since 2008, the European standard EN 12620 has included a new classification for recycled aggregates containing less crushed concrete. This classification is based on the proportion of the crushed concrete, crushed masonry, glass, unbound stone, bituminous material, floating material and other constituents present in C&D debris.

1.3 High-Quality Recycled Concrete Aggregate

Recycled concrete aggregates currently produced are usually of low quality and generally considered not suitable for use in ready-mix concrete. They are mainly used as base and sub-base materials in road carriageway construction or mixed in small fractions, up to 20%, with natural aggregate to be used in ready mix concrete (Shayan and Xu, 2003). Two main reasons have been suggested as the causes of the lower quality of the recycled concrete aggregates (RCA) compared to natural aggregates (NA):

1. Contaminants (impurities), chemical and physical, present in the concrete debris.

2. Mortar adhering to the recycled concrete aggregate particles which is of a porous and weak nature.

1.4 Elimination of Impurities\Contaminants

Currently, manual removal at the recycling plants is used to reduce the resultant amount of the impurities present to enhance the quality of RCA. However, this method is highly inefficient as only the larger pieces of impurities may be removed.

Ideally, prior to demolition of the structure, by incorporating a soft-strip stage, various non-concrete elements such as composite roofing, sanitary products, doors, window frames, suspended ceilings, raised floors, carpeting, furnishings, plant and machinery, etc can be removed in advance at the demolition site. However, even in this case, due to technical difficulties and the lack of suitable surface removal methods, impurities (such as plaster board, gypsum and tiles) present on the surface of typical concrete structural elements are not completely and efficiently removed.

In addition, depending on the building type, the concrete structure may have inherent chemical or physical contaminants (Table 1.4). Such contamination is normally limited to a thin layer of the concrete surface, depending on the age of the structure. Hence, if the contaminated surface can be efficiently removed, the remaining bulk of the concrete may be confidently used to produce good quality RCA.

Different possible surface removal methods that may be used for removing the contaminants\impurities from the concrete surface are reviewed in Chapter 3 of this thesis. Emphasis will be placed on using the microwave-assisted method which has been previously used in the removal of the radioactive contaminants from the surface of the concrete structures of decommissioned nuclear power plants and radioactive waste

processing plants (White et al., 1995) as well as in the breakage of rocks in mining technology (Hemanth Satish, 2005). Microwave-assisted surface removal seems to be more efficient and rapid than the other available surface removal techniques which are normally slow with many drawbacks such as dust and secondary waste generation and may pose potential health hazards.

It is well known that microwave heating at high frequencies can generate high temperature gradients inside the concrete, occurring between the microwave exposed surface and the cooler interior. Such non-uniform heating within a very short time duration leads to a high differential temperature gradient and thus high thermal stresses. Moreover, concrete is a material whose pores may be partially filled by water and air. Under ambient temperature conditions, part of the water is chemically bonded to the cement while the remainder is contained in the concrete pores as free water. When exposed to microwaves, as a result of dielectric losses, microwaves penetrating the concrete act as a volumetrically distributed heat source. Water in the concrete is a very strong dipole and is easily heated up, as it absorbs the microwave energy. As a result, the water within the concrete evaporates. When the evaporation rate overtakes the vapor migration rate, pore pressure builds up. The two phenomena of thermal stresses and pore pressure have been postulated as causes for delamination of the concrete surface layers when concrete is heated with high frequency microwaves. Hence, microwave heating may be used as an efficient surface removal tool. The basics of microwave heating, the microwave heating formulations and electromagnetic modeling concepts are reviewed in Chapter 4 of this thesis. Moreover, the microwave-assisted surface removal technique is

analytically modeled in Chapters 5 and 6 for a fuller understanding of the phenomena leading to concrete surface removal.

1.5 Removal of the Adhering Mortar

The presence of the adhering mortar on the surface of the crushed concrete particles has been identified as the most important factor lowering the quality of the recycled aggregates (De Juan and Gutierrez, 2009). The cementitious adhering mortar has a lower density, higher water absorption, lower Los Angeles abrasion resistance and higher sulfate content when compared to aggregates such as granite (De Juan and Gutierrez, 2009).

Recently, a number of methods have been proposed to improve the quality of RCA by removing the adhering mortar present. In these methods, known as RCA beneficiation methods, one or a combination of mechanical, thermal and acidic pre-soaking treatments may be used to remove the adhering mortar. Previous experiences on using these methods as reported in available literature are reviewed in Chapter 3 of this thesis.

In addition, a new microwave assisted RCA beneficiation technique is proposed in this study. The proposed microwave-assisted technique may increase the efficiency and speed and thus be more economical as a means of removing the adhering mortar from RCA in practice. This method uses microwave heating to generate high thermal stresses concentrated in the adhering mortar and at its interface with the original aggregate. In Chapter 7, the theoretical concepts behind this method are explained. In addition, a simple experimental study and numerical modeling of the RCA beneficiation process are used to illustrate the feasibility of applying this method in practice. Furthermore in Chapter 10, the results of an experimental study conducted to compare the properties of RCA

processed using the microwave-assisted beneficiation technique with the properties of RCA processed using the other proposed beneficiation methods are presented.

1.6 Objectives

The current study is aimed at investigating different methods to improve the quality of coarse RCA so that it can be confidently used as a replacement for coarse natural aggregates. The focus will be placed on investigating the feasibility of using microwave heating as a demotion tool to remove the surface contaminants of concrete debris and to remove the layer of adhering mortar from the RCA particles. In general the objectives of this study may be listed as:

- To review the properties of the coarse recycled concrete aggregates and identifying the main factors resulting in the lower quality of RCA compared to natural aggregates.

- To review different methods that may be used to improve the quality of recycled concrete aggregate.

- To investigate the possibility of using microwave heating as a demolition tool to remove the contaminants from the surface of concrete debris.

- To analytically study the phenomena leading to spalling of the concrete surface when concrete is exposed to microwave heating.

- To develop an easy-to-use analytical formulation for simulating the microwave heating of concrete that can be used as an estimation and optimization tool.

- To investigate the feasibility of using the microwave heating to remove the adhering mortar from RCA.

- To analytically simulate the microwave-assisted RCA beneficiation process for a better understanding of the underlying phenomena as well as providing an efficient optimization tool for the design of the microwave-assisted RCA beneficiation systems.

- To investigate the feasibility of using Fiber Bragg Grating (FBG) optical sensors for the measurement of concrete and RCA temperature during the microwave heating so that it can serve as a control tool for these applications.

- To design and assemble a pilot industrial high power microwave heating system to be used for microwave decontamination and microwave assisted RCA beneficiation applications.

- To experimentally investigate the effects of the microwave-assisted beneficiation technique on the properties of the RCA.

- To compare the properties of the RCA treated with microwave-assisted beneficiation technique with the RCA treated using the other available beneficiation methods.

1.7 Thesis Organization

This thesis is organized into 11 chapters. The content covered in each chapter is briefly explained as follows:

In Chapter 1, the necessity of using RCA as a replacement for the natural aggregate in Singapore, the previous experiences of other countries, the factors lowering the quality of RCA and thus limiting its application, and different solutions to deal with these factors are briefly discussed. Moreover, the objectives and scope of the current study are outlined.

In Chapter 2, available previous studies on the properties of recycled concrete aggregate are reviewed. Some of the more interesting results as reported in previous studies, especially with regards to the differences in properties between RCA and NA, are presented. Moreover, the effects of different RCA production techniques and equipments are investigated.

In Chapter 3, different techniques proposed to improve the quality of RCA are described. Based on the literature review presented in Chapter 2, the presence of contaminants (impurities) and adhering mortar on RCA particles are considered as the two main factors lowering the quality of RCA. In the first section of Chapter 3, different concrete surface removal techniques are reviewed and assessed for the possible use in the removal of contaminants from the surface of the concrete debris. The emphasis will be placed on using the microwave assisted surface removal (microwave decontamination) method which has been reported to be more efficient and less time consuming compared to other techniques. In the second section, the previously reported methods used to remove the adhering cementitious mortar from the RCA particles (RCA beneficiation methods) are reviewed. Moreover, a novel microwave-assisted RCA beneficiation technique is proposed to increase yield and quality and eliminate the drawbacks of previously proposed methods.

In Chapter 4, to facilitate a better understanding of the microwave decontamination process and the microwave assisted RCA beneficiation technique, fundamental concepts of microwave heating are presented. The concepts presented in this chapter are used in chapters 5 to 8 where the microwave-concrete and microwave-RCA interactions are investigated.

In Chapter 5, the microwave decontamination of concrete is numerically modeled by presenting the governing heat and mass transfer equations as well as a simple approximate method based on Lambert's law to estimate microwave power dissipation. The thermal stresses and pore pressure developed in the concrete, when heated with microwaves of three different frequencies, are presented. Moreover, the effects of the concrete water content, microwave frequency, microwave power and the heating duration on the microwave decontamination process are analytically investigated. The approximate microwave power dissipation formulation developed in this chapter is easy-to-use and can significantly reduce the mathematical difficulties of the more accurate electromagnetic modeling.

In Chapter 6, the more accurate Maxwell's equations are numerically solved to calculate the electromagnetic field, microwave power dissipation and the resulting thermal stress distributions in concrete heated with a common industrial microwave heating system comprising a rectangular waveguide as the applicator. The results are compared with the results obtained using the approximate Lambert's law formulation used in Chapter 6 to verify the accuracy of the approximations used.

In Chapter 7, the microwave assisted RCA beneficiation process is numerically investigated by modeling the microwave-RCA interaction and the resulting heat and mass transfer phenomena. The thermal stresses developed as a result of the differential heating of RCA are numerically calculated and used to investigate the capability of microwave heating to remove the adhering cementitious mortar from RCA. Moreover, the effects of the mortar's water content on the rate of temperature increase and thus on the thermal stress development are numerically examined. Furthermore, the results of a small-scale

experimental study conducted using a commercially available microwave oven are presented, examining the capability of microwave heating to remove the adhering mortar from the RCA particles.

In Chapter 8, an experimental and numerical study is conducted to investigate the capability of Fiber Bragg Grating (FBG) optical sensors for monitoring the concrete temperature during microwave heating. Moreover, the accuracy of the conventional thermocouples and infrared thermometry cameras are examined and compared with the FBG sensors as well as the temperatures obtained through numerical modeling.

In Chapter 9, the design and assembly stages of the pilot industrial microwave decontamination system set up in the NUS structural laboratory are explained in detail. The microwave heating system designed in this study can be used for either the microwave decontamination or the microwave assisted RCA beneficiation applications with minor reconfiguration of the hardware.

In Chapter 10, the microwave assisted RCA beneficiation technique using the industrial microwave heating system designed in Chapter 9 is used to remove the adhering mortar of RCA. The effects of incorporating this technique on the properties of RCA are investigated and compared with the effects of the other RCA treatment techniques proposed in previous studies.

In Chapter 11, the general conclusions drawn from the experimental and numerical studies presented in this thesis are reviewed and future research is proposed as a continuation of this work.

Table 1.1 Singapore's coarse aggregate (Granite) import history (Statlink, 2010)

Country	2004		2005		2006		2007	
	Import		Import		Import		Consumption	
	Qty (tonne)	Value (kS$)	Qty (tonne)	Value (kS$)	Qty (tonne)	Value (kS$)	Qty (tonne)	Value (kS$)
Indonesia	10861188	73366	9906855	71084	10936511	83825	5633430	98835
Malaysia	31400	189	478676	3162	582787	4105	3684759	77982
India	1938	303	3611	671	11380	2197	24	9
China	785	325	762	176	408	152	3776882	113149
Philippines	852	150	346	47	170	23	4646	651
Italy					100	6		
Total import for the above	10896163	74333	10390249	75139	11531356	90309	13099741	290626
Total import from other countries	66	12	42	11			469757	10025
total export to other countries	90	1016	37	728	42	1195	1039	409
Total market Use	10896139	73329	10390254	74422	11531314	89114	13568459	300242

Table 1.2 The change in the Singapore's coarse aggregate import origins (Statlink, 2010)

Country	2007	
	Qty (tons)	Value (kS$)
China	3,776,882	113,149
Indonesia	5,633,430	98,835
Malaysia	3,684,759	77,982
Vietnam	450,185	9,000
Thailand	16,133	689
Philippines	4,646	651
United States	203	119
Brunei Darussalam	2,753	85
Taiwan	404	59
Germany	48	47
Australia	30	14
India	24	9
Iran		9
Italy		2
Total	13,569,498	300,651

Table 1.3 Material composition for various building types, (EnviroCentre, 2005)

Material	Material Composition for different building types							
	4-storey concrete frame office		4-storey traditional masonry residence		Single storey steel framed retail development		2-storey steel framed office	
	%	Ton	%	Ton	%	Ton	%	Ton
High value aggregate: RCA	97.8	2581	48.6	1052	72.6	2568	60.2	1462
Medium value aggregate: RA	0.7	20	38.4	831	24.6	871	29.8	724
Recyclable steel	5.9	166	0.7	15	2.5	87	1.7	41
Recyclable hardwood, glass	0.1	3	neg	266	neg	11	neg	203
Physical contamination	1.5		12.3		0.3		8.4	

Table 1.4 Historical risk assessment of buildings chemical contamination.(EnviroCentre, 2005)

Historical Use	Likely Contaminants				
	Inorganic chemicals/reactions				pH
	SO$_4$	Cl$^-$	CO$_3$	ASR	
Building Type					
Airports	X	✓	✓	X	✓
Carparks	✓	✓	X	X	X
Ceramics works	✓	✓	✓	X	✓
Chemical works – paints	✓	X	X	✓	✓
Chemical works – cosmetics	✓	X	X	✓	✓
Chemical works – disinfectants	✓	✓	X	✓	✓
Chemical works – explosives	✓	✓	X	X	✓
Chemical works – fertiliser	✓	✓	✓	✓	✓
Chemical works – fine chemical	✓	✓	✓	X	-
Chemical works – sealants	✓	X	✓	✓	✓
Chemical works – organic chemicals	✓	X	✓	X	✓
Chemical works – soap manufacturer	X	X	X	X	✓
Dockyards	✓	✓	✓	X	-
Electronics	X	X	X	✓	
Engineering works	✓	✓	✓	X	✓
Gasworks	✓	X	✓	X	✓
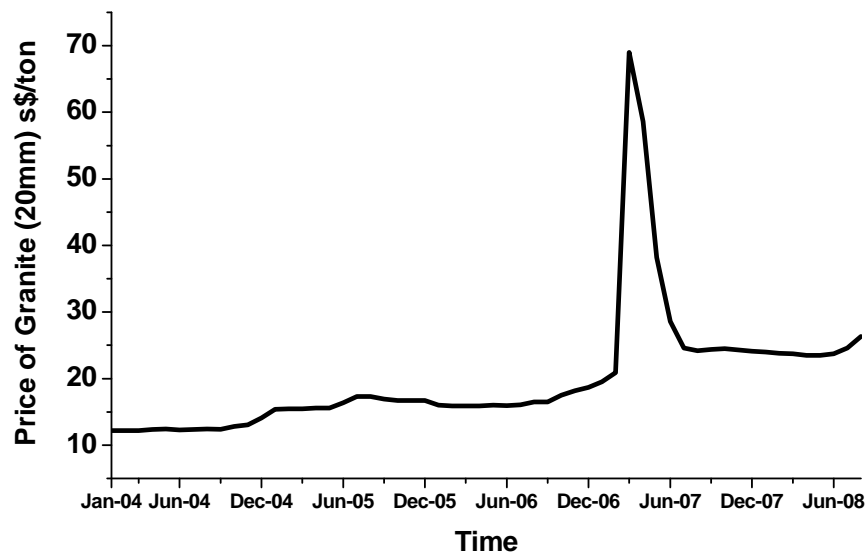
Figure 1.1 Price of Granite in Singapore Market (Statlink, 2010)

Chapter 2 : Recycled Concrete Aggregate- Literature Review

The significance of concrete recycling for Singapore and the experiences of other countries were briefly discussed in Chapter 1. The current chapter is divided into three sections. In the first section, **Section 2.1**, the state of art of the concrete recycling technology is reviewed. To investigate the possibility of incorporating new techniques and modifications to improve the quality of RCA, the full understanding of the processes involved in the current recycling technology is extremely important. In the second section, **Section 2.2**, the available literature on the properties of the recycled concrete aggregate produced using the current state of art technology is reviewed. The comprehensive literature review presented in this section is used to identify the main causes leading to the lower qualities of RCA compared to NA. Finally, in **Section 2.3**, available standards and specifications for the use of recycled concrete aggregates in concrete are reviewed.

2.1 Concrete Recycling Technology- State of Art

A concrete recycling plant refers to a central place where the recycling or reprocessing of construction and demolition waste materials is conducted to obtain the recycled aggregate. A concrete recycling plant generally involves four operations in

reprocessing the construction and demolition debris to produce recycled aggregates: sorting, crushing, refining and separating.

Sorting is first done on the incoming materials through grizzles, to set aside broken rock and concrete rubble suitable for recycling. The material is then passed through a primary jaw crusher which reduces the size to less than 250 mm. Crushing of the recycled material using a crusher is the principal step in processing recycled concrete lumps to reduce its size. Typically, crushing stages are followed by refining stages to ensure that the crushed concrete rubble are further reduced and properly processed. Separating of the recycled material involves other secondary processing steps. At this stage, a magnet is used to remove any reinforcement steel present in the concrete rubble and hand-sorting is used to remove other foreign substances. In addition, vibrating screens are usually utilized to separate the coarse and fine aggregates. The rock and concrete rubble are then crushed using secondary impact crushers and sorted into 40 mm, 20 mm, 10 mm sizes and fine fraction (5 mm down) through a set series of sieves.

The concrete recycling plant may be mobile (on-site) or permanent (fixed-site). A permanent plant usually needs an area of between 2 to 4 hectares. Even with mobile sites, space is usually required for resource and equipment storage. Whether a mobile or a fixed plant is set up, it is advantages to locate the site of the recycling operation close to either the sources of raw materials or product destinations.

Mobile plants require the ability to allow for the ease of set up and relocation. Most recycling occurs in urban areas with access to adequate transportation routes and infrastructure. Compared to a more permanent concrete recycling plant, a mobile single

trailer plant may be more suitable for small asphalt projects or where concrete does not contain rebar or other debris, involving less complicated operations.

2.2 Properties of Recycled Concrete Aggregate (RCA)

Many studies have been conducted to examine the properties of RCA produced using the current state of the art concrete recycling technology. In following, the results of the previous studies on different properties of RCA including the adhering mortar content, density, water absorption, toughness and soundness as well as the effect of various production parameters including the type of the crushing process, particle size and the strength of the parent concrete on these properties are reviewed.

2.2.1 Amount of Adhering Mortar

RCAs often contain a large amount of adhering mortar and cement paste. The volume percentage of old mortar may amount between 20% to 70% (Li et al., 2008). The adhering mortar content is one of the most important properties of RCA because it will directly or indirectly affect all other major RCA properties. The cementitious adhering mortar is considered to be main cause leading to inferior properties of recycled aggregates, e.g. lower density, higher absorption, lower Los Angeles abrasion resistance and higher sulphate content. Intuitively, the undesirable effect of the adhering mortar on the properties of RCA particles should be proportional to its content. Available literature reports that the volume of adhering mortar varies with the grain size, strength of the parent concrete and the crushing process used. The effects of these factors are reviewed in following subsections:

a) **Effect of Particle Size**

The relationship between the amount of the adhering mortar content and the size

of the RCA particle as reported by Fleischer et al. (1998) is shown in Figure 2.1. Moreover, the results of another study by De Juan et al. (2009) are summarized in Figure 2.2. As can be seen, the fine RCA particles may contain cementitious mortar up to 65% of their total weight. The amount of the adhering mortar content of coarse RCA is between 20% to 40%.

According to Torben and Narud (1983), The amount of mortar that remains adhering to natural gravel particles in recycled aggregate varies from around 30% for the 16-32 mm fraction to more than 60% for the 4-8 mm fractions.

b) Effect of the Parent Concrete Strength

The exact effect of the parent concrete's strength on the amount of the RCA's adhering mortar is still unknown. According to Hasse et al. (1998), for the same particle size, aggregates derived from weaker parent concrete have greater dry density and thus less adhering mortar. Hasse et al. explained that this dependency probably stems from the fact that the mortar in weaker parent concrete sheds off more readily in the crushing process, leaving more clean rock particles.

Contrary to the Hasse et al.'s study, Grubl et al. (1998) claimed that the strength of the parent concrete has practically no influence on the strength of the new concrete. He asserted that the amount of the adhering mortar is mainly dependent on the concrete crushing procedure. According to his studies, after the first stage crushing, only the strong portion of mortar remains adhering.

c) Effect of the Crushing Process

The crushing process can affect significantly the properties of the recycled concrete aggregates including the amount of its adhering mortar, the presence of cracks on the

RCA, and the shape of the particles. The significant effect of the crushing procedure on the amount of the adhering mortar and thus the properties of the recycled concrete aggregate has been investigated by a number of researchers. According to Fleischer et al. (1998), the properties of the recycled aggregates are largely determined by the crushing process. The amount of the adhering mortar may be diminished by increasing the number of crushing operations; however, this will increase the cost and hence a balance between the number of the stage-crushing processes and aggregate quality needs to be found (De Juan and Gutierrez, 2009).

The effect of the type of crusher has also been studied in available literature. Two types of crushers are usually applied at different stages of concrete recycling, jaw crushers and impact crushers.

Jaw Crushers reduce large size pieces by compressing the concrete chunks. A jaw crusher consists of a set of vertical jaws, one jaw fixed and the other being moved back and forth relative to it (Figure 2.3). The jaws are farther apart at the top than at the bottom, forming a tapered chute so that the material is crushed into progressively smaller and smaller sizes as it travels downward until it is small enough to escape through the opening at the bottom.

Impact crushers involve the use of impact rather than pressure to crush concrete (Figure 2.4). Concrete is contained within a cage, with openings of the desired size on the bottom, end, or side to allow the pulverized material to escape through.

Impact crushers use a plate hammer mounted on rapidly rotating rotors that generates high-speed impact to crush the concrete pieces in the crushing cavity and casts the crushed concrete pieces along a tangential direction to impact the plate at the other end of

the crushing cavity. The concrete pieces are crushed again, and are then returned to the plate hammer to undergo the process repeatedly. The concrete pieces bump against each other when propelled between the plate hammer and the impact plate. The concrete pieces become cracked, loose and then comminuted by knocking against the plate hammer, impacting with impact plate and bumping against adjacent concrete pieces. The crushed concrete of sizes smaller than the gap between impact plate and plate hammer will be discharged.

According to Fleischer et al. (1998), within the jaw crushers, the concrete chippings are squeezed. Hence, the incipient cracks may be induced in the chippings and this may reduce the strength, and above all, the frost resistance of the RCA. However, unlike the Jaw crushers, in the impact crushers, the reduction in size takes place without forces being exerted on the individual particles. On the other hand, in the impact crushers, the chippings break at their weakest points, such as at incipient cracks so that the result is a particle with better properties. Reduction by impact also causes the solid mortar to be removed off to a greater extent.

Nagataki et al. (2004) evaluated the recycled aggregate characteristics using fluorescent microscopy and image analysis. This study focused on the characteristics of recycled aggregates produced by further processing technology that can improve the quality of the product. The recycling technology reported in this study consisted of crushing the source concrete using a combination of jaw and impact crushers and processing the crushed material twice with a mechanical grinding equipment to minimize the amount of the adhering mortar. Results showed that double crushing can significantly reduce the amount of the adhering mortar.

d) Measurement Techniques

Several methods have been recently proposed to remove the adhering mortar from the surface of RCA. Even though most of these methods seem unpractical and uneconomical as means for the quality enhancement, they may be used to measure the adhering mortar content of RCA in the laboratory. These methods are briefly described in following sections. A more comprehensive explanation of these methods and introduction to a new microwave-assisted method will be discussed in Chapter 3.

d-1) Acid Pre-Soaking Method

In this method the adhering mortar is removed through exposure to an acidic solution such as HCL, H_2SO_4 or H_3PO_4. Previous studies have shown that by choosing the appropriate acid concentration, these methods can effectively remove the RCA's adhering mortar (Tam et al., 2007). Hence, the weight loss of RCA after being soaked in the acidic solution for 24 hours may be measured to obtain the adhering mortar content. (Tam et al., 2007)

d-2) Colored Cement

This method includes casting a new concrete with 100% coarse RCA content and colored cement. The difference in color between the new mortar, old adhering mortar and the original aggregate facilitates the detection of the original adhering mortar in a slice of the hardened specimen (Rilem, 1994).

d-3) Conventional Heating

In this method the adhering mortar of RCA is removed through the stresses generated by exposing the RCA to several cycles of soaking in the water and heating in a

conventional furnace. RCA is heated at 500 °C for 2 hours and then immersed into the cold water (De Juan and Gutierrez, 2009).

De Juan et al. (2009) measured the adhering mortar content of RCA using the three abovementioned methods. The results of this study are summarized in Figure 2.5.

2.2.2 Density

Similar to natural aggregates, ASTM C-127 standard {standard test method for specific gravity and absorption of coarse (or fine)} is used to calculate the density of the recycled concrete aggregates.

Available literature shows that the recycled concrete aggregate generally has a lower density than natural aggregate. According to Li et al. (2004), the bulk density of RCA is about 1290–1470 kg/m^3 which is somewhere in between rock materials and lightweight aggregate. Moreover, the SSD density of RCA is between 2310 and 2620 kg/m^3. According to previous studies, the density of RCA depends on the following:

a) Adhering Mortar Content

The lower density of RCA is directly attributed to the presence of adhering mortar in RCA which is of lower density compared to stone. De Juan et al. (2009) reported that the bulk specific density and SSD density of RCA are inversely proportional to the mortar content of RCA. The results of this study are summarized in Figures 2.6 and 2.7.

b) Particle Size

Generally the density of RCA has been reported to vary between 2290 and 2490 kg/m^3 depending on the size of the aggregates. Hansen et al. (1985) showed that the density of RCA varies with its size when the same crushing equipment and the same crushing stages are used.

The density (SSD) of RCA generally decreases with decreasing aggregate size. However, this decrease may be also attributed to the increase in the adhering mortar content in RCAs of smaller sizes.

2.2.3 Water Absorption

By testing 15 samples, Ravindrarajah et al. (2000) observed that the average value of water absorption of recycled aggregate and of natural aggregates were 6.35% and 0.90%, respectively.

Water absorption of recycled concrete aggregates is a function of their density and size and thus of the adhering mortar content. RUHL et al. (1997) examined the water absorption capacity of recycled concrete aggregates obtained from four different concrete recycling plants. The results of this study are summarized in Figure 2.8. As can be seen, the water absorption of RCA decreases almost linearly with the increase in its density.

The relationship between the water absorption and density was also investigated by De Juan et al. (2009). As can be seen in Figure 2.9, similar to the RUHL et al.'s results, the results of this study showed an almost linear decrease in the water absorption as the RCA density increases. Since the density of the RCA varies with its mortar content; the authors concluded that the water absorption of RCA is directly proportional to the amount of the adhering mortar present.

Poon et al. (2002) found that the absorption capacity of recycled aggregate increased with a higher amount of adhering mortar (=lower density). Poon et al. also asserted that in all the cases considered in their study, the absorption capacity did not seem to be dependent on the strength of the original parent concrete.

2.2.4   Toughness (Abrasion and Impact Resistance)

Crushing strength, abrasion resistance, and elastic modulus of aggregate are all interrelated properties that are greatly influenced by porosity (Tabsh and Abdelfatah, 2009). "The abrasion and impact resistance of an aggregate is its ability to resist being worn away by rubbing and friction or shattering upon impact. It is a general measure of aggregate quality and resistance to degradation due to handling, stockpiling, or mixing" (Concrete Knowledge Center, 2007). Due to their higher strength and density compared to other components in concrete, natural aggregates are not normally counted as the limiting factor in the overall compressive strength of concrete. However, due to the presence of the adhering mortar, recycled concrete aggregates are generally expected to have a lower toughness.

The resistance of aggregates against degradation due to the effects of abrasion, wear and impact is measured using the Los Angles test (ASTM C 131 for aggregate between 2.36 and 37.5 mm [No. 8 sieve opening and 1-1/2 in.], and ASTM C 535 for aggregate between 19 and 75 mm [3/4 and 3 in.]). This test subjects the aggregate participles to a combination of impact and abrasion by rubbing them against the steel balls placed in a slowly revolving drum.

The results of the Los Angles test conducted on recycled concrete aggregate by Tabsh et al. (2009) are presented in Figure 2.10. Tabsh et al. reported that the recycled concrete aggregates had on average 30% more Los Angles abrasion losses than natural aggregates. Moreover, according to this study, the strength of the parent concrete affects the abrasion resistance of the aggregate, i.e. stronger concrete results in less loss. Nevertheless, the authors asserted that the toughness of all the recycled aggregates tested was within

the acceptable limit of 50% for structural applications.

The effects of the RCA's adhering mortar content on its toughness were investigated by De Juan et al. (2009). According to the results of this study, Figure 2.11, the Los Angles abrasion increases with the adhering mortar content. Results showed that all samples with adhering mortar content lower than 44% can fulfill the requirement of the Spanish standard for aggregates in concrete. In Spanish standard, the Los Angles coefficient has been limited to a maximum of 40% (De Juan and Gutierrez, 2009). De Juan et al. observed that during the Los Angles abrasion test almost all the adhering mortar of the exposed individual recycled concrete aggregates was turned into powder and deposited at the bottom of the drum.

2.2.5 Soundness

Soundness of an aggregate refers to its ability in concrete to withstand aggressive exposure, particularly due to weathering (Concrete Knowledge Center, 2007). If an aggregate absorbs too much water so that its pores are nearly filled, expansion caused by turning the water into ice as a result of cold weather may be high enough to crack the aggregate particle and, when used in a concrete matrix, the surrounding concrete as well.

Soundness tests predict the resistance of aggregates to weathering by subjecting them to alternate cycles of wetting and drying, or freezing and thawing. In ASTM C 666, concrete specimens are subjected to alternate cycles of freezing, either in air or water, and thawing in water (Concrete Knowledge Center, 2007). In this method, the deterioration is determined by measuring the reduction in the frequency of an energy wave passed through the specimens.

The soundness test described in ASTM C88 is also used by some specifications. In this test, aggregates are immersed in sodium sulfate or magnesium sulfate for a prescribed number of cycles and oven dried subsequently. The deterioration is determined by measuring the percentage loss in mass. Tabsh and Abdelfatah (2009) studied the coarse recycled concrete aggregates soundness by subjecting them to sodium sulphate for 5 cycles. The tests results, Figure 2.12, show that compared to natural aggregates, recycled aggregates are more prone to soundness problem. However, only in one case, where recycled aggregates were produced from an unknown dump site, did the loss exceed the acceptable limit of 12 (Tabsh and Abdelfatah, 2009).

2.2.6 Impurities

Construction and demolition (C&D) wastes are normally composed of concrete rubble, bricks and tiles, sand and dust, timber, plastics, cardboard and paper, and metals (Kou and Poon, 2006). Impurities are present in recycled aggregates due to the heterogeneity of the raw material. However, the impurities content in recycled concrete aggregate can be controlled through quality assessment before accepting the concrete debris from the demolition site and through manual and automated removal techniques in the recycling plants. As long as the limits are observed, there will be minimal effect on the quality and properties of concrete made with recycled aggregates (Kou and Poon, 2006).

The effects of contaminants commonly found in construction and demolition wastes (bricks, tiles, clay, glass, wood) on the properties of RAC was investigated by Poon et al. (2005). In this study, impurities were blended to replace 10% of the recycled concrete aggregate in the production of concrete blocks. Results of this study showed that there was on average 5% decrease in density of the concrete blocks in which contaminants were

incorporated. For blocks with aggregate to cement (A/C) ratio of 3, the 28-day compressive strengths of contaminated blocks were in between 71.5% to 82.3% of the control blocks with 100% recycled concrete aggregates. Moreover, Poon et al. reported that the compressive strength increased with either a decrease in the A/C ratio or an increase in the density. Furthermore, based on the results obtained, Poon et al. claimed that the allowable contamination level in the recycled concrete aggregate can be increased from 1% (adopted by the current Hong Kong standard) to a maximum of 10% in the production of paving blocks (Poon and Chan, 2007).

According to Dhir et al. (2004), mixing 3% plaster with the coarse RCA aggregates led to 15% reduction in the concrete's compressive strength of the concrete produced. Dhir et al. recommended the use of sulphate resistant Portland cement when recycled aggregates containing plaster or gypsum are used in concrete.

2.3 Available Standards on RCA

With the increasing interest towards the use of recycled aggregates, most major standards bodies have recently published documentation on the general requirements for use of recycled concrete aggregate (RCA) and recycled aggregate concrete (RAC). Among the standards available, the Japanese standard (JIS) is most comprehensive. Japan was among the first countries to initiate research on RCA. Japan introduced the recycling law as early as 1991. Under the "recycled 21" programme launched by the ministry of construction (MOC) in 1992, targets were set to increase the percentage of recycled demolished concrete in the ensuing years. By 2000, 96% of demolished concrete was recycled against the MOC target of 90%. However, practically all the recycled concrete aggregate were used as sub-base material for road carriageways.

Previously, the Japanese standard **JIS A 5308** for ready mix concrete did not permit the use of the recycled aggregates. In response to the recommendation of JIS Civil Engineering Committee in 1998, the Japanese Concrete Institute formed a committee to draft a JIS technical report, as a preliminary document to be developed into a JIS standard. This report known as **TR A 0006**, released in 2000, permits recycled concrete to be used independently from **JIS A 5308**. However, according to this report, the strength of structural recycled concrete was capped at 18 MPa. Pre-soaking of the recycled aggregates for the control of workability and the use of blast furnace slag cement or fly ash to counteract alkali aggregate reaction are among the requirements of this standard.

Subsequently, in 2005, this report was published as the JIS standard, **JIS A 5021** [Japanese Standard Association, 2005] for high quality recycled aggregate '**H**' for concrete, which is produced through advanced processing, including crushing, grinding and classifying of concrete masses generated in the demolition of structures. Recycled aggregate **H** must have physical properties satisfying the requirements listed in Table 2.1. There are also upper limits for the amount of deleterious substances present in recycled aggregate **H**, as shown in Table 2.2. **JSI A 5023** has also been published as a standard for recycled concrete using low-quality recycled aggregate **L.** This type of concrete includes backfilling, filling and leveling concrete, and the use of Type B blended cement is required as a measure against alkali-silica reactivity.

In Hong Kong, two sets of specifications are used for the use of recycled aggregates in concrete production. The specifications requirements for RCA are listed in Table 2.3. According to these specifications, 100% recycled coarse aggregate may be used for low grade applications, while recycled fines are not allowed for use in concrete. The

29

compressive strength for concrete with 100% recycled aggregate concrete is capped at 20MPa which can be used in benches, planter walls, concrete mass, and other minor concrete structures. For higher grade applications, up to C35, the Hong Kong specifications allow a maximum of 20% replacement of virgin aggregate by recycled aggregate.

In UK, **BS 8500-2** and **BS EN 12620:2002-A1:2008** have included the general specifications for RCA and RAC in their new editions. United Kingdom has not been as active as the other European countries in concrete recycling, the old standards of **BS882** and **BS1047** only cover natural aggregates and air-cooled blast slag aggregates, respectively and did not include any provisions for recycled aggregates. However, these standards have already been withdrawn and replaced with **EN 12620:2002**. The use of recycled aggregates in concrete was first allowed in **BS 8500** published in 2002. According to **BS 8500-2**, the coarse RCA and coarse recycled aggregate (RA) shall conform to the requirements specified in Table 2.4. Composites of coarse RCA or coarse RA and natural aggregates shall conform to the general requirements for aggregate specified in **BS EN 12620** as appropriate and to the general requirements for normal-weight aggregates.

While RA can only be used in low grade concrete not exceeding 20 MPa characteristic strength, concrete containing RCA can be up to 50 MPa characteristic strength (Table 2.5). According to this standard, the maximum replacement level of natural aggregate with RCA in designated concretes RC20/25 to RC40/50 shall be not more than a mass fraction of 20% of coarse aggregate except where the specification permits higher proportions to be used. However, for the designed concrete, the judgment

shall be based on the performance. Furthermore, **BS 8500-2 Annex B** presents a test method to determine the composition of RCA and RA. The use of fine RA or RCA is not covered in the BS.

In Germany, after a wide range of tests conducted under a comprehensive research programme (Baustoffekreislauf im massivbau) between 1996 and 1998, a series of guidelines (Die Ricthlinie) for the use of recycled aggregates in concrete was published. The recommendations of this guideline on the allowable percentage of recycled aggregate for different applications are summarized in Table 2.6. The particle density of the recycled aggregate must not be less than 2000 kg/m^3. This guideline is expected to be eventually upgraded to a DIN standard.

In Austria, the production of recycled aggregate is governed by the "Richtlinie fur recycling-Baustoffe" (Guidelines for the recycled building materials), jointly published by the Austrian Association for the Recycling of Building Materials and the Austrian Quality Protection Association for Recycled Building Materials. The third edition of this guideline published in 1999 covers four types of recycled aggregates including: recycled asphalt aggregates, recycled concrete aggregates, mixed recycled asphalt and concrete aggregates, and mixed recycled asphalt, concrete and natural aggregates. Moreover, three quality classes are defined. Only quality class I recycled concrete aggregates are suitable for use in concrete construction. Aggregates in this class are to be tested for grain size distribution, grain strength, frost resistance, compactability, permeability, foreign materials content, contamination and environmental compatibility as instructed in this guideline.

In the Spanish standard, the use of recycled aggregate is restricted to mass concrete and reinforced concrete and its use for pre-stressed concrete is prohibited (W.K. Fung, 2005). Moreover, only the use of aggregate from the recycling of conventional concrete will be recommended, excluding special types of concrete such as light weight concrete, fiber-reinforced concrete and concrete made using aluminous cement, etc.

European standards are intended to unify practice in the member countries of the European Union, basically to remove the trade barriers. **BS EN 12620**- Aggregates for Concrete- was published in January 2003. The merit of **BS EN 12620** lies in the way recycled aggregates are treated on an equal basis with natural aggregates. Compliance requirements are implicitly the same for both types of aggregates.

Table 2.1 Physical properties requirement for Type H recycled aggregates, JIS standard

Items	Coarse aggregate	Fine aggregate
Oven-dry density, g/cm^3	Not less than 2.5	Not less than 2.5
Water absorption, %	Not less than 3	Not less than 3
Abrasion, %	Not more than 35	NA
Solid volume percentage for shape determination	Not less than 55	Not less than 53
Amount of material passing test sieve 75μm, %	Not more than 1	Not more than 7
Chloride ion content	Not more than 0.04	

Table 2.2 Limits of amount of deleterious substances for Type H recycled aggregates, JIS standard

Category	Deleterious Substances	Limit (mass %)
A	Tile, Brick, Ceramics, Asphalt	2.0
B	Glass	0.5
C	Plaster	0.1
D	Inorganic substances other than plaster	0.5
E	Plastics	0.5
F	Wood, Paper, Asphalt	0.1
Total		3.0

Table 2.3 Specification requirements for recycled concrete aggregate in Hong Kong (W.K. Fung, 2005)

Requirements	Limit	Test method
Min. dry particle density (kg/m^3)	2000	BS812:Part 2
Max. water absorption	10%	BS812:Part 2
Max. content of wood and other material less dense than water	0.5%	Manual sorting in accordance with BRE Digest 43
<ax. Content of other foreign materials (e.g. glass, plastics, clay lumps, asphalt, tar)	1%	
Max. fines	4%	BS 812: Section 103.1
Max. content of sand (<4mm)	5%	BS812:Section 103.1
Max. Sulphate content	1%	BS812:Part 118
Flakiness index	40%	BS812:Section 105.1
10% fines value	100KN	BS812:Part 111
Grading	Table 3 of BS 882:1992	
Max chloride content	Table 7 of BS 8820. 0.5% by mass of chloride ion of combined aggregate	

Table 2.4 Requirements for coarse RCA and coarse RA, (mass fraction %), BS 8500-2

Type of aggregate	Requirement [A]					
	Maximum masonry content	Maximum fines	Maximum lightweight material [B]	Maximum asphalt	Maximum other foreign material, e.g. glass, plastics, metals	Maximum acid-soluble sulfate (so_3)
RCA[A),C)]	5	5	0.5	5	1	1
RA	100	3	1	10	1	—[D]
[A] where the material to be used is obtained by crushing hardened concrete of known composition that has not been in use e.g. surplus precast units or returned fresh concrete, and not contaminated during storage and processing, the only requirements are those for grading and maximum fines						
[B] material with a density less than 1000 kg/m³						
[C] The provisions for coarse RCA may be applied to mixtures of natural coarse aggregates blended with the listed constituents.						
[D] The appropriate limit and test method needs to be determined on the case by case basis						

Table 2.5 Limitations on the use of coarse RCA, BS 8500-2

Type of aggregate	Limitation on use	
	Maximum strength class [A]	Exposure classes [B]
RCA	C40/50	X0,XC1,XC2,XC3,XC4,XF1,DC-1

[A] Material obtained by crushing hardened concrete of known composition that has not been in use and not contaminated during storage and processing may be used in any strength class.

[B] These aggregates may be used in other exposure classes provided it has been demonstrated that the resulting concrete is suitable for the intended environment, e.g. frezze-thaw resisting, sulfate resisting.

Table 2.6 German Guidelines on the maximum percentage of recycled aggregate in relation to the total aggregate (W.K. Fung 2005)

	Recycled aggregates and crushed sand > 2mm Volume (%)	Crushed sand < 2mm Volume %
< B25	35	7
Indoor concrete structures B35	25	
Concrete for outdoor exposure environment	20	0
water proofed concrete		
concrete with high forest resistance		
Concrete resistant to mild chemical attack.		
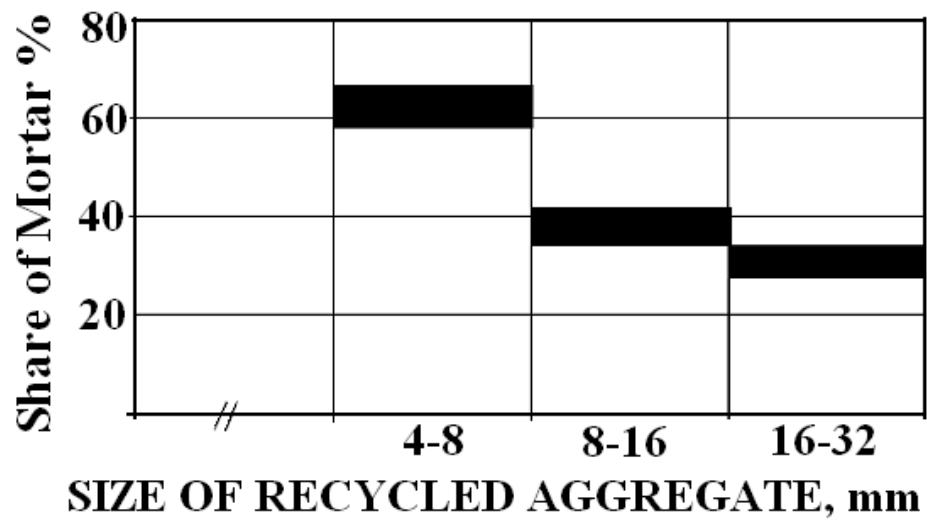
Figure 2.1Share of mortar for different RCA size fractions. (Fleischer and Ruby, 1998)
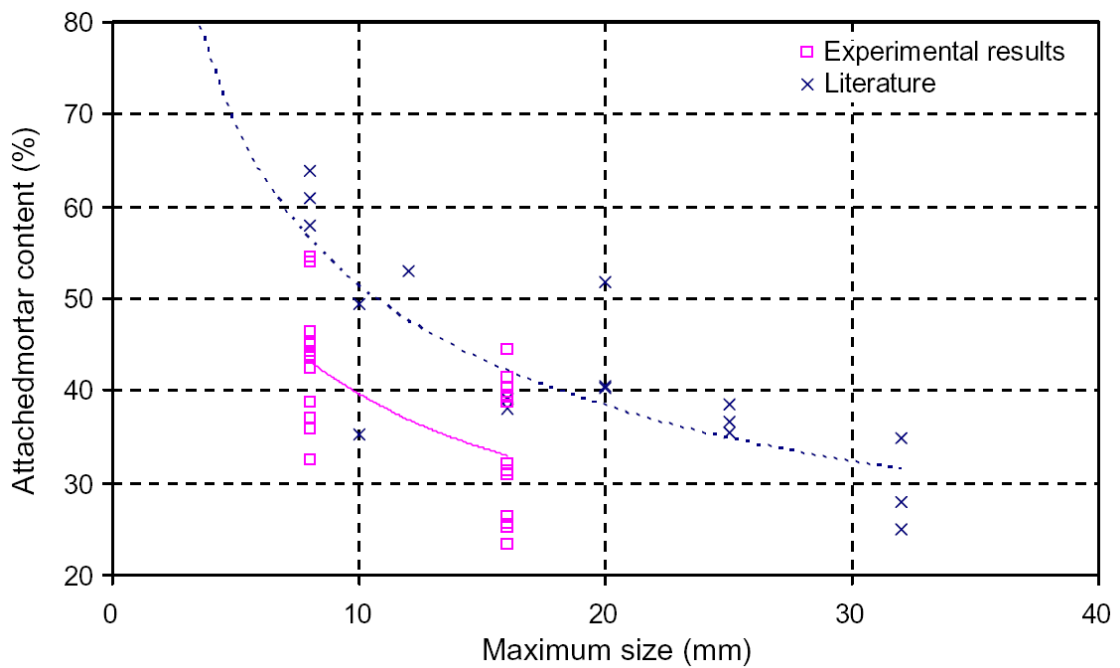
Figure 2.2 Share of mortar for different RCA size fractions. (De Juan et al., 2009)
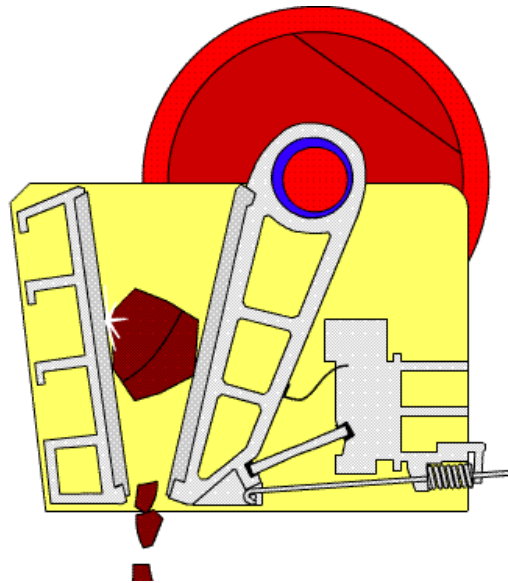
Figure 2.3 Jaw Crusher (www.sbmchina.com)
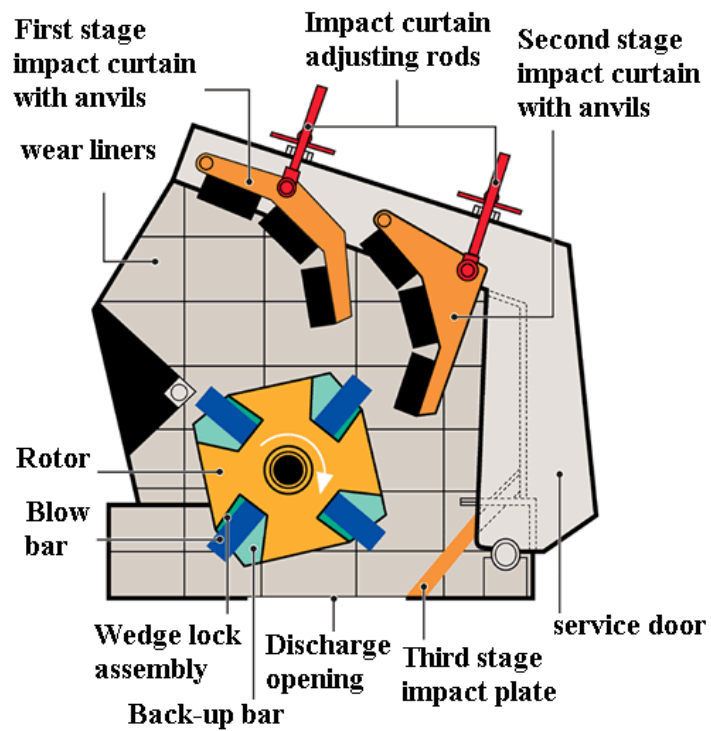
Figure 2.4 Impact Crusher (www.impact-crushers.com)
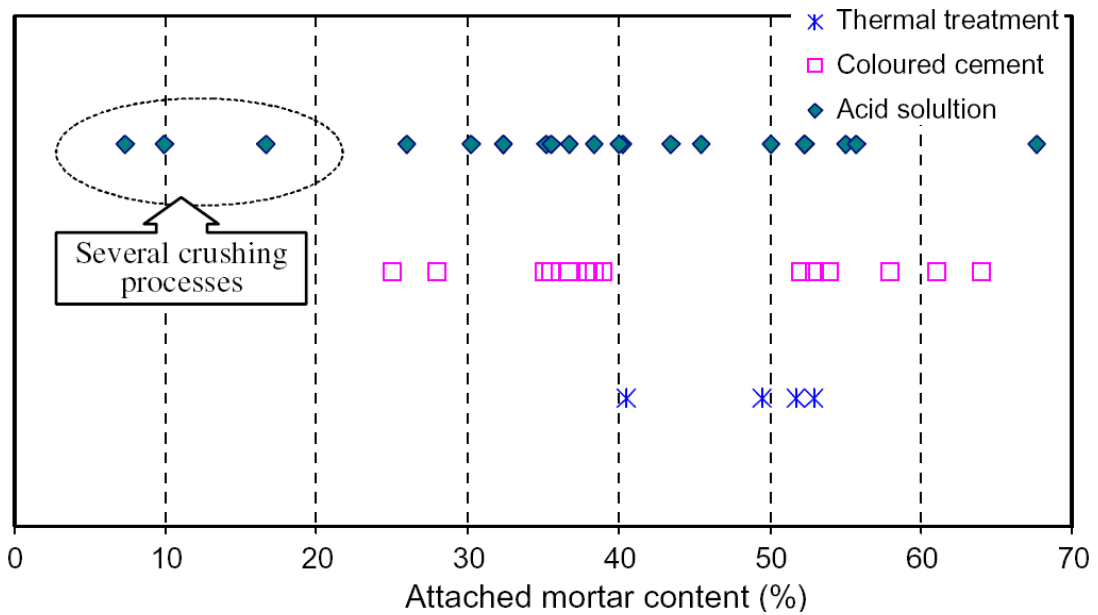
Figure 2.5 The adhering mortar content of RCA measured through different techniques. (De Juan et al., 2009)
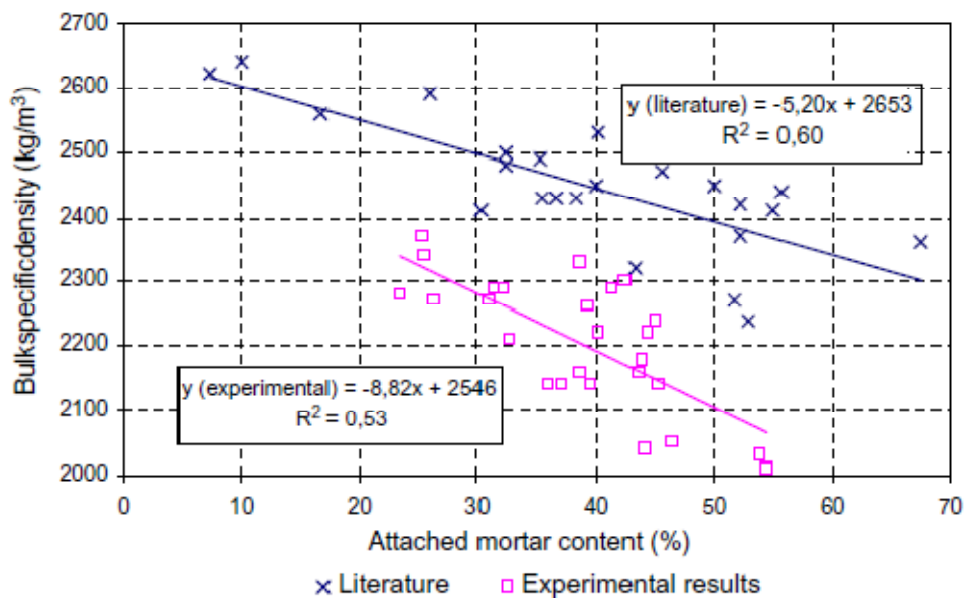
Figure 2.6 Variation of the bulk specific density of RCA with its adhering mortar content (De Juan et al, 2009)
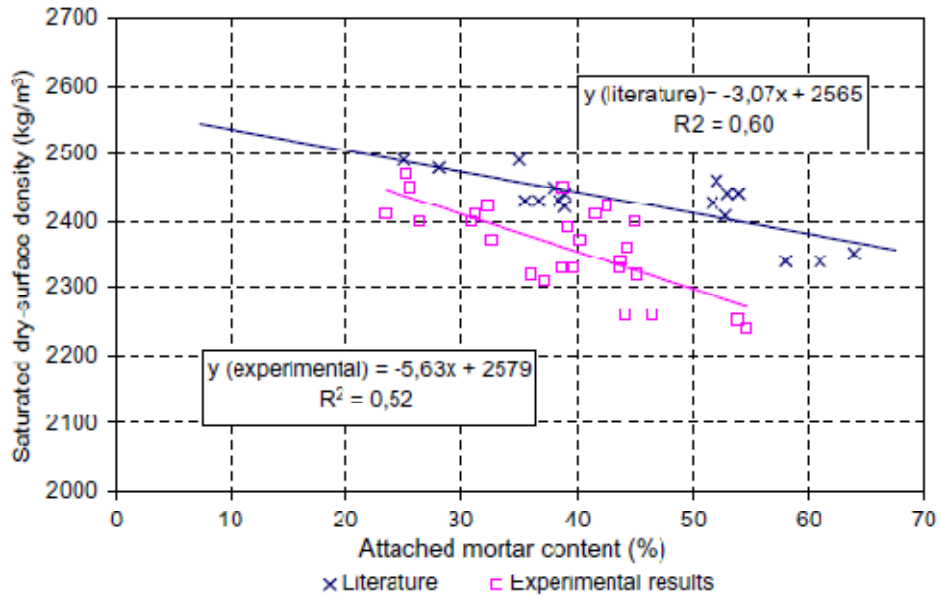
Figure 2.7 Variation of the SSD density of RCA with its adhering mortar content (De Juan et al., 2009)
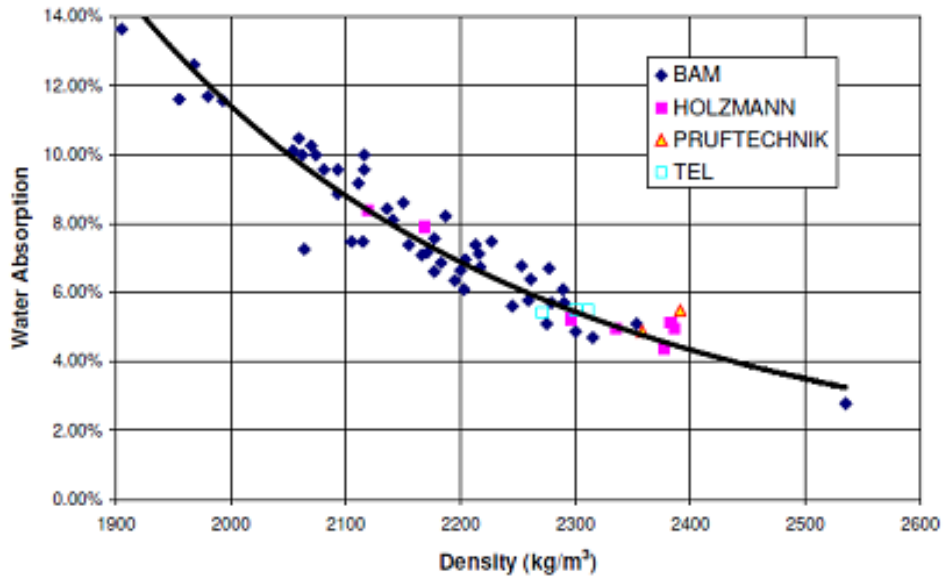
Figure 2.8 Relationship between the water absorption and density measured for RCA produced in four different recycling plants in Germany (RUHL and MARCUS, 1997)
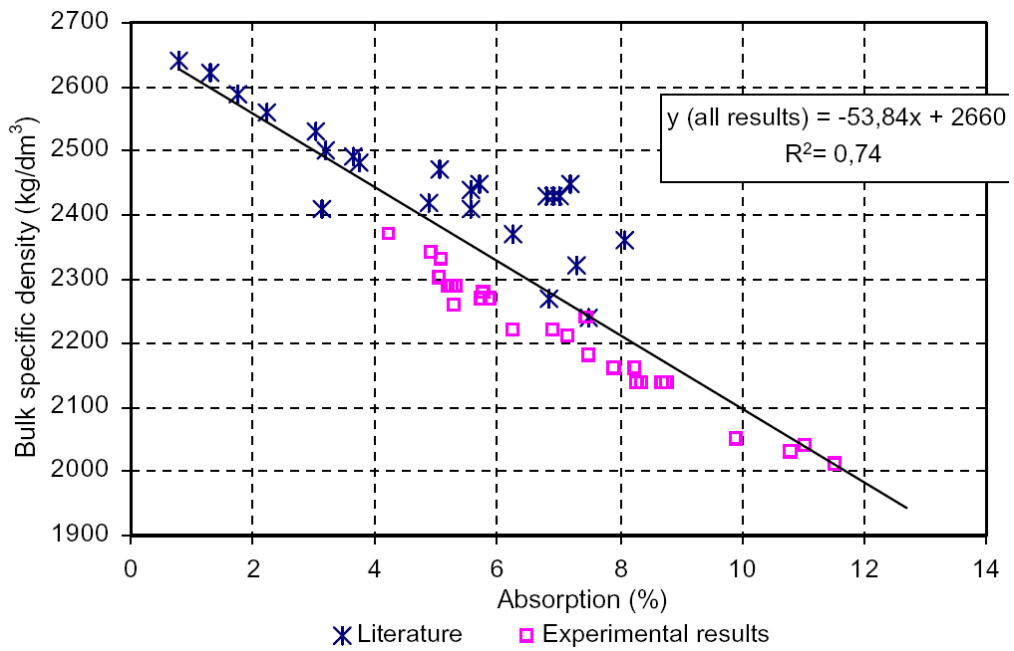
Figure 2.9 Relationship between the water absorption and bulk density measured (De Juan and et al., 2009)
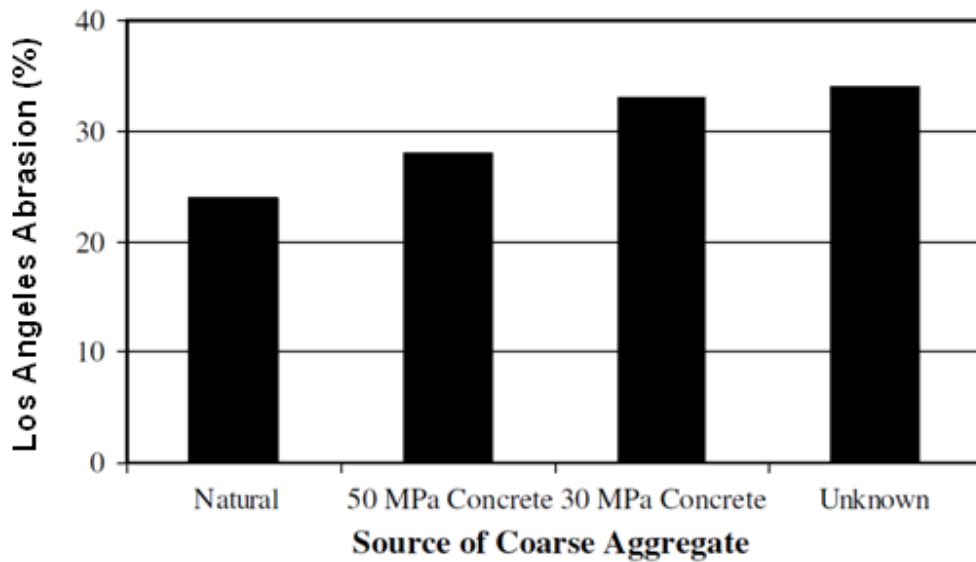
Figure 2.10 Results of the RCA toughness tests conducted by Tabsh and Abdelfatah (2009)
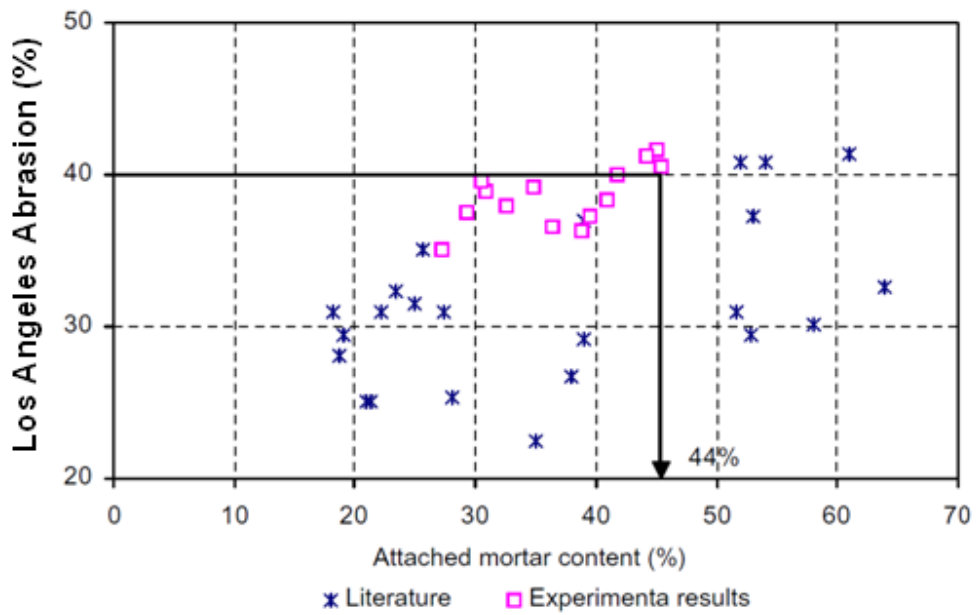
Figure 2.11 Relationship between the Los Angles abrasion coefficient of RCA and its adhering mortar content (De Juan and Gutierrez, 2009)
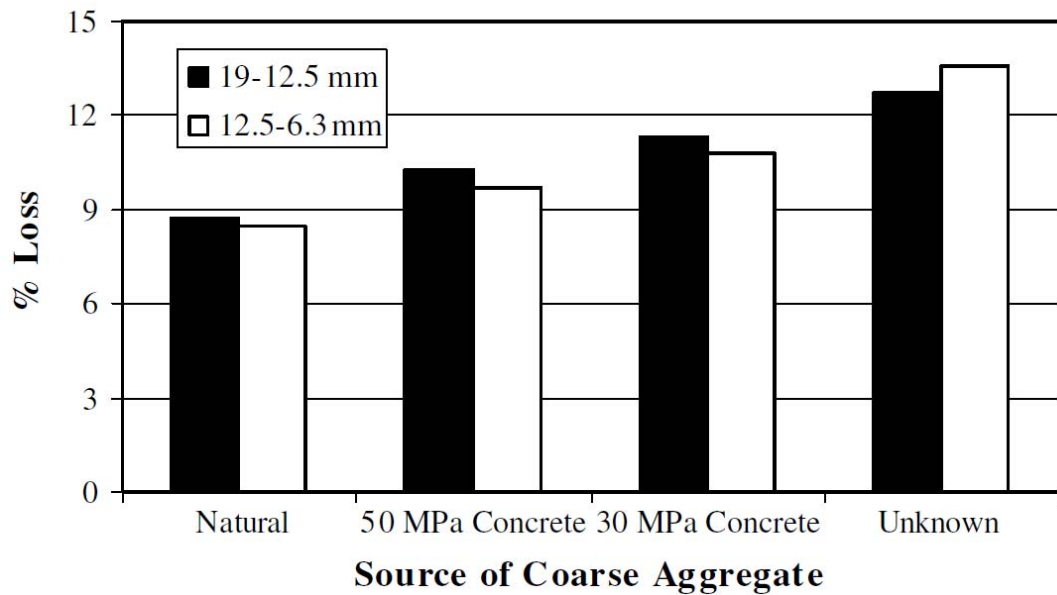
Figure 2.12 Results of the RCA soundness tests conducted by Tabsh and Abdelfatah (2009)

Chapter 3 : Proposed Methods to Improve the Quality of RCA

As reviewed in Chapters 1 and 2, there are mainly two factors leading to the lower quality of RCA compared to NA.

1. Impurities and Contaminants (chemical and physical) present in the concrete debris.

2. The adhering cementitious mortar, of a porous and/or weak nature which decreases the quality and strength of RCA compared to natural aggregates.

In this chapter the proposed methods to improve the quality of RCA through elimination of the abovementioned factors are discussed. This chapter is divided into two sections. The first section begins by reviewing decontamination methods which may be used to remove the impurities and contaminants from the concrete surface. The focus will be then shift to a novel microwave-assisted surface removal process. The basic concepts behind this method as well as findings from previous studies and corresponding patents are comprehensively reviewed.

The second section, first reviews previously used RCA beneficiation (removal of the adhering mortar from RCA) methods. In the second part, a novel microwave-assisted method is proposed to remove the adhering mortar in a much faster and more efficient way compared to the previous methods. The concepts of this method are then explained.

3.1 Removal of Contaminants from the Surface of Concrete (Surface Decontamination)

The general term of contaminants used here refers to all materials, hazardous or non hazardous, which when present in concrete demolition debris may lower the quality of the recycled concrete aggregates or make them unsuitable for some concreting applications. With this definition, contaminants may include hazardous contaminants such as chemical or radioactive which may pose health hazard as well as non-hazardous contaminants which may compromise concrete quality, e.g. concrete surface plasters, gypsum, tiles, glazing, etc.

The type of the contaminants present varies depending on the building type. The type of likely contaminants present in various building types are listed in Table 1.4. It is noteworthy that the building interior components such as sanitary products, doors, window frames, suspended ceilings, raised floors, furnishings, plant & machinery, etc are not considered as concrete surface contaminants. Prior removal of these items is assumed to be the normal practice either at the demolition site itself or at recycling plants receiving the demolition debris and thus, is not covered in this study.

Currently conventional techniques such as chisel and hammer may be used to remove contaminants\impurities from the surface of concrete; however, such techniques are slow, and have many drawbacks such as dust and secondary waste generation and pose potential

health hazard. In following, the more efficient and more widely used surface decontamination techniques are reviewed. These technologies vary widely in their effectiveness and processing rates.

3.1.1 Abrasive Jetting

The abrasive jetting (Figure 3.1) uses a high speed stream of particles carried in an air or gas jet to remove a thin layer (paint, concrete, rust) from the surface of the material (Dickerson et al., 1995). The abrasive material is normally aluminum oxide or silicon carbides. Abrasive particles should have sharp edges and diameters of about 10-50 micro meters. This process is most effective on flat surfaces and can also be used on 'hard to reach' areas such as ceilings. The process produces comparatively large amounts of secondary waste (Ayers, 1998). Depending on the specific configuration used, processing rates vary from 7.5 to 22 m^2/hr (Dickerson et al., 1995).

3.1.2 High Pressure Liquid Nitrogen Blasting

This technique is a variation of the abrasive jetting technique where the jet material is liquid nitrogen (Dickerson et al., 1995). Concomitant effect of the embrittlement caused by liquid nitrogen and the abrasive action of the grit is used to remove the contaminated surface layer.

3.1.3 Wet Ice Blasting

Wet ice blasting is another variation of abrasive jetting where a compressed air jet is used to propel a mixture of water and ice crystals onto the surface to be decontaminated (Ayers, 1998).

3.1.4 High Pressure and Ultra High Pressure Water Jets

In this technique a highly pressurized water jet is used to remove contaminants from the concrete surface. The jet pressure is optimized for the specific removal depth and speed requirements. Variations of this technique include the use of glycerine as the pressurized medium or the entrainment of grit in the water jet (Ayers, 1998).

3.1.5 Sponge Blasting

In this method an air-propelled open cell, water-based polyurethane foam cleaning media (also known as sponge media), is used (Figure 3.2). Surfaces are pneumatically blasted (>700 kPa) with various grades of foam cleaning media (i.e. sponges). During contact, sponges contract and expand, creating a scrubbing action. The performance of the media may be increased by impregnating the foam with abrasive grit. The average treatment rate of this method is 5.5 m^2/hr (DOE, 1994).

3.1.6 CO_2 Blasting (Dry Ice Blasting)

Dry ice blasting is somewhat similar to abrasive jetting; however, instead of using a hard abrasive media to remove the surface, in dry ice blasting, the soft dry ice accelerated at supersonic speeds is used to remove the surface contaminants by creating mini-explosions on the surface (www.coldjet.com, 2010). Dry ice (CO_2) pellets are propelled by nitrogen gas or compressed air to impact on the contaminated surface. The pellets shatter upon impact and, in turn, shatter the target material. The CO_2 sublimes immediately and returns to atmosphere, leaving behind shattered pieces of concrete. Processing rate of this technique has been reported to range from 0.9 to 8.5 m^2/hr (Dickerson et al., 1995).

3.1.7 Mechanical Scabbling

This technology uses mechanical impact methods to physically remove the contaminated surface. A set of high-speed, reciprocating, tungsten carbide-tipped pistons are used to simultaneously strike the concrete surface. Due to poor efficiency, this method used to be considered as a rudimentary approach until the last decade. However, the newly developed models have shown very satisfactory and reliable performance in practical applications. Processing rates range from 2 to 4 m^2/hr (DOE, 1994).

3.1.8 Electro-Hydraulic Scabbling

The concrete surface is removed (scabbled) by powerful hydraulic shock waves induced by electric discharges between two electrodes. A hydraulic shock wave propagates through the water between the electrical discharge channel and the concrete causing the concrete to crack and peel. The high impulse pressure developed at the liquid-solid interface creates stresses that crack or break the surface layer. Depth of scabbling is controlled by pulse energy, shape and electrode placement. Processing rates vary between 2 to 4 m^2/hr (DOE, 1997).

3.1.9 Drilling and Spalling

In this technique a uniform pattern of holes of approximately 75 mm depth and 25-40 mm diameter are drilled into the concrete surface. A hydraulic spalling tool having an expandable tube is then inserted into the holes. Spalling occurs as a results of the forces created through the expansion and the generated dust is controlled by filter or water spray. The production rate of this technique has been reported to range from 0.2 to 1 m^2/hr (DOE, 1994).

3.1.10 Grinding

In this method, a thin surface layer of the concrete is removed through the direct contact with a rotating diamond or tungsten carbide grinding wheel. The average grinding rate is about 10 m^2/hr.

3.1.11 Shot Blasting

Shot blasting strips and etches the surface simultaneously. Abrasive is fed into the center of a completely enclosed centrifugal blast wheel; as the wheel spins, the abrasives are hurled from the blades, to strike and clean the surface (Figure 3.4). Such commercial shot blasting equipment is widely used to remove contamination and laitance (soft concrete) to reveal a mechanical profile for improved bonding with the new concrete. Commercial units with design rates of 14 m^2/hr are available (Ayers, 1998).

3.1.12 Soda Blasting

In soda blasting, sodium bicarbonate grit is applied against the contaminated surface using compressed air. Soda blasting process rates approach 20 m^2/hr. Soda blasting has been shown to effectively remove concrete surface contamination. This method was first used to restore the US's Statue of Liberty (Dickerson et al., 1995).

3.1.13 Laser Ablation

Laser ablation utilizes high power repetition rate lasers for ablation of coating from metal and concrete surfaces. Laser ablation efficiency is controlled primarily by wavelength, pulse width, energy power densities on target, pulse repetition rate, scan rate and light sources (xenon, pinch plasma). Rates of up to 8 m^2/hr have been demonstrated (DOE, 1994).

3.1.14 Microwave Heating

Microwave heating has been recently considered as an efficient replacement for conventional methods in concrete surface decontamination. It is well known that microwaves of high frequencies can generate high temperature gradients inside the concrete, occurring between the microwave exposed surface and the cooler interior. Such non-uniform heating in a very short time duration leads to a high differential temperature gradient and thus high thermal stresses. Moreover, concrete is a material whose pores may be partially filled by water and air. Under ambient temperature conditions, part of the water is chemically bonded to the cement while the remainder is contained in the concrete pores as free water. When exposed to microwaves, as a result of dielectric losses, microwaves penetrating the concrete act as a volumetrically distributed heat source. Water in the concrete is a very strong dipole and is easily heated up, as it absorbs the microwave energy. As a result the water within the concrete evaporates. When the evaporation rate overtakes the vapor migration rate, pore pressure builds up. The two phenomena of thermal stresses and pore pressure have been postulated to cause delamination of the concrete surface layer when heated with high frequency microwaves.

This method has been reported to have higher processing rates compared to previously discussed methods (White, 1995). In this thesis, the possibility of using the microwave heating as a demolition tool to remove the contaminants\impurities from the concrete surface is investigated. The previous experience on using microwave heating as a demolition tool is presented in next section.

3.1.15 Previous Experiences on Using Microwave Heating as a Demolition Tool

The idea of using microwave as a demolition and surface removal tool for

concrete first appeared in a paper by Watson in 1968 (Watson, 1968). Watson et al. invented a device for cracking a structure such as concrete, brick or the like through microwave heating. According to the invention, the device uses the microwave energy passing along a waveguide to form a narrow beam of energy, by causing it to emerge from the waveguide through an opening having a width substantially less than that of any part of the waveguide, and by directing the said beam at a small area of the surface of the structure for a sufficient amount of time to cause such local heating of the structure that results in the cracking of the structure. Inventors recommended that the best performance may be achieved when device uses the frequencies higher than 800 megacycles per second. It was reported that a temperature rise of at least 200 °C at the depth of 7.5 centimeters and a temperature rise of at least 400 °C at the surface of the structure may be reached before cracking occurs (Alexander Watson and St. Albans, 1965).

Subsequently, several research groups, the Japan's Atomic Energy Research Institute (JAERI), UK's Harwell Laboratory and US's Oak Ridge National Laboratory (ORNL) (White, 1992; White, 1995), tried to develop methods and the necessary equipment to use microwave as demolition tool to remove radioactive wastes from the surfaces of concrete.

Also, in an application similar to concrete demolition, microwave heating has been proposed as a rock breakage tool for use in the mining industry. Considerable amount of work has been done in applying microwave radiation to rocks like granite, schist, pumice slate and sandstone. The type of the applicator used in all the works was resonant cavities, surface applicators or internal applicators. The power used by various researchers was as high as 100 kW with frequencies being kept constant at 2.45 GHz or 915 MHz (Santamarina, 1989). These studies showed that microwave heating can effectively soften

the rock and eventually lead to surface delamination. However, it was reported that application of microwave heating as the only breaking force is not economical and thus the combination of microwave heating and mechanical cutting was proposed.

In 1965, Puschner et al. patented a novel microwave heating device for rock breakage. This device is shown schematically in Figure 3.5. The apparatus was invented to cleave large blocks of rock and ore for the purpose of subsequent comminution. This equipment consisted of a microwave generator, a cooling device for the generator, and a hollow guide radiator for directing the microwave energy onto the material to be heated. The microwave device was mounted on the boom of a crane to enable application of microwave energy from its hollow guide radiator onto the material to be heated. It was claimed that with this movable apparatus, even blocks at the edge of a rock field can be reached. This device was also reported to be suitable for the thermal blasting of concrete roads and rock walls in quarries (Puschner, 1965).

In 1991, Lindroth et. al. patented a new apparatus for the sequential fracturing and cutting of subsurface volume of hard rock in the strata of a mining environment by subjecting the volume of rock to a beam of microwave energy to fracture the subsurface volume of rock by differential expansion and, then bringing the cutting edge of a piece of conventional mining machinery into contact with the fractured rock. This apparatus is shown schematically in Figure 3.6. Inventors claimed that this combined method leads to faster breakage of rock and less wear of the equipment compared to when only microwave heating or only conventional mining methods are used (David P. Lindroth et al., 1991).

Lindroth et al. (1993) selected two igneous rocks, namely dresser basalt and St cloud grey granodiorite to test a drilling method combining both microwave heating and

mechanical mining. During the entire test, the drilling parameters were held constant, with variables being microwave power and time of irradiation. The 401 kg drill thrust, rotation of 36rpm and the 1 minute drilling time were also held constant. A high power microwave generator providing power of up to 25 kW at a frequency of 2.45 GHz was used in this experiment. All the experiments were performed inside a closed copper screen room used for containing microwave energy. Experiments showed that microwave heating can significantly increase the penetration depth rates in the selected types of hard rock. For example, the penetration rate in granodiorite at a temperature of 1093 °C was in excess of three times that of the rates at 25 °C.

In 1997, White et al. invented a mobile system for microwave removal of concrete surfaces. This apparatus uses the thermal stresses generated through the microwave heating alone to etch the desired depth of the concrete surface. As can be seen in Figure 3.7, this apparatus comprised a housing adapted to pass over a support surface. The housing included a waveguide for directing microwave energy to the surface of concrete at angle maximizing the absorption of microwave energy by the surface. The apparatus was further provided with a source of microwave energy operably associated with the waveguide, wherein the microwave energy had a frequency of between about 10.6 GHz and about 24 GHz to remove the uppermost layer from the surface. The apparatus also contained a debris containment assembly and vacuum assembly operably associated with the housing.

As reviewed above, the possibility of using microwave heating as a demolition tool and/or a part of the process for demolition for concrete and hard rock has been extensively studied in available literature. However, it seems that the actual microwave breakage

process has not been properly monitored during the above experiments. There is a need to use more accurate and appropriate instrumentation for measuring the concrete temperature, stress, pore pressure and other phenomena associated with the process of surface breakage. This information can be helpful for a better understanding of the phenomenon leading to surface removal during the microwave heating and can be used to design operational microwave surface removal systems with better performances.

Among the above parameters, temperature is the most important and yet the most difficult parameter to measure. Having known the temperature rise throughout the microwave heated specimen, the developed stresses can be estimated. Hence, temperature monitoring may be used as a process control tool for the microwave surface removal process.

In Chapter 4 of this thesis, the concepts of the microwave heating phenomenon are reviewed. These concepts will be used in Chapter 5 to numerically simulate the microwave-concrete interaction and calculate the pore pressure and thermal stresses developed. Moreover in Chapter 8, the results of an experimental study to monitor the concrete's temperature during actual microwave heating are presented.

3.2. Removal of the Adhering Mortar from RCA Particles (RCA Beneficiation)

As mentioned previously, the existence of the adhering mortar is another and probably the most important cause for the lower quality of recycled concrete aggregates when compared to natural aggregates. A number of researchers have previously tried to find an economical and rapid method to remove the adhering mortar from RCA. In this section the state-of-art RCA beneficiation technologies are reviewed.

3.2.1 Thermal Beneficiation

In this method, RCA particles are heated to about 500 °C. The thermal stresses generated through thermal expansion lead to removal of the adhering mortar. After heating, RCA particles are sieved to separate the mortar powder. It is believed that saturating the adhering mortar can increase the efficiency of this method because it can lead to higher pore pressure development in the adhering mortar. The concomitant effect of the pore pressure can lead to faster removal of the adhering mortar. There have been also recommendations to immerse the heated aggregate in cold water immediately after heating to increase the differential thermal stresses (De Juan et al., 2009).

However, this technique is very time and energy consuming. Processing of each batch of RCA using this technique may take about 4 hours. Moreover, this method tends to degrade the quality of the original granite core of the recycled concrete aggregate, as it heats the RCA particles up to temperatures in the range of 500 °C. According to Homand et al. (1989), "heating at high temperatures can adversely affect the mechanical properties of granite. For example, the pressure resistance decreases by up to 16% when heated at about 400 °C and by 44% when heated at 600 °C. Also, the tensile strength decreases by 30% and by 60% for the same heating temperatures, respectively. Moreover, as for the elastic modulus, it decreases by 12% when comparing heating temperatures of 20 °C and 400 °C and by 55% when heated at 600 °C for the same granite samples."

3.2.2 Mechanical Beneficiation

In this method mechanical forces are used to remove the adhering mortar. In Japan, two technologies have been proposed; eccentric-shaft rotor (Yonezawa et al., 2001) and mechanical grinding (Yoda et al., 2003). In the eccentric shaft rotor method, crushed

concrete lumps are passed downward between an outer cylinder and an inner cylinder that eccentrically rotates at a high speed to separate the material into coarse aggregate and mortar through a grinding effect.

In the mechanical grinding method, a drum is partitioned into small sections. The adhering mortar of RCA is removed by rubbing against the iron balls housed in the rotating partitioned sections.

3.2.3 Thermal-Mechanical Beneficiation

In this method a combination of the thermal stresses generated through conventional heating up to 300 to 500 °C and the mechanical stresses generated through rubbing the RCAs are used to remove the adhering mortar. In 2000, Tateyashiki et al. proposed a thermal-mechanical RCA treatment technique known as "heating and rubbing". In this technique, concrete masses are first heated at 300° C in a vertical furnace to make the cement paste brittle due to dehydration. To remove the cement paste from the surface of aggregates, the heated concrete is sent to the rubbing equipment (Figure 3.8). The rubbing equipment comprises a tube type mill with outer and inner cylinders. In the equipment, the heated concrete is rubbed by steel balls as media and the mortar portion of the material generated by the process is discharged through a screen provided on the inner cylinder to increase efficiency of the rubbing treatment. Inventors of this method have claimed that it can increase the quality of RCA to comply with the JCI standard for high quality recycled concrete aggregates.

3.2.4 Acid Pre-Soaking Beneficiation

More recently, Tam et al. (2006) proposed a new method to remove the adhering mortar by presoaking RCAs in an acidic solvent for 24 hours and then washing them with

the distilled water (Figure 3.9). Three different acidic solvents (HCL, H_2SO_4, H_3PO_4) were considered in this study. The authors claimed that this method can effectively remove the adhering cementitious mortar. Tam et al. showed that the water absorption rates of RCA after treatment have been reduced with improvements of between 7.27% and 12.17%. However, a major drawback of this method is the increase in the chloride and sulfate content of aggregate after treatment which may cause durability problems in future. Moreover, this method is rather time consuming, taking more than 24 hours overall.

3.2.5 Chemical-Mechanical Beneficiation

Abbas et al. (2007) proposed an approach which uses combined chemical degradation through exposure of RCA to sodium sulfate solution and mechanical stresses created through subjecting RCA to freeze-and-thaw action to separate the adhering mortar. However, the main focus of the study was on quantifying the amount of adhering mortar present on the samples of RCA for use in classifying the material. The method does not seem suitable for a large scale RCA production as overall this technique requires 7 days to complete.

3.2.6 Microwave-Assisted Beneficiation

The thermal and thermal-mechanical treatment methods explained above are generally found to be too energy and time consuming. Moreover, in some of the methods aggregates are heated up to temperatures of about 500 °C which can degrade the quality of the original natural aggregate after heat treatment. The effects of the thermal and thermal-mechanical treatment methods on the properties of RCA are studied in chapter 10 of this thesis.

The acid presoaking method explained above is also too time consuming and may cause durability problem due to the potential for increasing the sulphate and chloride content of the RCA. Furthermore, the combined chemical-mechanical method proposed by Abbas et al. cannot be considered as a practical method as it takes almost 7 days to complete. The effects of the chemical and chemical-mechanical methods on the properties of RCA are also examined in Chapter 10 of this study.

An alternative method to remove the adhering mortar from RCA surface is presented in this section. This method uses microwaves to delaminate the adhering cementitious mortar by developing considerably high thermal stresses at the mortar-aggregate interface. Differences between the electromagnetic and thermal properties of the aggregate and cementitious mortar may lead to development of high thermal stresses especially at their interface. These stresses may be harnessed to detach the adhering mortar. Moreover, any fissure present in the aggregates may also be addressed by splitting of the aggregates when subjected to microwave heating resulting in better quality aggregates overall. Shorter processing time compared to methods proposed by Tam et al. (2006) and Abbas et al (2007), and less energy consumption in comparison with the heating and rubbing method are among the advantages of this method. Moreover, compared to conventional heating methods, the maximum heating temperature levels reached in microwave heating are considerably lower and heating temperature is maintained for significantly shorter time duration. Furthermore, unlike the acid pre-soaking method, this method does not seem to cause any durability issues

The concept of microwave heating is presented in Chapter 4 of this thesis. The fundamentals of the microwave RCA treatment method are discussed in Chapter 7.

Moreover, in Chapter 7, analytical modeling and preliminary experiments are used to better understand the RCA microwave heating beneficiation process. In Chapter 10, the efficacy of microwave-assisted beneficiation technique is compared experimentally with the acid-presoaking and conventional heating beneficiation methods.
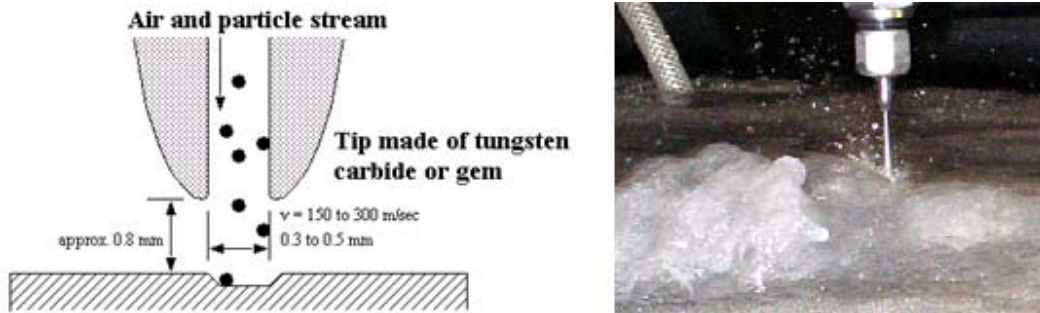
Figure 3.1 Abrasive Jetting (www.mech.unsw.edu.au)

Figure 3.2 Sponge Blasting (www.nstcenter.net)
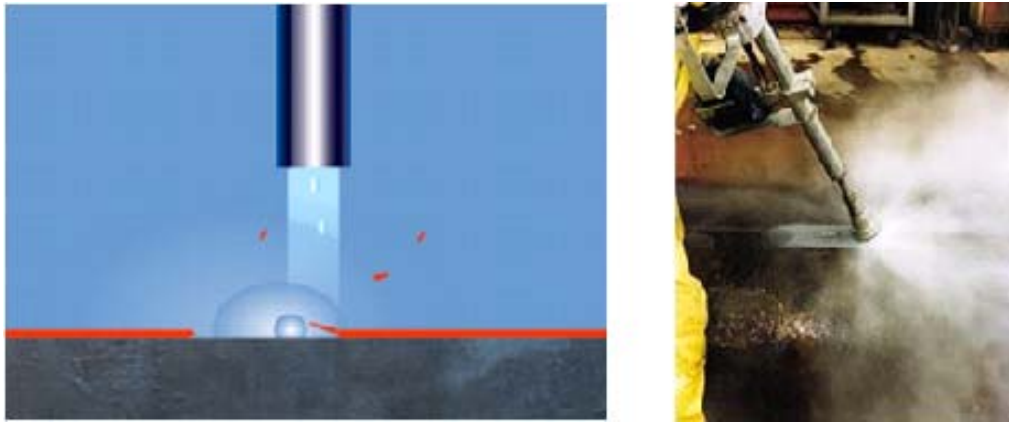
Figure 3.3 CO$_2$ Blasting (www.coldjet.com.au)

Figure 3.4 Shot Blasting (www.gritblasters.co.uk)
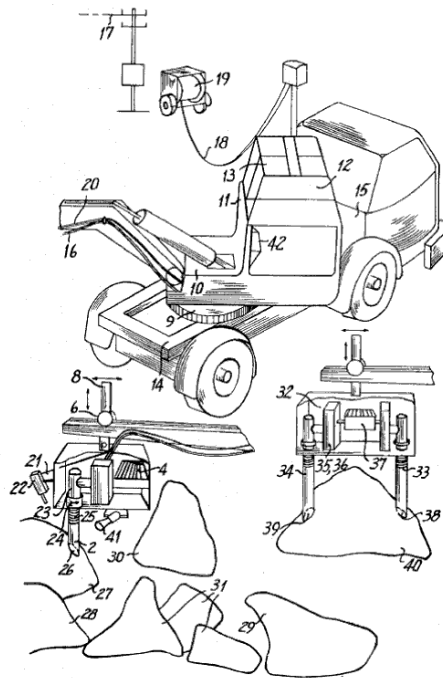
Figure 3.5 Microwave heating device for breakage of rocks (Puschner et al., 1965)
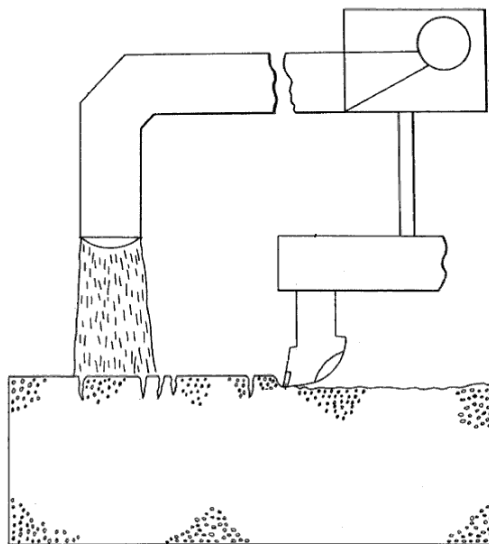
Figure 3.6 Microwave assisted fracturing and cutting device for hard rocks (Invented by Lindroth et al., 1991)
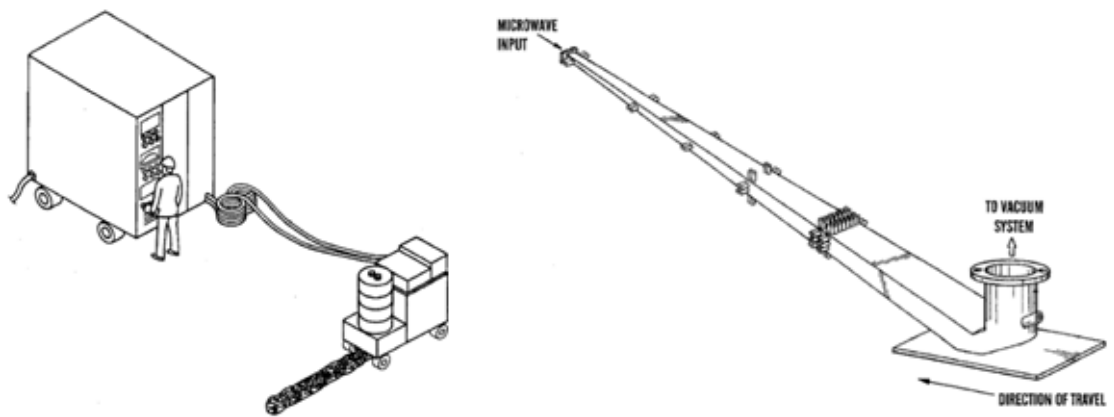
Figure 3.7 Mobile system for microwave removal of concrete surfaces (Invented by White et al., 1997)
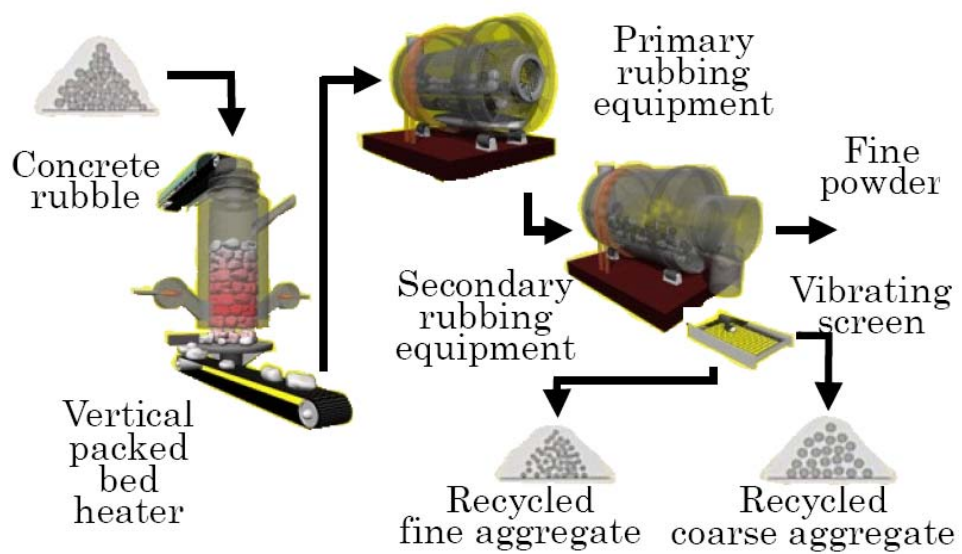
Figure 3.8 "Heating and Rubbing" RCA Beneficiation Method (Tateyashiki et al., 2000)
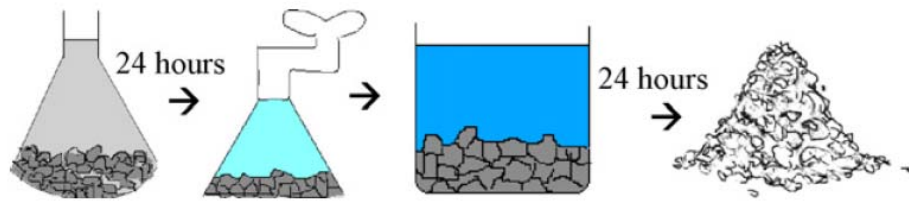
Figure 3.9 Acid Pre-Soaking RCA Beneficiation Method (Tam et al., 2006)

Chapter 4 : Fundamentals of Microwave Heating

4.1 Background

Microwaves are a portion of the electromagnetic spectrum lying between UHF (ultrahigh frequency) radio waves and heat (infrared) waves and span the frequency range of 300 MHz to 300 GHz (Figure 4.1). Intensive research during the Second World War into high-definition radar led to the development of microwave frequencies and in particular the magnetron valve as a microwave generator of very high power output with exceptional efficiency (Ayappa et al., 1991). In the post war years, further development resulted in microwaves being used for heating, especially for domestic purposes.

In order to minimize the interference with the microwave frequencies used in communication applications, specific frequencies often known as ISM "Industrial, Scientific and Medical" frequencies have been allocated for microwave heating applications. In general communications equipment should not be affected by any interference generated by ISM equipment. Among the ISM frequencies, 915 MHz, 2.450 GHz, 10.6 GHz and 18 GHz are the most commonly used frequencies for microwave

heating applications. At these frequencies, the wavelength of radiation in the medium ranges from 1 to 10 cm.

The largest market for microwave heating is the domestic microwave oven. However, commercial microwave heating units are also widely used in many industries such as food industry, tempering and thawing, continuous baking, vacuum drying, pasteurization and sterilization, and in the ceramics, rubber and plastic industries as well as in many specialized processes in the chemical industry especially that involve vacuum processing.

Microwave heating of concrete has also applications in various fields of civil engineering. These applications take advantage of the capabilities of the appropriate range of microwave frequency targeted to heat the concrete to different extents and degree of uniformity. Microwave heating at lower frequencies (such as 915 MHz) can be used to heat the concrete uniformly and accelerate its curing process at early ages. Previous studies have shown that, unlike steam cured concrete, microwave cured concrete can gain considerable strengths in just a few hours without compromising its long term properties (Leung and Pheeraphan, 1997; Phadungsak Rattanadecho et al., 2008).

In a contrasting application, as explained in Chapter 3, microwave heating at higher frequencies has been recommended as a potential replacement for more conventional concrete surface removal techniques (Bažant et al, 2003). Removal of the contaminated surface of concrete is of interest in the decommissioning of nuclear power plants where the contaminated surface of concrete should be removed before demolition (White, 1992; White, 1995) and in recycling of concrete where removal of physical and chemical contaminants from the surface of the concrete debris can significantly increase the quality

of the recycled concrete aggregates (Chi-Sun and Dixon, 2007). In the microwave-assisted surface removal technique which is also known as microwave decontamination, microwave heating at higher frequencies (> 2.45 GHz) and high powers is used to heat a thin surface layer of concrete and thereby generate a region of high thermal stress and pore pressure between the concrete's microwave-exposed surface and the cooler interior. Spalling of the concrete surface occurs when the pore pressure and/or thermal stresses exceed the concrete tensile and/or compressive strengths, respectively. In Chapter 5, the phenomena leading to the removal of the concrete surface when heated with microwaves is investigated. Focus will be placed on incorporating this technique to the concrete recycling process for removing the surface contaminants of concrete debris before sending them to recycling plant.

In addition, as explained in Chapter 3, another application of microwave heating in civil engineering is developed in this study. This application involves using microwave heating to increase the quality of recycled concrete aggregates (RCA) by removing their adhering cementitious mortar. In this technique which is known as microwave-assisted RCA beneficiation, high power microwave heating is used to develop high thermal stresses within the adhering cementious mortar as well as at its interface with the natural aggregate particles in RCA. These stresses can be harnessed to remove the adhering mortar of RCA and thereby increase the quality of the recycled aggregates.

The fundamental concepts of microwave heating are reviewed in this chapter. The information presented here are essential for a better understanding of microwave decontamination of concrete as well as the microwave assisted beneficiation of RCA which will be dealt with in Chapters 5 to 10.

4.2 Microwave Heating Mechanism

In general, microwave heating involves two primary mechanisms. In the first mechanism known as D.C. conductivity loss, the dielectric material behaves like a poor electrical conductor, having a finite resistivity measurable at DC. This type of loss is usually substantially constant as the frequency extends upwards.

The other mechanism is polarization due to an altering electric field. In this case, dipolar components of molecules in many dielectric materials couple electrostatically to the microwave electric field and tend to align themselves with the field mechanically. Since the microwave field is altering in time, the dipoles will attempt to realign each time the field reverses, and so are in a constant state of mechanical oscillation in tandem with the microwave frequency. Frictional forces generated within the molecules cause heat to be developed due to the motion of the dipoles.

Water is one of the most common materials displaying such polar characteristics. It absorbs microwave energy very strongly when highly pure, although it also has a very high DC electrical resistivity of approximately 105 Ω. However, when small quantities of solid are dissolved in water the DC resistivity falls and conduction via movement of the ionic charge carriers may become a significant component in heat dissipation. It is interesting to note that conduction heating tends to fall away when raising the frequency into the microwave domain, compared with dipolar heating, because the mass of the ions is such that their movement is curtailed.

Water is the main component in most of the dielectrics which show good microwave power absorption. Concrete, cementitious mortar and aggregate are also porous materials in which their pores are filled with water. In Chapters 5 to 10, the importance of the water

content of the concrete, mortar and aggregate on their microwave heating rate and pattern are analytically and experimentally investigated.

The microwave heating phenomenon may be generally thought as occurring in two stages. The first is the electromagnetic aspect, concerned with the propagation of radiation and power absorption by the medium as explained above. Second, the energy absorbed is converted into heat which is transported by convection, conduction and radiation. Propagation of microwaves is treated from the classical standpoint of Maxwell and the transport of heat is modeled using the constitutive equations of heat transfer. The electric field distribution is obtained by solving Maxwell's equations and the power absorbed by the medium is proportional to the intensity of the electric field. The power is then treated as a heat source when modeling the transport of heat.

4.3 Dielectric (Electromagnetic) Properties of Materials

Every material has a unique set of electromagnetic (EM) properties affecting the way in which the material interacts with the electric and the magnetic waves. Knowledge of dielectric properties of materials to be processed in the microwave regime is essential for the proper design of microwave applicators. A dielectric material can be characterized by two independent electromagnetic properties, the complex permittivity ε and the complex (magnetic) permeability μ (Rhim and Buyukozturk, 1998). The property which describes the behavior of a dielectric under the influence of a high frequency field is the complex permittivity. Complex permittivity is defined as

$$\varepsilon = \varepsilon' - i\varepsilon'' \quad (4.1)$$

Here, ε' is the real part of complex permittivity and ε'' is the imaginary part of complex permittivity. Dividing this by the permittivity of the free space ε_0, the property becomes dimensionless and relative to the permittivity of the free space:

$$\frac{\varepsilon}{\varepsilon_0} = \frac{\varepsilon'}{\varepsilon_0} - i\frac{\varepsilon''}{\varepsilon_0} \quad (4.2) \qquad \text{Or,} \qquad \varepsilon_r = \varepsilon_r' - i\varepsilon_r'' \quad (4.3)$$

Where, ε_0 is the permittivity of the free space, ε_r is the relative permittivity, ε_r' is the dielectric constant and ε_r'' is the loss factor of the material. Dielectric constant is a measure of how much energy from an external electric field is stored in a material and the loss factor is a measure of how dissipative or lossy a material is to an external field (Rhim and Buyukozturk, 1998). The ratio of the energy lost to the energy stored in a material is given as loss tangent:

$$\tan\delta = \frac{\varepsilon''}{\varepsilon'} = \frac{\varepsilon_r''}{\varepsilon_r'} \quad (4.4)$$

Electromagnetic wave attenuation occurs as a result of the conduction current through the lossy dielectric as well as the polarization in an altering field. The equivalent conductivity σ which accounts for both losses can be expressed in terms of the imaginary part of complex permittivity, as follows:

$$\sigma = \varepsilon''\omega = \left(\varepsilon'\tan\delta\right)\omega = \left(\varepsilon_r'\varepsilon_0\tan\delta\right)\left(2\pi f\right) \quad (4.5)$$

Where f and ω are the frequency and angular frequency of the electromagnetic wave respectively.

4.4 Reflection and Transmission of the Waves at Interfaces

The mismatch between the dielectric constants at the interface between two

different media causes some of the incident waves to be reflected and the rest to be transmitted into the next medium. The reflection coefficient can be obtained from:

$$R = \frac{\sqrt{\varepsilon_{r2}}\cos\theta_i - \sqrt{\varepsilon_{r1}}\cos\theta_t}{\sqrt{\varepsilon_{r2}}\cos\theta_i + \sqrt{\varepsilon_{r1}}\cos\theta_t} \qquad (4.6)$$

Where, R is the reflection coefficient, ε_{r1} is the dielectric constant for medium 1, ε_{r2} is the dielectric constant for medium 2, θ_i is the angle of incidence and θ_t is the angle of transmission. The square of reflection ($|R|^2$) is called reflectivity and denoted as r. The transmissivity, c, is obtained from:

c=1-r   (4.7)

When the parallel polarization mode (TM) is excited in microwave heating systems, there is an angle at which the incident wave will be totally transmitted to a dielectric material. This angle is known as the Brewester angle and may be obtained from:

$$\theta_B = \tan^{-1}\sqrt{\frac{\varepsilon_{r2}}{\varepsilon_{r1}}} \qquad (4.8)$$

Here, ε_{r1} and ε_{r2} are the dielectric constants of the medium 1 and 2, respectively. However, unfortunately, the Brewester angle is not applicable to the perpendicular polarization (TE) mode which is more commonly excited in microwave heating systems.

4.5 Penetration Depth & Attenuation Factor

As a result of the dielectric losses, the microwave energy attenuates inside the dielectric materials. The power penetration depth is defined as the depth at which the transmitted power drops to $1/e$ of its value at the surface and is given by

$$d_p = \frac{1}{2\beta} \qquad (4.9)$$

Where β is the attenuation factor. Having measured the electromagnetic properties of a dielectric material, its attenuation factor at a specific frequency may be calculated as:

$$\beta = \frac{2\pi f}{c} \sqrt{\frac{\varepsilon_r^{'}\left(\sqrt{1 + \tan^2 \delta} - 1\right)}{2}} \qquad (4.10)$$

Where, c is the speed of light, $\tan \delta$ the loss tangent, $\varepsilon_r^{'}$ the dielectric constant and f the microwave frequency.

4.6 Dielectric Properties of Concrete, Mortar and Aggregate

The amount of the energy dissipated in concrete, mortar and aggregate when they are exposed to microwaves varies significantly with their electromagnetic properties. Electromagnetic properties of concrete and mortar are a function of factors such as their ingredients, mix proportions, water content, microwave frequency and temperature. The dielectric properties of coarse aggregate and sand also vary with their composition, porosity, water content, microwave frequency, temperature, etc.

Compared to extensive information available on the mechanical properties of the construction materials, knowledge about their electromagnetic properties is very limited, especially over the wide frequency range. Previous research work has mostly been directed toward either the measurement of the electromagnetic properties of hardened concrete specimens at a limited frequency range (up to 1 GHz), or the measurements of changing electromagnetic properties of fresh concrete or cement pastes at their early ages of curing to monitor the hydration process (Rhim and Buyukozturk, 1998).

Hasted & Shah (1964), reported on the dielectric properties of building materials (brick, cement paste, concrete) at the microwave frequencies of 3GHz, 9GHz and 24 GHz as a function of their water contents. This study was aimed to introduce a new method to

find the water content of materials using electromagnetic waves. The authors reported that the real and imaginary parts of concrete's permittivity increase in an almost linear manner with its water content. Moreover, in another study by Hasted et al. (1964), the temperature dependency of 3.33 cm wavelength dielectric constant of hardened cement paste and brick was examined (Figures 4.2 to 4.5).

Li et al. (1994) conducted a test to obtain dielectric properties of concrete at different temperatures (Figures 4.6 and 4.7). However, because full specifications of the concrete specimens tested have not been reported, their results are not reliable for use in other studies.

Finally, in the most comprehensive and recent study by Rhim et al. (1998), the EM properties of concrete, cement paste, coarse aggregate and sand in the frequency range of 0.1 to 20 GHz were reported (Figures 4.8 and 4.13). Four different water contents were considered for the concrete and mortar specimens to investigate the effect of the water content on EM properties: 1) wet specimen, standing water on its surface 2) saturated, surface dry concrete 3) air-dried concrete exposed to ambient room temperature and humidity 4) oven-dried concrete with zero moisture content by weight. Concrete and mortar specimens tested by Rhim et al. were cast with water/cement/sand/coarse aggregate mix ratios of 1:2.22:5.61:7.12 (by weight) and 1:2.22:5.61:0 (by weight), respectively.

In the current study, the data reported by Rhim et al. are used in modeling of microwave heating of concrete (Chapters 5, 6, and 8) as well as the modeling of microwave-assisted beneficiation of RCA (Chapter 7). Hence, the raw data reported by Rhim et al. were processed using Equations 4.4 to 4.10 to calculate the basic

electromagnetic properties of concrete, mortar, coarse aggregate, sand and cement. The loss tangent, conductivity, reflection coefficient, transmissivity, Brewester angle, and attenuation factor of concrete, mortar and concrete constituents (i.e. Coarse aggregate, sand and cement) were calculated and are presented in Figures 4.14 to 4.31.

4.7 Maxwell's Equations

The problem of electromagnetic analysis on a macroscopic level is the problem of solving Maxwell's equations subject to certain boundary conditions. In 1873, the British physicist Maxwell published his famous 'Treatise on electricity and magnetism' including the Maxwell equations which embody and describe mathematically all phenomena of electromagnetism. Maxwell's equations are a set of equations, written in differential or integral form, stating the relationships between the fundamental electromagnetic quantities. These quantities are the electric field intensity $\mathbf{E}$, the electric displacement or electric flux density $\mathbf{D}$, the magnetic field intensity $\mathbf{H}$, the magnetic flux density $\mathbf{B}$, the current density $\mathbf{J}$ and the electric charge density $\mathbf{\rho_q}$. The electric field in particular is a recurring parameter in microwave and RF heating being the prime source of energy transfer to the workload.

The differential form of Maxwell's equations is presented here, because it leads to differential equations that the finite element method can handle. In the next few chapters, these equations will be numerically solved to investigate the microwave interaction with concrete, mortar and RCA. For general time-varying fields, Maxwell's equations can be written as:

$$\nabla \times H = J + \frac{\partial D}{\partial t} \qquad (4.11)$$

$$\nabla \times E = -\frac{\partial B}{\partial t} \qquad (4.12)$$

$$\nabla.D = \rho_q \qquad (4.13)$$

$$\nabla.B = 0 \qquad (4.14)$$

The first two equations are also referred to as Maxwell-Ampere's law and Faraday's law, respectively. Equations 4.13 and 4.14 are two forms of Gauss' law, the electric and magnetic form, respectively. Another fundamental equation is the equation of continuity, which can be written as:

$$\nabla.J = \frac{\partial \rho_q}{\partial t} \qquad (4.15)$$

Out of the five equations mentioned, only three are independent. To obtain a closed system, the constitutive relations describing the macroscopic properties of the medium, are included. They are given as:

$$D = \varepsilon E = \varepsilon_r \varepsilon_0 E \qquad (4.16)$$

$$B = \mu H = \mu_r \mu_0 H \qquad (4.17)$$

$$J = \sigma E \qquad (4.18)$$

Here, ε_0 is the permittivity of vacuum, μ_0 the permeability of vacuum, and σ the electrical conductivity. In the SI system, the permeability of vacuum is chosen to be $4\pi \times 10^{-7}$ H/m. The velocity of an electromagnetic wave in a vacuum is given as c_0 and the permittivity of vacuum is derived from the following relation:

$$\varepsilon_0 = \frac{1}{c_0^2 \mu_0} = 8.85 \times 10^{-12} \, F\!\!\left/\!\!m\right. \approx \frac{1}{36\pi} \times 10^{-9} \, F\!\!\left/\!\!m\right. \qquad (4.19)$$

4.8 Electromagnetic Energy

The electric and magnetic energies are defined as

$$W_e = \int_V \left(\int_0^D E \,.dD \right) dV = \int_V \left(\int_0^T E \,. \frac{\partial D}{\partial t} dt \right) dV \qquad (4.20)$$

$$W_m = \int_V \left(\int_0^B H \,.dB \right) dV = \int_V \left(\int_0^T H \,. \frac{\partial B}{\partial t} dt \right) dV \qquad (4.21)$$

The time derivatives of these expressions are the electric and magnetic power:

$$P_e = \int_V E \frac{\partial D}{\partial t} dV \qquad (4.22)$$

$$P_m = \int_V H \frac{\partial B}{\partial t} dV \qquad (4.23)$$

These quantities are related to the resistive and radiative energy, or energy loss, through Poynting's theorem

$$-\int_V \left(E \frac{\partial D}{\partial t} + H \frac{\partial B}{\partial t} \right) dV = \int_V J.E dV + \oint_S \left(E \times H \right).n ds \qquad (4.24)$$

Where V is the computation domain and S is the closed boundary of V. The quantity $E \times H$ is called the Poynting vector. Under the assumption of a linear and isotropic material, it holds that

$$E. \frac{\partial D}{\partial t} = \varepsilon E. \frac{\partial E}{\partial t} = \frac{\partial}{\partial t} \left(\frac{1}{2} \varepsilon E.E \right) \qquad (4.25)$$

$$H. \frac{\partial B}{\partial t} = \frac{1}{\mu} B. \frac{\partial B}{\partial t} = \frac{\partial}{\partial t} \left(\frac{1}{2\mu} B.B \right) \qquad (4.26)$$

By interchanging the order of differentiation and integration (justified by the fact that we have a constant volume and assuming that the fields are continuous in time), we get:

$$-\frac{\partial}{\partial t} \int_V \left(\frac{1}{2} \varepsilon E.E + \frac{1}{2\mu} B.B \right) dV = \int_V J.E dV + \oint_S \left(E \times H \right).n ds \qquad (4.27)$$

The integrand of the left-hand side is the total electromagnetic energy density:

$$W = W_e + W_m = \frac{1}{2}\varepsilon E.E + \frac{1}{2\mu}B.B \qquad (4.28)$$

The first term on the right-hand side represents the resistive losses:

$$P_h = \int_V J.E dV \qquad (4.29)$$

which results in heat dissipation in concrete. The current density **J** in this expression is the one appearing in Maxwell-Ampere's law. The second term on the right-hand side of Poynting's theorem represents the radiative losses:

$$P_r = \oint_S (E \times H).nds \qquad (4.30)$$

4.9 Dissipated Radiative Energy

The power flux associated with a propagating electromagnetic wave is represented by the Poynting vector S and the time average flux for the harmonic fields is given by:

$$S = \frac{1}{2}E \times H^* \qquad (4.31)$$

Where,* denotes the complex conjugate. According to the Poynting theorem the power dissipation in the medium is:

$$\oint_S S.nds = -\frac{1}{2}\omega\varepsilon_0\varepsilon_r'' \int_v E.E^* dv + i\omega\int_v \left(\frac{\mu_0}{2}H.H^* + \frac{\varepsilon_0\varepsilon_r'}{2}E.E^*\right)dv \qquad (4.32)$$

which states that the net power flow across a surface S enclosing a volume V equates to the power dissipated in the medium (real part), and that stored in the electric and magnetic fields (imaginary part). Applying the divergence theorem to Equation 4.32, the point form of Poynting theorem is:

$$\nabla . S = -\frac{1}{2}\omega\varepsilon_0\varepsilon_r^{"}E.E^* + i\omega\left(\frac{\mu_0}{2}H.H^* + \frac{\varepsilon_0\varepsilon_r^{'}}{2}E.E^*\right) \qquad (4.33)$$

Hence, the power dissipated per unit volume can be written as

$$P^M(r) = -\operatorname{Re}(\nabla . S) = \frac{1}{2}\omega\varepsilon_0\varepsilon_r^{"}|E|^2 \qquad (4.34)$$

As can be seen, the radiative microwave power dissipated per volume is directly proportional to the square of the electric field intensity's norm. In Chapter 5, this concept is used to develop an approximate formula to predict microwave power dissipation in concrete.

4.10 Lambert's Law

For an accurate description of heating with microwaves, Maxwell's equations which govern the propagation of electromagnetic radiation in a dielectric medium must be solved. However, owing to the complexity of Maxwell's equations, approximations are normally used to estimate microwave power dissipation in dielectric materials.

Lambert's law is the most common approximation used to estimate microwave power dissipation. This method considers an exponential decay of microwave energy absorption inside the dielectric material. The validity of Lambert's law to estimate the microwave energy distribution in a few materials has been investigated in available literature. Ayappa et al. (1991) compared numerical model predictions using Maxwell and Lambert's law to represent power dissipation in slabs. They obtained a critical thickness above which the use of Lambert's approximation is valid and showed that the two formulations predict identical power profiles for slabs at least 2.7 times thicker than the penetration depth. The original form of the Lambert's law may be written as:

$$I(x) = I_0 e^{-2\beta x} \qquad (4.35)$$

Where, $I(x)$ is the transmitted power flux into the medium, and I_0 the incident power of microwave. Equation 4.35 may be used to predict the change in the microwave energy with distance x from the microwave exposed surface of concrete. Hence, the microwave energy dissipated at a specific point inside the concrete specimen may be estimated by differentiating $I(x)$ with respect to x which results in:

$$PL(x) = -\frac{\partial I(x)}{\partial x} = 2\beta I_0 e^{-2\beta x} \qquad (4.36)$$

Lambert's law, when applicable, is easy to use and heating patterns can be analyzed with considerable ease. However, it must be noted that Lambert's law is restricted to semi-infinite samples and its use requires an estimate of the transmitted power density (Stuchly S. S. et al., 1972). Although, Lambert's law is valid for samples thick enough to be treated as infinitely thick, it is a poor approximation when applied in many practical situations. In applications where the object's dimensions are typically in the order of the wavelength of the radiation, the power distribution is very different from those predicted by Lambert's law. In such problems, usually, standing waves in the sample give rise to local hot spots where the power achieves a local maxima. Also corners and edges are known to focus radiation. Moreover, in a composite medium, the amount of radiation transmitted from one material to another depends on the dielectric properties of various components present in the medium. However, since Lambert's law ignores the wave characteristics of the radiation, heating patterns related to these effects cannot be accounted for.

In Chapter 5, a modified Lambert's law approximation will be used in the modeling of microwave heating of concrete slabs of a thickness of 200 mm. In Chapter 6, in order to verify the accuracy of the Lambert's law approximations, the results obtained using Lambert's law will be compared with the solutions obtained from Maxwell's equations.

4.11 Plane Wave Assumption

Since the plane wave assumption has been extensively used to simplify modeling of the concrete-microwave interaction in many previous studies, to be reviewed in next few chapters, its fundamental concepts are briefly explained in this section.

Plane wave is the simplest way in which electromagnetic waves can propagate. It consists of a vertically polarized sinusoidaly varying electric field E together with a horizontally polarized sinusoidaly varying magnetic field H, in phase with the electric field. Both components E and H lie in one plane while the direction of propagation of the field is at right angles to the plane. By definition the plane is infinite, requiring a generator of infinite power. In practice, only an approximation to a plane wave is possible.

Basically, the plane wave assumption is logical when the microwave source is far from the load and thus, it cannot be an accurate assumption in applications involving near field microwave heating such as that in the microwave heating of concrete or RCA. In practice, waveguides are used for transmission from generator to the load and the actual fields are more complicated than that of a plane wave.

In a plane wave, the electric and magnetic fields lie in a plane of constant intensity, with the intensity varying only in the direction of propagation. The electric field distribution for this case is obtained by solving:

$$\frac{d^2 E_z}{dz^2} + k^2 E_z = 0 \qquad (4.37)$$

Where k is the propagation constant of the medium.
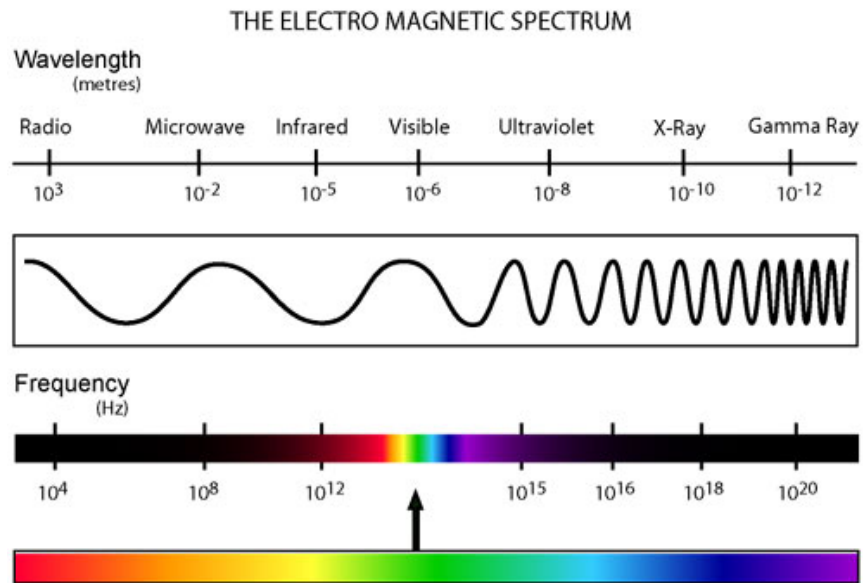
Figure 4.1 Electromagnetic Spectrum
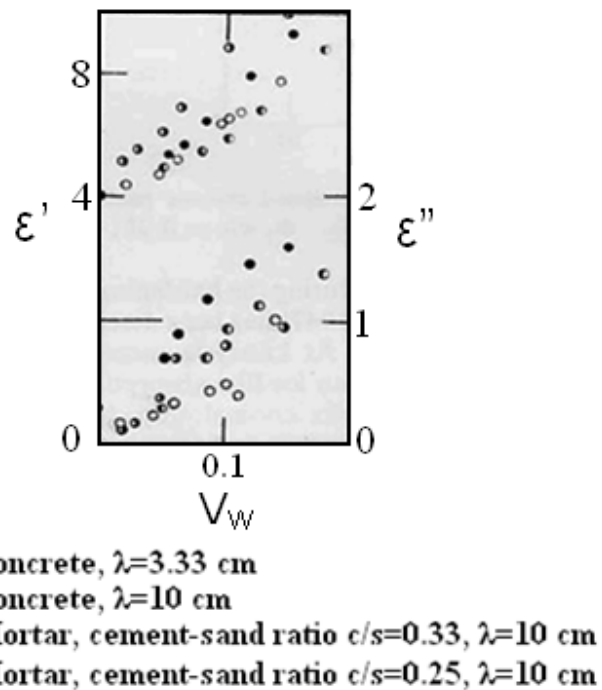
Figure 4.2 Concrete and Mortar Dielectric Constants (Hasted & Shah, 1964)
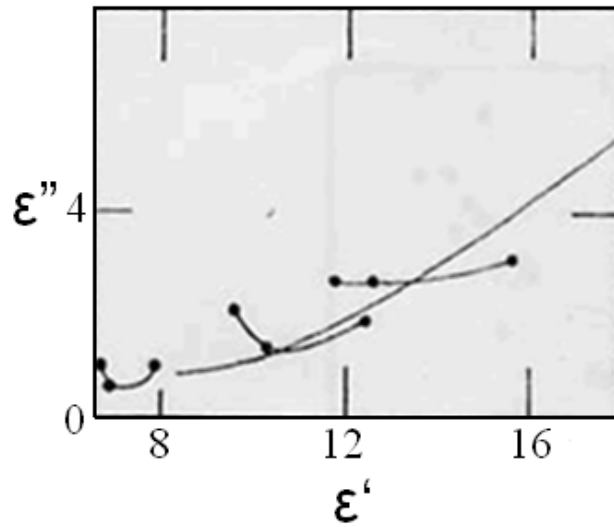
Figure 4.3 Cole-Cole diagram for w/c=0.28 hardened cement paste at Vw (volume of water)= 0.25,0.2,0.1. Full lines have been drawn arbitrarily through the closed circles, which represent, from right to left, the data at λ=10, 3.33 and 1.25 cm (Hasted & Shah, 1964).
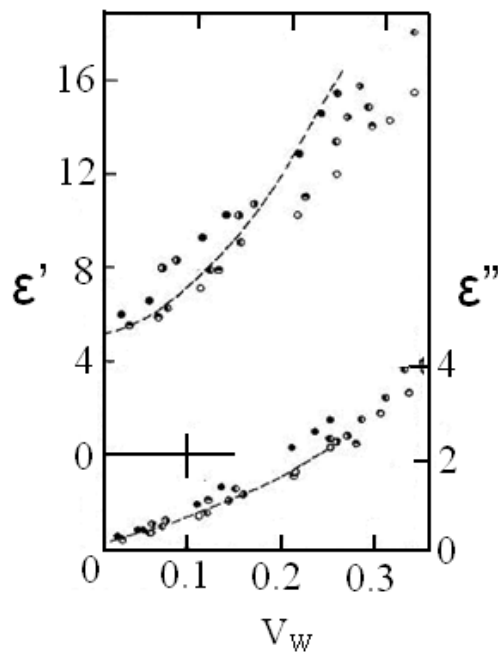
Figure 4.4 ε' and ε" (Vw) for hardened cement paste specimens at λ=10 cm (Hasted & Shah, 1964).
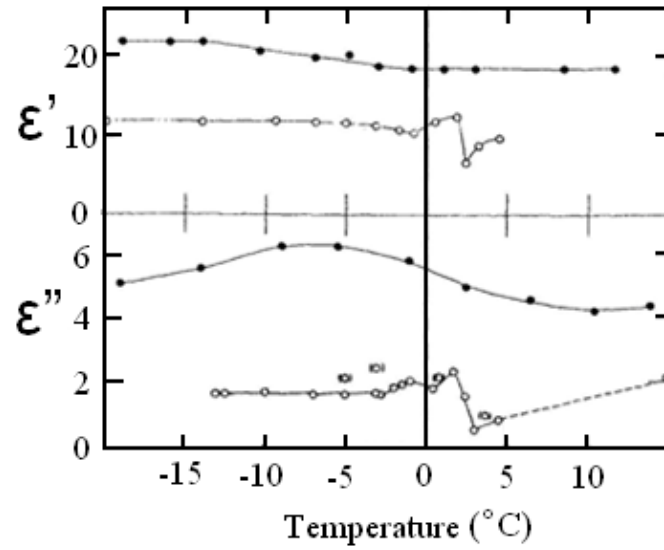
Figure 4.5 Typical ε'(T) and ε"(T) for water loaded hardened cement paste (closed circles) and brick (open circles). Circles in parentheses are considered non-typical (Hasted and Shah, 1964).
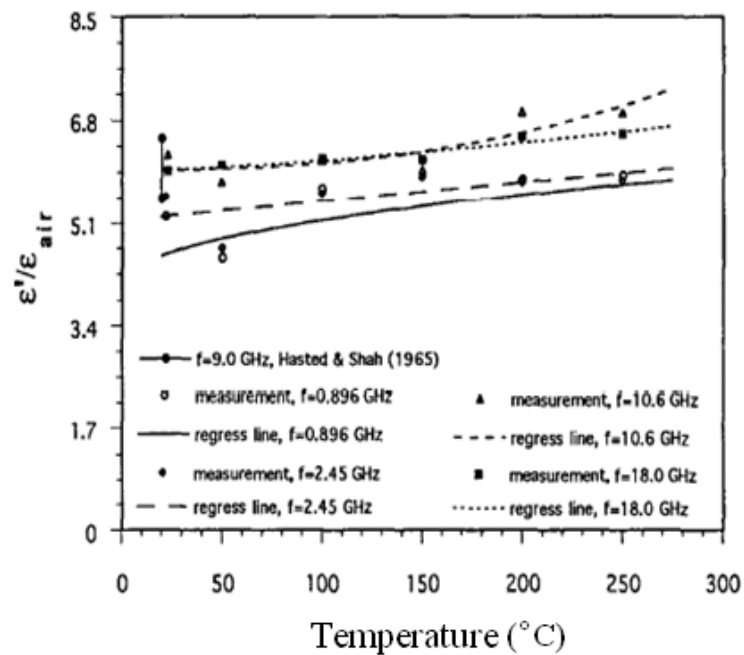
Figure 4.6 Variation of concrete's dielectric constant with temperature (Li et al, 1993).
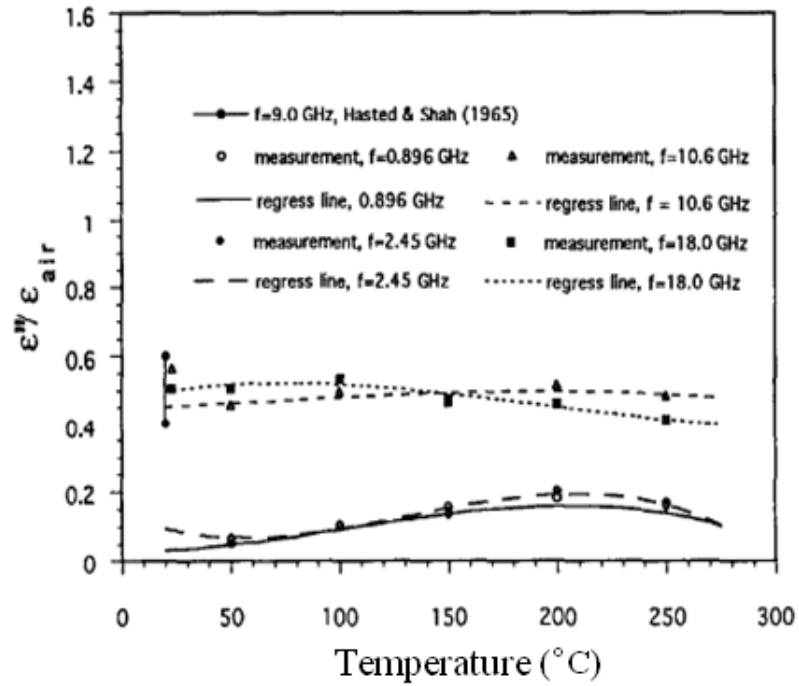
Figure 4.7 Variation of concrete's Loss Factor with temperature (Li et al, 1993)
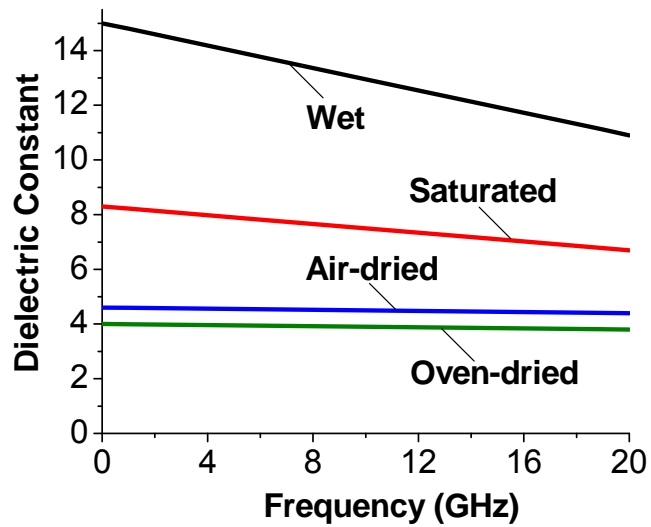
Figure 4.8 Dielectric constant of concrete at microwave frequency range, as reported by H.C. Rhim et al. (1998)
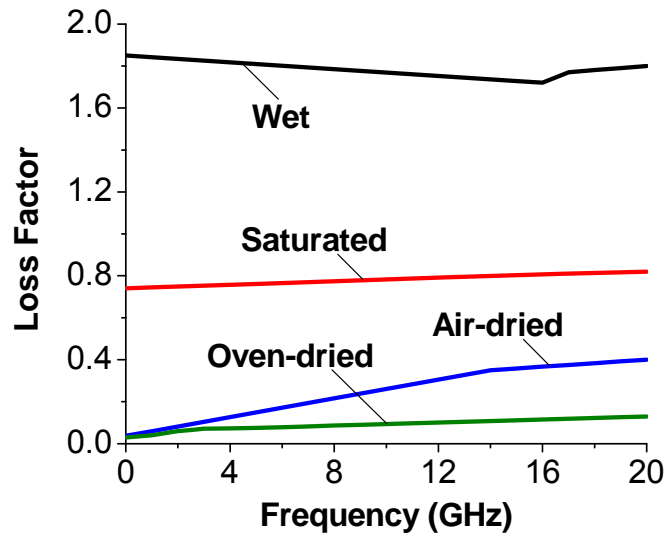
Figure 4.9 Loss factor of concrete at microwave frequency range, as reported by H.C. Rhim et al. (1998)
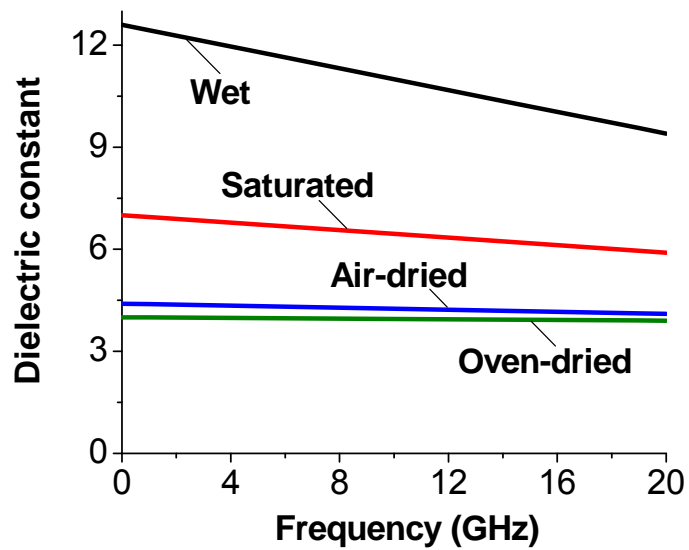
Figure 4.10 Dielectric constant of mortar at microwave range, as reported by H.C. Rhim et al. (1998)
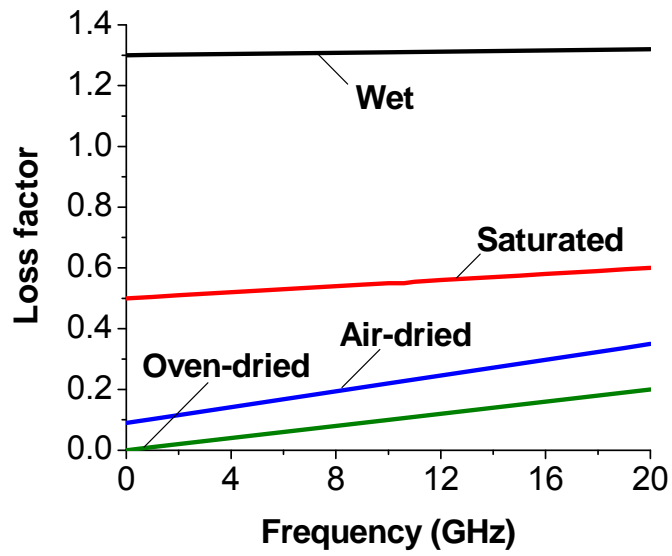
Figure 4.11 Loss factor of mortar at microwave range, as reported by H.C. Rhim et al. (1998)
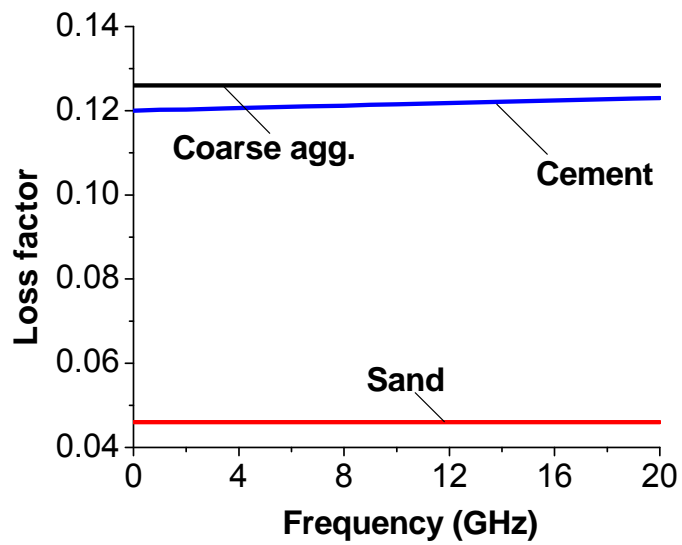
Figure 4.12 Loss factor of coarse aggregate, sand and cement at microwave frequency range, as reported by H.C. Rhim et al. (1998)
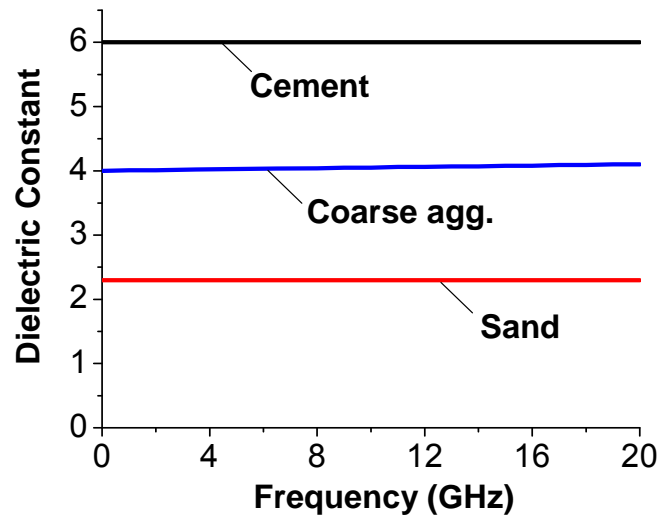
Figure 4.13 Dielectric constant of coarse aggregate, sand and cement at microwave frequency range, as reported by H.C. Rhim et al. (1998)
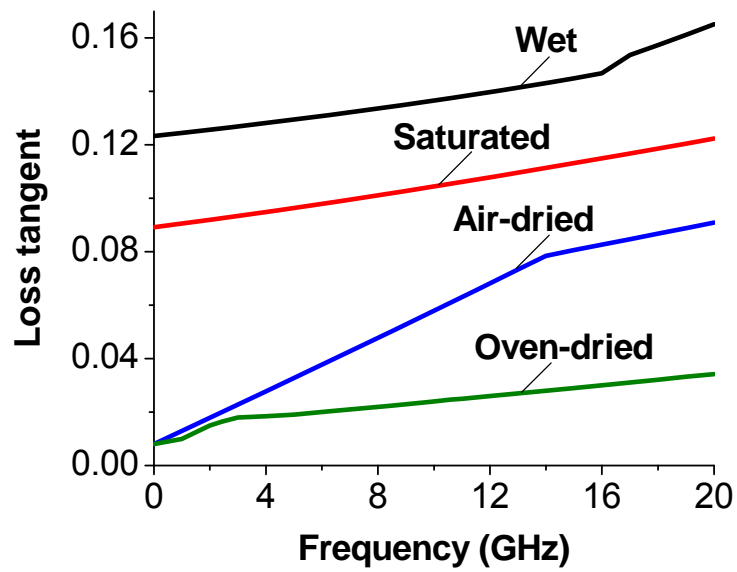
Figure 4.14 Loss tangent of concrete calculated using Equation 4.4
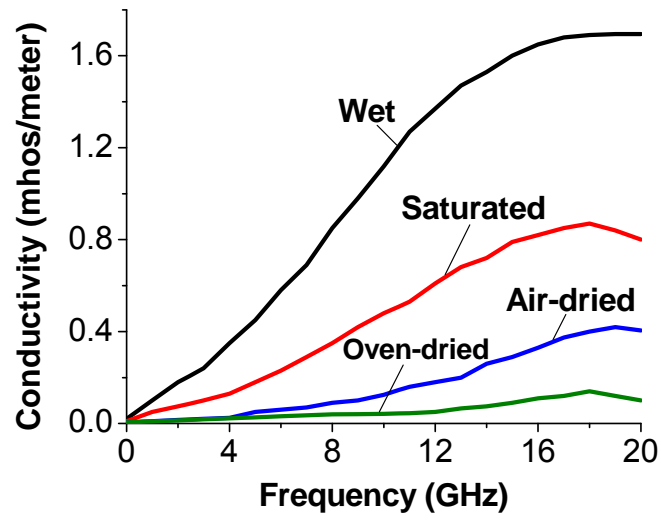
Figure 4.15 Conductivity of concrete calculated using Equation 4.5
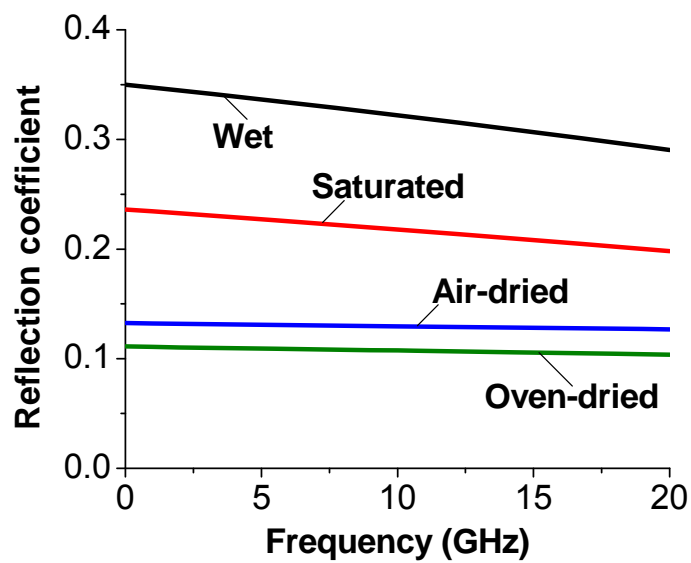
Figure 4.16 Reflection coefficient of concrete calculated using Equation 4.6.
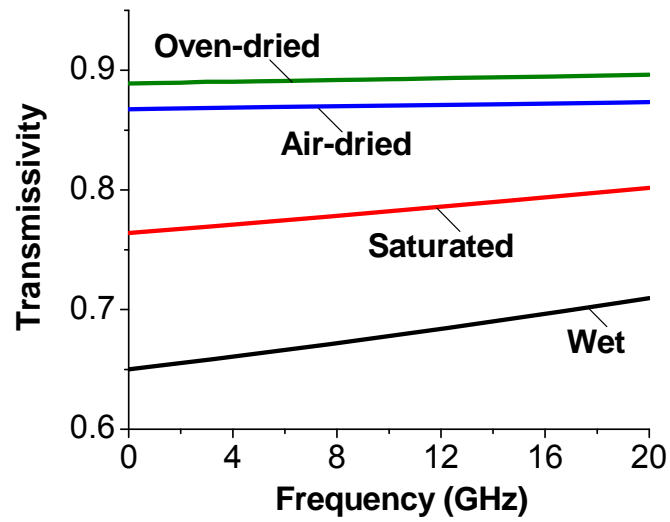
Figure 4.17 Transmissivity of concrete calculated using Equation 4.7.
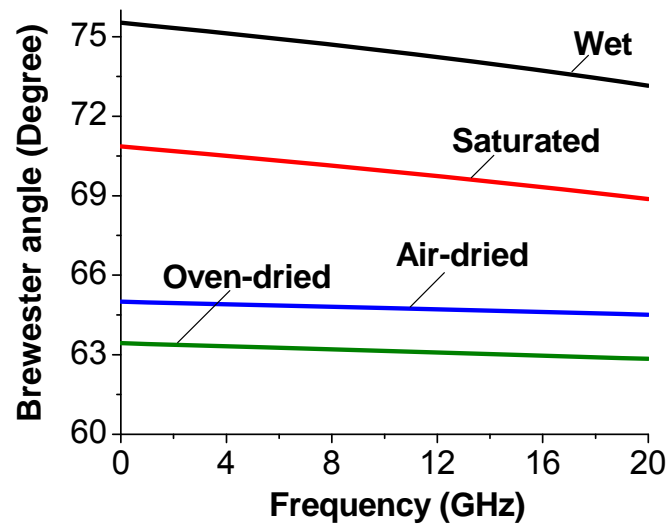
Figure 4.18 Brewester angle of concrete calculated using Equation 4.8
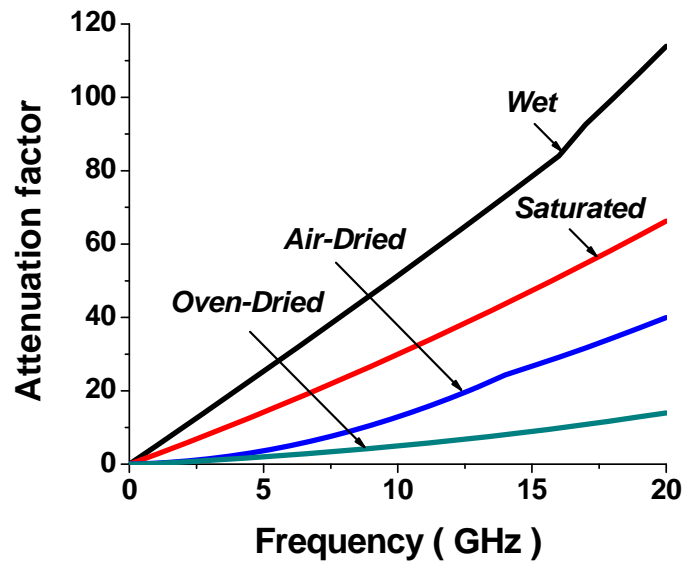
Figure 4.19 Attenuation factor of concrete calculated using Equation 4.10.
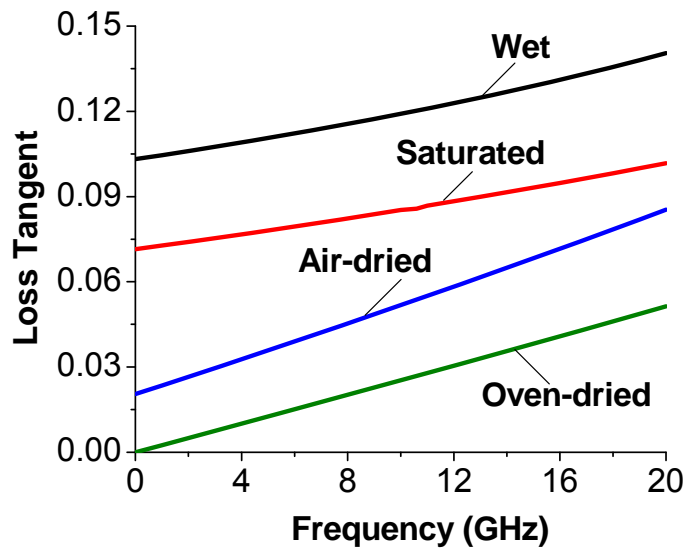
Figure 4.20 Loss tangent of mortar calculated using Equation 4.4.
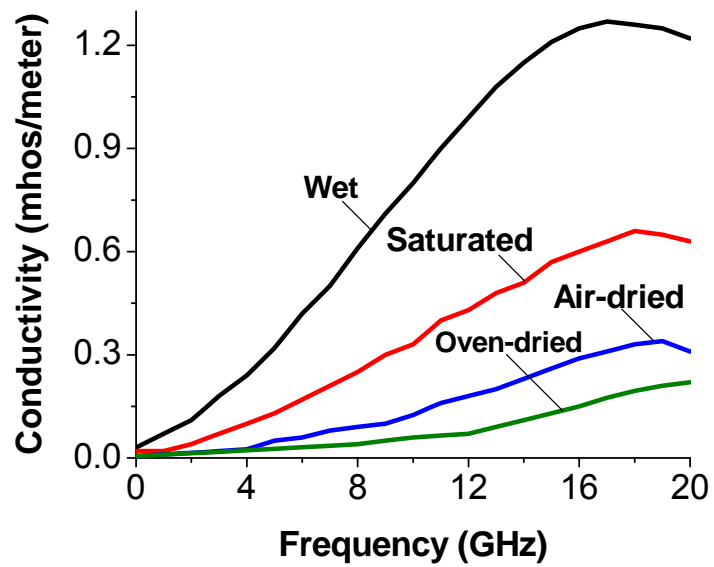
Figure 4.21 Conductivity of mortar calculated using Equation 4.5
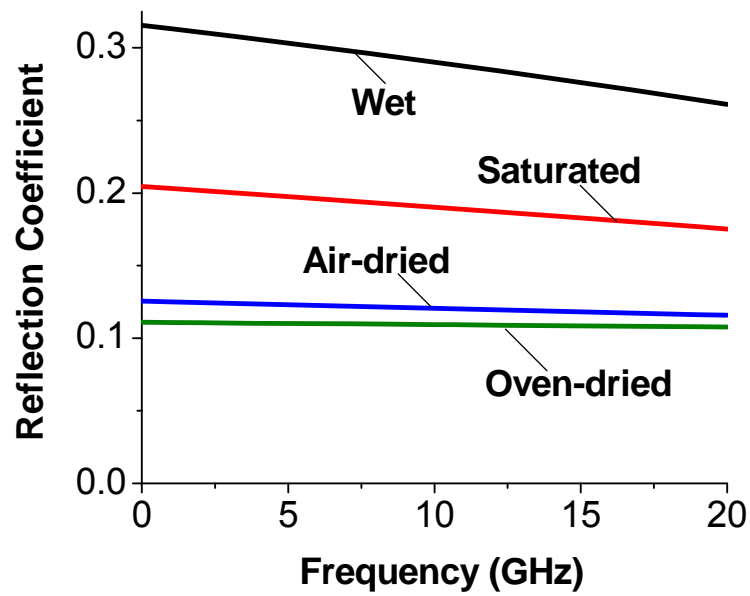
Figure 4.22 Reflection coefficient of mortar calculated using Equation 4.6
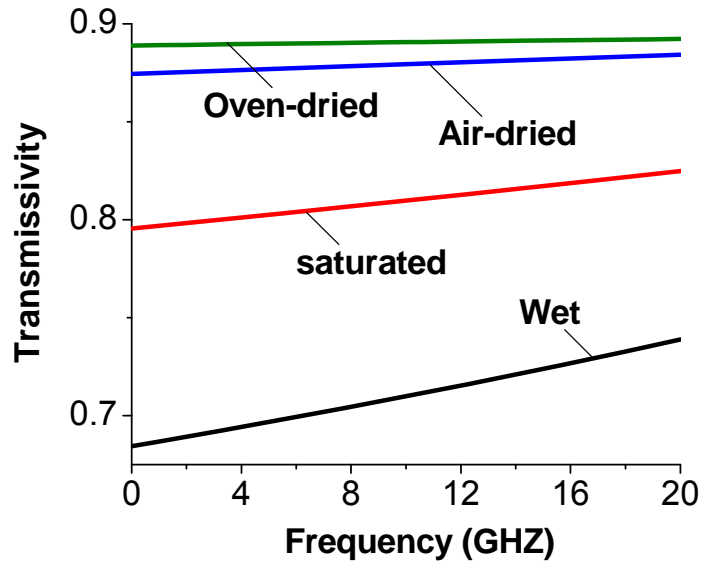
Figure 4.23 Transmissivity of mortar calculated using Equation 4.7
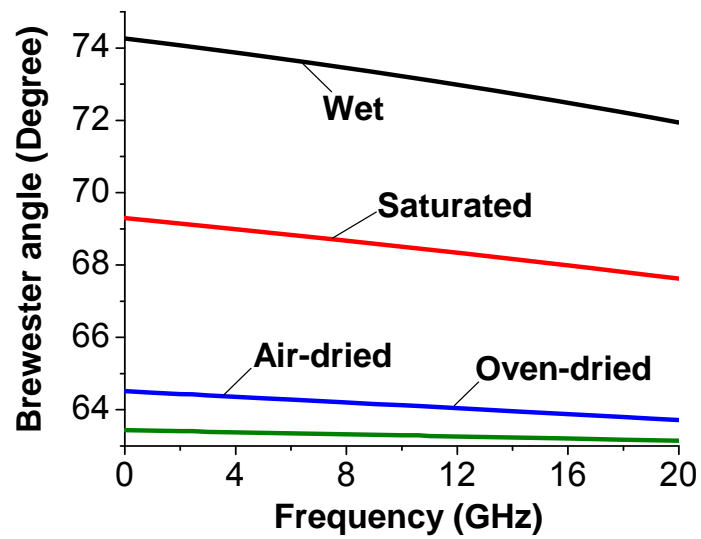
Figure 4.24 Brewester angle of mortar calculated using Equation 4.8.
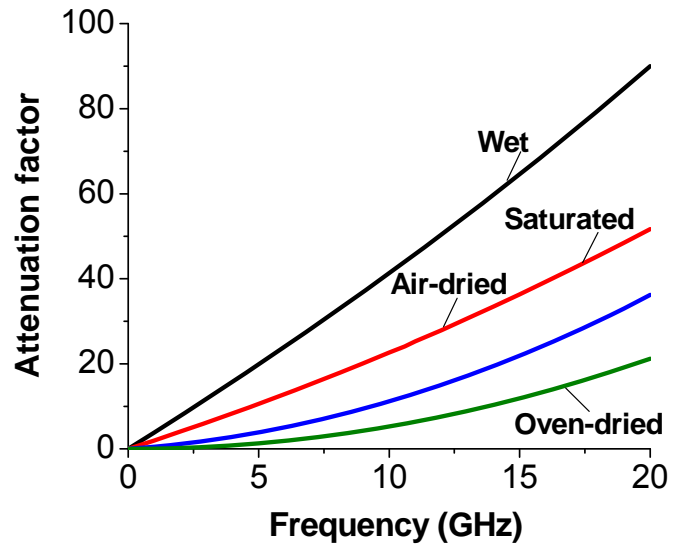
Figure 4.25 Attenuation factor of mortar calculated using Equation 4.10.
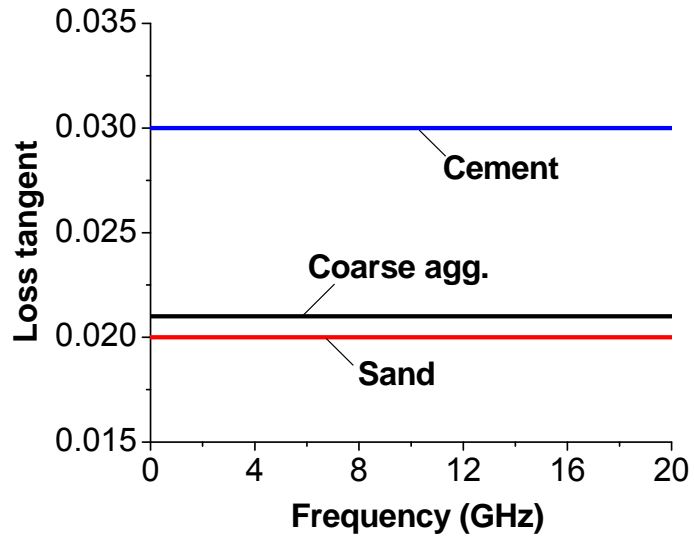
Figure 4.26 Loss tangent of coarse aggregate, sand and cement calculated using Equation 4.4.
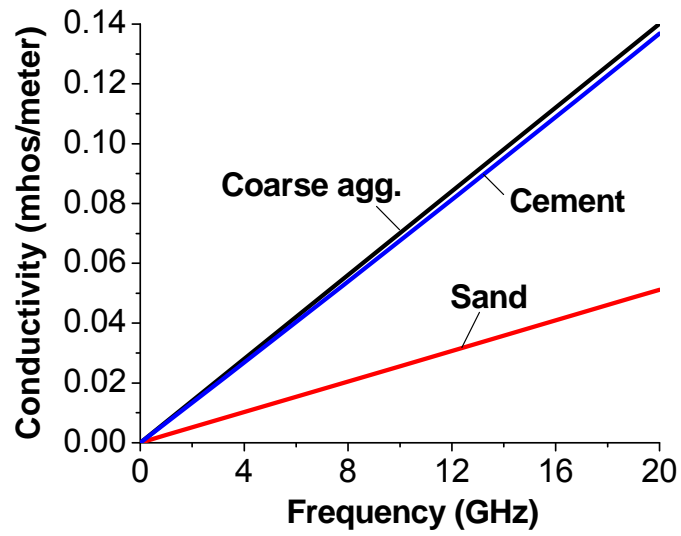
Figure 4.27 Conductivity of coarse aggregate, sand and cement calculated using Equation 4.5.
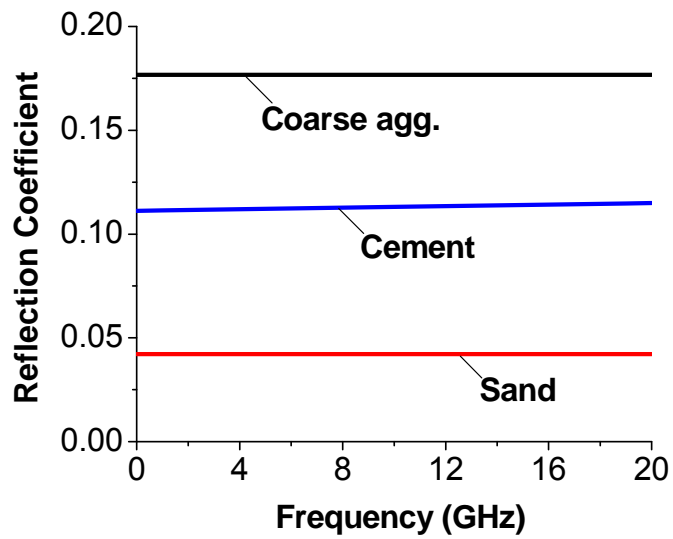
Figure 4.28 Reflection coefficient of coarse aggregate, sand and cement calculated using Equation 4.6.
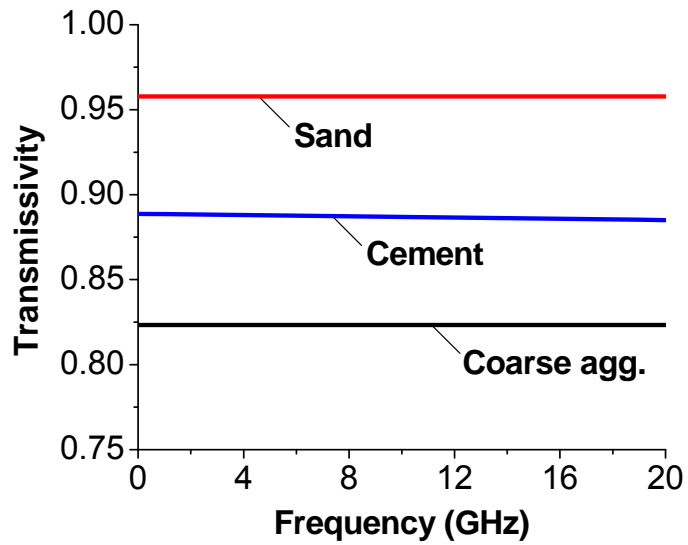
Figure 4.29 Transmissivity of coarse aggregate, sand and cement calculated using Equation 4.7.
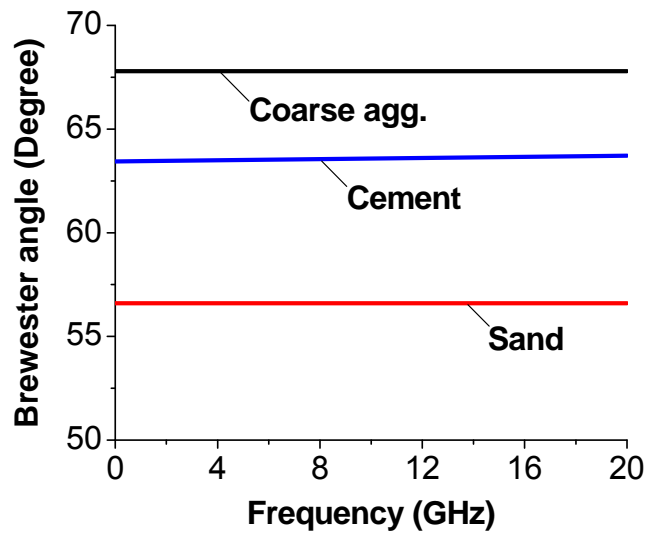
Figure 4.30 Brewester angle of coarse aggregate, sand and cement calculated using Equation 4.8.
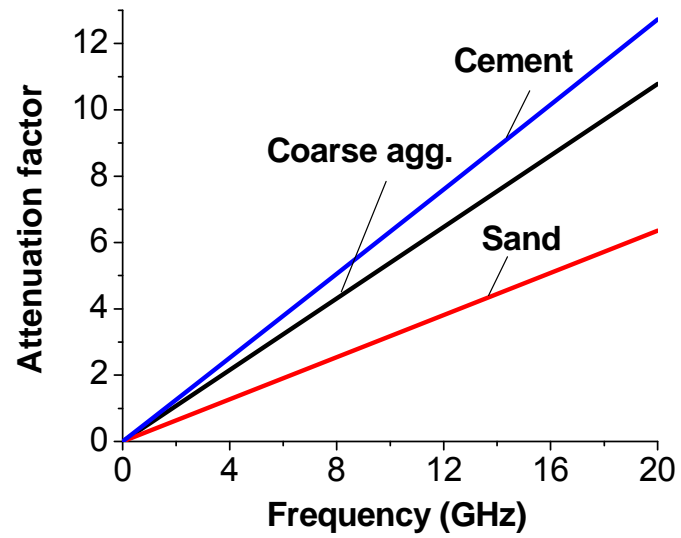
Figure 4.31 Attenuation factor of coarse aggregate, sand and cement calculated using Equation 4.10.

Chapter 5 : Microwave Decontamination of Concrete- Approximate Numerical Simulation

5.1 Background

In this chapter the possibility of using microwave heating to remove the contaminated surface of concrete is numerically investigated. Previous experimental studies on using this technique were reviewed in Chapter 3. As discussed earlier, thermal stresses and pore pressure are assumed to be the main factors leading to the concrete surface spalling when exposed to high power microwave heating. Modeling of microwave heating coupled with the heat and mass transfer in concrete can be used to investigate the development of these stresses and assess their relative contributions to the spalling of the concrete surface.

There have been a few analytical efforts to model the microwave heating phenomenon to correlate with experimental observations (Lagos et al., 1995). In general, the previous studies suggest two hypotheses dealing with the delamination phenomenon. The first adheres closely to studies on the effects of fire on the pore water pressure generated within the concrete mass. Li et al. (1993) examined the pore pressure and temperature distribution within a concrete sample with variable dielectric properties when

exposed to microwaves of frequencies, 0.896, 2.45, 10.6 and 18 GHz. Modeling of heat and mass transfer seemed to suggest generation of the pore water pressure within the concrete in excess of the concrete tensile strength (Li. et al., 1993; Lagos et al., 1995). This hypothesis overlooks the contribution of the thermal stresses generated in the concrete surface delamination.

The other hypothesis initiated by Bazant et al. (2003), postulates that the effects of the stresses caused by the differential thermal gradient generated play a more significant role in the decontamination process. Bazant et al. (2003) used the finite volume method to determine temperature and pore pressure development as well as thermal stresses that lead to spalling of the concrete surface when concrete is heated by microwaves. Their results showed that the thermal expansion of the saturated heated zone restrained by the colder surrounding concrete mass leads to very high compressive stresses parallel to the surface which either crush the concrete, or cause the surface layer to buckle or both (Zi. and Bažant, 2003; Bažant and Zi, 2003). Moreover, Bazant et al. asserted that since the porosity of a typical concrete is around 0.1, the actual pore pressures generated are only about a tenth of those predicted by the other researchers and does not seem sufficient to cause spalling (Bažant and Zi, 2003). Bazant et al. also claimed that the effect of pore pressure would in fact be even weaker because of the additional pore space created by the formation of microcracks.

Besides the current ambiguity relating to the relative contribution of thermal stresses vs. pore pressure to concrete surface spalling, there are a number of major drawbacks in the modeling procedure used in the previous studies. In general, the microwave decontamination problem involves solving the Maxwell's equations which govern the

propagation of microwave radiation through the material and microwave waveguide or cavity, the heat transfer equation which governs the heat absorption and the resulting temperature rise in the concrete block, and the mass transfer equation which governs the pore pressure development in the concrete block. However, due to the complexities of Maxwell's equations, previous studies have used approximate methods and made a number of simplifying assumptions to estimate the microwave power dissipation in concrete. Some of the drawbacks associated with the electromagnetic modeling of the microwave heating in a number of previous studies are reviewed, as follows:

1) As shown in Chapter 4, the electromagnetic (EM) properties of concrete vary significantly with its water content, the microwave frequency and temperature. However, despite its importance, the variation of concrete EM properties with water content does not seem to have been considered in the simulation of microwave heating of concrete. Li et al. (1994) considered microwave frequency and temperature dependence of the dielectric properties of concrete without reporting on the effects of water content of the concrete. Bazant et al. (2003) assumed that the volume fraction of water of the concrete in nuclear facilities is about 7% and seemed to have ignored the dependence of the electromagnetic properties of concrete on the incident microwave frequency.

2) The methods previously used to model microwave power dissipation in concrete are not easy to use and include many mathematical complexities.

3) The modeling procedures used in previous studies did not take into account reflections at the concrete surface and distribution of the incident microwave power. The distribution of the incident microwave power depends on the microwave mode

exited by the waveguides. The most popular mode used in microwave heating systems is TE_{10} which has a sinusoidal shape. However, all the previous studies assumed a uniform microwave power distribution at the concrete surface.

In this chapter, a finite element model is used to numerically study the relative contribution of thermal stresses vs. pore-pressure in surface delamination when concrete is subjected to microwaves of various frequencies. A simple microwave power dissipation estimate based on a modified Lambert's law formulation is used. The approximate method proposed in this study, can be easily used to estimate the microwave power dissipation in concrete without dealing with the mathematical complexities associated with more accurate electromagnetic analysis. Moreover, this study is aimed at illustrating the significant effect of the water content of concrete on the magnitude and pattern of the stresses developed. Furthermore, the variation of concrete EM properties with microwave frequency and its effect on stresses developed are examined.

5.2 Microwave Power Formulation: Modified Lambert's Law

As stated in Chapter 4, Maxwell's equations can be used to describe any microwave problem. However, owing to their complex formulation, approximations are usually used to predict the behavior of electromagnetic waves in materials. The most common approximation is Lambert's Law which considers an exponential decay of microwave energy absorption inside the medium. Ayappa et al. (1991) compared numerical model predictions using Maxwell and Lambert's law to represent power dissipation in slabs. They obtained a critical thickness above which the use of the Lambert's approximation is valid and showed that the two formulations predict identical power profiles for slabs at least 2.7 times thicker than the penetration depth. Similar results were reported by

Barringer et al. (1995), comparing predictions by the individual and combined models during heating of gel samples.

When applicable, Lambert's law can significantly simplify microwave heating modeling. However, there are two problems in using the Lambert's law when modeling a microwave heating system used in practice. Firstly, the original form of Lambert's law does not account for the reflections at the concrete-air interface and thus an estimate of transmitted power into the concrete is needed. Secondly, Lambert's law assumes a plane wave having a uniform power distribution at the incident surface of concrete which is not the case in practice. In practice, the microwave power distribution at the incident surface follows the shape of the excited mode delivered by the waveguides. In this chapter, the original form of Lambert's law, as explained in Chapter 4, is modified, taking into account the reflection at the concrete-air interface and the shape of the incident microwave power distribution.

5.2.1 Modifications for the Reflected Power

As explained in Chapter 4, If $I(x)$ is the variation of the transmitted power flux with distance x from the sample surface, then according to Lambert's law the microwave power dissipated at distance x from the concrete surface can be obtained from:

$$PL(x) = -\frac{\partial I(x)}{\partial x} = 2\beta I_0 e^{-2\beta x} \quad (4.36)$$

Where, I_0 is the incident power and β is the attenuation factor for a given material and frequency. As can be seen, the use of Lambert's law requires an estimate of the transmitted power intensity (I_0) which can be obtained from calorimetric measurements (Ohlsson and Bengtsson, 1971; Taoukis, Davis et al., 1987) or used as an adjustable

parameter to match model predictions to experimental temperature profiles (Nykvist and Decareau, 1976). Alternatively, as adopted in this study, if I_0 is the incident power flux, then Lambert's law should be modified to account for the decrease in power due to reflection at the surface of the concrete sample. In this study, in order to account for the reflection at the concrete-air interface, the transmissivity coefficient (c) is applied; hence, Lambert's law is modified to:

$$PL(x) = -\frac{\partial I(x)}{\partial x} \times c = 2\beta I_0 e^{-2\beta x} \times c \qquad (5.1)$$

The transmissivity coefficient can be calculated using Equation 4.7:

$$c = 1 - r = 1 - |R|^2 = 1 - \left| \frac{\sqrt{\varepsilon_{r2}} \cos\theta_i - \sqrt{\varepsilon_{r1}} \cos\theta_t}{\sqrt{\varepsilon_{r2}} \cos\theta_i + \sqrt{\varepsilon_{r1}} \cos\theta_t} \right|^2 \qquad (4.7)$$

Where, r is the reflection coefficient. The transmissivity coefficients and attenuation factors for concrete specimens with different moisture contents and subject to microwaves of different frequencies were calculated using the data reported by Rhim et al. (1998) and are illustrated in Figures 4.17 and 4.19, respectively. It is noteworthy that the dielectric constants and loss factors reported by Rhim et al. (1998) are considerably higher than similar values assumed by Bazant et al. (2003) and Li et al. (1994).

5.2.2 Modification for Microwave Modes

In practice, a hollow metallic tube either of rectangular or circular cross section, made of aluminum, copper, or brass of various sizes is usually used to transmit the generated microwave. Such a structure is commonly known as a waveguide.

In previous studies, the incident power has been postulated to be uniformly distributed in the transverse plane. However, this is not the case in practice. The

fundamental transverse electric and transverse magnetic modes, TE_{10} and TM_{11}, are usually excited in the waveguides. The transverse electric mode TE_{10} is the usual choice for the single-mode commercial waveguides. It does not vary in one of the transverse directions while having a sinusoidal distribution in the other. Hence, it represents a similar heating problem to that of heating a two dimensional slab. In this study, Equation 5.1 is modified to account for the sinusoidal shape of the TE_{10} mode.

The incident TE_{10} mode has the form of $E = (0,0,E_z) = \{0,0,\sin[\pi(a-y)/2a]\}$; where, $2a$ is the width of the waveguide. However, as can be seen in Equation 4.34, the dissipated energy is proportional to the square of the electric field's norm.

$$P^M(r) = -\text{Re}(\nabla S) = \frac{1}{2}\omega\varepsilon_0\varepsilon_r^{''}|E|^2 \qquad (4.34)$$

Therefore, it seems quite reasonable to consider a sine^2 shape to simulate the sinusoidal shape of the TE_{10} mode with the approximate Lambert's Law.

$$I(x) = P\sin^2\left(\pi\frac{a-y}{2a}\right)\times e^{-2\beta x} \qquad (5.2)$$

The sine^2-shape incident power equivalent to uniform power I_0 in Equation 5.1 may be computed as:

$$2aI_0 = 2\times\int_0^a P\sin^2\left(\pi\frac{a-y}{2a}\right) \Rightarrow P = 2I_0 \qquad (5.3)$$

Hence, the final power dissipation function may be written as:

$$PL(x) = -\frac{\partial I(x)}{\partial x}\times c = 2\beta\times(2I_0)\times e^{-2\beta x}\times c\times Sin^2\left(\pi\frac{a-y}{2a}\right) \qquad (5.4)$$

Comparing Equation 5.4 with Equation 5.1 illustrates that the incident microwave power delivered through a TE_{10} mode waveguide has a peak incident power that is twice

102

the equivalent uniform incident power adopted by most previous studies (Li et al., 1993; Li and Ebadian, 1994; Lagos et al., 1995; Zi. and Bažant, 2003; Bažant and Zi, 2003). Thus the maximum peak temperature expected locally as a result of heating the concrete with a TE_{10} microwave mode is expected to be twice the peak temperature reached when uniform microwave heating is assumed.

5.3 Problem Description

In this study, pore pressure and thermal stresses developed in the heated zone of a large concrete block subjected to microwave radiation through a waveguide applicator are numerically computed. A possible sketch of a typical microwave decontamination system is shown in Figure 5.1. To guarantee the accuracy of Lambert's Law, the concrete block is assumed to be thick enough to be treated as infinitely thick to microwave radiation. According to Ayappa et al. (1991), this is the case when the sample is at least than 2.7 times thicker than the penetration depth of microwave power. The power penetration depth d_p may be calculated using Equation 4.9:

$$d_p = \frac{1}{2\beta} = \frac{c}{2\sqrt{2}\pi f \sqrt{\varepsilon'} \left[\sqrt{1 + \tan^2 \delta} - 1 \right]^{1/2}} \qquad (4.9)$$

Here, β is the attenuation factor of concrete. Table 5.1 lists the abovementioned minimum thickness for the various concrete blocks considered in this study. These values were calculated using the electromagnetic properties presented in Chapter 4. The thicknesses of the concrete blocks assumed in this study are equal to the minimum values given in Table 5.1 at each frequency.

The area of the heated zone depends on the waveguide dimensions which vary with frequency as shown in Table 5.2. Dimensions of the concrete block are assumed to be

large enough in comparison with the size of the heated zone to ignore electromagnetic scattering and to provide structural restraint around the heated zone.

To study the significance of water content, four different types of concrete specimens are considered: 1) wet specimen, standing water on its surface 2) saturated, surface dry concrete 3) air-dried concrete, exposed to ambient room temperature and humidity 4) oven-dried concrete with zero moisture content by weight. In addition, the variation in dielectric properties with microwave frequency is taken into account in estimating the power dissipation.

5.4 Formulation

In this chapter, the modified Lambert's Law (Equation 5.4) is used to estimate the microwave power dissipation in concrete. Using Lambert's law can significantly eliminate the difficulties in solving the Maxwell's equations. In Chapter 6, the exact solution of Maxwell's equations will be used to verify the accuracy of the Lambert's law used.

In following, the general heat and mass transfer equations are simplified to model the heat and mass transfer equations in a concrete block when heated with microwaves. The coupled heat transfer, mass transfer, and structural analysis will be solved to obtain the temperature distribution, thermal stresses, and the pore pressure developed in concrete as a result of microwave heating

5.4.1 Heat Transfer and Thermal Stress Analysis

The basic heat transfer equation may be written as

$$\frac{\partial}{\partial t}(\rho C)T + \nabla \bullet q = PL(x) \qquad (5.5)$$

Where T= temperature, ρ= mass density of concrete, C= specific heat of concrete, ∇ = gradient operator, q= total heat flux vector including the conductive heat flux (q_{cd}) and the convective heat flux (q_{cv}), and PL(x) = distributed source of heat. The conductive heat flux q_{cd} may be expressed as linear combinations of the gradient of temperature T:

$$q_{cd} = -k\,\nabla T \qquad (5.6)$$

Where, K= heat conductivity. Moreover, heat may also be transferred through the movement of water in the concrete:

$$q_{cv} = C_w TJ \qquad (5.7)$$

Where, C_w is the specific heat of water and J is the water flux. The water flux (J) can be expressed in terms of the gradient of pore pressure:

$$J = -\frac{a}{g}\nabla P \qquad (5.8)$$

Where, a is the water permeability of concrete and g is the earth gravity. Hence:

$$q_{cv} = C_w TJ = -a\left(\frac{C_w}{g}T\,\nabla P\right) \qquad (5.9)$$

However, since the water permeability of concrete is about three orders of magnitude smaller than heat conductivity, this term can be neglected and thus Equation 5.5 may be simplified as:

$$\rho c\,\frac{\partial T}{\partial t} = -\nabla.\left(-K\,\nabla T\right) + PL(x) \qquad (5.10)$$

It is noteworthy that Equation 5.8 is the classical Darcy's law and hence its validity is known to be limited to saturated porous materials. However, Bazant and Najir (1972) showed that Darcy's law is applicable to a heated unsaturated material provided that P is

interpreted as the pressure of water vapor in the pores rather than the pressure of liquid capillary water.

Once the heat source (PL(x)) is known through Lambert's law, Equation 5.10 may be used to calculate the temperature distribution inside the microwave heated concrete. As the next step, the temperature distribution obtained is used as the input data for the thermal stress analysis.

5.4.2 Mass Transfer

The mass conservation equation for microwave heating of concrete can be formulated as:

$$\frac{\partial w}{\partial t} + \nabla \bullet J = HD(w) \qquad (5.11)$$

Here, $w = $ specific water content, $t = $ time, $\nabla = $ gradient operator, $J = $ water flux vector, and $HD(w) = $ change in free water content because of hydration and dehydration. The free water content in the liquid phase within the concrete can be determined by means of the so-called 'Equation of state of pore pressure' (Bazant and Kaplan, 1996). For temperatures above the critical point of water (374.15 °C), all free water is assumed to have been vaporized and thus there is no liquid phase. For temperatures below the critical point of water, the free water content was found to depend on temperature and the ratio of water vapor pressure to saturation vapor pressure. In this study, the semi-empirical expressions from Ref. (Bazant and Kaplan, 1996) are used. For non-saturated concrete, the following formula has been proposed:

$$\frac{w}{C} = \left(\frac{W_{s1}}{C} \times h \right)^{\frac{1}{m(T)}} \qquad h \le 0.96 \qquad (5.12)$$

Here, w is the water content of concrete, w_{s1} is the saturation water content at 25 °C, C is

the mass of (anhydrous) cement per m³ of concrete, $h = \dfrac{P}{P_s(T)}$ where $P_s(T) = $ saturation

pore pressure at temperature T, and $m(T)$ is an experimentally determined empirical

expression as follows (Ref.(Bazant and Kaplan, 1996)):

$$m(T) = 1.04 - \frac{(T+10)^2}{22.3(25+10)^2 + (T+10)^2} \qquad (5.13)$$

For saturated concrete, the free water-to-cement ratio is determined by: (Bazant and

Kaplan, 1996)

$$\frac{w}{C} = \frac{w_{s1}}{C}\left[1 + 0.12(h - 1.04)\right] \qquad h \geq 1.04 \qquad (5.14)$$

In this study, the transition between $h = 0.96$ and $h = 1.04$ is assumed to be a straight line

joining the value $w_{0.96}$ and $w_{1.04}$; Thus:

$$w = w_{h=0.96} + (h - 0.96) \times \frac{w_{h=1.04} - w_{h=0.96}}{1.04 - 0.96} \qquad 0.96 \leq h \leq 1.04 \qquad (5.15)$$

The saturation pore pressure at different temperatures can be calculated using the

following semi-empirical equation: (Rei R.C., Prauznitz J. M. et al., 1987)

$$Ln\left(\frac{P_s}{P_c}\right) = \frac{T_c}{T}\left[a(1-T_r) + b(1-T_r)^{1.5} + c(1-T_r)^3 + d(1-T_r)^6\right] \qquad (5.16)$$

Where, $T_r = T/T_c$, $T_c = 647.7K$, $P_c = 22.07MPa$, $a = -7.7645, b = 1.45938, c = -2.7758,$

and $d = -1.23303$. Substituting Equations 5.8, 5.12, 5.14, and 5.15 into Equation 5.11, we

obtain:

$$\frac{\partial}{\partial t}\left(C\left(\frac{W_{s1}}{C}\times\frac{P}{P_s(T)}\right)^{\frac{1}{m(T)}}\right)+\nabla\bullet\left(-\frac{a}{g}\nabla P\right)=HD(w)\,,\qquad\frac{P}{P_s(T)}\leq 0.96\qquad(5.17)$$

$$\frac{\partial}{\partial t}\left(w_{\frac{P}{P_s(T)}=0.96}+\left(\frac{P}{P_s(T)}-0.96\right)\times\frac{w_{\frac{P}{P_s(T)}=1.04}-w_{\frac{P}{P_s(T)}=0.96}}{1.04-0.96}\right)+\nabla\bullet\left(-\frac{a}{g}\nabla P\right)=HD(w)\,,\quad 0.96\leq\frac{P}{P_s(T)}\leq 1.04$$

(5.18)

$$\frac{\partial}{\partial t}\left(w_{s1}\left[1+0.12\left(\frac{P}{P_s(T)}-1.04\right)\right]\right)+\nabla\bullet\left(-\frac{a}{g}\nabla P\right)=HD(w)\ ,\qquad\frac{P}{P_s(T)}\geq 1.04\qquad(5.19)$$

Which can be solved for the pore pressure P. At ambient temperatures, the permeability of concrete is controlled by nanopores, which explains the extremely low permeability at these temperatures. But this is not the case at high temperatures. When the temperature is increased above 100 °C, the permeability increases sharply. This can be explained by heat-induced changes in the structure of small pores. The following expressions have been proposed by Bazant and Thonguthai (1978) to predict the variation of permeability with temperature:

$$a = a_0 f_1(h) f_2(T)\qquad\text{for } T \leq 100$$

and   (5.20)

$$a = a_0 f_2(100) f_3(T)\qquad\text{for } T\rangle 100$$

Where, $a_0 =$ Reference permeability at T=25 °C and, $f_1(h), f_2(T), f_3(T)$ are functions described by following expressions:

$$f_1(h)=\alpha+\frac{1-\alpha}{1+\left(\frac{1-h}{1+h_c}\right)^4}\qquad\text{for } h\leq 1;\text{ and } f_1(h)=1 \text{ for } h\geq 1\qquad(5.21)$$

108

Here, $\alpha = 1 / \left[1 + 0.253 \left(100 - \min \left(T, 100°C \right) \right) \right]$ and, $h_c = 0.75$

$$f_2(T) = \exp\left[\frac{Q}{R_g} \left(\frac{1}{\overline{T_0}} - \frac{1}{\overline{T}} \right) \right] \qquad\qquad (5.22)$$

$$f_3(T) = 5.5 \left\{ \frac{2}{a + \exp\left[-0.455(T - 100) \right]} - 1 \right\} + 1 \qquad\qquad (5.23)$$

Where, $\overline{T}$ = Absolute temperature, Q = activation energy for water migration, and R_g= gas constant. Having taken the above into consideration, the pore pressure and the moisture distribution in the concrete specimen can then be obtained by coupling Equations 5.10 and 5.11.

5.4.3 Heat and Mass Transfer Boundary Conditions

At the boundaries with ambient air and surrounding unheated concrete, both conductive and radiative heat losses occur. Hence, the heat transfer boundary condition may be written as:

$$\nabla T . n + B_i \left(T - T_a \right) + S \left(T^4 - T_a \right) = 0 \qquad (5.24)$$

Where, B_i is the Biot number, a measure of the relative effect of convective heat loss compared to thermal conduction, S_r is the radiation number, a measure of the relative effect of radiative heat loss compared to thermal conduction, n is the normal to the boundary and T_a is the ambient temperature. For a small heat-loss limit ($B_i, S_r \to 0$), a zero heat flux boundary condition results; while for the large heat-loss limit ($B_i, S_r \to \infty$), a fixed-temperature boundary condition is obtained. Similarly, for mass transfer the following boundary condition is imposed:

$$J.n + B_w \left(P_a - P \right) = 0 \qquad (5.25)$$

Where, P_a is the ambient pressure, P is the vapor pressure at the surface, and B_w is the moisture transfer coefficient which may vary from 0 for a sealed surface to ∞ for the case of free air convection near the concrete surface. In this study, a sealed concrete surface is considered.

5.4.4 Structural Boundary Conditions

As part of a large concrete block, the heated zone displacement is restrained by the unheated parts of the block and therefore, simply supported boundary condition may be considered:

$$U_x = U_y = U_z = 0 \qquad (5.26)$$

5.5 Results and Discussions

The commercially available COMSOL Multiphysics finite element software is used to solve the coupled mass transfer, heat transfer and structural problem explained. The equation-based modeling module of COMSOL Multiphysics can be used to solve the general form of differential equations and PDE's for the defined model. In this study, the general form equation module was used to perform the mass transfer analysis formulated. The effect of a number of different parameters such as variation of concrete porosity and saturation pore pressure with temperature were taken into account using the Matlab codes which can be simultaneously run through COMSOL Multiphysics' Matlab interface. Finally, structural and heat transfer modules were coupled with the general form equation module and solved simultaneously to account for the coupling effects in this multiphysics problem.

The mechanical and thermal properties of concrete used in this numerical study are summarized in Table 5.3. Moreover, the transmissivity and the attenuation factor of concrete as calculated in Chapter 4 (Figures 4.17 and 4.19) are used. Since the results for the full range of frequencies would be too numerous and to make it possible to compare the results obtained with the results reported in available literature, three frequencies of 2.45 GHz, 10.6 GHz and 18 GHz are considered. These three frequencies are representative of the characteristics of typical low, intermediate and high frequencies used in microwave heating. Moreover, a constant incident microwave power of 1.1 MW/m^2 is considered. To increase the legibility of figures, only the variation of results within the first 10 cm thick surface layer of the concrete blocks is illustrated.

5.5.1 Temperature Distribution

Temperature distribution in the microwave heated concrete and its variation with microwave frequency and the water content of the concrete are plotted in Figures 5.2 to 5.4. As expected, the temperature distribution patterns at different frequencies and different water contents of concrete resemble the approximate microwave power dissipation pattern (Equation 5.4), decaying exponentially.

As can be seen in Figures 5.2 to 5.4, for a microwave power of 1.1 MW/m^2, at higher frequencies and higher water contents, microwave penetration is reduced and more energy is dissipated near the concrete surface. This results in a higher temperature rise and temperature gradients within the thin surface layer of the concrete sample. Figure 5.5 shows the temperature distribution across the microwave incident surface of concrete. As can be seen, the sinusoidal shape of the TE_{10} mode results in a sine^2-shape temperature distribution across the microwave incident surface.

5.5.2 Thermal Stresses

Temperature gradient in the heated zone of concrete results in non-uniform expansion of this area and may lead to relatively high compressive stresses developing. The results of the thermal stress analysis for different microwave frequencies and the concrete's water contents are shown in Figures 5.6 to 5.8. Moreover, the stress developed across the microwave incident surface of concrete is plotted in Figure 5.9. Such plots may be of use when choosing the appropriate microwave specifications for a given nominal strength and depth of spalling. Similarly, for a specific incident microwave power, microwave frequency and concrete water content, the approximate spalling depth can be easily estimated. As can be seen, after just a few seconds of microwave heating, especially at high frequencies and water contents, considerably high compressive stresses may develop. The radial compressive stress developed may crush the concrete surface layer when it exceeds the concrete's compressive strength under the actual confined condition. Hence, the results confirm the capability of high frequency microwaves to remove the surface layer of concrete through development of a localized field of high thermal stresses.

5.5.3 Pore Pressure

The pore pressure development in saturated concrete specimens subjected to microwave at different frequencies is illustrated in Figures 5.10 and 5.11. As can be seen, the pore pressure variation with the microwave frequency and the concrete's water content shows a similar pattern as that for temperature and thermal stress effects. Pore pressure may lead to concrete surface spalling when the stresses generated exceed the concrete's tensile strength. Comparing the values of pore pressure obtained to the compressive thermal stresses developed for similar cases of microwave exposure serves to

highlight the prominent role that the thermal stresses play in the spalling of the concrete surface. Nevertheless, considering the inherent weakness of concrete in tension, the contribution of pore pressure should also be considered in the predictions.

5.5.4 Effect of Water Content

According to Equation 5.4, the microwave energy dissipation in any material depends on its attenuation factor and transmissivity values. Moreover, these two factors vary with microwave frequency and the water content of the concrete. The significant effect of the water content of concrete on the magnitude and pattern of stress development has been demonstrated in Figures 5.2 to 5.9. As can be seen, a higher water content leads to faster and more concentrated stress development in the heated concrete specimen which speeds up the surface delamination process. In practice, most of the contaminated concrete blocks are old and most likely to be in an air-dried condition; hence, drenching the concrete surface may be used, both to speed up the process and control the spalling depth.

5.5.5 Effect of Microwave Frequency

Generally, for a given microwave power and heating period, higher microwave frequencies result in higher stresses and pore pressure being generated within a thinner surface layer of concrete. The effect of microwave frequency on the maximum thermal stresses generated in concrete specimens with different water contents is shown in Figure 5.12. As can be seen, an increase in microwave frequency can lead to significantly higher compressive stresses.

5.5.6 Comparison with Available Literature

To compare the results obtained in this study with those from available literature,

the maximum temperatures predicted using the proposed method are compared with the results of the selected previous studies conducted by Bazant et al. (Zi. and Bažant, 2003; Bažant and Zi, 2003). These results are depicted in Figures 5.13 and 5.14. As mentioned earlier, it seems that the variation of the concrete's electromagnetic properties with the concrete's water content and the microwave frequency has been overlooked in previous studies. All the previous studies have considered constant electromagnetic properties for all the microwave frequencies investigated. This questionable assumption will significantly affect the accuracy of the results. To illustrate this, the results are compared at two different frequencies of 2.45 GHz and 10.6 GHz.

For purposes of comparison, results of the current study (as shown in Figures 5.13 and 5.14) were re-calculated using the similar assumptions (i.e. similar incident microwave power, incident power distribution and boundary conditions) as reported by Bazant et al. As can be seen in Figures 5.13 and 5.14, the both sets of results are roughly in agreement. For the microwave frequency of 2.45 GHz, the temperatures reported by Bazant et al. are in between the results obtained for the saturated concrete and the wet concrete while for 10.6 GHz microwave frequency are almost identical to the results obtained for the air-dried concrete. This shows that the ratio of temperatures reported by Bazant et al to those obtained in this study decreases with an increase in the microwave frequency. This reduction may stem from the negligence of the frequency dependency of dielectric properties by Bazant et al. In general, the loss factor of concrete increases with the microwave frequency (Figure 4.9); resulting in a higher temperature rise when subjected to microwaves. However, Bazant et al. assumed a constant loss factor for all microwave frequencies.

5.6 Conclusions

The well known Lambert's Law approximate method was modified to account for the TE$_{10}$ microwave mode used in common microwave heating systems and the reflections at the concrete surface. This method can be easily used to predict microwave power dissipation in concrete while avoiding the mathematical complexities of accurate electromagnetic modeling using Maxwell's equations. According to the results of the numerical modeling of microwave decontamination of concrete obtained by solving the coupled heat transfer, mass transfer and Lambert's law equations, the following conclusions may be made:

1. The results confirm the capability of high frequency microwaves to remove the surface layer of concrete by developing a localized field of both high thermal stresses and pore pressure.

2. The results of finite elements analysis confirm the prominent role that thermal stresses play in concrete surface spalling, as first highlighted by Bazant et al (2003).

3. Drenching of the concrete surface with copious amount of water may be used to increase the efficiency of the microwave decontamination process, as considerably higher stresses in a thinner surface layer may be generated.

4. Electromagnetic properties of wet and saturated concrete considered in this study {Ref. (Rhim and Buyukozturk, 1998)} are considerably higher than the values assumed by Bazant et al (2003) and Li et al. (1994). Moreover, instead of a uniform incident power distribution, an equivalent sine^2-shape power distribution

with twice the peak power was used to simulate the TE_{10} microwave mode. As a result, considerably higher temperatures and stresses were developed locally.

5. The results reveal the high sensitivity of the microwave heating process to the water content of concrete. Therefore, prior to any analytical or experimental investigation, the water content of concrete and its corresponding electromagnetic properties should be measured.

6. The spalling depth of the concrete surface layer and the time for spalling to occur are inversely proportional to the microwave frequency.

7. The results of this study should be verified using the more accurate methods and benchmarked against the results obtained via experimental studies.

Table 5.1 The minimum thickness of concrete block to guarantee the validity of Lambert's Law

Frequency (GHz)	Moisture Condition			
	Wet	**Saturated**	**Air-Dried**	**Oven-Dried**
	Minimum Thickness of Concrete Block , cm , (in.)			
2.45	10.96 (4.31)	19.97 (7.86)	122.53 (48.24)	161.30 (63.50)
10.6	2.47 (0.97)	4.23 (1.66)	9.40 (3.70)	25.09 (9.88)
18	1.36 (0.53)	2.31 (0.91)	3.93 (1.55)	11.40 (4.49)

Table 5.2 Standard waveguide dimensions at different frequencies

Microwave Frequency (GHz)	Designation	Width, mm (in.)	Height, mm (in.)
2.45	WR340	86.36 (3.4)	43.18 (1.7)
10.6	WR90	22.86 (0.9)	10.16 (0.4)
18	WR42	10.66 (0.42)	4.31 (0.17)

Table 5.3 Mechanical and thermal properties of concrete

Property	Assumption	Unit
Density	2300 (143.58)	Kg/m^3 , (lb/ft^3)
Specific heat	1000 (0.24)	$J/[Kg\,°K]$, ($Btu/[lb.°F]$)
Thermal conductivity	3 (1.73)	$W/[m.K]$, ($Btu/[ft.hr.°F]$)
Thermal expansion coefficient	12×10^{-6} (6.67×10^{-6})	$1/°C$, ($1/°F$)
Heat transfer coefficient of heat flux	10.0 (1.76)	$W/[m^2.°K]$, ($Btu/[ft^2.hr.°F]$)
Modulus of Elasticity	48.5 (7034.33)	GPa, (ksi)
Poisson's ratio	0.12	
Surface emissivity	0.9	
Initial Temperature	25 (77)	$°C$, ($°F$)

Figure 5.1 Sketch of the Microwave Decontamination System
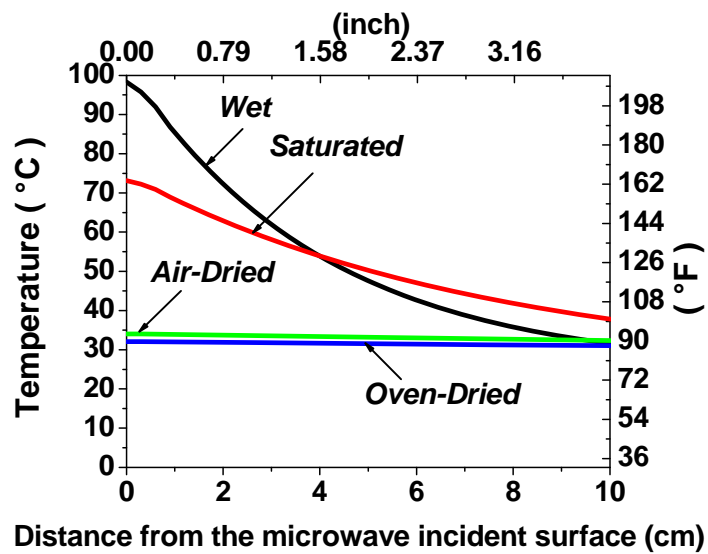
Figure 5.2 Temperature distribution in concrete after 5 seconds of microwave heating at 2.45GHz frequency
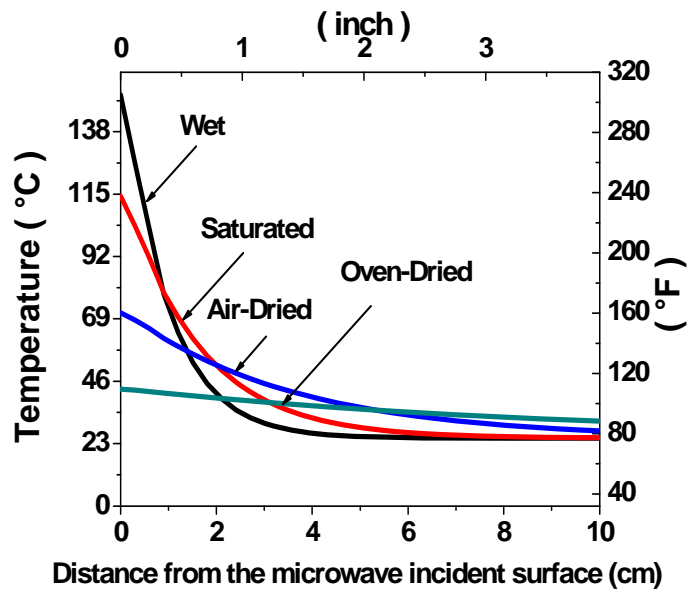
Figure 5.3 Temperature distribution in concrete after 2 seconds of microwave heating at 10.6GHz frequency
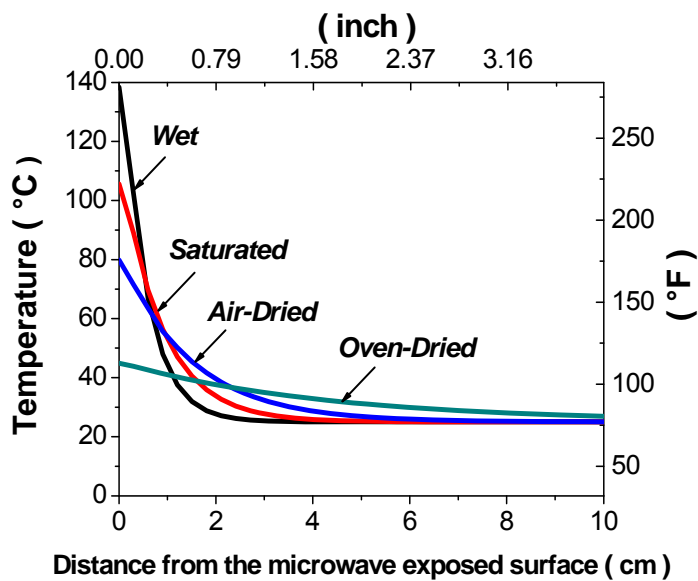
Figure 5.4 Temperature distribution in concrete after 1 second of microwave heating at 18GHz frequency
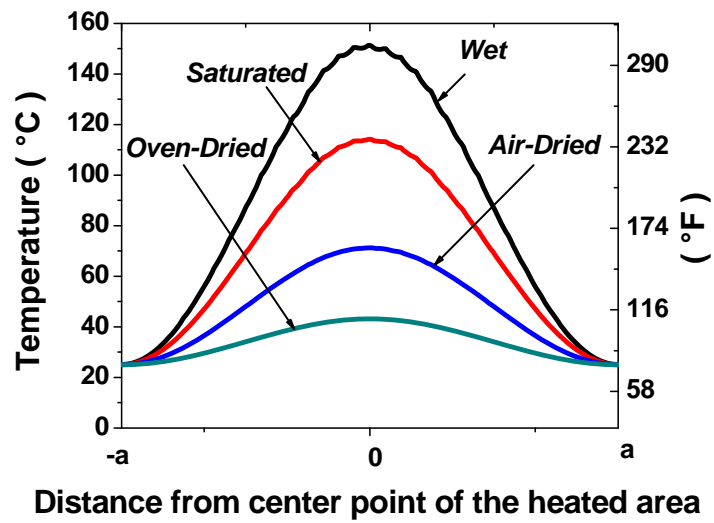
Figure 5.5 Temperature distribution across the microwave incident surface of concrete after 2 seconds of microwave heating at 10.6GHz frequency
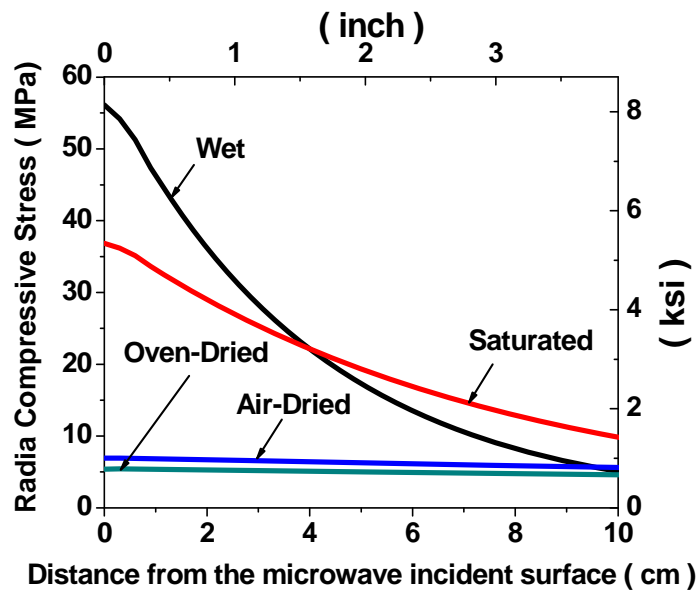
Figure 5.6 Radial compressive stress in concrete after 5 seconds of microwave heating at 2.45GHz frequency
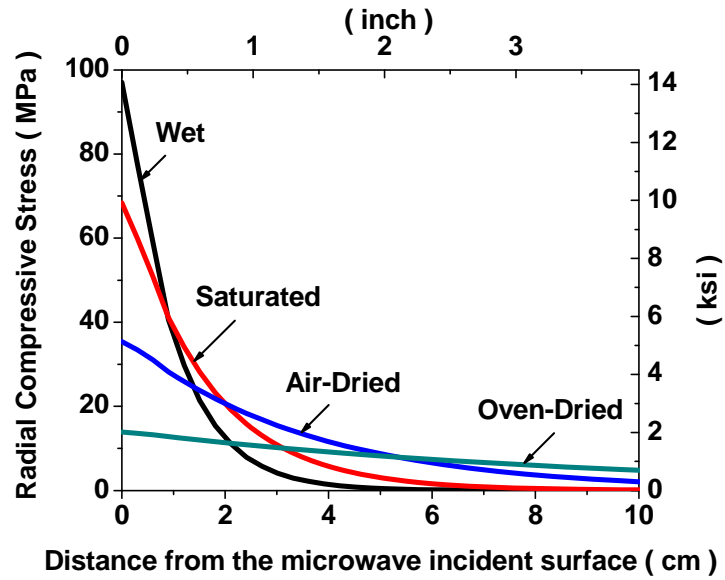
Figure 5.7 Radial compressive stress in concrete after 2 seconds of microwave heating at 10.6GHz frequency
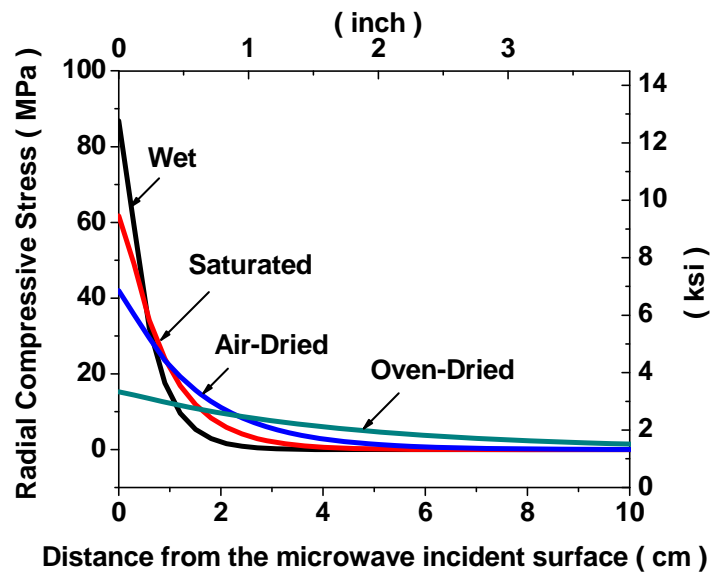
Figure 5.8 Radial compressive stress in concrete after 1 second of microwave heating at 18GHz frequency
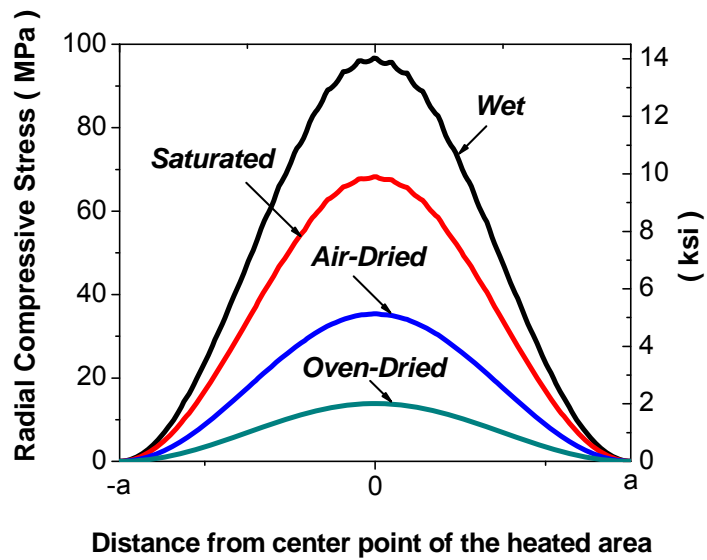
Figure 5.9 Radial compressive stress distribution across the microwave incident surface of concrete after 2 seconds of microwave heating at 10.6GHz frequency
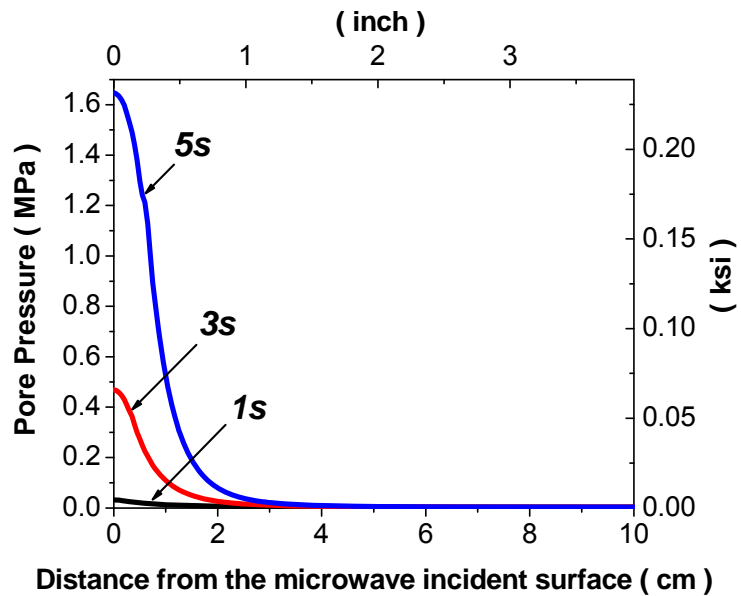
Figure 5.10 Pore Pressure in saturated concrete after 5 seconds of microwave heating at 10.6 GHz frequency

122
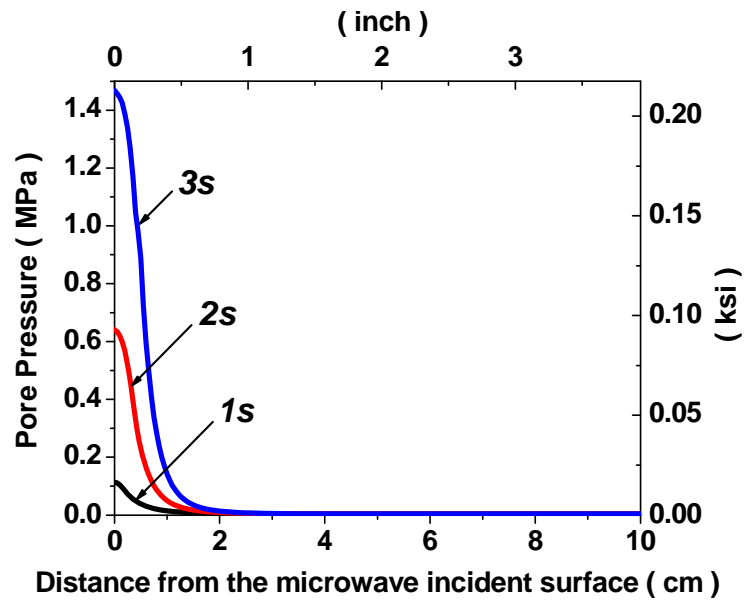
Figure 5.11 Pore Pressure in saturated concrete after 3 seconds of microwave heating at 18 GHz frequency
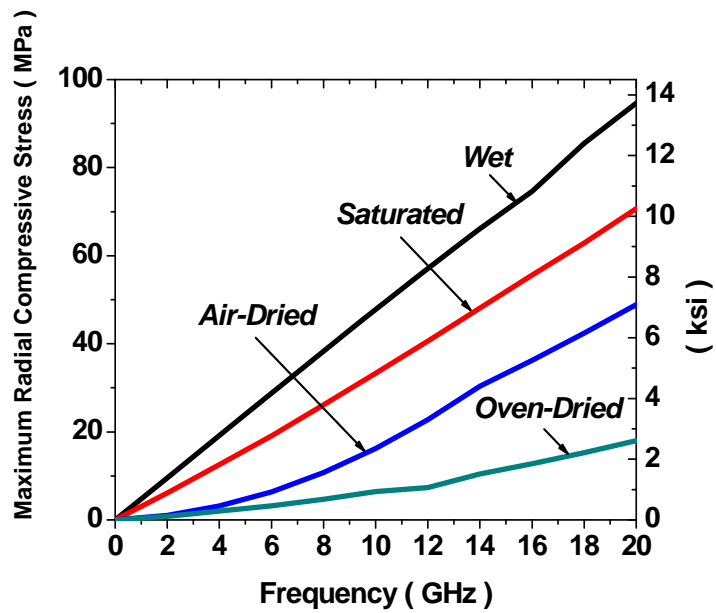
Figure 5.12 The variation of maximum compressive stress in concrete with frequency after 1 second of microwave heating
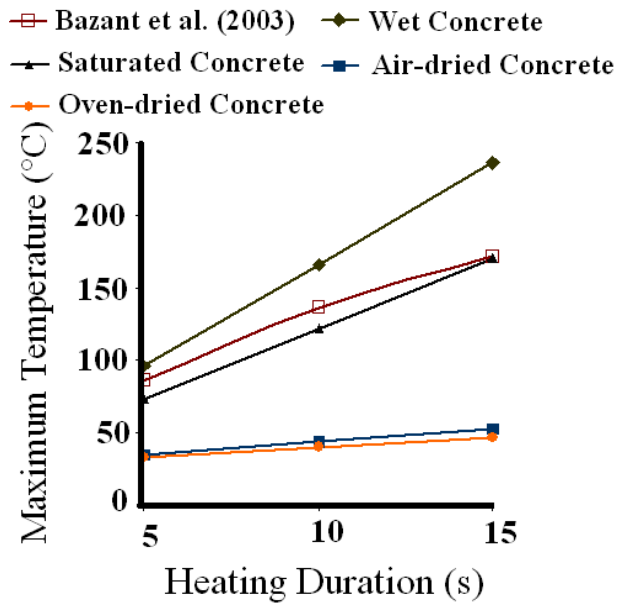
Figure 5.13 Comparison between the maximum temperatures in concrete obtained in this study and the results reported by Bazant et al. for the same microwave frequency of 2.45 GHz and microwave incident power of 1.1 MW/m^2
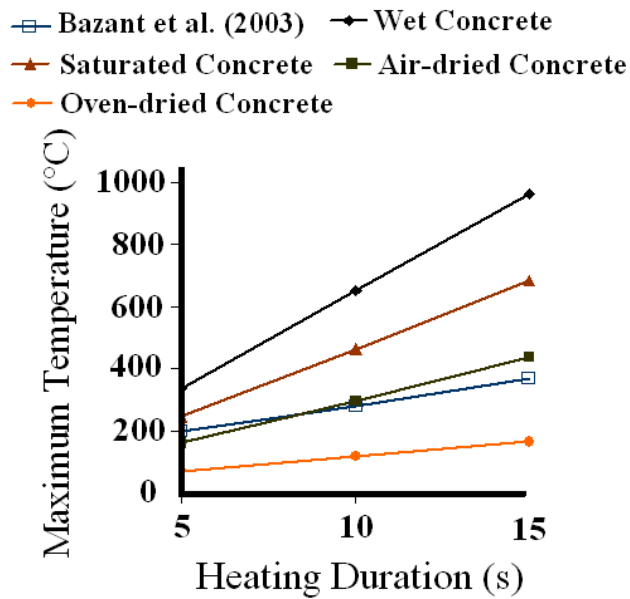
Figure 5.14 Comparison between the maximum temperatures in concrete obtained in this study and the results reported by Bazant et al. for the same microwave frequency of 10.6 GHz and microwave incident power of 1.1 MW/m^2

124

Chapter 6 : Microwave Heating of Concrete-Accurate Numerical Simulation

6.1 Background

As reviewed in Chapter 5, a number of analytical studies have been conducted to predict the temperature rise, pore pressure and thermal stresses developed in concrete when subjected to microwaves (Li et al., 1993; Li and Ebadian, 1994; Lagos et al., 1995; Zi. and Bažant, 2003; Bažant and Zi, 2003). Even though, all the studies had focused on modeling microwave decontamination of concrete, the simulation techniques used were general and can be readily applied to other applications such as microwave curing of concrete. Generally, modeling of the microwave heating process of concrete involves solving Maxwell's equations which govern the propagation of microwave radiation through the material and microwave waveguide or cavity, the heat transfer equation which governs heat absorption and the resulting temperature rise in the concrete block, and the mass transfer equation which governs the pore pressure development in the concrete block. However, because of the complexity of Maxwell's equations, approximations and

simplifying assumptions are usually used to estimate the dissipation of microwave power in concrete.

Li et al. (1993) and Lagos et al. (1995) used the plane wave assumption to simplify modeling of the microwave power dissipation in concrete. However, the plane wave assumption may only be reasonable when the microwave source is located very far from the concrete and thus may not be a good assumption to make for concrete decontamination and heating applications.

Subsequently, Bazant et al (2003) used a Lambert's law approximate formulation to estimate the microwave power dissipation in concrete. Bazant et al. modified the original Lambert's law to account for power reflection by the reinforcing rebars present in concrete. However, they did not take into account the shape of the incident power distribution associated with the microwave excited mode and considered a uniform incident microwave power distribution at the incident surface of concrete.

In Chapter 5 of this study, the original form of Lambert's law was modified to account for reflections at the concrete incident surface and also for the sinusoidal distribution of the TE_{10} microwave mode which is normally excited in common microwave heating systems. The modified formulation was used to estimate the microwave power dissipation in concrete exposed to microwaves of different frequencies and the resulting thermal stresses and pore pressures were calculated.

The formulation used in Chapter 5 is very simple and if proven to be accurate, can considerably reduce the mathematical complexities encountered in the simulation of the microwave-concrete interaction. However, according to available literature, even though Lambert's law is valid for samples thick enough to be treated as infinitely thick, it may be

a poor approximation for many practical situations (Ayappa et al., 1991). Therefore, prior to its use in applications involving microwave heating of concrete, its accuracy in estimating the microwave power dissipation in concrete blocks of commonly encountered thicknesses needs to be evaluated. In this chapter, both a modified form of Lambert's law and Maxwell's equations are used in the numerical model to calculate the microwave energy dissipation in concrete. Comparisons between the results obtained using both methods are used to verify the validity of the Lambert's Law approximate method to predict the microwave power dissipation in concrete blocks of normal thicknesses. Furthermore, the resulting temperature rise and thermal stresses developed in the concrete are calculated accordingly.

Since the focus of this study is geared to remove the contaminated surface of concrete, the simulation method presented in this chapter will be illustrated with this application in mind. However, the formulations can be extended for use for other applications such as microwave curing of concrete.

6.2 Industrial Microwave Heating Systems

Unlike the approximate methods which assume a predetermined distribution and power for the incident wave at the concrete surface, in the accurate modeling of microwave heating, the shape and configuration of the microwave heating systems will greatly affect the distribution, power, and transmission of the microwave at the concrete incident surface. Hence, the exact configuration of the microwave heating system to be modeled should be known in advance. In this chapter, microwave heating of the concrete surface using a basic system with a commonly utilized

configuration is simulated using the Maxwell's equations. For clarity, the components of a normal microwave heating system are briefly explained in following section.

The configurations of the microwave heating systems differ according to their application. In microwave curing application, concrete specimens are normally heated in a chamber. A waveguide is used to transfer the waves from the microwave generator into the chamber. Curing chambers are designed to provide a uniform microwave power distribution.

On the other hand, in microwave decontamination of concrete, the system is designed to concentrate the microwaves on the incident surface area of the concrete. A sketch of the fixed microwave decontamination system considered in this study is depicted in Figure 6.1. A basic microwave decontamination system may comprise of a microwave source to generate the waves and a waveguide and horn to transmit the generated waves onto the incident surface of the concrete. Other attachments such as a vacuum system, safety cavity and measurement instrumentation may also be incorporated.

6.2.1 Microwave Source

The most commonly used source of microwave energy, primarily for reasons of efficiency, is the magnetron. Because of mass production, magnetrons at 2.45 GHz are particularly cheap; however, magnetrons for other frequencies are also available. Other microwave sources are available such as the traveling wave tube (TWT), klystron, gyrotron and solid state devices. Each of these has characteristics that can be exploited. For instance, at higher frequencies (e.g. 10.6 GHz and 18 GHz), klystron and gyrotron are normally more efficient than magnetrons.

6.2.2 Waveguides

The wave travels in an unrestricted manner in free space. If metallic wall boundary conditions are applied, the waves are confined to the space within the walls and are guided by them. A hollow metallic tube of either rectangular or circular cross section made of aluminum, copper or brass of various sizes is generally used in practice. Such a structure is commonly known as a waveguide.

6.2.3 Waveguide Fields

Because of the boundary conditions, the waves that propagate inside a homogeneously filled waveguide are different from the TEM (transverse electromagnetic) waves assumed by most of the previous studies, and they are known as transverse electric (TE) waves and transverse magnetic (TM) waves. TE waves have $E_x = 0$ while TM waves have $H_x = 0$. For TE waves, there is a component of H along the direction of propagation, while for TM waves it is the E component which exists in the same direction. In both cases, energy is carried by the electric and magnetic fields associated with the wave. The wave forms a field pattern inside the waveguide known as a mode. It is possible to have several modes of propagation inside a particular waveguide. The modes correspond to the solutions of Maxwell's equations. The mode that has the lowest frequency in a particular waveguide is known as the dominant mode. Generally, the waveguide used for microwave heating has dimensions such that only the dominant mode propagates along it.

The fundamental transverse electric and transverse magnetic modes, TE_{10} and TM_{11}, are usually the two most dominant modes (Constantine A. Balanis, 1989). In the present study, the TE_{10} mode, which is excited by most of the basic microwave heating systems

available, is considered. Field lines for the TE_{10} mode in a rectangular waveguide are shown in Figure 6.2.

6.2.4 Waveguide Cutoff Frequency

There is a minimum frequency below which a given waveguide cannot transmit waves, and this is known as the cutoff frequency. A waveguide has a cutoff frequency for each allowed mode. If the frequency of the excited mode is above the cutoff frequency, electromagnetic energy will be transmitted down the guide with little attenuation. If it is below the cutoff frequency, the wave is described as evanescent and will be attenuated strongly within a short distance. For a homogeneously filled waveguide, the cutoff frequency, f_c, is given by

$$f_c = \frac{1}{2\pi\sqrt{\mu_0 \varepsilon_0 \varepsilon}} \sqrt{\left(\frac{m\pi}{a}\right)^2 + \left(\frac{n\pi}{b}\right)^2} \qquad (6.1)$$

where a and b are the dimensions of the waveguide and m and n are the mode indices. The cutoff frequency characteristic of a waveguide must be used to choose the appropriate waveguide and horn for a specific frequency and microwave mode. The chosen waveguide dimensions for the three different frequencies used in this study are listed in Table 6.1. The dimensions of the waveguides are calculated using Equation 6.1 so that just the TE_{10} mode exists at each frequency.

6.3 Problem Description

In this study, the incident microwave power dissipation and the resulting temperature rise and thermal stresses generated in a 20 cm thick saturated concrete slab heated through a waveguide are numerically predicted by using both the approximate Lambert's Law and

the more accurate Maxwell's equations. The area of the heated zone varies with the waveguide dimensions as listed in Table 6.1.

6.4 Problem Formulation

The microwave power dissipation, heat transfer, and mass transfer phenomena in the concrete block heated using the microwave heating system described above are formulated in the following section.

6.4.1 Power Dissipation: Maxwell's Equation

As explained in Chapter 4, the power dissipated per unit volume can be obtained from

$$P(r) = -\mathrm{Re}(\nabla S) = \frac{1}{2}\omega\varepsilon_0\varepsilon_r^{"}\left|E\right|^2 \qquad (4.34)$$

In above equation, ω is the angular frequency which has the following relationship with the chosen microwave frequency

$$\omega = 2\pi f \qquad (6.2)$$

Moreover, ε_0 and $\varepsilon_r^{"}$ are the permittivity of the free space and the loss factor of the concrete, respectively. Hence the only unknown parameter is the electric field intensity (E) which can be obtained through solving the Maxwell's equations (Equations 4.11 to 4.14).

6.4.2 Power Dissipation: Lambert's Law

The attenuation factor and the minimum thickness of the concrete calculated based on Ayappa et al.'s recommendations such that Lambert's Law is valid, are listed in Table 5.1. However, to investigate the validity of Lambert's law for simulating the actual microwave

decontamination process, in the current study, the accuracy of this method to estimate the microwave power dissipation in a concrete block with a more commonly used thickness of 20 cm is verified with the results obtained through the more accurate Maxwell's equations. According to the modified Lambert's law presented in Chapter 5, if I_0 is considered as the power transmitted into the concrete, and considering the sinusoidal shape of the TE_{10} mode, the power dissipated at distance x from the microwave incident surface may be estimated as:

$$PL(x) = 2\beta \times (2I_0) \times e^{-2\beta x} \times Sin^2 \left(\pi \frac{a-y}{2a} \right) \qquad (6.3)$$

Here, $2a$ is the width of the waveguide.

6.4.3 Heat Transfer

Once the microwave energy dissipation in concrete has been determined using either of the abovementioned methods (Lambert's law or Maxwell's equations), the heat absorption and resulting temperature rise in the concrete may be obtained using the heat transfer equation:

$$\rho C \frac{\partial T}{\partial t} = -\nabla.(-K \nabla T) + Q_{Lambert}(x) \qquad \text{(6.4-a) or,}$$

$$\rho C \frac{\partial T}{\partial t} = -\nabla.(-K \nabla T) + Q_{emw}(x) \qquad \text{(6.4-b)}$$

Here, ρ = mass density of concrete, t = time, ∇ = gradient operator, C= specific heat of concrete, K=heat conductivity, T= temperature, $Q_{Lambert}$ = dissipated energy estimated using the modified Lambert's approximation and Q_{emw} = dissipated energy obtained from the solution of Maxwell's equations.

6.4.3.1 Heat Transfer Boundary Conditions

Both conductive and radiative heat loss boundary conditions are imposed at the model boundaries. Hence, the heat transfer boundary condition may be written as

$$\nabla T \cdot n + B_i \left(T - T_a \right) + S \left(T^4 - T_a \right) = 0 \qquad (6.5)$$

Where B_i is the Biot number, S is the radiation number, n is the normal to the boundary and T_a is the ambient temperature

6.4.4 Structural Boundary Conditions

As part of a large concrete slab, the heated zone displacement is restrained by the unheated parts of the slab and, therefore, simply supported boundary conditions may be considered:

$$U_x = U_y = U_z = 0 \qquad (6.6)$$

6.4.5 Electromagnetic Boundary Conditions

Since we are dealing with the accurate near-field electromagnetic modeling of microwave heating, besides the structural and heat transfer boundary conditions, the electromagnetic boundary conditions must be appropriately imposed to ensure that the wave propagation in the concrete matches its actual behavior. The EM boundary conditions used in this study are briefly explained in the following section.

6.4.5.1 Perfect Electric Conductor (PEC)

A perfect electric conductor (PEC) boundary (also called an electric wall) is a surface on which the tangential component of the vector electric field vanishes. A neighboring conductor from the model can be removed and replaced with a PEC boundary condition if the losses of the metallic conductor can be ignored. In many applications, a thin metallic

object simplifies to an infinitesimally thin metallic sheet with a PEC boundary condition. In addition, the model size can be reduced by applying PEC boundary conditions to symmetry planes that have a zero tangential component of the vector electric field. In this study, as can be seen in Figure 6.3, the PEC boundary condition is imposed at the waveguide walls and unattached surfaces of the Perfectly Matched Layer (PML) regions.

6.4.5.2 Surface Impedance

Surface impedance boundary conditions can be used to approximate a radiation boundary and an electrically small lossy/dielectric layer where a very fine mesh would usually be required. For the case of the interface between the free space and the model, the following expression may be used to compute impedance:

$$Z = \sqrt{\frac{\mu_0}{\varepsilon_0}} \qquad (6.7)$$

6.4.5.3 Perfectly Matched Layers (PML)

The purpose of an absorbing boundary condition is to absorb the outgoing electromagnetic wave so that there are no reflections back into the FE computational domain. Perfectly matched layers (PML) are the layers of electromagnetic wave absorbing elements designed for mesh truncation of an open FE domain in a harmonic or modal analysis. It is an artificial anisotropic material that is transparent and heavily lossy to incoming electromagnetic waves. PML can reduce the size of the computational domain significantly with very small numerical reflections. A PEC boundary condition should be imposed at the external boundary of the PML region.

6.4.6 Effects of the Reinforcing Bars

Bazant et al. (2003) examined the effects of the presence of reinforcing bars on the microwave decontamination process by considering the area fraction of the steel bars (by projecting on the surface of the wall) to be about 19%. For simplicity, a parallel combination of reinforced and unreinoreced strips in the direction normal to the surface were considered. The overall average volumetric heat generation was postulated as the average heat generation of two adjacent strips. The authors concluded that, at high microwave frequencies applied for microwave decontamination purposes, the effect of the reinforcing bars is negligible.

The Lambert's law approximation used in Chapter 5 of this study has been shown to provide a satisfactory approximation of the microwave power dissipation where reflections are negligible (Basak, 2004). However, the use of Lambert's law to approximate the microwave power dissipation in multi-layer materials usually leads to unsatisfactory results, as reported by Basak (2004). Therefore, the application of Lambert's law to estimate the microwave power dissipation in reinforced concrete is not recommended. In this study, the electric field distribution and its resulting temperature distribution in reinforced concrete are examined using the more accurate solution of Maxwell's equations. The reinforcing bars may be considered as perfect electric conductors. Hence, microwaves are assumed to be completely reflected at the interface between the concrete and the reinforcing bars.

6.5 Results and Discussions

The commercially available COMSOL Multiphysics finite element software is used to solve the coupled electromagnetic, heat transfer and structural problems detailed in the

previous sections. The mechanical and thermal properties of concrete considered in this study are summarized in Table 6.2. Three frequencies of 2.45 GHz, 10.6 GHz and 18 GHz are considered. These frequencies are representative of the characteristics of low, intermediate and high frequencies. Moreover, a constant incident microwave power of 1.1 MW/m^2 is assumed.

It should be noted that in all the graphs presented in the results section, the distribution along the center line of the heated zone of the concrete block is presented, unless otherwise stated. The center line refers to the line passing through the centers of the incident and distal surfaces of the heated zone of the concrete block. The area of the heated zone of the concrete block varies with the dimension of the waveguide used (Table 6.1). The dielectric constant, loss factor and conductivity of the saturated concrete specimens considered in this study are summarized in Table 6.3.

6.5.1 Electric Field in Concrete

The variation of the z component of the electric field inside the concrete block at microwave frequencies of 2.45 GHz, 10.6 GHz and 18 GHz is shown in Figures 6.4, 6.5 and 6.6, respectively. Moreover, the variation of the electric field's norm in concrete at different microwave frequencies is shown in Figures 6.7 to 6.9. Having computed the electric field's norm inside the concrete, Equation 4.34 can be used to compute the average dissipated energy per unit volume of concrete which can be used as the power source in the heat transfer equation to calculate the temperature rise. As can be seen in Figures 6.4 to 6.9, an increase in microwave frequency leads to faster dissipation of the electric field within a thinner layer at the surface of the concrete.

6.5.2 Temperature Distribution

Temperature distributions in saturated concrete specimens subjected to microwaves of different frequencies have been computed using both Maxwell's equations and the Lambert's law approximation. The temperature distributions across the horizontal line passing through the center of the microwave heated zone are illustrated in Figures 6.10 to 6.12. As can be seen, both methods predict relatively similar microwave dissipation depths and temperature distribution patterns in concrete. As expected, at a fixed incident microwave power of $1.1 \, MW/m^2$ and at higher frequencies, microwave penetration is reduced and more energy is dissipated near the concrete's surface. This results in a faster temperature rise and higher temperature gradients within a thin surface layer of the concrete block. Results show that the approximate Lambert's law method can be satisfactorily used to predict the temperature distribution inside the concrete without having to deal with the computational complications of Maxwell's equations. Moreover, according to the results, the sine^2-shape incident power distribution used in Lambert's law to simulate the sine-shape of the TE_{10} microwave mode appears to provide a satisfactory approximation.

The 3D temperature distribution plots of the temperature distribution in the heated zone are depicted in Figures 6.13 to 6.15 for 2.45 GHz, 10.6 GHz and 18 GHz, respectively. As can be seen, the sine^2 shape of the incident microwave power dissipation leads to a sine^2-shape temperature distribution across the concrete exposed surface with the peak temperature at the vertical center line. Moreover, as can be seen in these figures, the size of the microwave heated zone decreases with an increase in the microwave frequency.

6.5.3 Thermal Stresses

The temperature gradient in the heated zone of the concrete results in non-uniform expansion of this area and may develop relatively high compressive stresses. The results of the thermal stress analysis of the saturated concrete specimens subjected to microwaves of different frequencies have been computed using both the approximate Lambert's law and the more accurate Maxwell's equations. These are illustrated in Figures 6.16 to 6.18. As can be seen, both methods predict relatively similar stress development patterns inside the concrete.

6.5.4 Effects of the Presence of Reinforcing Bars

The temperature distribution in saturated reinforced concrete subjected to microwaves of different frequencies is illustrated in Figures 6.19 to 6.21. As can be seen, the presence of reinforcing bars will generally lead to a higher temperature rise within the surface layer of the concrete. The effect of the reinforcing bars on the decontamination process is expected to decrease with a decrease in microwave penetration depth, especially when the penetration depth is less than the concrete cover to the embedded reinforcing steel. The microwave penetration depth may decrease with an increase in microwave frequency or the concrete's water content. As can be seen in Figures 6.20 and 6.21, the effect of the presence of reinforcing bars on the temperature distribution generated in saturated concrete for microwave frequencies of 10.6 GHz and 18 GHz is almost negligible.

6.6 Conclusions

In this chapter, the finite element method was used to solve Maxwell's equations

for concrete blocks subjected to microwaves. From the results of Maxwell's equations, the electric and magnetic field distributions in the concrete can be obtained. These outputs can be used to compute the resistive heat dissipation in the concrete after some straightforward manipulations. The resulting heat dissipation is used to compute the temperature rise and thermal stress development in the concrete in subsequent steps. In this study, both Maxwell's equations solution and Lambert's law approximation were used to compute the temperature rise and thermal stress development in the concrete. According to the results, the following conclusions may be made:

1. Both Lambert's law and Maxwell's equations predict relatively similar patterns. Hence, Lambert's law can be confidently used as a satisfactory approximation to simplify the analytical modeling of the microwave heating process in concrete.

3. The $sine^2$-shape assumption for the incident power distribution at the concrete's surface can be a good approximation of the sine-shape of the TE_{10} mode used in most basic microwave heating systems.

4. The presence of reinforcing bars in concrete will generally lead to a higher temperature rise in the concrete's surface layer. The effect of reinforcing bars on the microwave decontamination process decreases with a decrease in the microwave penetration depth. The microwave penetration depth appears to decrease with an increase in microwave frequency or water content of the concrete.

Table 6.1 Waveguide dimensions

Frequency (GHz)	Designation	Width, mm (in.)	Height, mm (in.)	Cutoff Frequency (GHz)
2.45	WR340	86.36 (3.4)	43.18 (1.7)	
10.6	WR90	22.86 (0.9)	10.16 (0.4)	7.847
18	WR42	10.66 (0.42)	4.31 (0.17)	14.05

Table 6.2 Mechanical and thermal properties of concrete

Property	Assumption	Unit
Density	2300 (143.58)	Kg/m^3 , (lb/ft^3)
Specific heat	1000 (0.24)	$J/[Kg°K]$, ($Btu/[lb.°F]$)
Thermal conductivity	3 (1.73)	$W/[m.K]$, ($Btu/[ft.hr.°F]$)
Thermal expansion coefficient	12×10^{-6} (6.67×10^{-6})	$1/°C$, ($1/°F$)
Heat transfer coefficient of heat flux	10.0 (1.76)	$W/[m^2.°K]$, ($Btu/[ft^2.hr.°F]$)
Modulus of Elasticity	48.5 (7034.33)	GPa, (ksi)
Poisson's ratio	0.12	
Surface emissivity	0.9	
Initial Temperature	25 (77)	$°C$, ($°F$)

Table 6.3 Electromagnetic properties of saturated concrete

Frequency (GHz)	Dielectric Constant	Loss Factor	Conductivity (mhos/meter)	Attenuation Factor
2.45	8.1	0.750	0.086	6.76
10.6	7.45	0.785	0.51	31.91
18	6.86	0.813	0.87	58.47
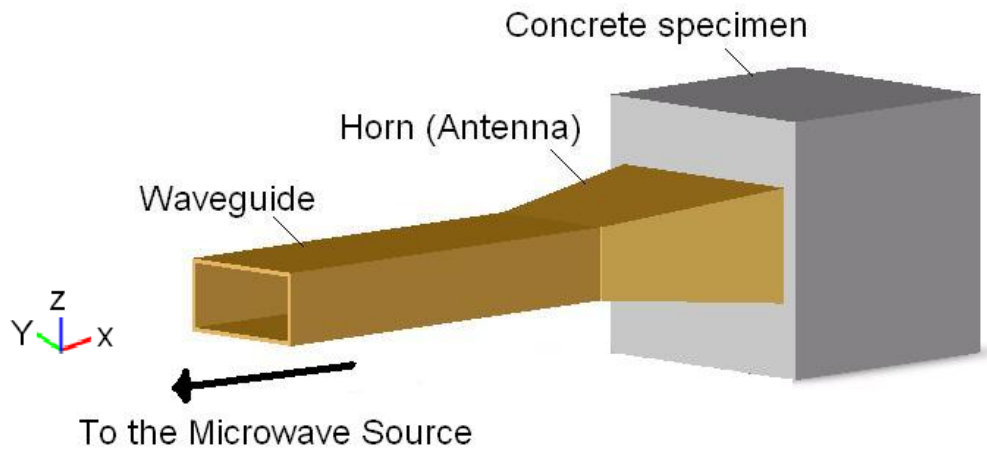
Figure 6.1 Sketch of the microwave applicator
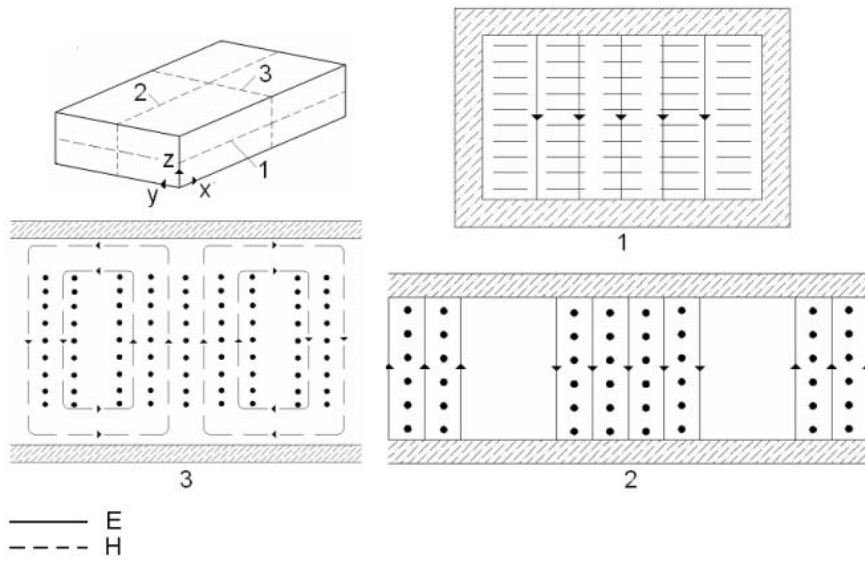
Figure 6.2 Field lines for the TE$_{10}$ mode in a rectangular waveguide
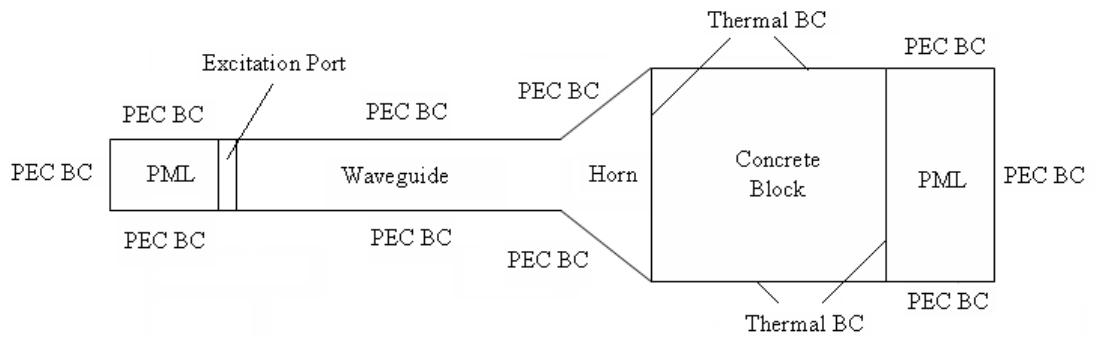
Figure 6.3 Boundary conditions
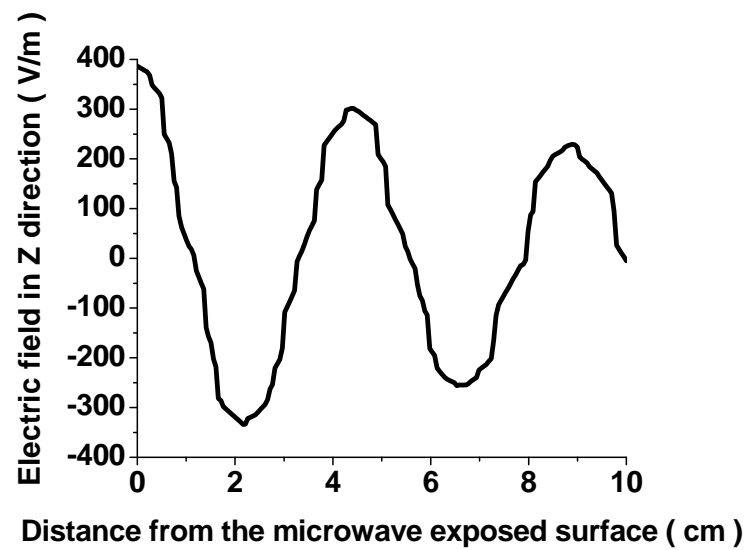
Figure 6.4 The z component of electric field inside concrete subjected to microwave at 2.45 GHz frequency and 1 W power.
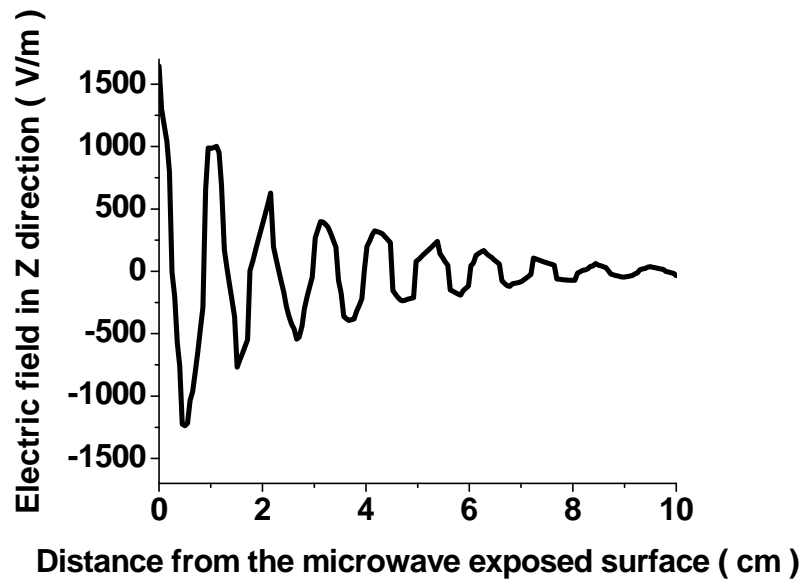
Figure 6.5 The z component of electric field inside concrete subjected to microwave at 10.6 GHz frequency and 1 W power.
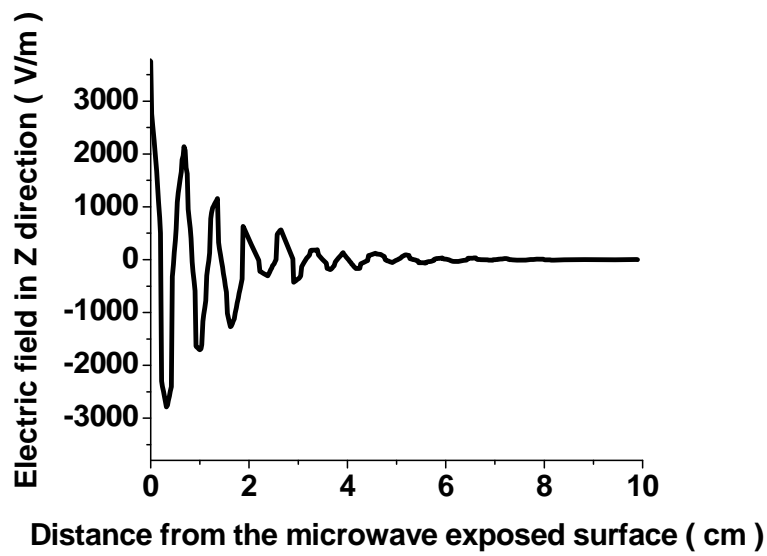
Figure 6.6 The z component of electric field inside concrete subjected to microwave at 18 GHz frequency and 1 W power.
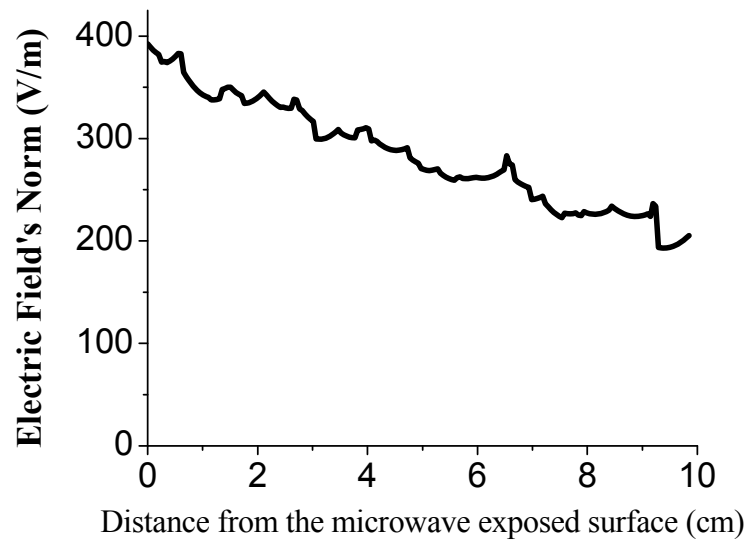
Figure 6.7 Variation of the electric field's norm inside concrete subjected to microwave at 2.45 GHz frequency and 1.1 MW/m^2 power.
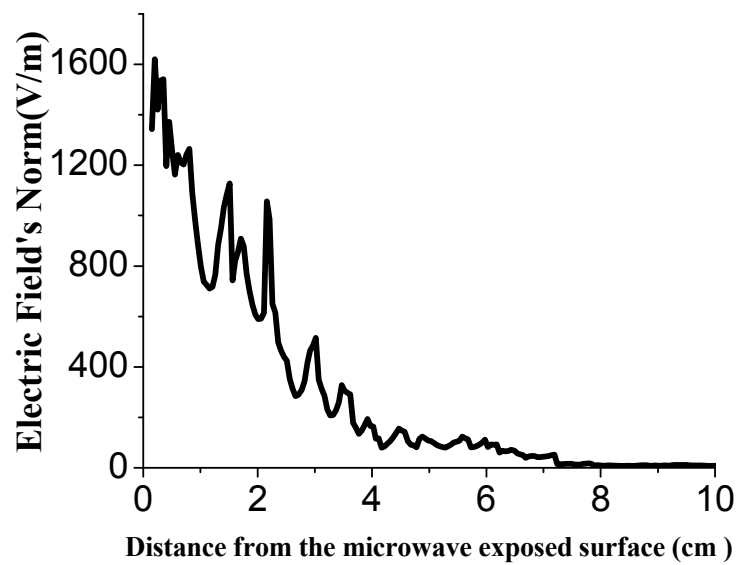
Figure 6.8 Variation of the electric field's norm inside concrete subjected to microwave at 10.6 GHz frequency and 1.1 MW/m^2 power.
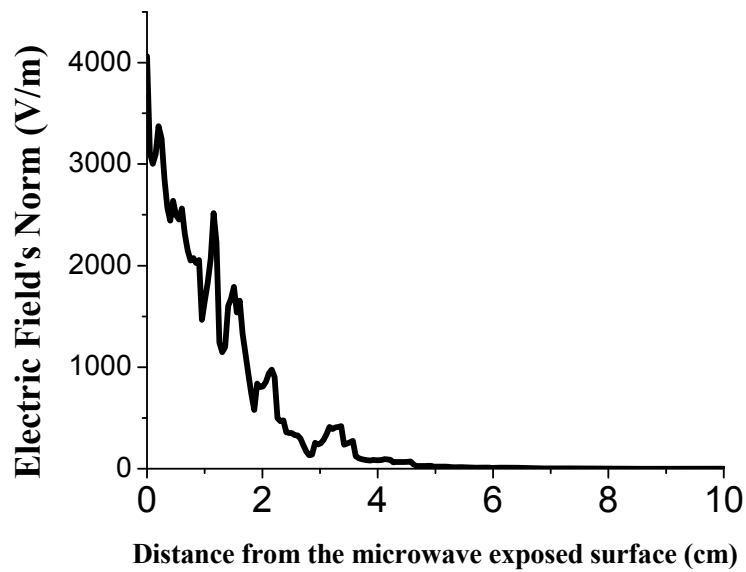
Figure 6.9 Variation of the electric field's norm inside concrete subjected to microwave at 18 GHz frequency and 1.1 MW/m² power.
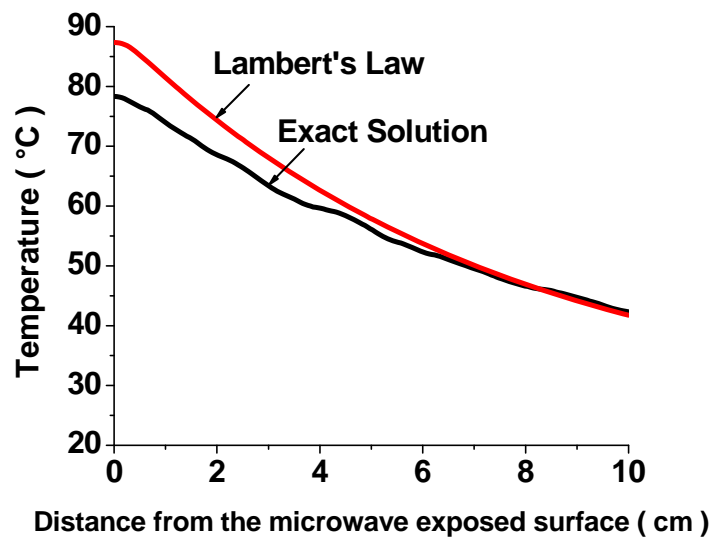
Figure 6.10 Temperature distribution in saturated concrete after 5 seconds of microwave heating at 2.45 GHz frequency and 1.1 MW/m² incident power
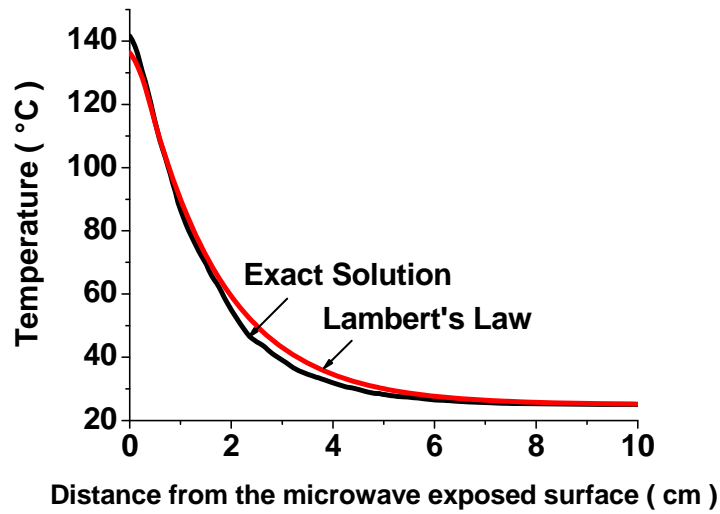
Figure 6.11 Temperature distribution in saturated concrete after 2 seconds of microwave heating at 10.6 GHz frequency and 1.1 MW/m² incident power
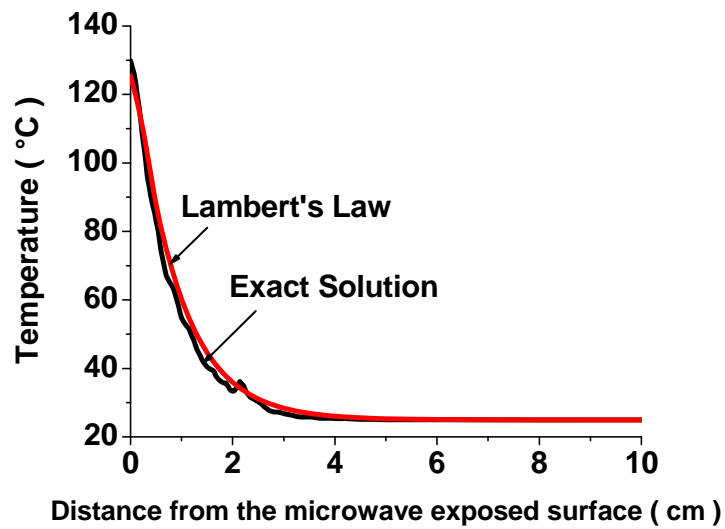
Figure 6.12 Temperature distribution in saturated concrete after 1 second of microwave heating at 18 GHz frequency and 1.1 MW/m² incident power

146
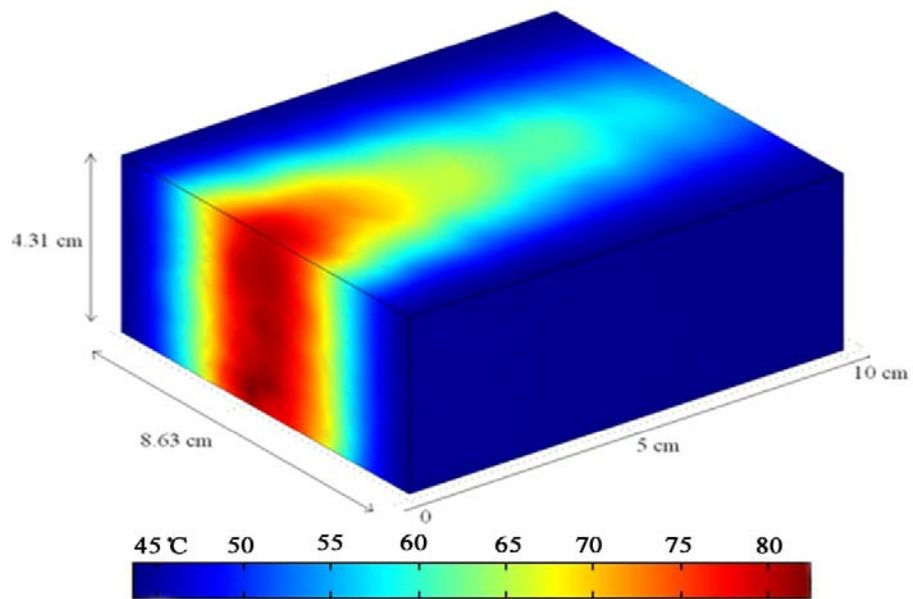
Figure 6.13 Temperature distribution across the heated zone of a saturated concrete after 5 second of microwave heating at 2.45 GHz frequency and 1.1 MW/m^2 incident power
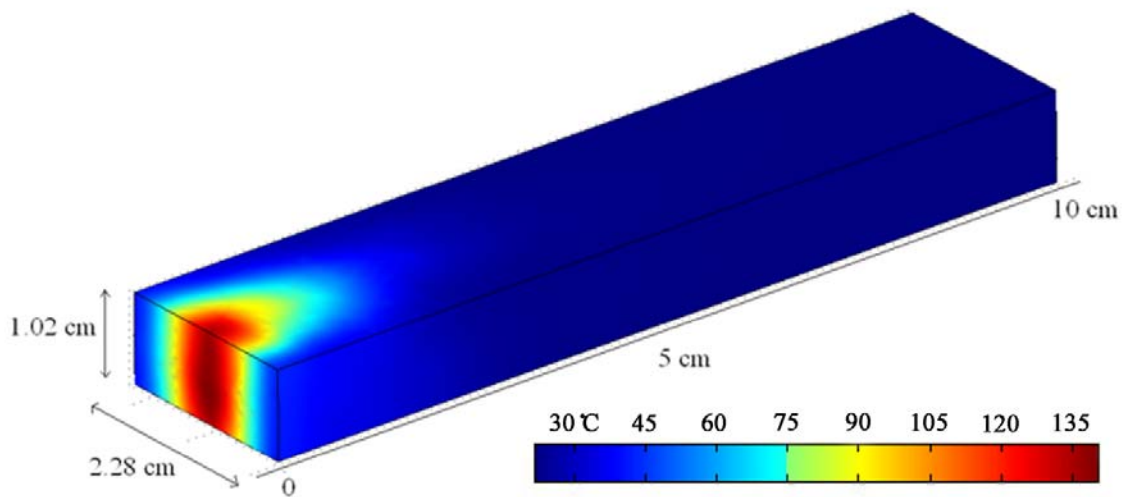
Figure 6.14 Temperature distribution across the heated zone of a saturated concrete heated after 2 seconds of microwave heating at 10.6 GHz frequency and 1.1 MW/m^2 incident power
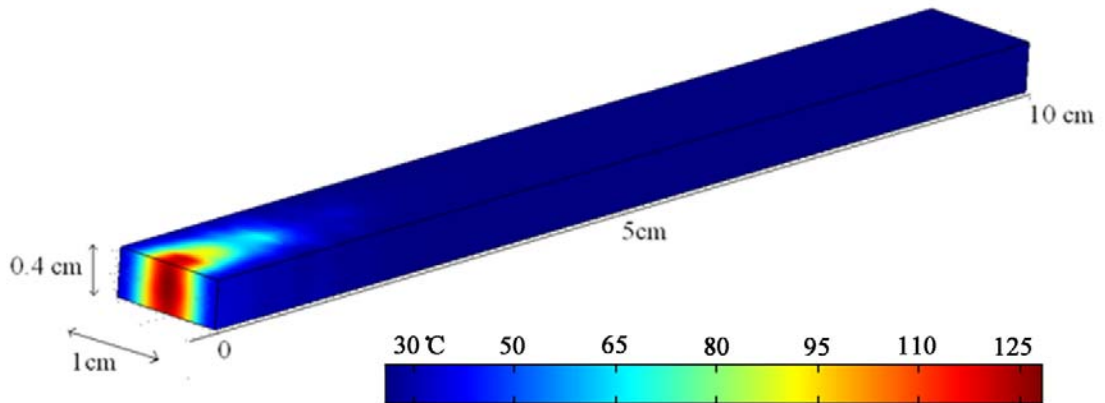
Figure 6.15 Temperature distribution across the heated zone of a saturated concrete after 1 second of microwave heating at 18 GHz frequency and 1.1 MW/m² incident power
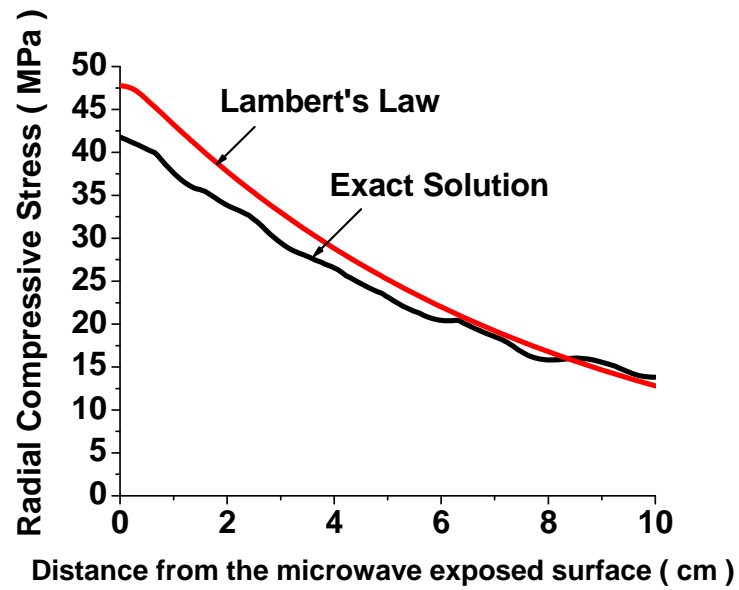
Figure 6.16 Radial compressive stress in saturated concrete after 5 seconds of microwave heating at 2.45GHz frequency and 1.1 MW/m² incident power
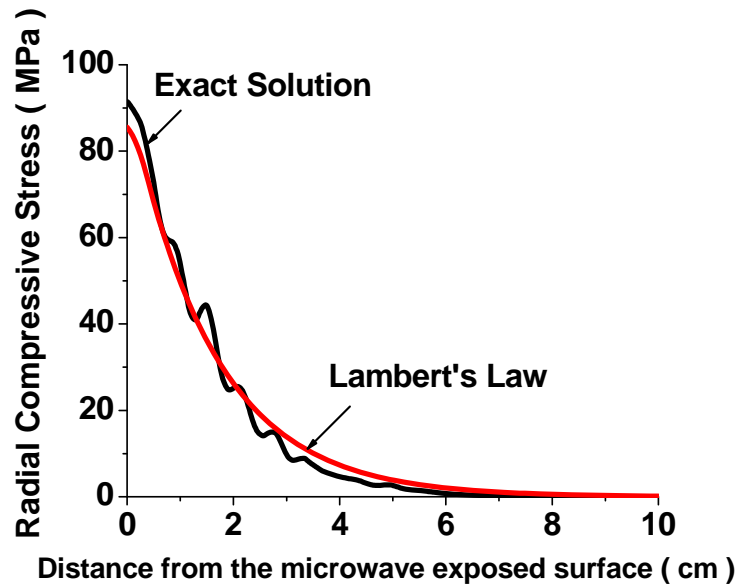
Figure 6.17 Radial compressive stress in saturated concrete after 2 seconds of microwave heating at 10.6 GHz frequency and 1.1 MW/m^2 incident power
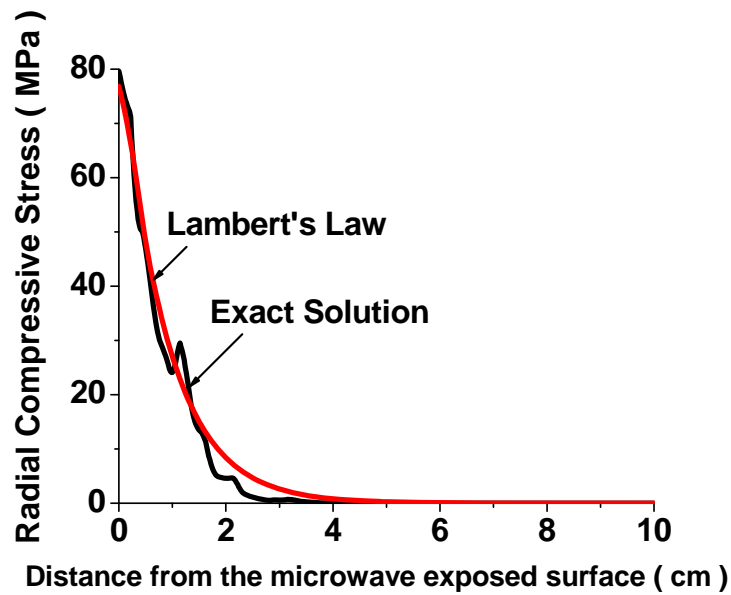
Figure 6.18 Radial compressive stress in saturated concrete after 1 seconds of microwave heating at 18 GHz frequency and 1.1 MW/m^2 incident power
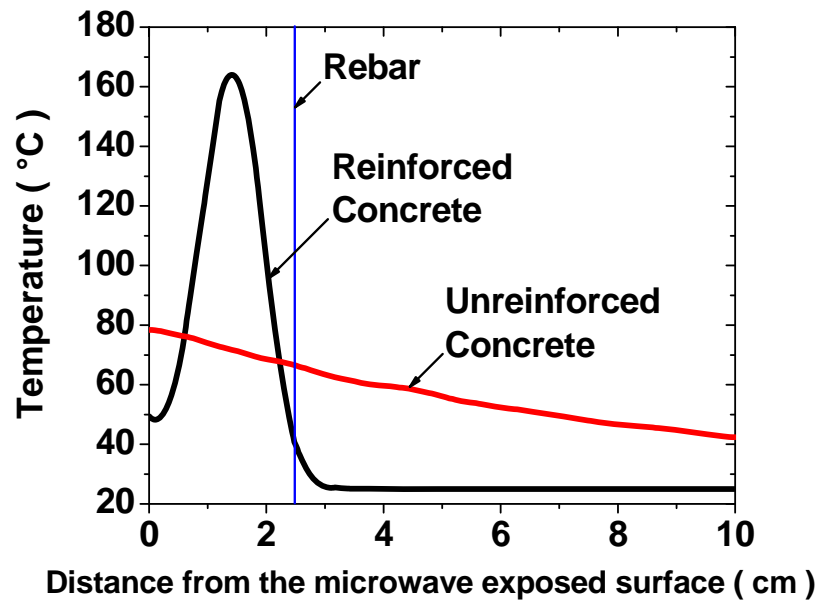
Figure 6.19 Temperature distribution in reinforced saturated concrete after 5 seconds of microwave heating at 2.45 GHz frequency and 1.1 MW/m^2 incident power
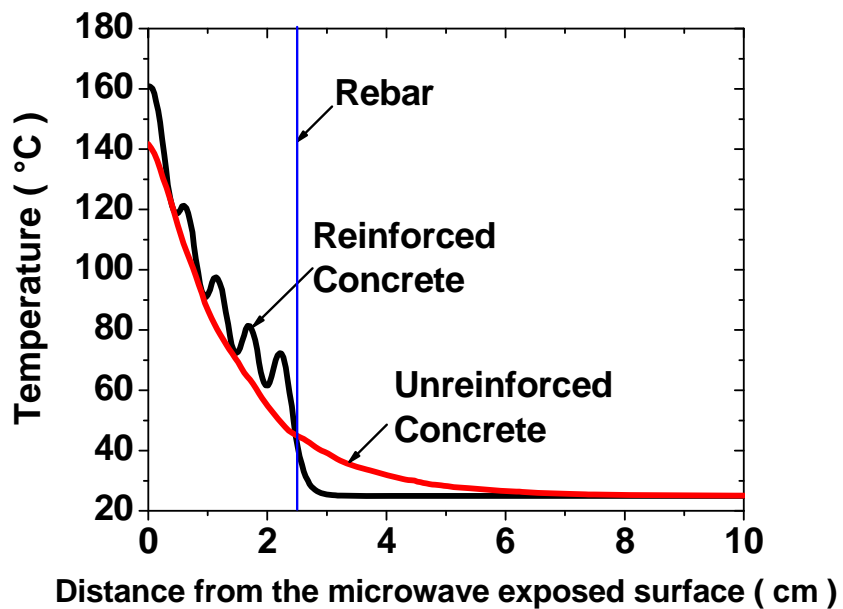
Figure 6.20 Temperature distribution in reinforced saturated concrete after 2 seconds of microwave heating at 10.6 GHz frequency and 1.1 MW/m^2 incident power
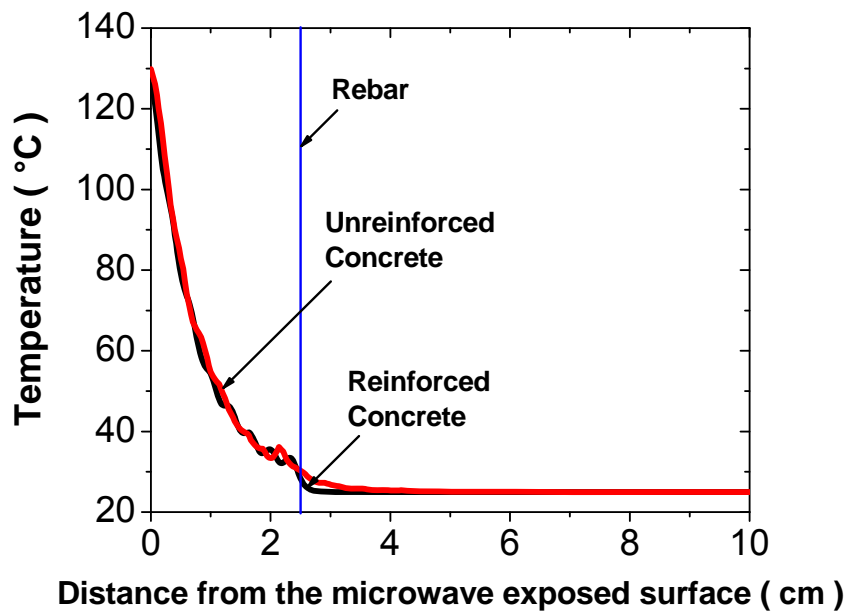
Figure 6.21 Temperature distribution in reinforced saturated concrete after 1 second of microwave heating at 18 GHz frequency and 1.1 MW/m^2 incident power

Chapter 7 : Microwave-Assisted RCA Beneficiation- Numerical Simulation and Preliminary Experiments

The adhering mortar has been reported as one of the main causes contributing to the inferior properties of RCA compared to natural aggregates (NA). The adhering mortar results in higher porosity, higher water absorption, lower modulus of elasticity and weaker interfacial zone (ITZ) between newly cast cementitious mortar and the recycled aggregates.

Different techniques proposed to increase the quality of RCA through removal of the adhering mortar (RCA beneficiation methods) were reviewed in Chapter 3. In the current chapter, the fundamentals of a novel microwave-assisted RCA beneficiation technique developed during the current study are presented. In this technique, the inherent difference in the EM and thermal properties of mortar and coarse aggregate and the unique capability of microwaves to heat the materials selectively based on their EM properties are used to develop high differential thermal stresses at the ITZ between Adhering Mortar (AM) and

Embedded Natural Aggregate (ENA) to remove the adhering mortar and thereby increase
the yield and quality of RCA.

To facilitate understanding of this method, in the first section of this chapter, **Section
7.1**, the basic differences between the thermal, mechanical, and electromagnetic properties
of mortar and aggregate which can lead to differential stresses in the adhering mortar and
its interface with the recycled natural aggregate (RNA) during the microwave heating are
reviewed.

In the second section, **Section 7.2**, results of a preliminarily experimental study using
a commercially available microwave oven are presented. Results are used to investigate
the capability of microwave heating in the removal of the adhering mortar of RCA. A
comparison between the properties of RCA before and after microwave beneficiation is
used to investigate RCA quality enhancement.

In the third section of this chapter, **Section 7.3**; to investigate the feasibility of using
the microwave beneficiation technique in practice, the temperature rise and thermal
stresses developed in the RCA particles heated with a prototype industrial microwave-
assisted RCA beneficiation system is numerically modeled.

7.1   Different Electromagnetic and Thermal Properties

The decay in the incident microwave energy in RCA along with the different
microwave power absorption rates of the natural aggregate and the adhering mortar may
lead to a temperature gradient and thus thermal stress development in RCA, especially at
the aggregate-mortar interface. The higher the temperature gradient, the higher thermal
stresses developed.

As explained in Chapter 4, the microwave power dissipation in RCA may be estimated using the Lambert's law. The simple form of Lambert's law may be stated as:

$$PL(x) = -\frac{\partial I(x)}{\partial x} = 2\beta I_0 e^{-2\beta x} \qquad (4.36)$$

Here, PL(X) is the microwave energy dissipated at a distance x from the microwave exposed surface of RCA, I_0 is the microwave power transmitted into RCA and β is the attenuation factor of RCA. Attenuation factor is the EM property which can best illustrate the microwave power decay in the materials. It is a measure of the magnitude and decay rate of microwave power inside the material. As can be seen in Equation 4.36, a higher attenuation factor results in a higher microwave power dissipation and thus a faster decay of the microwave energy in the material.

Considering a material comprising two layers with the different attenuation factors of β_1 and β_2 and different thicknesses of L_1 and L_2, respectively, exposed to a uniform microwave power from its top surface, the microwave power dissipation in the upper layer (Layer 1) may be calculated as:

$$PL_1(x) = 2\beta_1 I_0 e^{-2\beta_1 x} \qquad (7.1)$$

While the dissipated microwave power at distance x from the top surface of the next layer (Layer 2) is calculated through:

$$PL_2(x) = 2\beta_2 (I_0 - \int_0^{L_1} PL_1(x)) e^{-2\beta_2 x} \qquad (7.2)$$

Now, consider that layer 1 has a considerably higher attenuation factor compared to the layer 2. In this case, according to the above equations, more energy tends to be dissipated in layer 1 and thus layer 1 would be heated up much faster than layer 2.

$$\begin{gathered} \beta_1 \rangle \beta_2 \\ I_0 \rangle I_0 - \int_0^{L_1} PL_1(x) \end{gathered} \Rightarrow 2\beta_1 I_0 \gg 2\beta_2 (I_0 - \int_0^{L_1} PL_1(x)) \Rightarrow PL_1(x) \gg PL_2(x) \qquad (7.3)$$

Hence, in this case, microwave heating leads to a differential heating, especially at the interface of the two layers.

Now, consider RCA as a composite material comprising of two layers; the adhering mortar (AM) and the recycled natural aggregate (RNA). Comparing the attenuation factors of air-dried mortar to coarse aggregate, Figure 7.1, shows that for similar moisture condition, the attenuation factor and thus the microwave energy absorption rate of mortar is higher than natural aggregates.

Hence, if RCA is exposed to microwaves, the mortar layer would be heated up much faster than RNA and thus significant differential thermal stresses may develop at the AM-RNA interface. These differential thermal stresses may be harnessed to remove the adhering cementitious mortar from RCA and thereby increase the quality and yield of the RCA products.

In addition, it must be noted that the EM properties vary significantly with the water content of a material among other parameters. As can be seen in Figure 7.1, the attenuation factor of mortar varies significantly with its water content and the microwave frequency used. There is a considerable difference, between the attenuation factor of the saturated mortar and natural aggregate. Hence, by saturating the adhering mortar in RCA, the difference between the attenuation factors of AM and RNA can be significantly increased. Such a difference may lead to high differential thermal stresses at the AM and RNA interface.

It is noteworthy that comparing to natural aggregate portion, mortar paste portion of RCA has considerably higher porosity. Hence, when immersed in water, the adhering mortar may absorb significantly more water than the natural aggregate portion of the RCA.

Moreover, it is well known that the w/c ratio increases at the interfacial transition zone and can be quite significant if bleeding is predominant; hence, ITZ normally has a higher porosity and water absorption than the bulk cementitious mortar. As a result of higher water content, ITZ is expected to heat up even faster when RCA is exposed to microwaves. Hence, higher differential thermal stresses are expected to develop at the ITZ.

Besides the differences between the water absorption and the EM properties of mortar and aggregate, the differences in the thermal properties such as the specific heat, thermal conductivity, and expansion coefficient may also contribute to the differential stresses at the mortar-aggregate interface when RCA is subjected to microwave heating. However, the effects of these properties are considered to be much less significant compared to the effects of the different EM properties. These differences are considered in the numerical simulation of the microwave –assisted beneficiation which will be presented in following.

7.2   Preliminary Experiments

In this section, the results of a preliminary study using a commercially available microwave oven conducted to investigate the feasibility of using the microwave assisted beneficiation technique to remove the adhering mortar from RCA are presented. Moreover, the effects of the RCA beneficiation on the properties of RCA is investigated

by comparing the density, water absorption and the mortar content of RCA before and after the microwave beneficiation.

The microwave oven used in this experimental study operates on an intermediate maximum power level of 1.9 KW and the limit imposed on the maximum heating time is 2 minutes at maximum power. Hence, it can only be used for small samples of RCA.

In Chapter 9 of this thesis, the design and installation procedure of an industrial microwave heating system is presented. This system may be used to operate continuously and treat enough RCA particles for further testing on the properties of RCAs treated using microwave-assisted beneficiation method. The results of the experiments conducted using the industrial microwave heating system installed in NUS structural laboratory are presented in Chapter 10 of this thesis.

7.2.1 Experimental Procedure

7.2.1.1 Sample Preparation

This experimental study was carried out on aggregates obtained from one of the Singapore's largest recycling plants; Samgreen. The production procedure of this plant includes initial crushing using a jaw crusher, manual removal of the contaminants, removal of the reinforcing bars using magnets, secondary crushing using the impact crusher, and a series of sieving and further crushing to obtain the RCA particles of the desired size fractions. Inspection showed that the original aggregate of the RCA samples taken is predominantly granite. This plant is fed from different demolition projects, having concretes with different mix proportions. The RCAs produced have very little (<1%) impurities. In this plant, RCA particles are sieved into 5 to10 mm, 10 to 20 mm and 20 to 30 mm size fractions. In the current study, RCA particles within the 20 to 30

mm size fraction were used. The density, water absorption and the adhering mortar content of RCA after microwave beneficiation were then measured (Table 7.3). To investigate the effect of the AM water content, two different moisture conditions were considered:

1. Saturated (SA): 2 kg oven-dried RCA samples were saturated by immersing them in water for 24 hours.

2. Air Dried (AD): 2 kg oven dried RCA samples were saturated by immersing them in water for 24 hours and were then kept at ambient indoor laboratory temperature and humidity conditions for 21 days.

7.2.1.2 Microwave Heating

Unlike conventional ovens, in microwave ovens, the degree of the heating and temperature rise is directly proportional to the volume of the material heated. Hence, because of the limitations of the microwave power and heating duration of the commercially available microwave oven used in this study, only batches of 150 g (oven dried weight) RCA were heated each time. The experiment was repeated for 20 batches to obtain 3 kg of the microwave treated RCA.

Each sample was heated at the maximum power of 1.9 kW for the maximum duration allowed (2 minutes). An infrared thermal camera was used to record the surface temperature of the RCAs at the end of the microwave heating. After 5 minutes cooling, samples were sieved through a 4 mm sieve to separate the delaminated adhering mortar. The density, water absorption and the remaining adhering mortar content of RCA after microwave beneficiation were then measured.

7.2.1.3 Determination of the adhering Mortar Content

The total mortar content of RCA samples before and after microwave beneficiation was determined by soaking the RCA particles in a sulfuric acid solution. The acid pre-soaking method proposed by Tam et al. (2007) was briefly reviewed in Chapter 3 of this thesis. Tam et al. (2006) used 0.1 molar solutions of HCL, H_2SO_4 and H_2PO_4 acids to remove the adhering mortar of RCA. They reported that acid pre-soaking resulted in 7.27% to 12.17% reduction in the RCA water absorption. However, such a small improvement shows that there is still a rather large amount of adhering mortar present on the RCA treated with 0.1 molar acidic solutions. Hence, this method may not be suitable for the present study.

In a preliminary experiment conducted in the present study, three different concentrations of sulfuric acid and three different soaking durations were tested to investigate whether higher acid concentrations or higher soaking durations can achieve the desired level of removal. As can be seen in Figure 7.2, the results of this study showed that only when the RCA samples were soaked for 5 days in sulfuric acid solutions of 2 molar or higher concentrations, would the adhering mortar of RCA be completely removed. Besides visual inspection, comparison between the water absorption and bulk specific gravity of RCA samples after acid soaking with that of the original granite aggregates used to produce RCA confirmed that the adhering mortar has been completely removed. Based on these results, the following procedure was used to measure the adhering mortar content of RCA in this study:

- RCA samples were oven dried at 105 °C for 24 hours.

- 1 kg samples were placed in a plastic container and soaked in two liters of sulfuric acid at a concentration of two molar.

- Samples were soaked for five days and were then washed on a 4 mm sieve to remove the detached mortar.

- The RCAs retained on the 4 mm sieve were oven dried and re-sieved through the 4 mm sieve for 5 minutes. The total RCA retained on the 4 mm sieve was weighed (Wr). The percentage of detached mortar was calculated as:

$$Mc = \frac{Wi\text{-}Wr}{Wi} \times 100 \qquad (7.4)$$

Here, Wi is the initial oven dried weight of the RCA sample.

7.2.1.4 Density and Water Absorption

As explained in Chapter 2, the presence of adhering mortar leads to a lower density and higher water absorption of RCA compared to NA. Since density and water absorption are directly related to the amount of the adhering mortar of RCA, a comparison between the density and water absorption of RCA before and after treatment can be used to investigate the efficiency of the RCA beneficiation methods. In this study, the pykometer method recommended by ASTM C127 was used to measure the density and water absorption of the RCA samples.

7.2.2 Results

The RCA particles before and after microwave heating are depicted in Figure 7.3. The amount of adhering mortar detached from RCA, as a result of microwave heating, was measured by manually sorting the detached mortar and granite aggregates and is listed in Table 7.1. Results confirmed that microwave heating can be used to effectively

remove a significant portion of the adhering mortar from RCA. A visual inspection of
particles after microwave heating showed that in most cases, especially when saturated
RCAs were heated, detachment of most of the adhering mortar had occurred at the ITZ so
that the original surface of the granite was clearly visible. The delamination of mortar was
accompanied by moderate noises and took place within 30 seconds of microwave heating
for all batches of RCA with SA moisture condition. The RCA particles of AD moisture
condition required longer heating times, up to 2 minutes. Visual inspection of the RCAs
after microwave heating showed that even though a considerable proportion of the
adhering mortar had been detached through microwave heating, there was still a small
amount of cementitious mortar that remained adhering to some of the RCA particles.
However, it was observed that the remaining adhering mortar had been significantly
softened and fissured so that it could be easily removed by exerting a small mechanical
force. Hence, incorporating a crushing or rubbing stage after microwave heating might be
used to remove the remaining weakened adhering mortar. On the other hand, as can be
seen in Table 7.1, the detached adhering mortar may contain large pieces, up to those
retained on a 10 mm sieve, which may cause difficulties in the screening and separation of
the original aggregate. Moreover, some RCA particles comprise solely of mortar. A
crushing or rubbing stage after microwave heating may be useful in turning the large
loosened mortar pieces into powder which can be easily sieved.

The surface temperature of the RCA particles after 2 minutes of microwave heating
captured using an infrared camera are shown in Figure 7.4. As can be seen the maximum
surface temperature of the RCA particles is about 140 °C which is much lower than the
temperatures required for RCA beneficiation using conventional heating methods

explained in Chapter 3. Hence, unlike the conventional heating beneficiation, microwave-assisted beneficiation should not lead to degradation in the quality of RNA due to the excessive heating.

Table 7.2 compares the density, water absorption and the amount of adhering mortar of RCA before and after microwave-assisted beneficiation. As can be seen, the water absorption of RCA reduced by 30.7 % after microwave beneficiation. Moreover, microwave beneficiation resulted in a 3.5 % percent increase in the RCA density. The increase in density and reduction in the water absorption of RCA may be directly related to the 43.2 % reduction in the amount of adhering mortar of RCA after microwave-assisted RCA beneficiation as shown in Table 7.2. Compared to the 7 to 12 % reduction in the water absorption of RCA after acid-presoaking beneficiation as reported by Tam et al. (2006), the 30.7 % reduction in the water absorption of RCA after microwave heating may be considered as a significant achievement. It should be noted that in the current experiment utilizes a commercially available microwave oven with limited power. The efficacy of microwave beneficiation is expected to increase tremendously by using a suitably designed industrial microwave heating systems in combination with an appropriate RCA rubbing stage, after microwave heating.

7.3. Numerical Study

The capability of microwave heating to detach the adhering mortar of RCA was confirmed through the experimental study reported above. To examine the feasibility of using the microwave-assisted RCA beneficiation technique on an industrial scale and to investigate the effect of RCA water content on the beneficiation process, a possible

industrial microwave-assisted aggregate beneficiation system is numerically modeled in this section.

7.2.1 Model Description

As can be seen in Figure 7.5, a simple microwave assisted RCA beneficiation system may include the microwave generator unit, the microwave waveguides to transfer the microwave power from generator to the horn, a horn (antenna) to spread the microwave power over an specific area, a microwave chamber to contain the RCA particles, a stirrer to provide a more uniform heating pattern within the chamber and churning of the RCA particles during microwave heating, and a conveyor belt to transfer RCA to the sieving facility after microwave beneficiation. The microwave generator simulated in this study is considered to operate at a frequency of 2.45 GHz and 10 kW power. Two different moisture content conditions, saturated and air-dried, are considered to investigate the effects of the water content of RCA on the magnitude and pattern of the development of temperature rise and thermal stresses across the RCA particle.

Perfectly spherical RCA particles comprising a 10 mm granite core and a 2 mm thick adhering mortar are considered (Figure 7.6). The RCAs are assumed to be directly exposed to a TE_{10} microwave mode of 10 kW power through a standard waveguide (Table 5.1) and a horn of 10 cm × 10 cm dimensions at its larger end as shown in Figure 7.5. Hence, the microwave power is distributed over an area of 100 cm^2. The temperature rise and stresses developed in the RCA particle located at the center of the microwave applicator (horn) are presented in the results of this study.

7.2.2 Formulation

Similar to the microwave heating of concrete discussed in Chapters 5 and 6, simulation of the microwave heating of RCA also involves coupled electromagnetic, thermal and structural analysis. Maxwell's equations are solved to investigate the propagation of microwave radiation through the microwave waveguide, horn, and inside the heating chamber and RCA particles. The resulting microwave power dissipation in RCA particles are calculated using the similar modeling procedure as explained in Chapter 6. The microwave power dissipation is used as the input for the heat transfer analysis to calculate the temperature rise and temperature distribution across the RCA particles. Moreover, the structural-thermal analysis is conducted to calculate the developing differential thermal stresses inside AM, recycled granite aggregate (RNA) and their ITZ.

7.2.3 Results

Similar to Chapters 5 and 6, the Comsol Multiphysics finite element package is used to model the coupled electromagnetic, thermal and structural analysis to evaluate the temperature rise and thermal stress development in RCA particles during the microwave beneficiation process explained above. Properties of the adhering mortar and the granite RNA are listed in Table 7.2.

7.2.3.1 Temperature Rise and Thermal Stresses

The temperature distribution, temperature gradient, and thermal stresses developed in the saturated and air-dried RCA particles are illustrated in Figures 7.7 and 7.8, respectively. The tensile and compressive stresses are illustrated by positive and negative signs, respectively. As can be seen, as a result of the differences in the EM, thermal and mechanical properties of granite and the cementitious mortar, the temperature gradient

164

and thus thermal stresses increase significantly at the interfacial zone. Moreover, comparing the temperature rise and stresses developed at saturated and air-dried moisture conditions confirms that saturating the adhering cementitious mortar can significantly increase the efficiency and speed of the RCA beneficiation process. As can be seen in Figure 7.7, at saturated moisture condition, after a considerably short microwave heating duration, the normal tensile stresses at the ITZ can easily exceed the strength of the bond between the mortar and aggregate particle in normal concretes. Taking into account, the higher water content at the ITZ due to its higher porosity and water absorption (especially when bleeding is possible), in practice, the temperature gradient at the ITZ may be even higher. Moreover, considering the significantly higher tensile strength of natural granite compared to the cementitious mortar, the stresses developed in the granite aggregate particles are not expected to cause any damage to the integrity of the granite particle unless fissures are present.

The microwave beneficiation system modeled in this study uses a microwave horn to direct microwave power from the top of the microwave chamber towards the incident surface of the RCA particles. Hence, as can be seen in Figures 7.7 and 7.8, only the mortar adhering to the top exposed surface of the RCA particles is substantially heated and stressed. In practice, stirrers should be used in the RCA beneficiation chamber to ensure a uniform microwave power distribution so that the RCA particles can be heated uniformly from all directions. Using a stirrer in microwave beneficiation systems may lead to a more uniform delamination of the mortar adhering to the RCA particles and thus higher quality RCA. However, due to the lack of the accurate techniques to model the

stirrers' function using the finite element method, they were not considered in the RCA beneficiation system simulated in this study.

7.2.3.2 Estimation of the Production Rate

Given the 100 cm^2 area of the microwave applicator considered in the numerical study and assuming 5 seconds as the average time required to reach a stress level exceeding the bond strength between mortar and aggregate, approximately 650 kg/hr of RCA may be processed using just one 10 kW microwave generator. By using an array of microwave generators and applicators in practice, higher yields seem to be easily achievable. However, field tests are necessary to confirm the results of this study.

7.3 Conclusions

The feasibility of using microwave heating to increase the quality of RCA through removal of its adhering mortar was experimentally and numerically investigated in this chapter. Results confirm that microwave heating may be effectively used to remove cementitious mortar adhering to RCA particles through developing high temperature gradients and thus high thermal stresses, especially at the interfacial zone. Furthermore results showed that saturating the RCA particles prior to exposure to microwaves can significantly increase the yield and quality of the RCA produced.

In addition, besides removal of the adhering mortar, the microwave beneficiation of RCA is also expected to increase the quality of RCA by breaking the aggregates along the possible fissures present in the particle. Results showed that unlike conventional heating beneficiation, in microwave assisted beneficiation method, RCA particles are heated to a much lower temperature and for a significantly shorter duration which should eliminate the concerns about the possible degradation of the aggregate particle during processing.

Shorter processing time compared to methods proposed by Tam et al. (2006) and Abbas et

al. (2007), and less energy consumption in comparison with the heating and rubbing

method are among the advantages of microwave-assisted beneficiation. Moreover, unlike

the acid presoaking method, microwave assisted beneficiation method seems to raise

virtually no foreseeable durability concerns.

Table 7.1 Percentages of the cementitious mortar detached and original aggregate extracted after microwave heating of saturated RCA particles

Sieve Size (mm)	Mass Percentage of the RCA Retained on the Sieve (%)	
	Granite Extracted	**Delaminated Cementitious Mortar**
20	57.72	
10	22.59	6.77
4.75	2.79	5.09
2.36		2.31
1.18		1.33
0.075		1.10
Total	**83.39**	**16.60**

Table 7.2 Input data for numerical modeling

	Granite	Adhering Mortar
Dielectric Constant	6	6.42
Electric Conductivity (mohs/m)	0.071	0.372
Thermal Conductivity (J/m^{2}s°C)	4.3	1.3
Expansion Coefficient (10^{-6}/°C)	11	19
Specific Heat (J/kg°K)	800	1600
Modulus of Elasticity (GPa)	50	25
Microwave Frequency (GHz)	2.45	
Incident Microwave power (kW)	10	
Ambient Temperature (°C)	25	

Table 7.3 Comparison of the RCA properties before and after microwave beneficiation

Property	Before Microwave Beneficiation	After Microwave Beneficiation	Improvement %
Water absorption	5.2	3.6	30.7
Bulk Specific Gravity (kg/m^3)	2290	2370	3.5
Adhering Mortar Content (%)	≈ 37	≈ 21	43.2
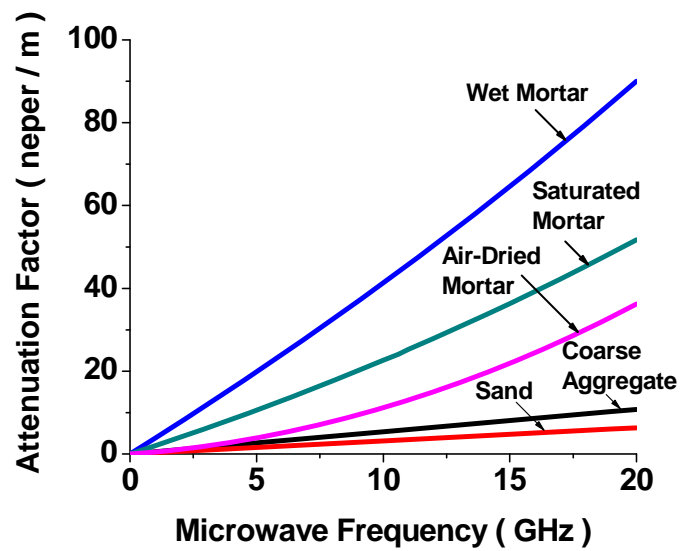
Figure 7.1 The attenuation factors of coarse aggregate, sand, and cementitious mortar
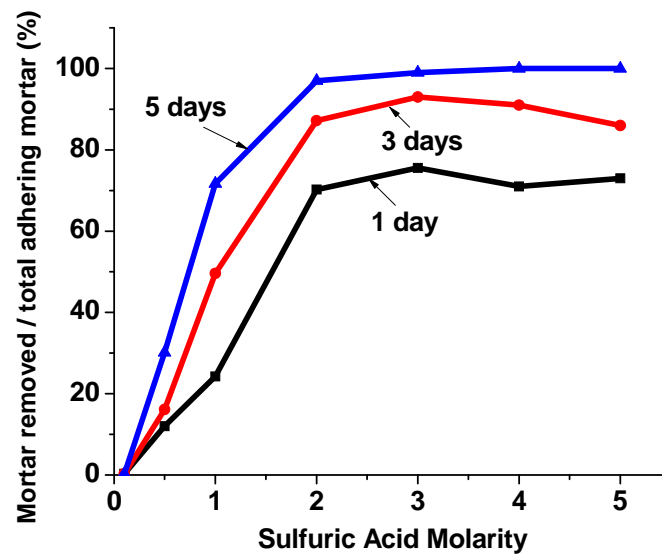
Figure 7.2 variation of the percentage of the adhering mortar removed with the sulfuric acid concentration and soaking duration

Figure 7.3 RCA particles before and after two minutes of microwave heating at 1.9 kW power in a commercially available microwave oven.
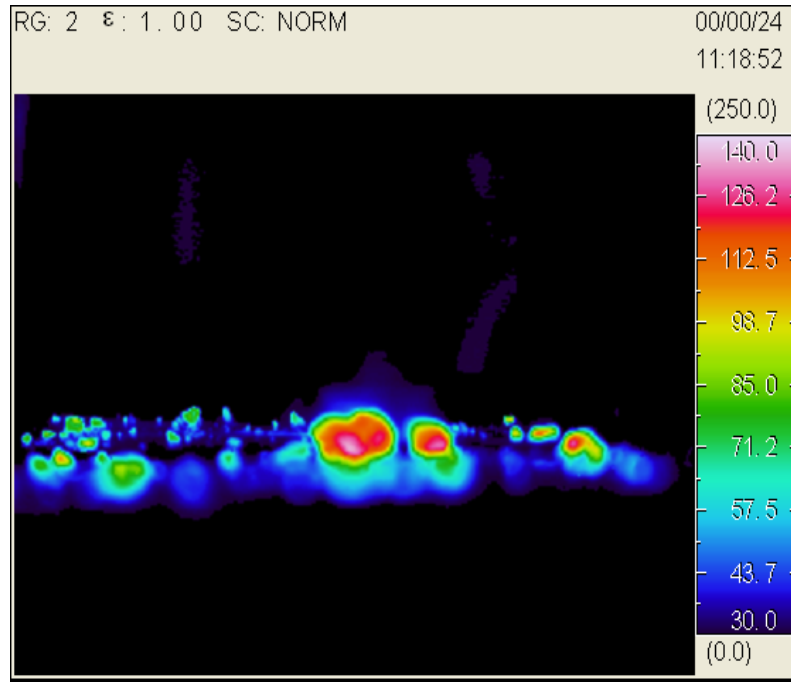
Figure 7.4 Surface temperature of RCA particles after two minutes microwave heating at 1.9 kW in a commercially available microwave oven.
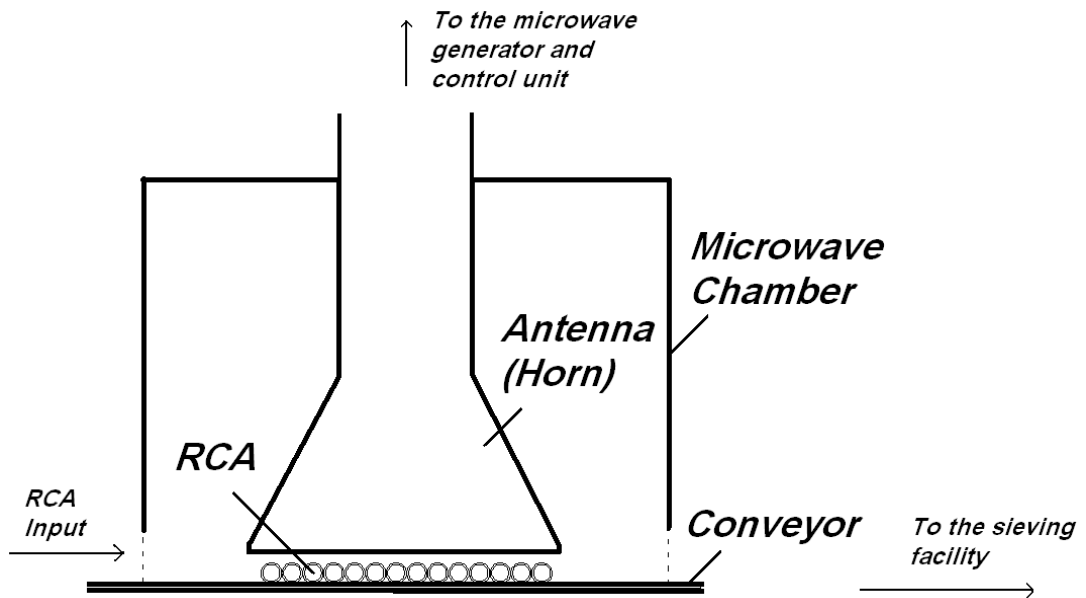
Figure 7.5 The RCA beneficiation system considered for numerical simulation
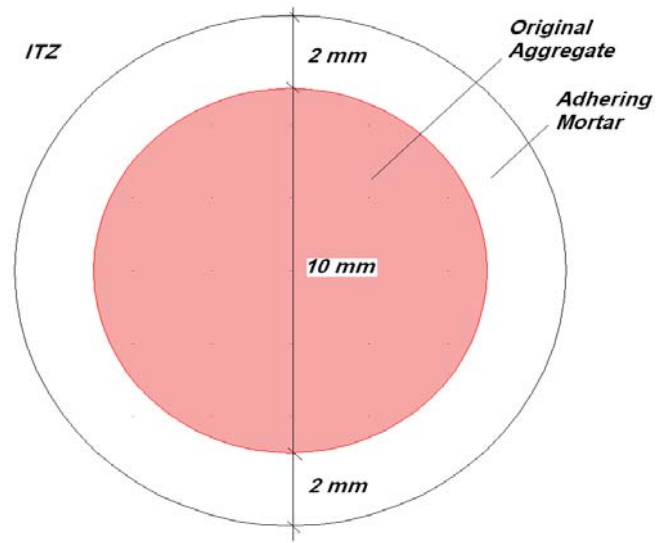
Figure 7.6 The RCA particle considered in numerical model
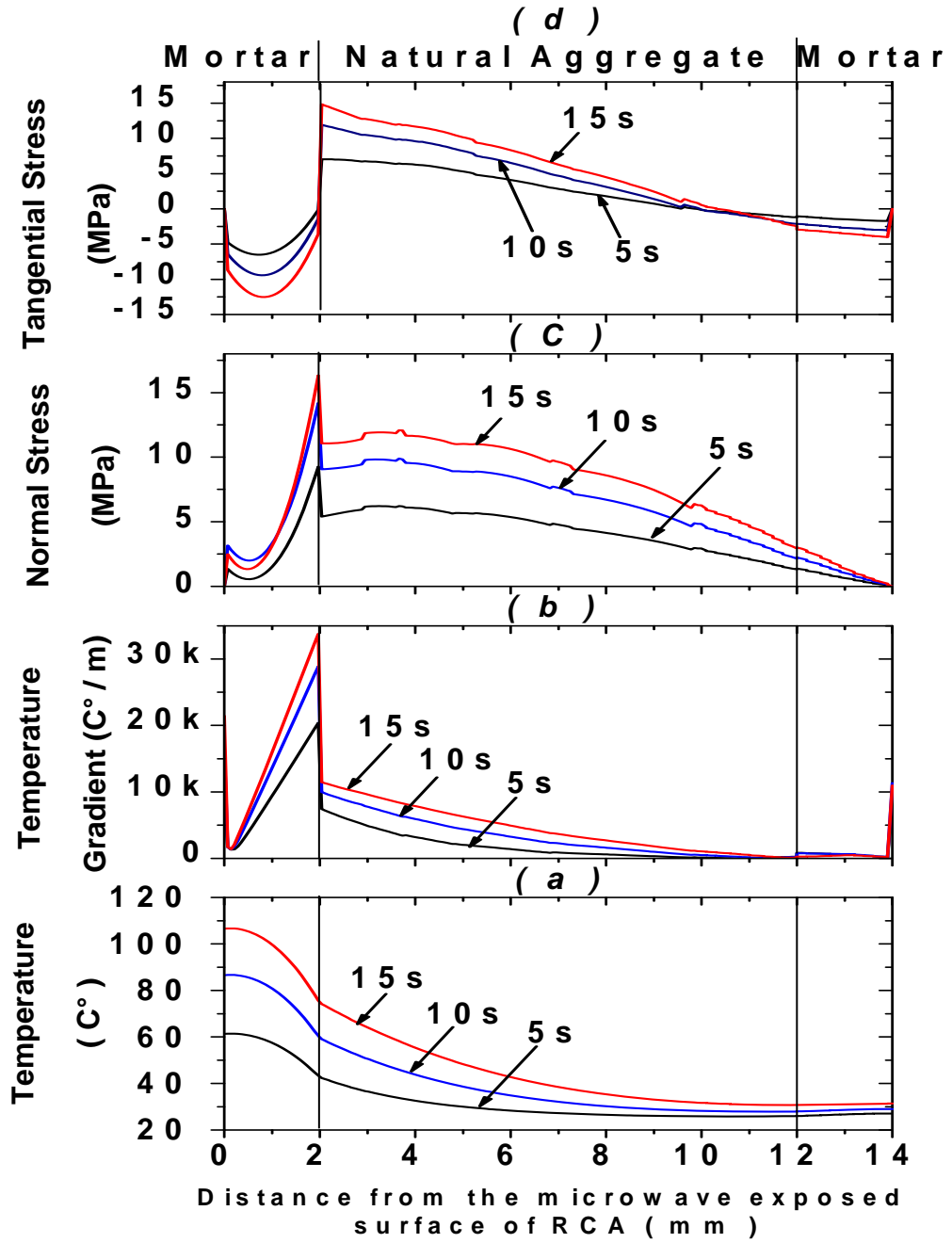
Figure 7.7 (a) Temperature, (b) Temperature gradient, (c) Normal stress, and (d) Tangential stress in a saturated RCA particle subjected to microwave of 2.45 GHz frequency and 10kW power
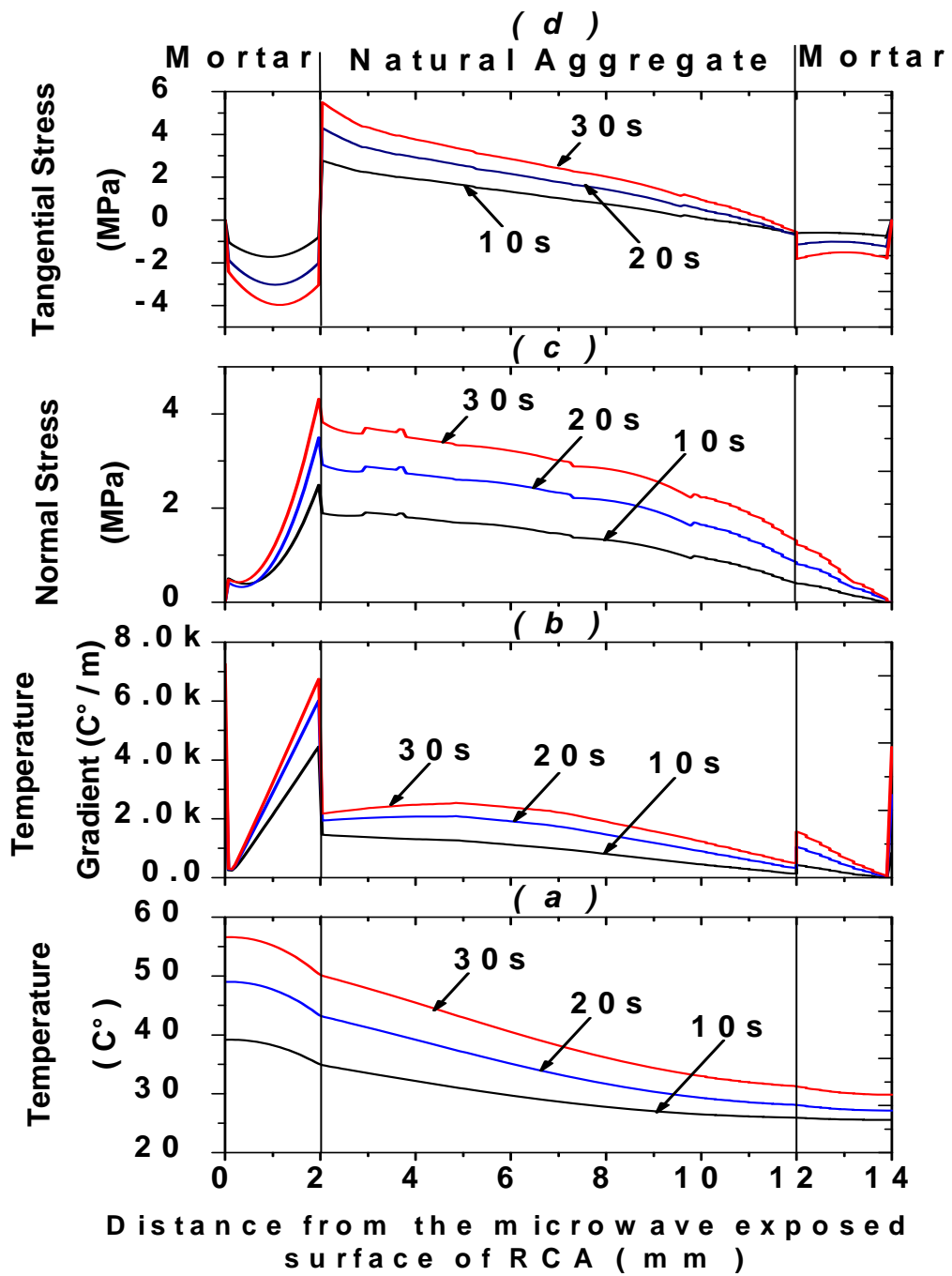
Figure 7.8   (a) Temperature, (b) Temperature Gradient, (c) Normal Stress, and (d) Tangential Stress in an air dried RCA particle subjected to microwave of 2.45 GHz frequency and 10kW power

Chapter 8 : Temperature Sensing in Microwave Heating of Concrete Using Fiber Bragg Grating Sensors

8.1 Background

The application of microwave heating in the removal of the contaminated surface layer of concrete as well as in the removal of the adhering cementitious mortar of RCA were numerically investigated in Chapters 5 to 7.

As shown in Chapters 5 and 6, in the microwave decontamination of concrete, the thermal stresses and pore pressure that develop in the concrete block are a function of the temperature and its gradient. Hence, temperature monitoring inside the concrete block can be used as a simple method to monitor the thermal stresses and pore pressures developed and thus can be used as a process control tool to predict the removal thickness and to estimate the microwave power dissipation pattern in the microwave heated concrete.

Moreover, as explained in Chapter 3, heating of aggregates such as granite at high temperatures, e.g. above 300 °C, may lead to degradation in their quality. As was shown in Chapter 7, the microwave assisted beneficiation can be used to remove the adhering mortar from RCA by developing high thermal stresses in the adhering mortar and its

interface with the natural aggregate portion of the RCA (RNA) while heating the RCAs to much lower temperatures, e.g. 150-300 °C, and for a significantly shorter heating duration compared to the conventional heating beneficiation methods. Hence, in microwave assisted beneficiation of RCA, temperature monitoring can be used as a control process tool for choosing the appropriate microwave power and heating duration for a specific volume of RCA to prevent unnecessary excessive heating which may lead to degradation of the extracted aggregate.

Besides the above two applications which were dealt with in this study, temperature monitoring can be a very important process control tool in other microwave assisted applications in civil engineering such as curing of the prefabricated concrete at early ages.

Microwave heating has been reported to be a rapid and efficient concrete curing method. Previous studies have shown that, unlike steam cured concrete, microwave cured concrete can gain considerably high strengths in just a few hours without sacrificing its long term properties. To achieve a uniform microwave heating pattern, besides choosing an appropriate microwave frequency, the microwave curing chamber should also be properly designed. However, there are not yet any reliable design techniques to guarantee the uniformity of microwave power across a microwave curing chamber. Thus, the design is usually based on the engineer's experience. Hence, a process control technique is required to monitor the uniformity of the microwave heating throughout the curing process. Undoubtedly, the simplest and most logical way to control a heating process is temperature monitoring. Moreover, it has been reported that overheating of the concrete specimens during microwave curing may adversely affect their long term properties (Leung and Pheeraphan, 1995). Leung et al. (1997) showed that an optimal microwave

curing process which provides high strength at both the early and later stage can be achieved with the help of feedback temperature control.

In General, temperature, despite its importance, is one of the most difficult parameters to measure in a microwave environment. Aside from concrete curing, RCA beneficiation and concrete surface decontamination applications, sampling temperature is the most common process-control parameter of microwave processing in almost all applications. Inaccuracies in temperature measurements can lead to erroneous indications of process temperature and provide misleading representations of the process efficiency.

The current study is aimed at examining the capability of conventional temperature measurement instruments as well as evaluating new sensing techniques and instrumentation to measure the temperature rise of concrete when subjected to microwave heating.

In the microwave heating of concrete, the temperature measurement has to be made directly on or within the sample, not merely in its vicinity. This is because microwaves heat the sample volumetrically and not its surroundings. Hence, any temperature probe used must maintain good contact with the sample for accurate temperature measurements.

Thermocouples are the most commonly used temperature measurement sensors. Leung et al. (Leung and Pheeraphan, 1995 and 1997) used K type thermocouples to measure the concrete's temperature during microwave curing. However, because of their metallic nature, thermocouples are not immune to electromagnetic interference and may be inaccurate when utilized in a microwave field. The presence of an electrically large ($>\lambda/10$, where λ is the wavelength of the electromagnetic wave) metallic temperature probe in a microwave environment may cause distortions to the electromagnetic field

distribution and induce currents that can affect the electronics used for temperature measurement. The presence of an electromagnetic field may also give rise to errors due to self heating, heat conduction or excessive localized heating, particularly at the tip of the probe.

Optical fiber sensor is well-known to be virtually immune to electromagnetic fields (Schmaup, 1995; Pennisi et al., 2002; Degamber, 2003; McSheny et al., 2004). Because of their glass-based nature, optical fibers do not interact with the electromagnetic field and hence, maintain their accuracy in the presence of microwaves. Moreover, optical fiber sensors are small in size, rendering them suitable for microwave heating ovens where opening sizes are intentionally made small due to safety considerations.

The properties of optical fibers allow for innovative approaches in the design of optical sensors. For this reason, an enormous number of fiber-optic sensor types have been developed over a very short period of time. Recently, Fiber Bragg Grating (FBG) optical sensors have attracted a great deal of attention as reliable temperature and strain sensors. These sensors have found a wide spread applications in civil engineering (Maher, et al., 1996; Yong Wang et al., 2001; Yung Bin Lin et al., 2004; Chuan Wang, 2006). The concept of these sensors is to relate the changes in the wavelength of the reflected wave to the desired measurand. Besides the general advantages of optical fibers, FBGs have the capability to be used in multiplex arrangements. This characteristic enables the possibility of placing different sensors along a single fiber and measuring the desired properties at different points along the fiber, simultaneously. Even though commercially packaged FBGs have been used in strain, pressure, and temperature measurements in civil

engineering, their performance in the presence of strong electromagnetic fields has not been investigated previously.

Besides thermocouples and optical fibers, non-contact instruments such as infrared cameras may be also used to measure the concrete's temperature during the microwave heating. Rattanadecho et al. (2008) used a temperature feedback system including an infrared camera to improve the performance of the microwave curing of concrete specimens.

The current study was aimed at investigating the accuracy of thermocouples and FBG sensors for measuring the sample's temperature during microwave heating of the concrete. In order to verify their measurement accuracies, both the FBG sensor and the thermocouple measurements were collected and compared with the results obtained using numerical modeling and measurements taken using an infrared thermo-tracer camera.

8.2 Temperature Sensors

In the following sections, the basic concepts of temperature monitoring and previous experiences on the use of thermocouples, thermo tracer cameras and optical fiber temperature sensors for measuring the concrete's temperature are reviewed.

8.2.1 Thermocouples

Thermocouples are one of the most widely used types of temperature sensors in civil engineering experiments and practice. A thermocouple consists of two dissimilar metals joined together at one end. When the junction of the two metals is heated or cooled, a voltage is produced that can be correlated back to the temperature. The thermocouple alloys are commonly available as wires. A thermocouple is available in different

combinations of metals or calibrations. The four most common calibrations are graded as type J, K, T and E. There are also high temperature calibrations R, S, C and GB. Each type (or calibration) has a different temperature range, although the maximum temperature varies with the diameter of the wire used in the thermocouple (www.temperatures.com, 2007). In this study, T type thermocouples capable of measuring temperatures up to 250 °C are used to measure the concrete's internal temperature when heated by microwaves.

8.2.2 Infrared Thermo Tracer Cameras (Radiation Thermometry)

Infrared imaging is widely used for nondestructive testing of industrial products, in aircraft surveillance and for medical diagnostics. It has also been used for quick characterizations of microwave components (Kiwamoto et al., 1997).

The thermo tracer is a non-contact and highly sensitive infrared radiometric camera. A surface of temperature **T** emits infrared radiation of intensity $\mathbf{I = A\ T^4}$, where **A** is a constant. Radiometric measurements of **I** serve as an accurate indication of **T.**

The infrared radiation emitted from the measuring object is detected and converted to an electric signal by the two-dimensional uncooled focal plane array detector and the amplitude analog temperature signal is converted to a digital signal. The digital signal is displayed as a thermal image in color or black and white. In the current study, a NEC TH9100 infrared camera capable of measuring surface temperature up to 250 °C is used to capture the concrete's surface temperature immediately after microwave heating.

8.2.3 Optical Fiber Sensor

As previously stated, in an electromagnetic field, the use of conventional temperature sensors such as thermocouples may not be satisfactory. The main reasons being the

electromagnetic interference caused by induced currents and voltages in the metallic conductors and the local heating of the sensor due to electromagnetic induction (Pennisi et al., 2002). In order to reduce or eliminate errors due to such effects, temperature sensors based on optical fibers have been studied. Besides of their relative immunity to electromagnetic fields, the extremely small size (125 μm in diameter) of the optical fiber can facilitate wiring of the needed instrumentation inside the microwave heating chamber. The size of the openings on the microwave heating chamber is usually designed to be small due to safety considerations. The small opening makes it difficult to deploy conventional thermocouples for measurement.

The use of optical fibers as temperature sensors has been investigated by many researchers in different fields (Lagakos et al., 1981; Berkoff, 1992; Jaehoon Jung et al., 1998; Ramesh and Wong, 1999; Protopopov et al., 2000; Yong Wang et al., 2001; Pennisi et al., 2002; Yonglin Huang et al., 2003; Silva et al., 2004; Piotr Kisala et al., 2004; Yage Zhan et al., 2004; Yung Bin Lin et al., 2004; Yage Zhan et al., 2005). Several researchers developed optical fiber-based temperature sensors by replacing a length of the optical fiber's cladding with materials that have a temperature-dependent refractive index (Pennisi et al., 2002). The variation of the refractive index which may lead to a variation in the optical power transmitted along the fiber can be related to temperature change. The fluorescence life-time approach has also been used in a few studies to develop fiber optic temperature sensors. These sensors have been reported to work satisfactorily in conditions ranging from below room temperature to above 300 °C (Wade et al., 2004).

8.2.3.1 Fiber Bragg Grating (FBG) Sensors

In recent years several studies have been conducted to investigate the possibility of using FBGs as temperature sensors in civil engineering. In these studies, FBG sensors have been used mainly for the temperature monitoring of the concrete structures (Yong Wang et al., 2001) and concrete laboratory specimens (Yung Bin Lin et al., 2004; Chuan Wang, 2006) subjected to elevated temperatures while negligible or weak electromagnetic fields were present. There is very limited information on the potential of using the FBG sensors to monitor the concrete's temperature in the presence of strong electromagnetic fields, such as that present in the microwave curing or microwave decontamination of concrete. Nevertheless, there have been few reports on the satisfactory employment of FBGs in other non-civil engineering applications involving the strong electromagnetic fields (Romero et al., 1997; Protopopov et al., 2000; Pennisi et al., 2002; Degamber, 2003).

8.2.3.2 Operating Principle of FBG Sensors

A Bragg grating is a periodic structure fabricated by exposing a photosensitized fiber core to ultraviolet light (Meltz et al., 1989) .When light propagating along a single-mode fiber encounters periodic variation in the refractive index of the in-fiber grating, at each point of the refractive index transition, a small amount of light is reflected. If each of the reflections is in phase, they will add coherently and produce a large net reflection from the grating. This phase matching occurs at only one specific wavelength, and this wavelength is called the Bragg wavelength. A change in the length of the grating due to thermal expansion, strain or pressure leads to a change in the grating spacing. This change in the grating spacing and the change in the FBGs refractive index with temperature produce a

shift in the Bragg wavelength (Hill, 1997). The Bragg wavelength is related to the grating period Λ and the effective refractive index of the fiber n by:

$$\lambda_B = 2\Lambda n \qquad (8.1)$$

Both the effective refractive index and the grating period vary with changes in strain (ε), temperature (T) and pressure (P) imposed on the fiber. An applied longitudinal strain or pressure (radial strain) will shift the Bragg wavelength through expansion or contraction of the grating periodicity and through the photo-elastic effect. Temperature affects the Bragg wavelength through thermal expansion and contraction of the grating periodicity and through the thermal dependence of the refractive index. These effects are well understood and, when adequately modeled, provide a means for measuring strain, pressure and temperature. The shift of the Bragg wavelength with temperature and strain is given by the expression:

$$\Delta\lambda_B = 2n\Lambda\left[\left(1 - P_{eo}\right)\Delta\varepsilon + \left(\alpha + \xi\right)\Delta T\right] \qquad (8.2)$$

where P_{eo} is the effective elastic-optic coefficient, $\Delta\varepsilon$ is the applied strain change, α is the thermal expansion coefficient, ξ is the thermo-optic coefficient and ΔT is the temperature change. The strain response depends on the physical elongation of the sensor and the change of fiber index owing to photo-elastic effects, whereas the temperature response depends on the fiber material's thermal expansion and the temperature dependence of the refractive index due to thermo-optic effects. Such a thermally induced Bragg wavelength shift is given by (Lagakos et al., 1981):

$$\Delta\lambda_B = 2\Delta n\Lambda + 2n\varepsilon_z\Lambda = 2n\Lambda\{\frac{\partial n}{\partial T}\frac{1}{n}\Delta T + \varepsilon_z - \frac{n^2}{2}\left(P_{11} + P_{12}\right)\varepsilon_r + P_{12}\varepsilon_z\} \qquad (8.3)$$

Where, ε_z and ε_r represent the axial strain and the radial strain in the core, respectively, and P_{11} and P_{12} are the Pockels coefficients of the core (Seo and Kim, 1999). Considering Equation 8.1, if the lateral and longitudinal strains of the fiber are set to zero, temperature would be directly related to the change in the wavelength:

$$\Delta\lambda_B = 2\Delta n \Lambda + 2n\varepsilon_z \Lambda = 2n\Lambda \frac{\partial n}{\partial T}\frac{1}{n}\Delta T = K_T \Delta T \qquad (8.4)$$

The lateral and longitudinal displacement freedom of FBGs can be provided through the design of the sensor's coating or by avoiding the constraints when installing the FBG sensors on the structures to be instrumented. Equation 8.4 clearly illustrates the concept behind an FBG temperature sensor. The coefficient K_T may be obtained through calibration.

Many researchers have tried to increase the sensitivity of FBG temperature sensors. Generally, two techniques have been used for this purpose. In the first technique, the FBG sensors are coated using different coatings with higher expansion coefficients than the bare FBG itself (Albin, 1998; Seo and Kim, 1999). By using such coatings, a given temperature change will translate to a higher thermal expansion of the FBG and hence, will increase the sensitivity of the FBG sensors.

In the second technique, usually two metallic pieces are connected to both ends of the FBG sensors and the difference in the expansion of these two different metals, due to the difference in their thermal expansion coefficients, is translated into a temperature difference (Yage Zhan et al., 2005).

Theoretically, the optical fiber sensors used for temperature measurement in an electromagnetic field cannot have coatings unless the coating is transparent to electromagnetic waves. This is because microwaves heat the sample itself volumetrically

and not the surroundings. Hence, if the fiber's coating is made of a microwave absorbent material, it will itself be heated up and as a result, the optical fiber would measure the temperature of its own coating rather than the temperature of the material which is meant to be monitored. Moreover, optical fibers with a metallic coating or those based on the differential expansion of two metallic pieces at the FBG ends cannot be used for temperature measurement in electromagnetic fields. The main reasons for this are the electromagnetic interference caused by the currents and voltages in the metallic conductors and the local heating of the sensor head due to electromagnetic induction (Pennisi et al., 2002).

8.3 Experiments

In this study, a series of experiments were conducted to investigate the feasibility of using FBGs as temperature sensors for concrete specimens during microwave heating. These experiments were also targeted at illustrating the inaccuracy of conventional thermocouples for temperature measurement in a microwave field.

A commercially available microwave oven generating microwaves at 2.45 GHz frequency and a maximum power of 1900 W was used. This oven consists of two magnetrons each having a maximum power of 950 W. The microwaves generated are transferred to the microwave cavity through two WR340 rectangular waveguides. As can be seen in Figure 8.1, this oven originally included a mode stirrer to help increase the uniformity of the microwave power inside the cavity. However, due to difficulties in the numerical modeling of the stirrer, it was removed so that the results of the experimental work can be compared with the results of the numerical modeling.

8.3.1 Type of the FBG Sensors

As stated earlier, in many of the techniques reported in available literature, optical fiber temperature sensors have a metallic shielding and/or two metallic plates are usually used in the optical fiber to correlate the difference in the strain of these metals to the temperature (Albin, 1998; Seo and Kim, 1999; Yage Zhan et al., 2005). However, the existence of metallic pieces in the temperature sensors makes them unsuitable for use in an electromagnetic field. On the other hand, coated optical fibers which are usually used for strain and temperature measurements in civil engineering also do not seem suitable for temperature measurement in a microwave oven, as microwaves may heat the coating to different extents compared to the concrete specimen, depending on the difference between the dielectric properties of the coating material and concrete. Figure 8.2 shows a commercially-packaged FBG sensor before and after exposure to microwave heating. The commercial sample used contains metallic fiber splicers within the outer sheath and proved to be unsuitable for the present study. A simple test demonstrated that, after a few seconds of microwave heating, the plastic coating next to the metallic splicers began to ignite as it absorbed microwave energy. As the metallic splicer was exposed to microwave radiation directly as a result of loss of the plastic coating, the induction phenomenon led to sparks being generated inside the microwave chamber. This finally led to the splitting of the fiber next to the metallic splicer. This simple experiment clearly showed that the commercially-packaged FBGs sample tested was not suitable for temperature measurement in a microwave filed. In view of this, bare FBGs without any kind of coating and metallic splicer were chosen in the current study. The two bare FBG sensors chosen had the Bragg wavelengths of 1538 nm (FBG1) and 1547 nm (FBG2).

8.3.2 Calibration of FBG Sensors

Prior to the tests, temperature calibration of the FBG sensors was conducted. The calibration process allows for the determination of the thermal-optic coefficient (K_T) of the sensors used. Two T type thermocouples were fixed in position next to the grating section of the FBG in a conventional oven. The change in the wavelength of the fibers and the temperature measurements of the thermocouples were recorded using an FBG interrogator system and a data logger, respectively, as the oven's temperature was increased from 20°C to 120 °C. The calibration curves of the two bare FBGs used in this study are shown in Figures 8.3 and 8.4.

8.3.3 Instrumentation

As shown in Figure 8.5, three T type thermocouples capable of measuring temperatures up to 250 °C were embedded at different depths inside the concrete specimens during casting to monitor the internal temperature change, while FBG sensors were mounted on the surface of the specimens at the time of testing to measure the surface temperature. These configurations of FBGs and thermocouples were chosen to address two issues. Firstly, the thermocouple's metallic head should not be exposed when placed in the microwave oven. The exposure of the metallic head of a thermocouple leads to induction phenomenon between the thermocouple's head and the microwave cavity which will most likely lead to erroneous readings. Secondly, to verify the accuracy of the FBG sensors in this application, the readings of the FBG sensors need to be compared with measurements obtained using another accurate and reliable instrument. The non-contact infrared camera used for verification of the FBG measurements in these experiments

could only capture the surface temperature. Hence, for comparison purposes, FBGs were used to monitor the same surface as monitored by the infrared camera.

8.3.4 Microwave Heating

The concrete specimens used in this study were all 70 day old and in a saturated condition at the time of testing. Specimens were heated using the commercially available microwave oven at two different power levels of 50% (950 W) and 100% (1900 W) for 2 minutes. Immediately after the heating was completed, the cavity's door was immediately opened and the surface temperatures of the specimens were captured using the infrared camera.

8.4 Numerical Modeling

In order to double-check the accuracy of the experimental results and also to verify the accuracy of the analytical modeling methods presented in Chapter 6, the microwave oven used in these experiments was accurately simulated using the electromagnetic module of the COMSOL MULTIPHYSICS commercial finite element package. The model created is schematically shown in Figure 8.6.

The analytical modeling of the microwave heating process involves solving Maxwell's equations which govern the propagation of microwave radiation through concrete and the microwave's waveguide or cavity, and the heat transfer equation which governs heat absorption and the resulting temperature rise in the concrete block. A detailed explanation of the numerical modeling was presented in Chapters 5 and 6.

The mechanical, thermal and electromagnetic properties of concrete used for modeling are similar to those assumed in Chapter 5 and are listed in Table 5.3. It is noteworthy that as explained in Chapter 4, each concrete specimen has a unique set of

electromagnetic properties affecting the way it interacts with microwaves. These
properties vary with the chemical composition of concrete, proportion of the various
constituents used, water content, temperature, and the microwave frequency. The
electromagnetic properties calculated in Chapter 4 using the data reported by Rhim et al.
(1998) are used in the current numerical study.

8.5 Results and Discussions

The experimental test described above was conducted on 6 concrete specimens. A
summary of the results obtained for all the specimens tested are presented in Tables 8.2
and 8.3. Figures 8.7 and 8.8 show the results of temperature measurement using
thermocouples, the infrared thermo tracer camera and FBG sensors as well as the
temperatures predicted through numerical modeling, for two typical concrete specimens
when heated at two different microwave power levels of 50% (950 W) and 100% (1900
W).

It should be noted that the temperature distribution is a function of the
electromagnetic energy distribution in the microwave oven and in the concrete specimen.
The electromagnetic energy distribution varies with the design of the microwave chamber
and with the electromagnetic properties of concrete. Investigating the phenomena leading
to different microwave heating and temperature patterns is beyond the scope of this
chapter. The current study was only aimed at searching for appropriate instrumentation for
temperature measurement of typical microwave heated concrete specimens in applications
such as microwave curing of prefabricated concrete or microwave decontamination of
concrete.

8.5.1 Thermocouples Accuracy

Prior to the tests, considering the metallic nature of the thermocouples' wires, it was expected that the thermocouples would be either dysfunctional or inaccurate in an electromagnetic field such as microwave oven. As expected, the results of this study (Table 8.2) confirmed that the conventional thermocouple is not suitable for use as temperature sensors for concrete in a microwave filed. As can be seen in Table 8.2, it was observed that in 3 (out of 6) of the tests conducted, at least one of the embedded thermocouples was totally damaged or that the temperatures monitored were erroneous. Figures 8.7 and 8.8 present the temperature measurement results for two of the three cases in which all the thermocouples were functional during microwave heating. The results of temperature measurements using thermocouples embedded at three different depths (Fig 8.2) within the concrete specimens heated at two different microwave power levels of 50% and 100% are shown in Figures 8.7(c) and 8.8(c). All the results are presented over a 4 minutes (240 s) period which includes 2 minutes microwave heating (0 to 120s) and two minutes cooling (120s to 240s).

Furthermore, the temperatures at the locations monitored using embedded thermocouples predicted through numerical modeling are shown in Figures 8.7(d) and 8.8(d). As can be seen, temperature increases almost linearly to the peak temperature during microwave heating and the rate of this increase is directly proportional to the microwave power level. Moreover, as can be seen in Figures 8.7(d) and 8.8(d), during the cooling period (120s to 240s), the temperature at each location tend to converge to a stable average value as heat transfers from the hotter point to the cooler point. By comparing the temperature readings of the thermocouples with the temperature

measurements obtained through numerical modeling, it is obvious that during microwave heating (0 to 120 s), the thermocouples' readings were obviously erroneous. As can be seen in Figures 8.7(c) and 8.8(c), the thermocouple measurements are nonlinear and fluctuate in some cases, e.g. the T2 thermocouple in Figure 8.7(c). In addition, there is a considerable difference between the thermocouples measurements and the numerical predictions during the microwave heating period.

The inaccurate thermocouple's measurements during microwave heating period clearly highlight the disruptive effect of microwaves on the accuracy of the thermocouples. This suggests that conventional thermocouples cannot be used to monitor the concrete specimen's temperature in applications such as microwave curing or microwave decontamination of concrete. Nevertheless, comparing the thermocouples' temperature measurements during the cooling period (120s to 240s) with the numerical predictions (Figures 8.7(d) and 8.8(d)) shows that while inaccurate during the microwave heating period, the thermocouples measurements show acceptable accuracy during the cooling period without any microwave radiation present.

8.5.2 FBG Sensors

The temperature measurements of the FBG sensors are shown in Figures 8.7(e) and 8.8(e). Moreover, the numerical temperature predictions at the same locations monitored by the FBGs are depicted in Figures 8.7(f) and 8.8(f). As can be seen, the results are very encouraging, showing almost similar development and peak temperature reached during both microwave heating and cooling.

As can be seen in these figures, for both FBG sensors (FBG1 and FBG2), experimental measurements and numerical predictions show an almost linear increase in

the concrete's surface temperature during the microwave heating period. Moreover, during the cooling period (120s to 240s), the temperature measurement curves converge as heat is transferred from hotter locations (measured by FBG2) to the cooler locations (measured by the FBG1).

It must be noted that the small discrepancy between the numerical results and FBG sensors' measurements may be attributed to the actual magnitude of the electromagnetic properties of concrete used. Generally each concrete specimen has a unique set of electromagnetic properties that should be measured using the dielectric measurement kit. However, due to equipment limitations, the electromagnetic properties considered in the current numerical study were extracted from values reported in previous studies (Rhim and Buyukozturk, 1998). Some slight variations are expected in the EM properties of the actual specimens tested experimentally.

The surface temperatures recorded by the infrared thermo tracer camera may also be used directly to investigate the accuracy of the temperature measurements of the FBG sensors. The temperatures at the same locations monitored by the FBG sensors were measured using the infrared camera and are shown in Figures 8.7(a) and 8.8(a). Comparison between the maximum temperatures measured by the FBG sensors and the temperatures at the same locations monitored by the thermo tracer camera confirm that the accuracy of the bare FBG sensors as temperature sensors is satisfactory in microwave heating of concrete.

8.6 Conclusions

The accuracy of thermocouples for measuring the temperature of concrete during microwave heating was investigated in this chapter. Moreover, the feasibility of using

both bare and coated fiber Bragg grating optical sensors for monitoring the concrete's temperature during microwave processing of concrete was experimentally investigated. The results of the temperature measurement using a non-contact infrared thermo tracer camera as well as the results obtained using numerical modeling of the concrete heating process were used to verify the experimental results. According to the results presented, it may be concluded that:

1- The thermocouple readings were not accurate and mostly overestimated the actual temperature of the concrete. Hence, the results confirm that conventional thermocouples are not suitable for measuring the concrete temperature during the microwave decontamination or the microwave curing applications. It might be also similarly concluded that thermocouples are not suitable for use as process control instrumentation during the microwave assisted beneficiation of RCA.

2- The commercially-packaged off-the-shelf FBG sensors currently used for strain and temperature measurements of concrete in normal environments cannot be used in the presence of strong microwave fields. This is mainly due to the errors caused due to self-heating of the outer polymer sheath of the FBG sensors as well as the electromagnetic interference caused by the presence of metallic connectors in such optical fibers.

3- Bare FBG fibers can accurately measure concrete temperature when heated by microwaves and hence, may be used as a reliable process control tool in applications such as microwave curing of prefabricated concrete, microwave decontamination of concrete, and microwave-assisted RCA beneficiation.

Table 8.1 Thermal properties of concrete

Property	Assumption	Unit
Specific heat	1000 (0.24)	$J/[Kg\,°K]$, $(Btu/[lb.°F])$
Thermal conductivity	3 (1.73)	$W/[m.K]$, $(Btu/[ft.hr.°F])$
Heat transfer coefficient of heat flux	10.0 (1.76)	$W/[m^2.°K]$, $(Btu/[ft^2.hr.°F])$
Surface emissivity	0.9	
Initial Temperature	25 (77)	$°C$, $(°F)$

Table 8.2 Thermocouples' readings at t=120s

Specimen	Microwave Power (W)	Thermocouples readings (°C)			Analytically Predicted temperatures (°C)		
		D1	D2	D3	D1	D2	D3
C1	900	77	DF*	80	77.53	67.95	70.53
C2	1800	140.13	90.40	116.04	134.54	90.88	117.62
C3	900	72.7	78.8	68	77.53	67.95	70.53
C4	1800	140.01	96.81	122.59	134.54	90.88	117.62
C5	900	DF	82.77	DF	77.53	67.95	70.53
C6	1800	174.32	DF	127.33	134.54	90.88	117.62

* DF: Dysfunctional; i.e. the thermocouple was damaged as a result of the electromagnetic interference.

Table 8.3 Summary of the results obtained by thermo-tracer camera, FBGs sensors, and numerical modeling at t=120s

Specimen	Microwave Heating Power (W)	Thermo-tracer readings at t=120s (°C)		FBG readings (°C)		Analytically Predicted temperatures (°C)	
		S1	S2	S1	S2	S1	S2
C1	950	39.0	57.5	39.0	58.3	36.2	60.9
C2	1800	67.0	119.5	67.2	119.2	65.3	119.0
C3	950	38.5	59.0	37.6	58.2	36.2	60.9
C4	1800	66.5	120.0	65.7	120.4	65.3	119.0
C5	950	36.0	118.0	35.6	117.8	36.2	60.9
C6	1800	70.0	124.0	70.0	123.7	65.3	119
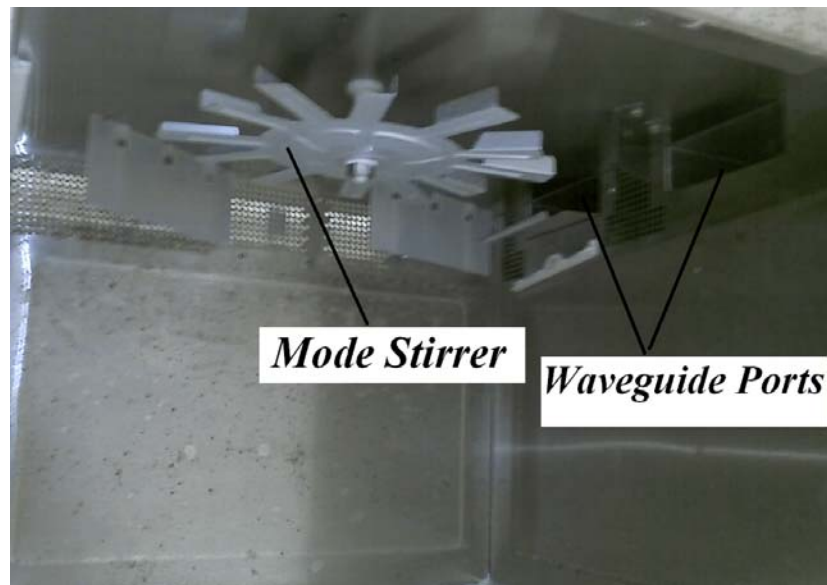
Figure 8.1 Interior of the microwave oven
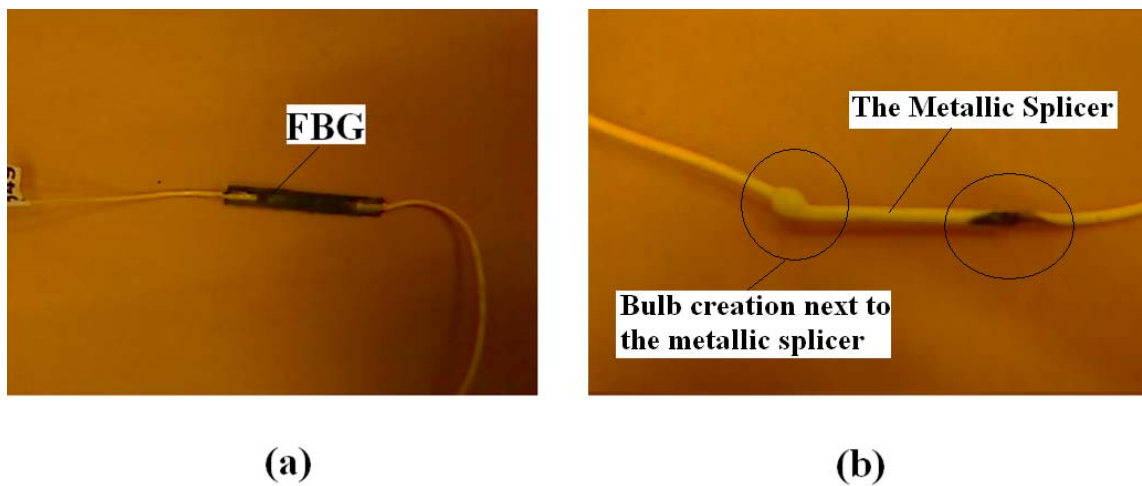
**Figure 8.2 (a) A commercially packaged FBG before microwave heating (b) burning of the
plastic coating next to the metallic splicer after microwave heating**
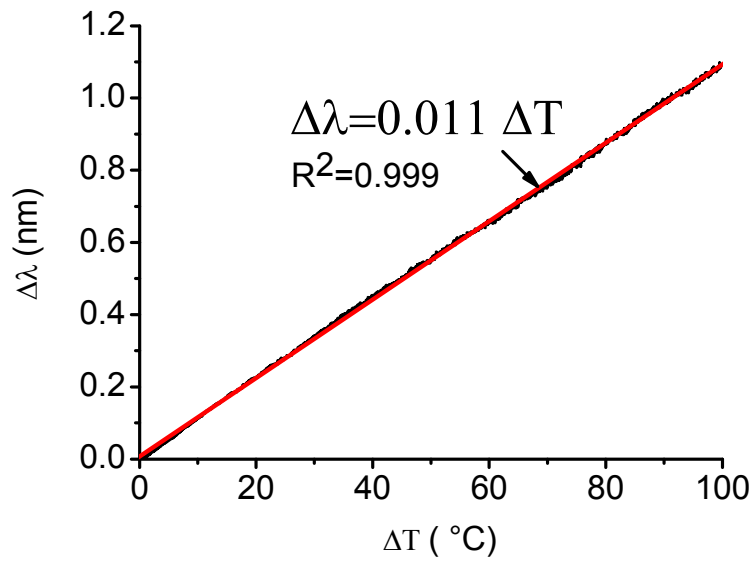
Figure 8.3 Calibration curve for FBG1
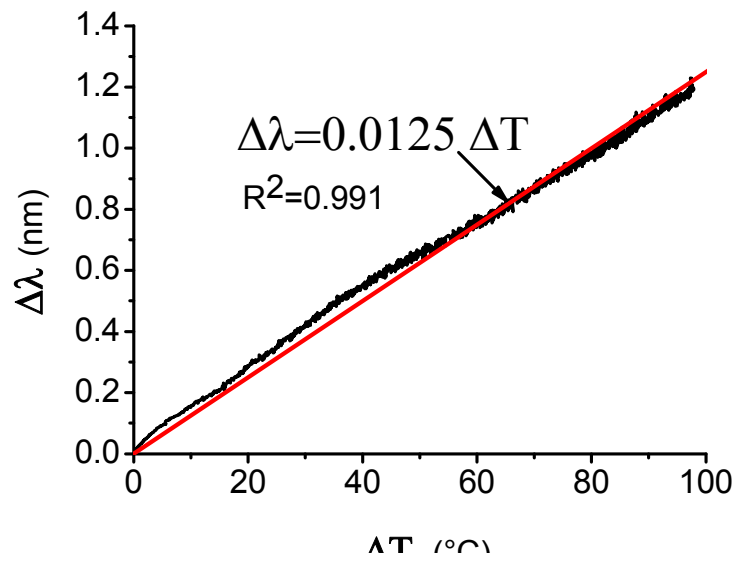
Figure 8.4 Calibration curve for FBG2
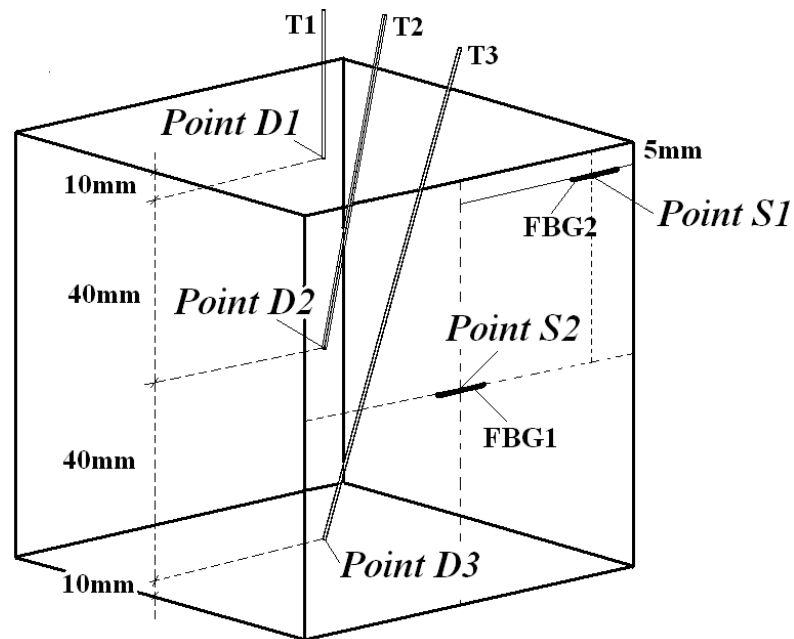
Figure 8.5 Instrumentation of the concrete specimens; positioning of thermocouples and FBG sensors
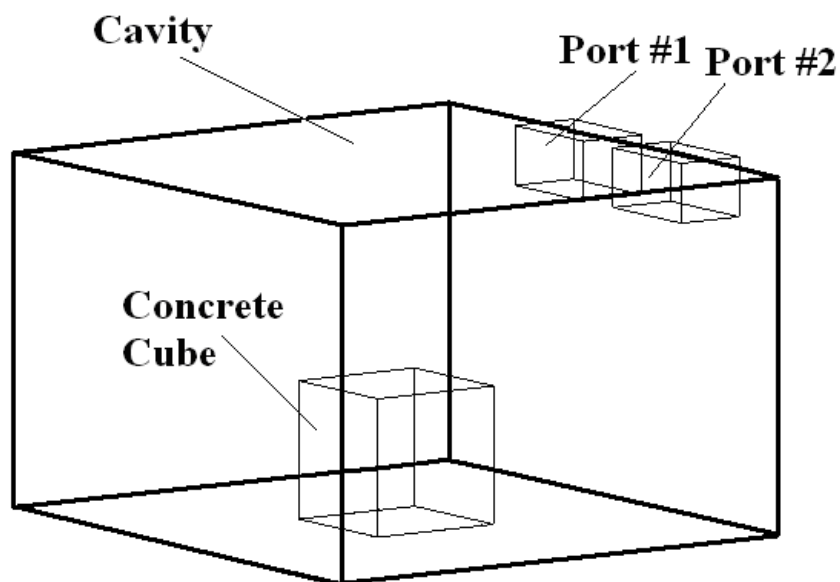
Figure 8.6 Sketch of the microwave oven for numerical modeling
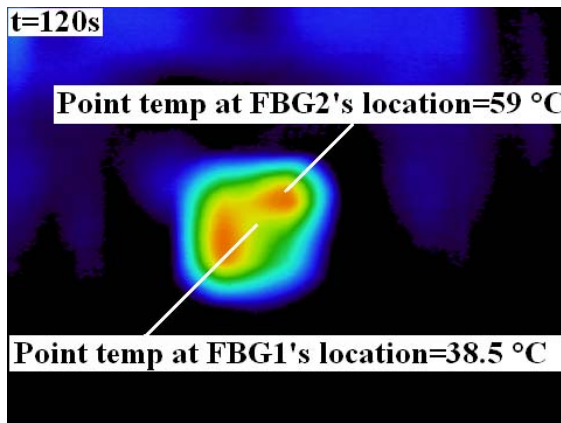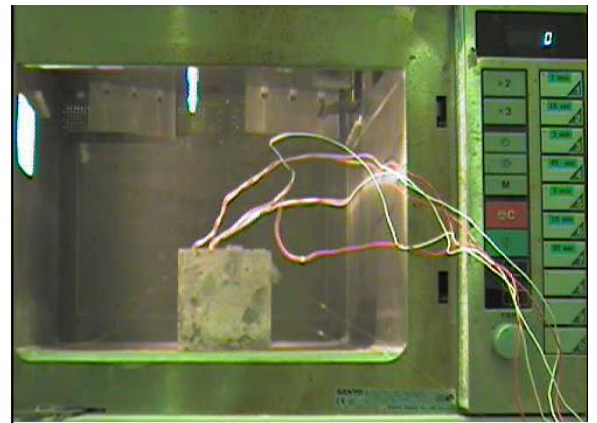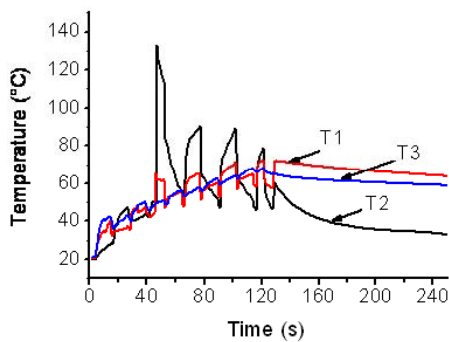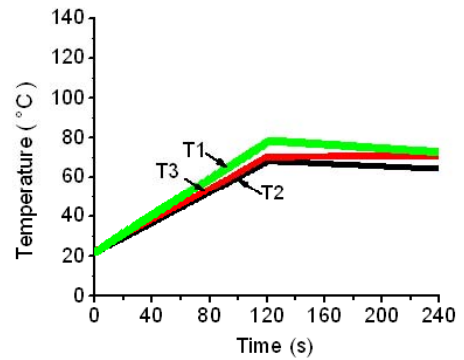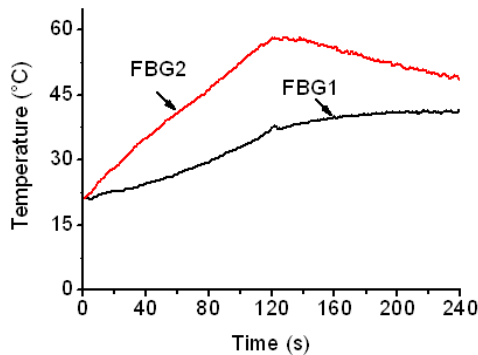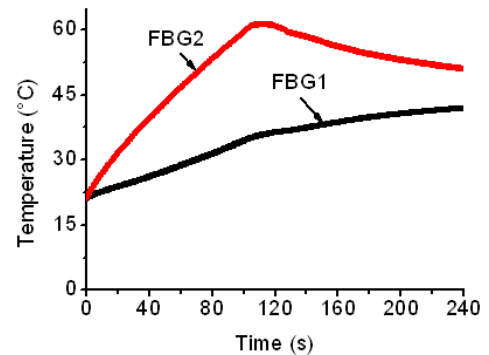
Figure 8.7 . (a) Temperature profile captured using the infrared camera, (b) the specimen under test, (c) embedded thermocouples' readings, (d) temperature at the locations monitored by thermocouples predicted using numerical modeling, (e) Temperature measured using bare FBG sensors, (f) Temperature at the locations monitored by bare FBG fibers predicted using numerical modeling, for a saturated concrete specimen (C3) heated at 950W microwave power for 2 minutes.
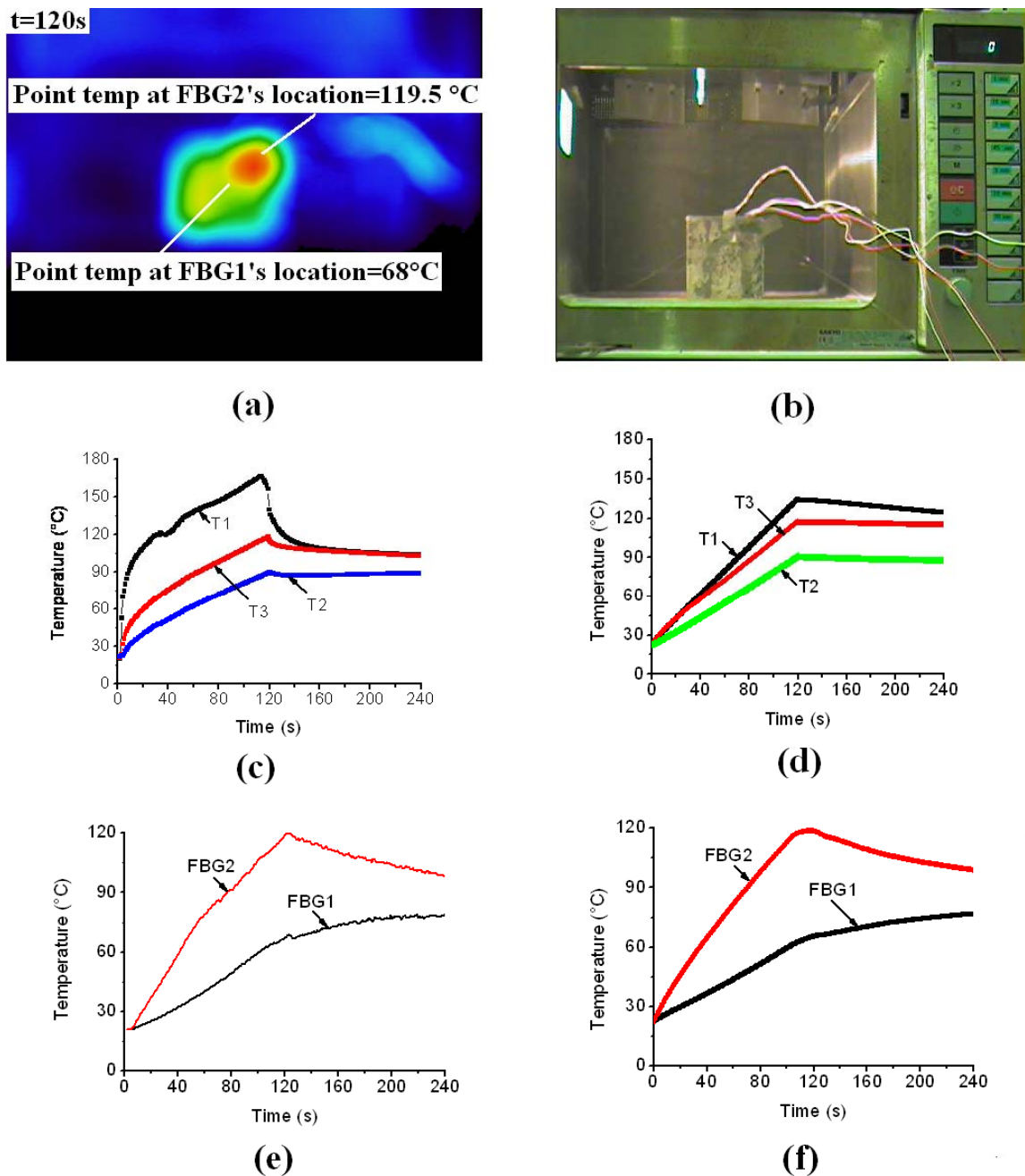
Figure 8.8 **(a) Temperature profile captured using the infrared camera, (b) the specimen under test, (c) embedded thermocouples' readings, (d) temperature at the locations monitored by thermocouples predicted using numerical modeling, (e) Temperature measured using bare FBG sensors, (f) Temperature at the locations monitored by bare FBG fibers predicted using numerical modeling, for saturated concrete specimen (C2) heated at 1800W microwave power for 2 minutes.**

Chapter 9 : Design and Installation of the 10 KW Microwave Heating System

Two novel microwave-assisted methods to improve the quality of the recycled concrete aggregate through removal of the contaminated surface of concrete and removal of the cementitious mortar adhering to RCA particles were introduced in Chapters 5 to 8 of this thesis. One of the most important steps to commercialize these methods is to design an efficient, safe and economical industrial system that can be eventually incorporated in an actual RCA production facility. In this chapter, the different stages of design, assembly, and installation of a pilot microwave heating system installed in the NUS Structural Engineering Laboratory are presented. Through this chapter, this system is referred to as NUS10KWGEN.

9.1 Configuration and Components

The microwave system designed comprises five main units:

1) *Microwave Generator Unit:* This unit comprises active microwave components used to generate the microwave power.

2) *Microwave Delivery Unit (Waveguide Components):* This unit includes a variety of waveguide components used to deliver the generated microwave power to concrete/RCA while minimizing the power reflection.

3) *Cooling Unit:* This unit comprises pumps, pipelines, cooling tower and heat exchanger to dissipate the internal heat generated during operation.

4) *Control Unit:* This unit comprises a PLC (Programmable Logic Controller) programmed to control microwave generation based on data input by the operator as well as the feed-back sent by a network of sensors used to control the function associated with the microwave generation and delivery units.

5) *Microwave Heating Chamber (Cavity):* The heating chamber is used to contain the load (concrete/RCA) and is designed to prevent microwave leakage.

In the following, the configuration, working principle and the installation procedure of each of the abovementioned units designed for NUS10KWGEN are explained.

9.1.1 The Microwave Generator Unit

The microwave generator unit is the heart of the microwave heating system. It consists of the microwave source and the power supply. The commonly used source of microwave energy, primarily for reasons of efficiency, is the magnetron. Because of mass production, magnetrons at 2.45 GHz are particularly cheap; however, magnetrons are available for other frequency ranges as well. Other sources available include traveling wave tube (TWT), Klystron, Gyrotron, and solid state devices. Each has characteristics that can be exploited to suit the needs of the user.

As illustrated previously, results of numerical modeling suggest that compared to 2.45 GHz frequency, the higher microwave frequencies (e.g. 10.6GHz or18 GHz) may be

more efficient for the purpose of concrete surface decontamination and RCA beneficiation applications. However, due to limitations on the availability of commercial components at higher frequencies and considering the economic justification of the project, a magnetron capable of generating microwaves at 2.45 GHz and max power of 10 kW was selected for this experimental study. The H0915 Hitachi magnetron used in the NUS10KWGEN system is shown in Figure 9.1.

As can be seen in Figures 9.1 and 9.2, magnetron consists of a hot filament as the cathode (source of the electrons) which is placed in the center of an evacuated circular chamber. A permanent magnet is used to impose a magnetic field parallel to the filament to force the electrons, attracted to the outer part of the chamber, to spiral outwards in a circular path rather than moving directly to the anode. As the electrons sweep past the cylindrical cavities spaced around the rim of the chamber, they induce a high frequency electromagnetic field in the cavity. A portion of the field is extracted using an antenna and is directed to the waveguides through the magnetron's ceramic dome.

To generate the microwave, the magnetrons filament should be kept at a high negative voltage. A high power DC power supply is used to provide such a high negative voltage. The 10 KW SM1690x Alter microwave DC power supply used in the designed system is shown in Figure 9.3. The output power of the power supply is adjusted through an analog signal from 1 to 10Vdc.

In order to warm up the magnetron's filament before commencing microwave generation, a filament transformer is used to preheat the magnetron. The FIL250 filament transformer used is shown in Figure 9.4. The FIL250 heats the filament by passing a 30 Amps current through it for almost 4 minutes.

9.1.2 Power Delivery Unit

The microwave power generated is delivered to the load (concrete/RCA) through a set of waveguide components. As can be seen in Figure 9.5, common high power configurations of the waveguide components usually include an isolator (circulator + water load), an impedance tuner, a power measurement tool and some combinations of waveguide straight and bent sections. Depending on the application and cost considerations, some of these components may not be needed. In the following, the waveguide components used in NUS10KWGEN are briefly described.

9.1.2.1 Isolator (Circulator and Water Load)

The isolator is a two port device made of a ferrite material and magnets which does not permit the flow of power in the reverse direction. For low power applications, an isolator is normally used to protect the magnetron from the damaging effect of the reverse power. However, in high power applications, instead of using the standard two-port isolator, an isolator is formed by connecting a circulator to the dummy waveguide load to absorb the reverse power. The circulator is a three port device used to control the direction of power flow. Dummy loads are used to dissipate the microwave power with little or no reflection. Two types of dummy loads are available, wet loads and dry loads. Wet loads absorb the microwave power directly into a high loss fluid medium, usually water, while dry loads absorb power directly into a high loss solid, usually silicon carbide. Each type of dummy load has distinct advantages and disadvantages. The most important advantage of wet loads is their small size and high power rating as compared to dry loads. Wet loads are often preferred in the high power microwave heating, while dry loads are preferred for

applications where standing waves must be minimized such as with traveling wave applicators.

Based on the above discussion, the combination of a circulator and water load was chosen as the isolator for the NUS10KWGEN microwave heating system. The circulator and water load used are shown in Figures 9.6 and 9.7, respectively.

9.1.2.2 Directional Coupler and Power Monitor

The directional coupler is used to take samples of the power propagating in one direction. This sample can be used to obtain an accurate measure of the total microwave power propagating in the waveguide. The coupler then sends a signal, which is usually a D.C voltage, to the meter or some other calibrated signal measuring device.

Similarly, Dual directional couplers are used to take a sample of the power in both directions. Hence, they can be used to measure both the forward and reverse power. In the NUS10KWGEN system, a dual directional coupler with a power monitor is used to measure the forward and reflected powers. The dual directional coupler and power monitor used are shown in Figure 9.8.

9.1.2.3 Tuner

In microwave heating, the microwave power should be transferred from generator to the workload with minimum loss. The transfer efficiency of microwave heating is limited by two factors, the energy absorbed by the walls of the transmission line through resistive heating and the power reflected from the load. In most cases, the power loss through resistive heating of the waveguide components is negligible and the second factor plays a more significant role. To achieve the optimum power transfer from the source to the load,

the load resistance (impedance) R_L should be equal to the generator internal resistance R_G. This concept is known as impedance matching.

A common method to achieve impedance match is to insert a metallic element into the waveguide. By adjusting the position and the depth of the insertion of the metallic element in the applicator, either the phase or amplitude of the source impedance can be adjusted. Multi-stub tuners are normally used to adjust the position and depth of the insertion by inserting one, or more stubs into the waveguide. When the change in the properties of the load during microwave heating is insignificant, manually adjusted tuners are usually used. The adjustment of the stubs in a manual tuner is mostly done based on the experience.

In applications where there is a significant change in the load impedance during the microwave heating, manual tuning is inconvenient and too slow to keep pace with the changes. In this case, auto-tuners are usually used. Auto-tuners can achieve a superior impedance match by adjusting the stubs within milliseconds. Auto-tuners are usually very costly compared to manual tuners but can significantly increase the efficiency of microwave heating and increase the life of the microwave generator by minimizing the reverse power reversals.

Because of the expected high variation in the electromagnetic properties of concrete and RCA samples to be tested using the NUS10KWGEN system, a 3 stub auto-tuner shown in Figure 9.9 was chosen to provide the highest energy transfer and to prevent damage to the generator by minimizing the amount of reflected power. The tuners should be located as close to the load being matched as possible.

9.1.2.4 Straight Waveguide Sections

A hollow metallic tube of either rectangular or circular cross section is generally used in practice to transfer microwave power from one component to the next or to the load. Such a structure is commonly known as a waveguide. Waveguides are usually made of aluminum, copper or brass of various sizes. To choose the appropriate waveguide section, operating frequency, power rating, component availability and cost should be considered. The standard waveguide sizes for 2.45 GHz frequency are listed in Table 9.1. The WR284 waveguide is often the preferred choice for 2.45 GHz operation at average power levels up to 6kW. WR340, WR430 are recommended for higher power levels.

Waveguide Flanges are used to connect one waveguide section to another. Standard flange types are available for each waveguide type. In most industrial heating applications, "flat face" flanges are the most cost effective choice whereas "choke" type flanges are more popular for military and communication applications.

Most commercial waveguide components are made of aluminum due to its low cost and good performance. In cases where heat loss is of concern, copper waveguides may be more appropriate; although the cost usually outweighs the slightly lower heat loss advantage. Where sanitation is of high importance, such as in the food processing industry, stainless steel waveguides may be used. In the system designed for this study, the aluminum WR430 waveguide and CR430 flange type were used (Figure 9.10).

9.1.2.5 Waveguide Bends

Waveguide bends are used to change the direction of the waveguide transmission system. H-bend and E-Bend are two types of common waveguide bends used to change the direction of the transmission line in the horizontal and vertical directions, respectively.

In the NUS10KWGEN system, H-Bend is used to connect the generator to the RCA heating chamber, while an E-bend is used to direct the microwave power downward onto the concrete slab surface to be decontaminated. The H-bend and E-bend used are shown in Figure 9.11 and 9.12, respectively.

9.1.3 Cooling Unit

Water cooling system is used to absorb the heat generated by the magnetron and circulator when in operation and the heat absorbed by the water load as a result of the reflected power. The cooling system used in NUS10KWGEN is divided into an internal closed cooling loop designed for water to circulate through the magnetron, circulator, and water load and an external cooling loop designed to dissipate the heat generated in the internal loop using a heat exchanger.

9.1.3.1 Internal Cooling System

The internal cooling system comprises a pump and three sets of closed pipe line loops. The first loop circulates water through the magnetron while the second and third loops provide the cooling water for the circulator and water load, respectively. The components of the internal cooling network are illustrated in Figure 9.13.

The internal loop is filled with distilled water to prevent the formation of deposits within the cooling passages. The presence of deposits in water can lead to overheating which can shorten the life of the magnetron and circulator.

9.1.3.2 External Cooling System

As can be seen in Figures 9.14 and 9.15, the external cooling system comprises a cooling tower, a pump and a heat exchanger. The external cooling water absorbs the heat

of the internal cooling water using the heat exchanger. The cooling tower is used to keep the temperature of the external cooling water within the prescribed range of 20-25 °C. A pump is used to circulate the external cooling water through the heat exchanger and cooling tower.

9.1.4 Control Unit

The control unit is designed to ensure optimum and safe operation of the system through a network of sensors, relays and contactors controlled using a PLC (Programmed Logic Controller) programmed to operate the system according to input of the user and other safety requirements. Various components of the control unit are briefly explained in following.

9.1.4.1 PLC (Programmable Logic Control)

PLC is the heart of the control unit. An Allen Bradley FlexLogix PLC is used to control the NUS10KWGEN system and to communicate with external computers, processors, and Ethernet/IP networks. The PLC includes three main modules; I/O (Input/output) module, Processor, and communication module. The I/O module is used to send and receive commands to/from sensors and controllers. The output and input information, from operator or sensors, are processed within the processor unit according to the logic control program written using the RSLogix 5000 programming software. The PLC communication module comprises Ethernet/IP and modem modules to communicate with the external computer and processors. The communication module can be used to change and modify logic programming, and monitor the processor operation remotely. Different components of the PLC used in GEN10KW-NUS are shown in Figure 9.16.

The PLC is connected to a touch-screen panel view through a local control module. The panel view is used to receive the operator's input commands and show the system status prior to and during microwave generation. The Panel view used in GEN10KW-NUS is shown in Figure 9.16.

9.1.4.2 Sensors and Relays

Sensors and relays are used to monitor the operation of various parts of the microwave generator. Relay is an electronic switch that can stop or start the operation of a specific part of the generator based on the sensors' signals. The most important sensors and relays used in NUS10KWGEN are listed as follows:

1. *Door Interlocks:* Both the generators cabinet door and the control panel door are protected by safety interlock preventing generator operation when the door is opened or unlatched. These switches are monitored by the main control system for operator safety and are checked for proper operation each time the system started. If any door switch is cycled during system operation, the system is shut down and a fault appears on the generator operator interface identifying the switch involved.

2. *Lower Breaker Monitor:* This sensor is used to check whether the lower circuit breaker is switched on to provide the mains power to the active microwave components.

3. *Circulator Arc Detector Relay:* An optical sensor is used to detect the arc in the circulator. The sensor is connected to the circulator arc detector relay, Figure 9.16, which stops the generator operation in case of arc detection.

4. *Internal Pump Pressure and Flow Sensors:* These sensors are used to ensure that enough water flow and pressure is provided for the cooling of the circulator,

magnetron and water load. The pressure and flow of the switch can be adjusted using the pressure switch shown in Figure 9.13.

5. *E-Stop Relay:* This relay stops generator operation in an emergency when the signal is sent through the remote E-Stop connection or the E-Stop button.

6. *Coolant Temp Sensor:* This sensor is used to control the temperature of the internal cooling water.

7. *Magnetron's Fan Sensor:* This sensor is used to check whether the magnetron fan is on, before starting microwave generation.

8. *External Cooling Water, Pressure and Temperature Sensors:* These sensors are located at the output of the heat exchanger to control the temperature and pressure of the external cooling water.

9. *K2 Overload (overload relay):* This relay is used to stop microwave generation if the pump is not working properly.

10. *Magnetron Over-current and Over-Voltage Relay (K35):* These relays are used to stop generator operation, in case of detection of over-current and over-voltage which can damage the magnetron.

11. *Alter Sensors:* These sensors are used to monitor the operation status of the power supply and control pre-heating of the magnetron using the filament transformer.

9.1.5 Microwave Heating Chamber

Microwave heating chambers or cavities are used to contain the heating loads and provide the required safety for operating personnel against microwave radiation. Two microwave heating chambers with different sizes were built for the NUS10KWGEN to

address the two different applications expected for the system; the microwave surface decontamination of concrete and the microwave-assisted RCA beneficiation.

9.1.5.1 Concrete Surface Decontamination Chamber

As explained in Chapters 5 and 6, in the microwave surface decontamination technique, the applicator (waveguide) is used to transmit microwaves directly to the concrete surface. Hence, ideally, if the microwave applicator can be placed in a 100% fit contact with the concrete surface, there is no need to provide shielding against the microwave leakage. However, normally, the surfaces of concrete specimens are not completely flat. Moreover, the concrete surface becomes even more uneven after the surface spalls off during the microwave heating. Hence, there is a need for a shielding chamber to contain microwave heating applicator and the concrete specimens. In the system designed in this study, a 2.2×2×2.2 (m) microwave heating chamber was manufactured and installed to provide the required shielding for the microwave surface decontamination process.

2 mm thick mild steel plates were cut in the workshop and assembled the microwave generator room. As shown in Figure 9.17, the steel plates were welded continuously to minimize possible microwave leakage through the joints. The chamber was connected to the microwave generator cabinet through a tunnel (Figure 9.18) tightly bolted to the generator cabinet using the same openings provided to connect the waveguide launcher to the generator's cabinet. Before welding the base plate, a layer of thermal insulation sheet was spread on the floor to reduce as much as possible the conductive heat transfer from the base plate which can damage the floor finishes (Figure 9.19).

Perhaps the most critical part and the weakest link against the microwave leakage in the microwave heating chamber is the door. As can be seen in Figure 9.20, in NUS10KWGEN, conductive RF gaskets were used to fill in the gap of the door and minimize possible leakage while the door is pressed firmly against the chamber using five strong latches. The front view of the decontamination chamber is shown in Figure 9.21.

9.1.5.2 The RCA Heating Chamber

A small 50×40×40 (cm) chamber was fabricated to contain the RCA particles during the microwave heating. The basic concepts in the fabrication of this chamber are similar to the microwave decontamination chamber explained above. In this chamber, 2 mm thick galvanized steel plates were welded continuously. An opening of the same size as the WR430 waveguide with the required openings was cut on the top center of the left wall of the chamber for connection to the microwave applicator (auto-tuner). Similar gaskets and door latches as the microwave decontamination chamber were used to minimize possible leakage from gaps around the door.

9. 2 Assembly and Installation

The circulator, power supply, internal pump, heat exchanger and the control unit were assembled in the supplier's factory and were shipped to NUS. The magnetron, directional coupler, auto tuner, external cooling system, waveguides, and the heating chambers were installed and assembled locally.

9.2.1 Installation of Magnetron

Magnetron was installed by carefully inserting its ceramic dome into the opening provided in the waveguide. M5 flange nuts were used to tighten the PEM studs from the

bottom of the waveguide bracket. The filament leads from the magnetron were connected to the secondary of the filament transformer and the HV cable from the high voltage power supply. The water pipes from the internal cooling system were then connected to the magnetron.

9.2.2 Installation of the Cooling System

The internal cooling loops were assembled in the supplier's plant. The internal closed loop system was filled through the radiator cap located on the top of the water to water heat exchanger (Figure 9.14).

The external cooling tower was placed outside the structural workshop at a level lower than the generator. Due to the existence of many bends in the pipe line, a strong pump of 30 m water head was needed to provide the sufficient water pressure. Cooling input water and output pipes were connected to the water to water heat exchanger.

9.2.3 Waveguide Components

After assembly of the active microwave components, the dual directional coupler, straight waveguides, bends, auto-tuner and RCA heating chamber were added to the system consecutively. After assembly of each of these waveguide components, the microwave generator was tested by terminating the system using a water load. A pump was used to circulate water between the water load and a small tank. The temperature rise of the water after microwave heating was used to calculate the total absorbed microwave energy. A comparison of the absorbed microwave energy calculated and the microwave power set on the control panel was used to check whether there is any significant loss due to the installation of the new components and to check whether the actual microwave power generated is equal to the value measured by the directional coupler. The internal

views of the NUS10KWGEN microwave generator and microwave delivery units, after assembly, are shown in Figures 9.23 and 9.24, respectively.

9.3 Safety

Safety is one of the most important aspects of any industrial process. All industrial machinery should be designed to ensure the safety of its operators. In general, the previous studies conducted on the safety of microwave heating show that microwave heating can be as safe as conventional heating. The two main safety concerns about microwave heating and the measures taken in the design of the NUS10KWGEN to address these concerns are briefly explained in the following section.

9.3.1 Radiation Hazards

It is well known that unlike Gamma and X-ray frequencies, the photonic energy at microwave frequencies is not enough to ionize the exposed material. Available literature does not show any confirmed relationship between exposure to electromagnetic waves at microwave frequencies and various cancers (Elwood JM, 1999). The only proven effect of microwave heating on the biological materials is thermal heating. Hence, thermal injury may be considered as the only known health hazard of microwave heating. The danger of thermal injury due to exposure to microwaves increases with an increase in microwave frequency and power. As illustrated in Chapters 5 and 6, higher frequencies lead to a more concentrated heating because of their shorter penetration depth. Thus, a much lower power may be needed to cause burns when exposed to higher frequencies. Shielded chambers are used to protect the operators against the microwave radiation. In NUS10KWGEN, besides the microwave decontamination and RCA beneficiation chambers, as shown in Figure 9.21, the generator cabinet was designed to contain all the

active and delivery microwave components. The generator chamber may be relied upon to prevent microwave radiation leakage in case of leakage from any of the microwave generator components. Moreover, a leakage meter is used on a periodic basis to detect any microwave leakage. Upon detecting excess emissions, the equipment should be immediately shut down and the cause of emissions investigated and corrected before restarting operation. Under the IEC standard, which is applicable to equipments operating in the frequency range from 300 MHz to 300 GHz, power density is measured at least 5 cm from any accessible location on the equipment and should be limited to 5 mW/cm^2 during "normal" operation and 10 mW/cm^2 during abnormal operation. During the installation of NUS10KWGEN, a HI-1501leakage meter shown in Figure 9.25 was used to test all the connections as well as the seals of both chambers fabricated.

9.3.2 High Voltage Hazards

Although most of the public concern about microwave heating has been focused on the health hazards due to the exposure to the electromagnetic radiation, experience shows that the hazards associated with the exposure to high voltage in the microwave generators is of, at least, equal importance. In almost all microwave generators, depending on the design, very high voltages, up to tens of thousands Volts, may be present during operation. High voltages may even be present during the non-operation stage as most microwave generators include one or more capacitators that stores high voltage electric charge. These high voltages can cause serious injury or death if the human body becomes a part the electric circuits due to inadvertent contact with or in close proximity to the high voltage conductors or capacitators. To address these issues, NUS10KWGEN is equipped with door interlocks that prevent generator operation when the doors are open. Moreover,

all active microwave components have been designed for safe automatic discharge of any stored energy.

Table 9.1 Popular waveguide sizes used for industrial microwave heating at 2.45 GHz

Inside Dimensions (inches)	Frequency Band	Official Designation		
		IEC	RCSC (ccc)	EIA (US)
2.84×1.34	s	R32	WG10	WR284
3.40×1.70	s	R26	WG9A	WR340
4.30×2.15	s	R22	WG8	WR430
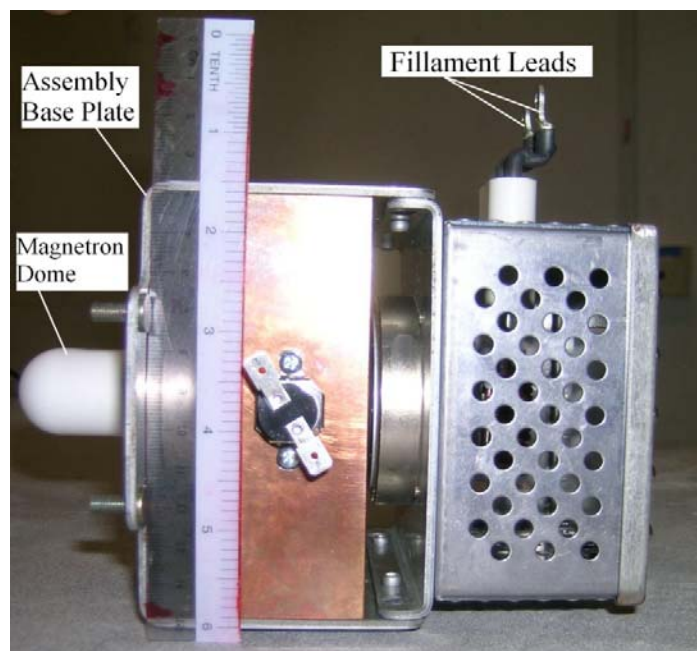
Figure 9.1 The magnetron used in NUS10KWGEN
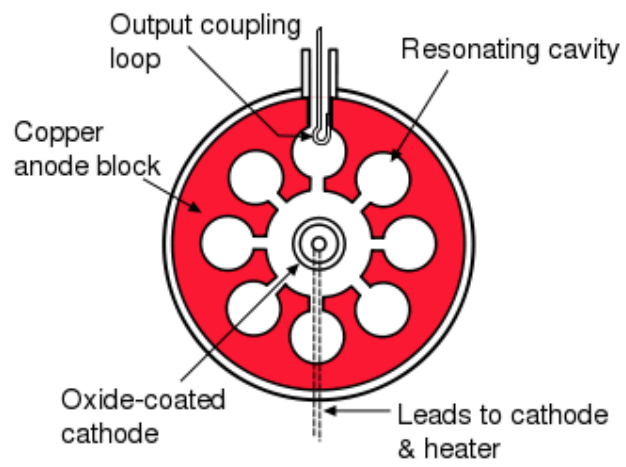
Figure 9.2 Internal structure of magnetron

Figure 9.3 Switch mode power supply
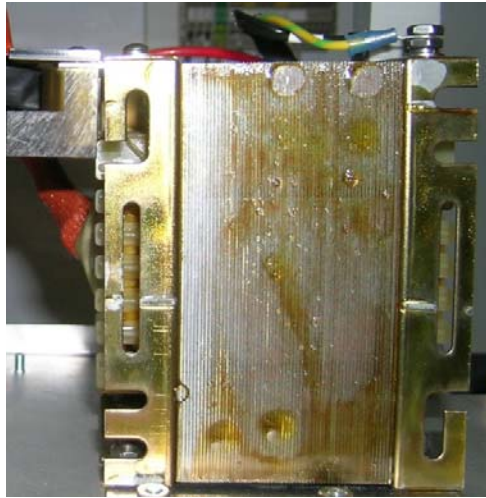
Figure 9.4 The filament transformer
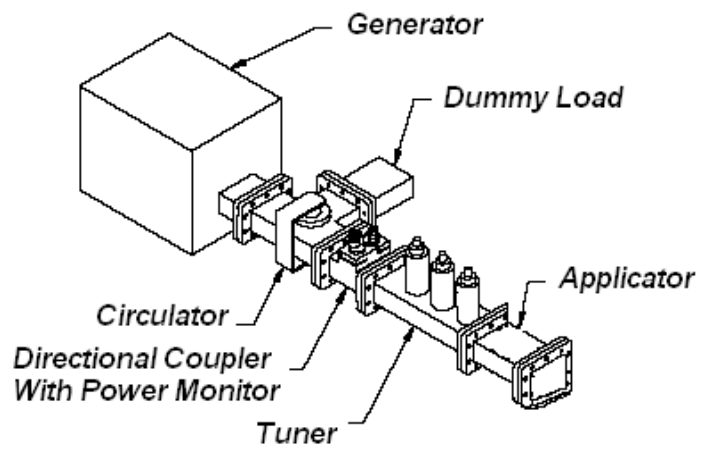
Figure 9.5 Common configuration of the power delivery unit
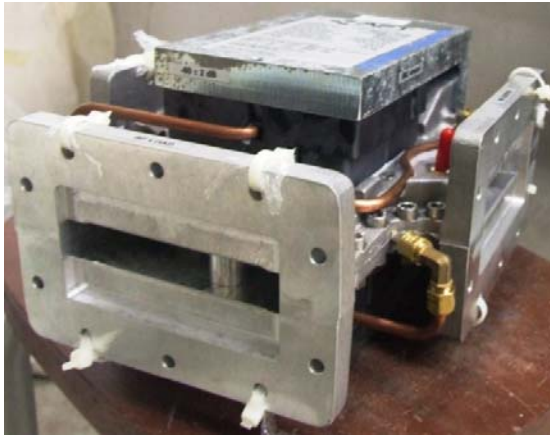
Figure 9.6 Circulator

Figure 9.7 Water Load

Figure 9.8 Dual directional coupler with power monitor
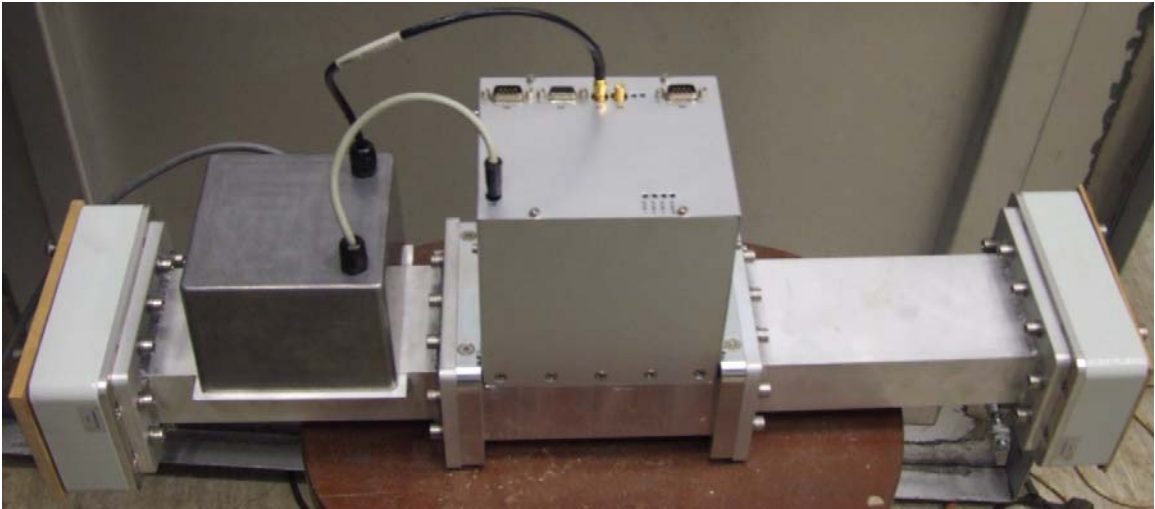
Figure 9.9 Auto-Tuner

Figure 9.10 Straight WR430 waveguide section with CR430 flange

Figure 9.11 H-bend
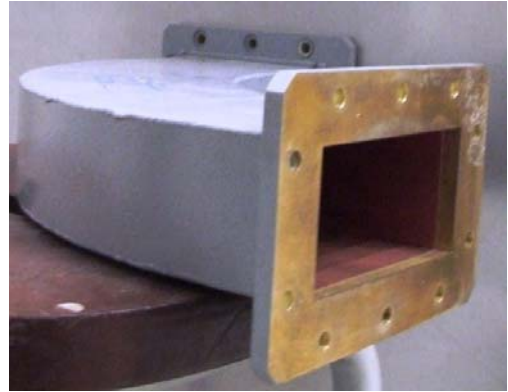
Figure 9.12 E-bend
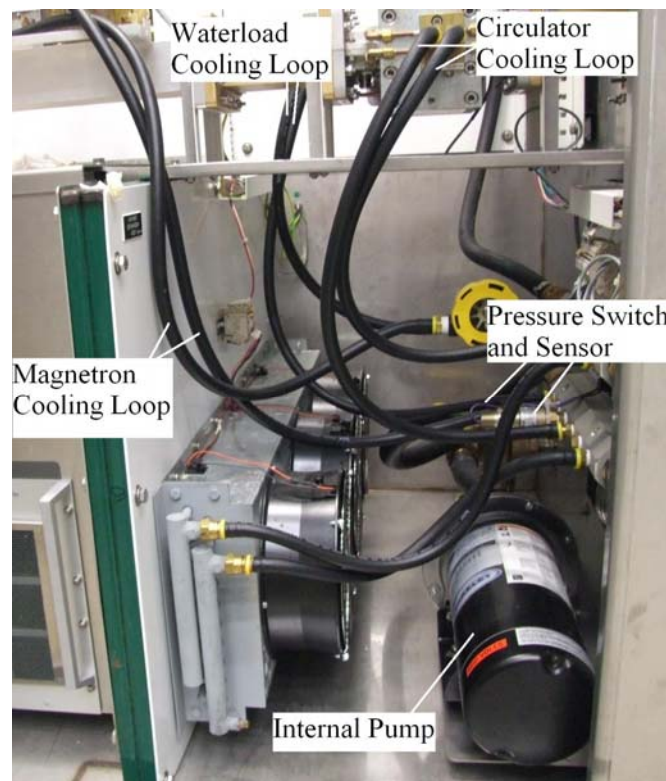
Figure 9.13 The Internal Cooling Loop
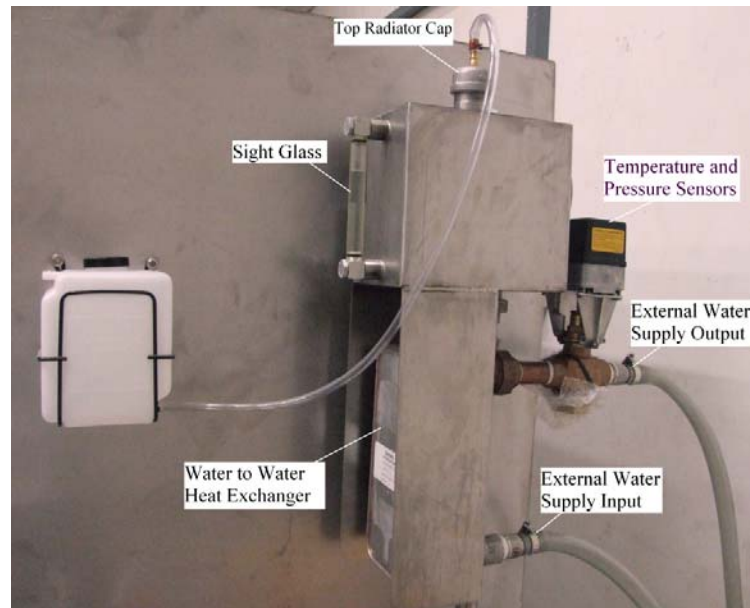
Figure 9.14 Heat Exchanger

Figure 9.15 Cooling tower and external pump
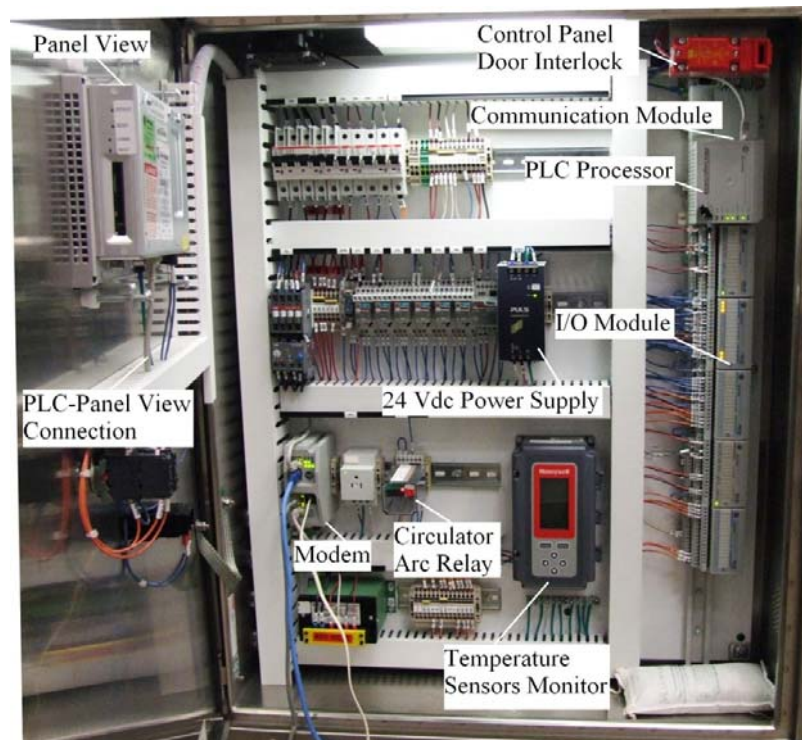
Figure 9.16 Control Panel

Figure 9.17 Continuous welding of the steel plates

Figure 9.18 Small tunnel to connect the chamber to the generator's cabinet

Figure 9.19 the thermal insulation beneath the chamber's base plate

Figure 9.20 RF Gasket of the chamber's door

Figure 9.21 The large chamber connected to the generator's cabinet

Figure 9.22 The RCA beneficiation chamber
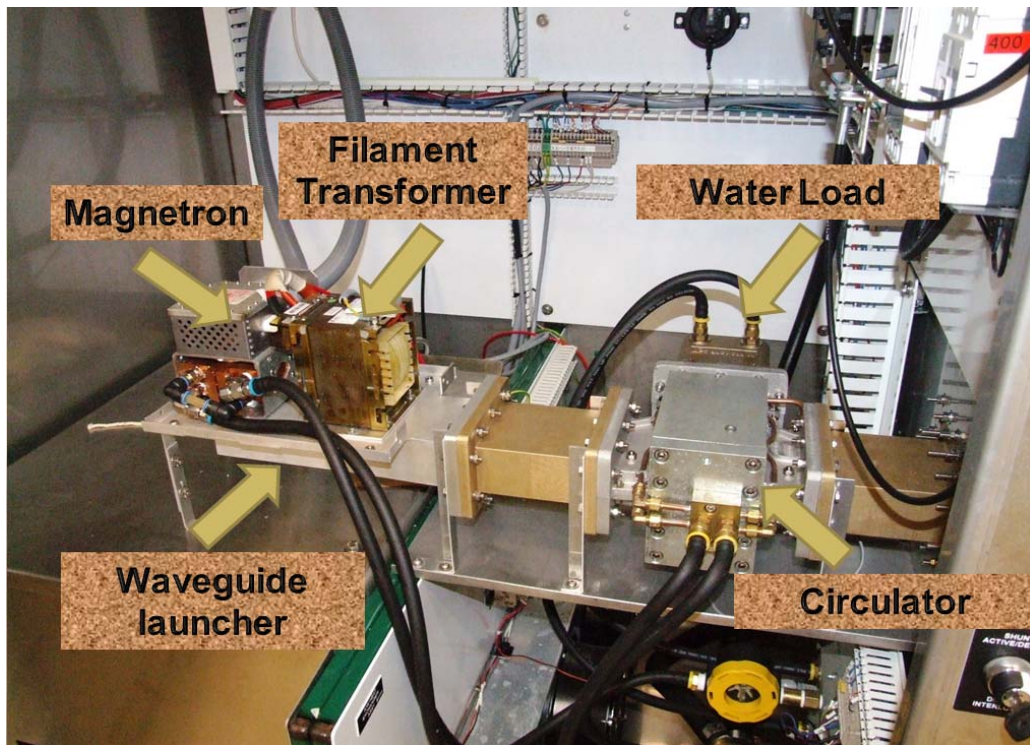
Figure 9.23 The microwave generator unit after assembly
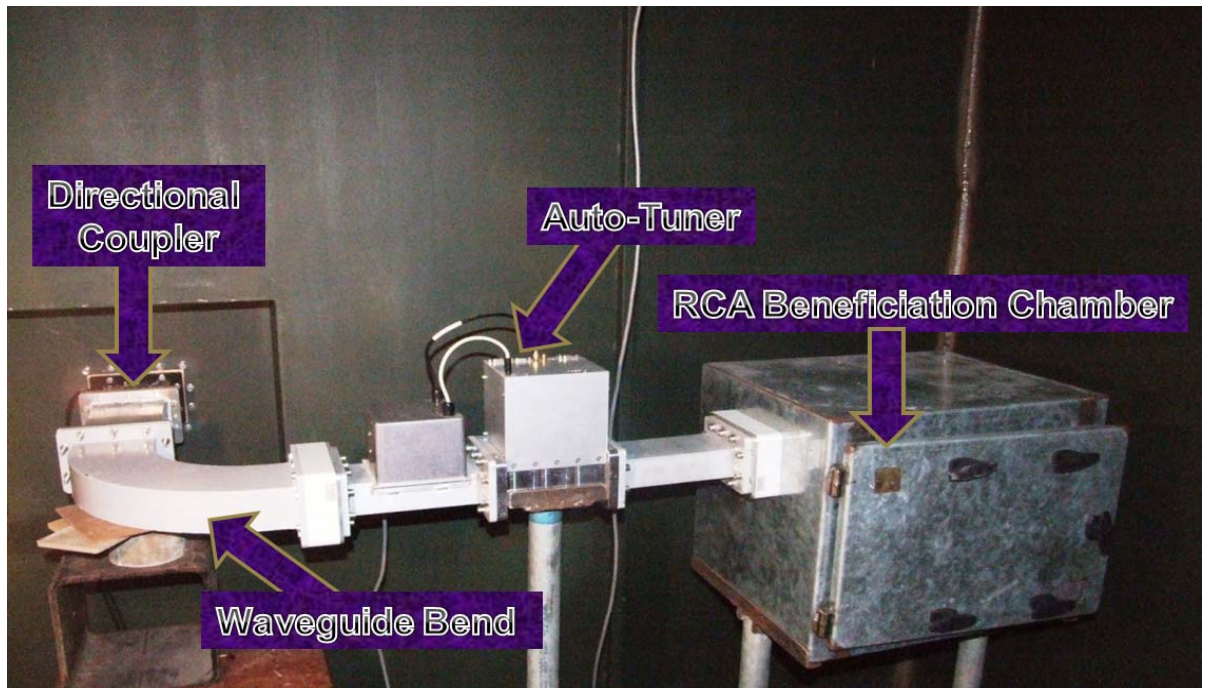
9.24 The microwave delivery unit components after assembly

Figure 9.25 Leakage meter

Chapter 10 : Experimental Investigation of the Effects of the Adhering Mortar Content and Comparison of Various Beneficiation Methods

10.1 Background

According to the available literature reviewed in Chapter 2, the presence of the adhering mortar was identified as the main factor lowering the quality of RCA compared to natural aggregates. A number of techniques to improve the quality of RCA through removal of the adhering cementitious mortar were reviewed in chapter 3. In addition, in chapter 7, a new microwave assisted RCA beneficiation technique developed during this study was introduced. The feasibility of using microwave heating to remove the adhering mortar from RCA was confirmed through preliminary experiments as well as numerical simulation. In chapter 9, the design and fabrication of a pilot microwave heating system to be used for RCA beneficiation was presented.

The study reported in the current chapter was divided into two phases. In the first phase, the effects of the adhering mortar content on the properties of RCA including water absorption and bulk specific gravity were investigated. Moreover, the effects of different production parameters including number of the crushing stages, strength of the parent

concrete, and particle size on the amount of the adhering mortar and thus the specific gravity and water absorption of RCA were examined.

Having determined the effects of different adhering mortar contents on the properties of RCA, for the second phase, the efficacy of a number of different beneficiation methods in removing the adhering mortar of RCA was investigated. Focus was placed on the microwave-assisted RCA beneficiation method proposed in this study. The properties of RCA treated using the 10 kW microwave heating system designed and fabricated during this study were experimentally examined and compared with the properties of RCA processed using acid pre-soaking at various acid concentrations and various soaking durations and using conventional heating at various temperatures.

Four different sources of RCA were used throughout this study:

1) **RCA-SAM:** RCA obtained from the biggest concrete recycling plant in Singapore, Samgreen. This recycling plant is supplied mainly with concrete from demolition debris from concrete road pavements. In this recycling plant, the large concrete chunks are first broken into smaller pieces that can be handled with the jaw crusher. After the initial crushing using a Jaw crusher the impurities are manually sorted and removed while the crushed concrete pieces move on the conveying belt to reach the magnet. The Magnet is used to separate the remaining reinforcing rebars. In the next stage, RCA particles are crushed using an impact crusher to the final required size. The products are sieved and large pieces are again crushed to the desired size using an impact crusher. Throughout this chapter, the RCA from this source are referred to as RCA-SAM.

2) **RCA30**: RCA from Grade C30 laboratory crushed specimens, representative of RCA produced from concrete of a grade commonly used in the 1980's and earlier.

3) **RCA60**: RCA from Grade C60 laboratory crushed specimens, representative of RCA produced from normal strength concrete currently used in Singapore.

4) **RCA90**: RCA from Grade C90 laboratory crushed specimens, representative of RCA produced from high strength concrete.

The coarse RCA-SAMs are produced in two different size fractions; 5-20 mm and 20-40 mm. The RCA composition test (BS 8500-2: 2006, ANNEX B) conducted on RCA-SAM samples, Table 10.1, showed that the amount of impurities were well below the level permitted by BS standard.

To prepare the laboratory crushed RCA samples (RCA30, RCA60, and RCA90), three different concrete grades of C30, C60, and C90 with characteristic cube compressive strengths of 30 MPa, 60 MPa and 90 MPa, respectively, were cast. The concrete specimens were cured in Fog room for 7 days and were then kept in lab air for another 35 days when they were crushed into a maximum size of about 12 mm using a Jaw crusher. The mix proportions and mechanical properties of C30, C60, and C90 concrete specimens cast are presented in Appendix A.

10.2 Phase 1 Experiments

The first phase of the experimental program was targeted at investigating the effects of the adhering mortar content of RCA on its properties as well as examining various parameters involved in the current state of art concrete recycling technology that may affect the amount of the adhering mortar.

10.2.1. Relationship between RCA Properties and Adhering Mortar Content

According to the literature available, mortar content, directly or indirectly, affects the RCA properties such as density, water absorption, and abrasion resistance. In this study a comprehensive experimental programme was conducted to investigate the relationship between RCA properties and adhering mortar content. The experimental study involved production of RCA samples with various adhering mortar contents and measurement of their basic properties.

In order to produce RCA containing different percentages of adhering mortar, thirty batches comprising 1 kg RCA samples obtained from the laboratory crushed concrete specimens (RCA60) were soaked in sulfuric acid at various concentrations for various soaking durations. After soaking in sulfuric acid solution, depending on the acid concentration and soaking duration used, a portion of the adhering mortar of the RCA samples was removed, producing RCA samples with different mortar contents. The water absorption and specific bulk gravity of each sample were measured in accordance with ASTM C127-07. Moreover, the remaining adhering mortar content of RCA samples was measured using the method described in Section 7.2.1.3.

10.2.2 Effects of the Production Parameters on the Adhering Mortar Content of RCA

Prior to investigate the efficacy of various beneficiation methods for reducing the adhering mortar content of RCA, it is worthwhile to examine the various parameters involved in the RCA production procedure that might affect the adhering mortar content. These parameters include the RCA particle size which is determined by the distance between the jaws of the crusher, the number of crushing stages, the strength of the parent

concrete used to produce RCA, etc. As a part of the first phase of this study, the effects of these parameters on the adhering mortar content as well as on the water absorption and bulk specific gravity which are deemed to be directly related to the amount of the adhering mortar were investigated. The adhering mortar content of RCA samples were measured using the acid soaking method described in section 10.2.1.1 and the water absorption and bulk specific gravity tests were conducted in accordance with ASTM C127-07.

10.2.2.1 Particle Size

To investigate the effects of the particle size, the adhering mortar content, water absorption and bulk specific gravity of RCA-SAM samples sieved into 4-8 mm, 8-12 mm, 12-16 mm and 16-20 mm size fractions were measured.

10.2.2.2 Strength of the Parent Concrete

During the past few decades, the average strength grade of the concrete used in Singapore's construction has been increasing consistently. Hence, the effect of strength of the parent concrete used to produce RCA should be investigated. The effects of the parent concrete strength on the mortar content, water absorption, and bulk specific gravity of RCA were investigated using samples of RCA30, RCA60 and RCA90 recycled concrete aggregates produced in the laboratory.

10.2.2.3 Number of Crushing Stages

To examine the effect of number crushing stages, the RCA-SAM samples of 20-40 mm size were re-crushed to 12 mm maximum size using a jaw crusher. Re-crushed samples were then sieved into 4-8 mm and 8-12 mm size fractions. The adhering mortar

content, water absorption and bulk specific gravity of 4-8 mm and 8-12 mm re-crushed

RCA-SAM samples were compared with the respective properties of the original 4-8 mm

and 8-12 mm RCA samples obtained from the recycled plant without any further

laboratory crushing as well as the respective properties of the original 20-40 mm RCA

particles.

10.3 Phase 2 Experiments: Efficacy of Different RCA Beneficiation Methods

Once the relationship between the properties of RCA and the adhering mortar content

was investigated in the first phase, the second phase studies were targeted at comparing

the efficacy of various beneficiation methods to improve the properties of concrete by

reducing the adhering mortar content. The focus was placed on investigating the efficacy

of the microwave-assisted beneficiation technique on a larger scale by using the pilot

microwave heating system fabricated during the current study. Moreover, the

improvements in the RCA properties achieved using microwave–assisted RCA

beneficiation were compared with that achieved using acid pre-soaking and conventional

heating beneficiation methods as proposed in available literature. The efficacy of various

RCA beneficiation methods was examined by comparing the bulk specific gravity, water

absorption and the mortar content of RCA before and after beneficiation.

This experimental study was carried out on the RCA produced by crushing the

laboratory-cast concrete specimens using a jaw crusher (RCA60). Only RCA particles of

8-12 mm size fraction were used. The water absorption, bulk specific gravity, and mortar

content of 8 to 12 mm RCA were measured as 4.2%, 2370 kg/m^3, and 47%, respectively.

10.3.1 Microwave-Assisted RCA Beneficiation

To investigate the effect of the RCA water content on the efficiency of the microwave-assisted beneficiation, samples with two different moisture conditions were prepared:

1. Saturated (SA): 2 kg oven-dried RCA-SAM samples were saturated by immersing them in water for 24 hours.

2. Air Dried (AD): 2 kg oven dried RCA-SAM samples were saturated by immersing them in water for 24 hours and were then kept at ambient indoor laboratory temperature and humidity conditions for 21 days.

Each sample was heated using the 10 kW microwave heating system designed and installed during this study at full power for 2 minutes. The samples were then sieved on 4 mm sieves to separate the delaminated adhering mortar.

10.3.2 Acid Soaking Beneficiation

As previously mentioned, 0.1 molar acidic solutions proposed by Tam et al. (2007) were reported to lead to only 7.27% and 12.17% decrease in the water absorption and thus were not suitable for the present study. In the current study, to investigate the capability of acid pre-soaking to be used on a larger scale, the effects of three different sulfuric acids concentrations of 0.1, 0.5, 1 molar and two different soaking durations of 1 day and 5 days were examined. 1 kg oven dried batches were placed in a plastic container and soaked in sulfuric acid solutions of various concentrations for various durations. After soaking, the RCAs were washed on 4 mm sieves and any detached mortar collected.

10.3.3 Conventional Heating Beneficiation (Thermal Beneficiation)

As reviewed in chapter 3, in this method RCA particles are heated at 300 °C to 500 °C. The thermal stresses generated through thermal expansion lead to the removal of the adhering mortar. It is believed that saturating the adhering mortar can increase the efficiency of this method because it can lead to pore pressure development in the adhering mortar. The concomitant effect of the pore pressure development and thermal stresses can lead to faster removal of the adhering mortar. In some cases, recommendations to immerse the hot aggregates in cold water immediately after heating have also been made. In the present study, saturated RCA batches of 1 kg (oven-dried weight) were heated in a conventional furnace at 300 °C and 500 °C for 2 hours. After heating, the RCA samples were immediately cooled down by immersion in a water tank cooled to 10 °C.

10.3.4 Measurement of the Delaminated Adhering Mortar Percentage

After going through the beneficiation processes explained above, each batch was washed on a 4 mm sieve and the delaminated adhering mortar collected. The RCAs retained on the 4 mm sieves were oven dried and sieved again for 5 minutes to collect any lose material detached. The portion of the sample remained on the 4 mm sieve was weighed and the percentage of the mortar detached was calculated. The bulk specific gravity and water absorption of the samples were then measured. Moreover, the acid soaking method presented in section 7.2.1.3 was used to measure the remaining adhering mortar content of the RCA samples after beneficiation.

10.4 Results and Discussion

10.4.1 Phase 1

10.4.1.1 Effects of the Adhering Mortar Content on the Bulk Specific Gravity and Water Absorption of RCA

The variations of the water absorption and bulk specific gravity of the RCA particles with the amount of the adhering mortar present are shown in Figures 10.1 and 10.2, respectively. As can be seen, a higher amount of adhering mortar present leads to higher water absorption and lower bulk specific gravity of RCA. Results showed that the water absorption of RCA increased from 0.6% to 4.8% as the adhering mortar content increased from 0 to 58%. Moreover, for a similar increase in the adhering mortar content, the bulk specific gravity of RCA decreased from 2590 to 2340 kg/m^3.

As can be seen, once the adhering mortar of RCA has been completely removed, the water absorption and bulk specific gravity of RCA approach those of the original natural aggregates, 0.6% and 2590 kg/m^3, respectively. Moreover, linear regression showed a relative proportionality of bulk specific gravity and water absorption of RCA to adhering mortar content. It may be noted that compared to the results obtained in the present study, the results reported by De Juan et al. (2009) showed greater variability. This is probably because in the current study, RCA samples produced from a specific concrete source were used. As a result of variation in sources of the concrete debris, the RCA produced in a typical concrete recycling plant may show a larger variability.

10.4.1.2 Effects of the Particle Size on the Properties of RCA

The adhering mortar content, water absorption and bulk specific gravity of various size fractions of the RCA-SAM batches are compared in Figures 10.3, 10.4 and 10.5,

respectively. As can be seen, the adhering mortar content and thus water absorption and density vary significantly with the size of the RCA particle. Results showed that an increase in the size of the RCA particles led to a smaller amount of adhering mortar present. This might be due to the fact confirmed by physical observations that some of the smaller RCA particles comprised entirely of mortar chunks. As expected, results showed that a decrease in the adhering mortar content with an increase in the particle size resulted in an almost proportional decrease in water absorption and increase in bulk specific gravity.

10.4.1.3 Effects of the Parent Concrete Strength on the Properties of RCA

The adhering mortar content, water absorption and bulk specific gravity of the RCA batches produced by crushing concrete specimens of three different compressive strengths are compared in Figures 10.6, 10.7 and 10.8, respectively. As can be seen, the adhering mortar content of both "4 to 8 mm" and "8 to 12 mm" RCA samples increased with an increase in the parent concrete compressive strength. This may be attributed to the fact that stronger mortar present in the RCA produced from higher strength concretes results in less mortar being removed during crushing. As expected, for all cases except for the 4 to 8 mm RCA produced from C30 concrete, 4 to 8 mm RCA samples contained more adhering mortar than 8 to 12 mm RCA samples. The unexpectedly low adhering mortar content of 4 to 8 mm RCAs produced from C30 concrete may be due to the fact that the mortar is weaker and should be easier to remove and is more prone to breaking into sand and powder. Thus a smaller amount of material between the 4 to 8 mm size fraction is collected.

In addition, as can be seen in Figure 10.7, except for the 4 to 8 mm RCAs produced from C30 concrete which exhibited unexpectedly low water absorption, the water absorption decreased with an increase in the parent concrete strength. This may attributed to the fact that the adhering mortar in RCA produced from higher strength concrete is denser and thus absorbs less water.

10.4.1.4 Effects of the Number of Crushing Stages on the Properties of RCA

Table 10.2 compares the properties of "4 to 8 mm" and "8 to 12 mm" RCA produced by re-crushing "20 to 40 mm" RCA-SAM particles to the properties of respective size fractions before re-crushing in the laboratory. As can be seen, further crushing may significantly increase the quality of RCA. The results of this study showed that reducing the size of RCA from 20-40 mm to 4-12 mm through an additional crushing stage resulted in a significant decrease in the adhering mortar content of the RCA particles (from 57% to less than 28%, by mass).

In addition, when compared to the original RCA belonging to the similar size fraction, it was observed that as a result of the additional crushing, the adhering mortar content of 4 to 8 mm and 8 to 12 mm RCAs decreased from 67% to 27% and from 63% to 18%, respectively. As can be seen in Table 10.2, this reduction led to almost 61% and 67% reduction in the water absorption of the 4-8 mm and 8-12 mm RCA particles, respectively. Moreover, the bulk specific density increased from 2190 to 2427 kg/m^3 and from 2216 to 2501 kg/m^3 for 4 to 8 mm and 8 to 12 mm RCA particles, respectively. Results also showed that re-crushing resulted in a significant reduction in the Los Angeles abrasion loss of the RCA-SAM samples. However, it should be noted that further

crushing may significantly lower the yield of the coarse recycled concrete aggregate by producing a large amount of fine.

10.4.2 Phase 2: RCA Beneficiation Methods

The results of the experiments conducted in the first phase of this study confirmed that a reduction in the amount of adhering mortar can increase the bulk specific gravity and reduce the water absorption of RCA. These generally imply an increase in the overall quality of RCA. Moreover, the effects of various parameters involved in the current state of art concrete recycling technology on the amount of the adhering mortar were investigated. In the following, the efficiency of various RCA beneficiation techniques that may be incorporated into the current recycling technology is examined. The effects of the microwave-assisted RCA beneficiation on the properties of RCA is examined and compared with the acid pre-soaking beneficiation and conventional heating beneficiation methods.

10.4.2.1 Microwave-Assisted Beneficiation

The surface of a 30 mm RCA-SAM particle before and after microwave heating using the 10 kW microwave heating system is depicted in Figure 10.9. As previously confirmed through the experiments presented in chapter 7, the results of this study also showed that in most cases, especially when saturated RCA batches were heated, a considerable portion of the adhering mortar was effectively detached from the RCA and the detachment seemed to have occurred at the ITZ as the original surface of the granite was clearly visible. Moreover, the remaining adhering mortar seemed to have been significantly weakened and fissured.

The properties of RCA processed using different RCA beneficiation techniques are listed in Table 10.3. As can be seen, microwave-assisted beneficiation of the RCA samples in a saturated (SA) condition led to 33.3% reduction in the water absorption and 3.8% increase in the specific bulk density of RCA. This may be directly related to the 48.9% reduction in the adhering mortar content of RCA after microwave-assisted RCA beneficiation at SA moisture condition. It must be noted compared to the results obtained using the commercially available microwave oven used in chapter 7, the results of this study seemed to show an improvement. In practice, a combination of high power microwave systems in a continues microwave heating chamber may be used to increase the yield and efficiency of the microwave-assisted beneficiation technique.

10.4.2.2 Acid Pre-Soaking Beneficiation

As can be seen in Table 10.3, the results of the acid soaking beneficiation method at different acid concentrations showed that soaking the RCA particles in 0.1 molar sulfuric acid as proposed by Tam et al. (2007) removed only about 2.1% of the adhering mortar and reduced the water absorption of RCA by only 2.4%. Moreover, results showed that a longer soaking duration at such concentrations may not result in any significant improvement in the quality of RCA produced. However, results showed that higher acid concentrations may be used to remove the adhering mortar more effectively. Soaking the RCA particles at 0.5 molar sulfuric acid solutions for 1 and 5 days led to 12.8% and 29.8% reduction in the amount of adhering mortar present and 7.1% and 19% reduction in water absorption, respectively. Moreover, soaking the RCA samples in 1 molar sulfuric acid solutions for 1 and 5 days resulted in 23.4% and 72.3% reductions in the adhering mortar content, respectively. However, concentrations as high as 0.5 and 1 molar may

pose safety and health concerns in practical applications and may significantly increase the sulfate content of RCA. Furthermore, this method is rather time consuming, taking at least 24 hours overall. Hence, the acid pre-soaking method at high acid concentrations may be effective only as a testing method to measure the amount of adhering mortar present on the RCA particles.

10.4.2.3 Conventional Heating Beneficiation

As can be seen in Table 10.3, the results of this study showed that conventional heating at 300 °C and 500 °C can reduce the adhering mortar content of RCA by only 6.4% and 12.8%, respectively. However, inspection of the RCA particles after conventional heating showed that after heating at 500 °C, the adhering mortar seemed to have been significantly weakened and could be more easily removed by robust brushing. Hence, incorporating a rubbing or crushing stage after conventional heating may significantly increase the efficacy of this method. De Juan et al. (2009) reported that the adhering mortar of RCA could be removed from individual RCA particles using a plastic hammer after being heated at 500 °C for 2 hours.

However, this technique is also very time and energy consuming. Processing of each batch of RCA using this technique may take about 4 hours. Moreover, as reviewed in chapter 3, according to Homand et al. (1989), heating at 300 °C to 500 °C used in this method can adversely affect the mechanical properties of the aggregates.

10.5 Conclusions

The relationship between the RCA properties and the amount of the adhering mortar present on RCA particles was experimentally investigated in this study. Results confirmed

that a higher amount of the adhering mortar generally leads to a higher water absorption and lower bulk specific gravity of RCA. Moreover, results confirmed that the amount of the adhering mortar present on RCA particles significantly vary with the size of RCA and the number of crushing stages used to produce RCA. In addition, the results showed that microwave-assisted RCA beneficiation can significantly improve the quality of RCA by reducing the adhering mortar content. The improvements achieved through the microwave assisted beneficiation seemed to be considerably higher that through conventional heating and acid pre-soaking methods.

Table 10.1 RCA-SAM composition

	Test 1	Test 2	Average	Maximum permitted by BS 8500-2	Remarks
Concrete and Aggregate, $P_{concrete}$ %	98.66	99.55	99.1		
Masonry, $P_{masonry \%}$	0.26	0.09	0.2	5	satisfactory
Lightweight, $P_{lightweight}$ %	0.25	0.02	0.1	0.5	satisfactory
Asphalt, $P_{asphalt}$ %	0.81	0.32	0.6	5	satisfactory
Others, P_{others} %	0.02	0.02	0	1	satisfactory

Table 10.2 RCA properties before and after re-crushing

RCA Property	Commercially Produced RCA-SAM			Re-crushed	
	4-8 mm	8-12mm	20-40 mm	4-8 mm	8-12mm
water absorption	8	6.8	6.37	3.14	2.28
Bulk specific Gravity	2190	2216	2229	2427	2501
Los Angles Abrasion resistance	38	37	35	25	24
adhering mortar content	67	63	57	27	18

243

Table 10.3 Results of the RCA beneficiation experiments

Beneficiation Method		Duration	RCA Properties After Beneficiation			Reduction in Water Absorption (%)	Increase in Bulk Specific Gravity (%)	Reduction in Adhering Mortar Content (%)
			Water absorption (%)	Bulk Specific Gravity (kg/m^3)	Adhering Mortar Content (%)			
Microwave-assisted	SA [1]	2 Min	2.8	2460	24	33.3	3.8	48.9
	AD [2]	2 Min	3.4	2430	32	19	2.5	31.9
Conventional Heating	300 °C	2 Hr	4.1	2380	44	2.4	0.4	6.4
	500 °C	2 Hr	3.8	2390	41	9.5	0.8	12.8
Acid Pre-soaking	0.1 molar	1 day	4.1	2380	46	2.4	0.4	2.1
		5 days	4.1	2380	46	2.4	0.4	2.1
	0.5 molar	1 day	3.9	2400	41	7.1	1.3	12.8
		5 days	3.4	2410	33	19	1.7	29.8
	1 molar	1 day	3.5	2410	36	16.7	1.7	23.4
		5 days	1.6	2500	13	61.9	5.5	72.3
	2 molar	5 days	0.6	2590	0	85	9	100

[1] Saturated
[2] Air-Dried
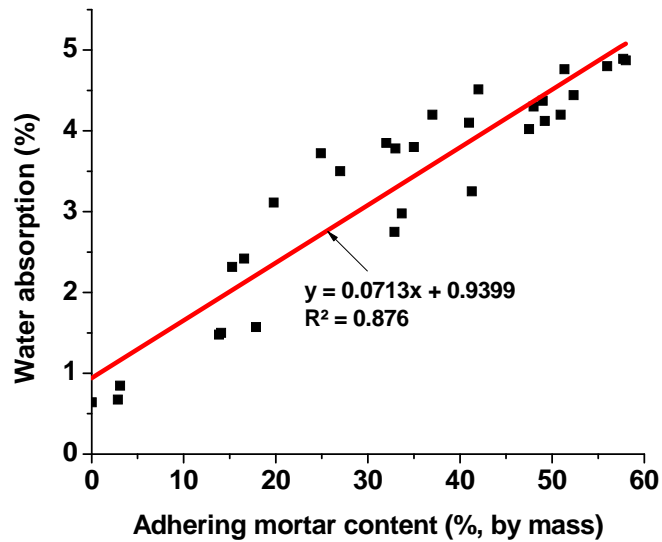
Figure 10.1 Relationship between adhering mortar content measured using acid soaking method and water absorption
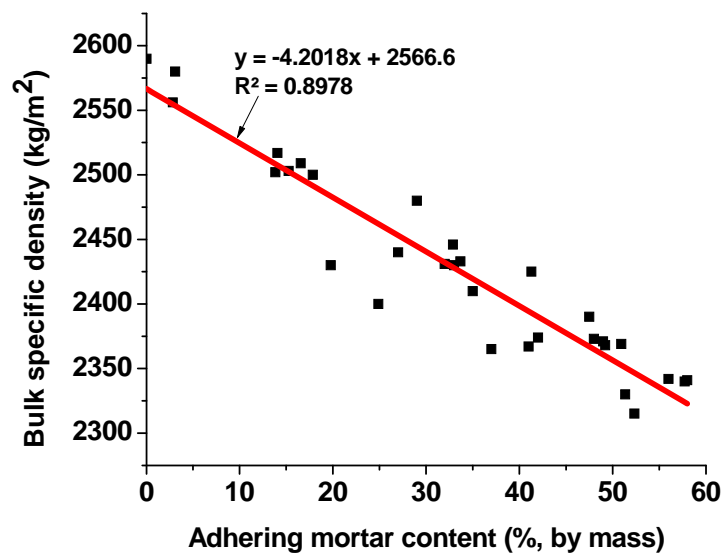
Figure 10.2 Relationship between adhering mortar content measured using acid soaking method and bulk specific gravity
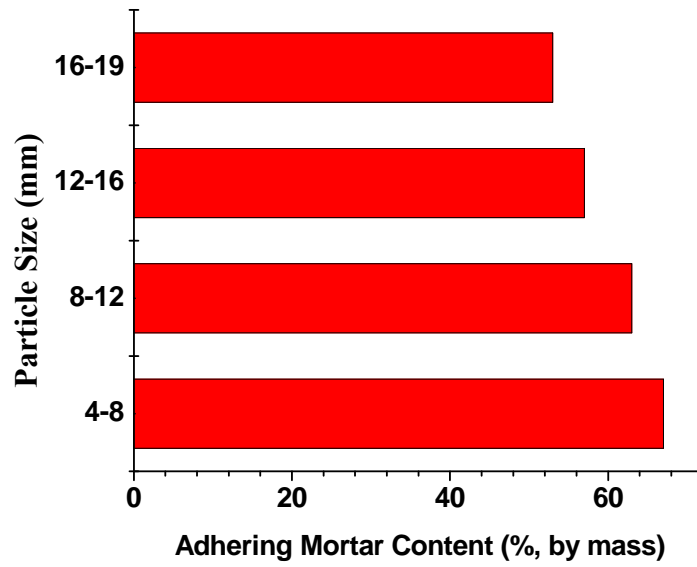
Figure 10.3 Variation of the adhering mortar content measured using acid soaking method with the RCA size
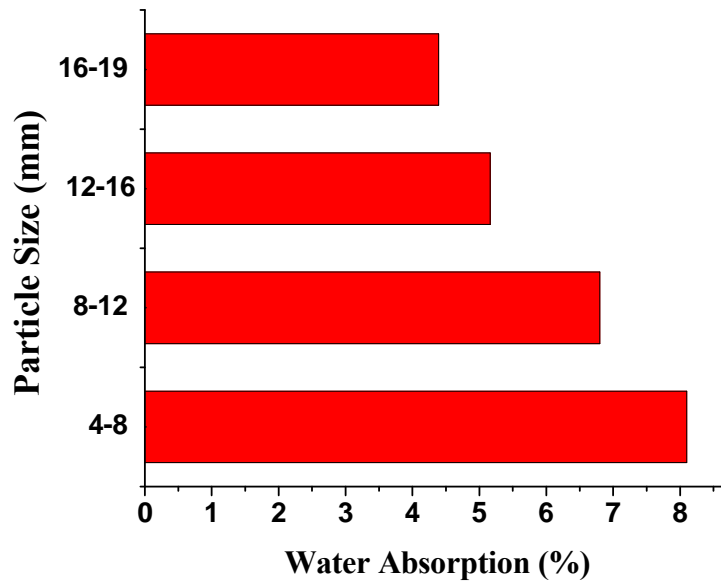
Figure 10.4 Variation of the RCA water absorption with its size
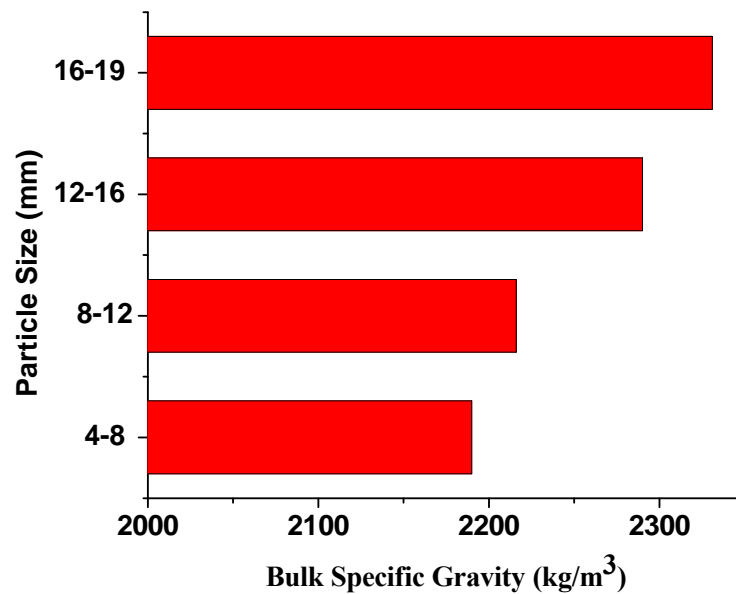
Figure 10.5 Variation of the bulk specific gravity of RCA with its size
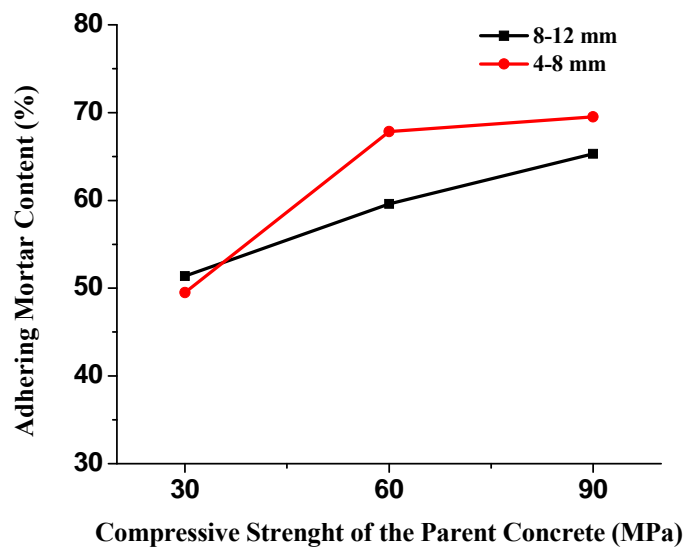
**Figure 10.6 Relationship between the adhering mortar content of RCA measured using acid
soaking method and the compressive strength of the parent concrete**
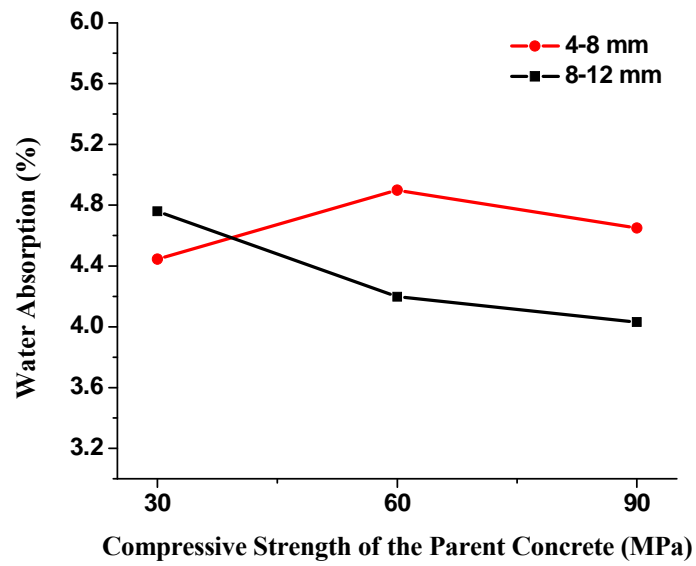
Figure 10.7 Relationship between the water absorption of RCA and the compressive strength of the parent concrete
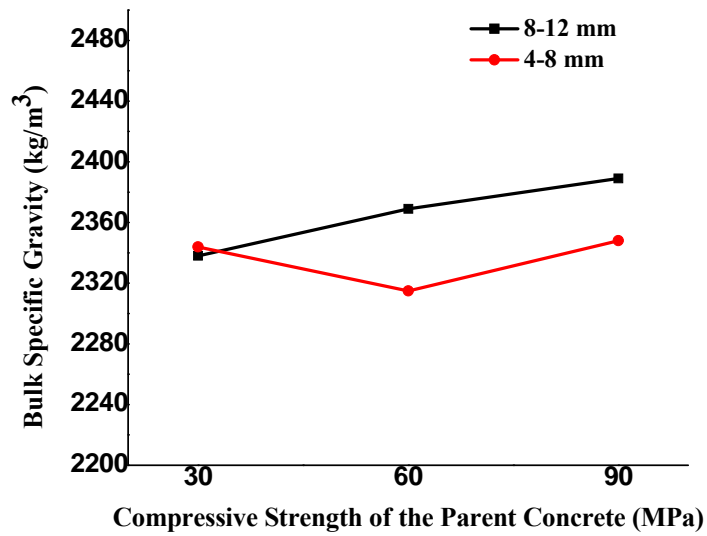
Figure 10.8 Relationship between the bulk specific gravity of RCA and the compressive strength of the parent concrete

A 30 mm RCA-Sam particle before beneficiation

Same particle crushed to three pieces after microwave heating

Figure 10.9 Surface of a 30 mm RCA particle before and after microwave heating

Chapter 11 : Summary, Conclusions and Future Work Recommendations

11.1 Summary

The results of a comprehensive study on different methods to improve the quality of the recycled concrete aggregate (RCA) were presented in this thesis. A comprehensive literature review on the properties of aggregates, produced using the currently available recycling techniques, was presented in Chapter 2 of this thesis. Based on the available literature, the two main factors lowering the quality of RCA compared to NA were identified as:

1- Contaminants (impurities), chemical and physical, present in the concrete debris.

2- Mortar adhering to RCA particles, which is of a porous and weak nature.

Having known the main factors attributing to the inferior properties of RCA, the current study was focused on investigating the capability of various methods to eliminate them. In the first section of chapter 3, different concrete surface removal techniques were

reviewed and assessed for possible use in removing the contaminants\impurities from the surface of concrete debris. Emphasis was placed on using the microwave-assisted surface removal (microwave decontamination) method which has been reported to be more efficient and less time consuming compared to other techniques. In the second section of chapter 3, methods previously used to remove the adhering cementitious mortar from the RCA particles (RCA beneficiation methods) were reviewed. Moreover, a novel microwave-assisted RCA beneficiation technique was proposed to increase the yield and speed of the RCA beneficiation process and to eliminate the drawbacks of previously proposed methods. In order to pave the way for a better understanding of the microwave assisted methods considered in this study, the fundamentals of microwave heating were reviewed in chapter 4. Various assumptions, estimations and modeling techniques as well as the electromagnetic properties of concrete, mortar and aggregate were discussed in chapter 4.

To investigate the feasibility of using the microwave decontamination method to remove the impurities and contaminants from the concrete surface and for a better understanding of the underlying phenomenon causing concrete surface delamination during microwave heating, an analytical study was reported in chapters 5 and 6. In chapter 5, a simple microwave power estimation formulation based on Lambert's law was used to predict the microwave-concrete interaction during the microwave decontamination process. The original Lambert's law formulation was modified to account for reflection at the exposed concrete surface as well as the sinusoidal distribution of the incident microwave power. By using the microwave heat dissipation estimated through the modified Lambert's law as the heat source, the coupled heat and mass transfer

formulation was solved to model the thermal stresses and pore pressure development in concrete when exposed to microwave heating. To investigate the effects of microwave frequency and concrete moisture condition on the efficiency of the microwave decontamination process, three different common microwave frequencies and four different concrete water contents were considered.

However, according to available literature, the approximate method used in chapter 5 to estimate microwave power dissipation in concrete may not be accurate, especially when the thickness of concrete is lower than the microwave penetration depth at the particular microwave frequency used. Moreover, this method does not account for reflections occurring at the distal surface of concrete as well as reflections when microwaves encounter the embedded reinforcing bars. In order to verify the accuracy of the approximate Lambert's law method and to accurately model the effects of reinforcing bars on the microwave decontamination process, in chapter 6, microwave-concrete interaction was modeled using the more accurate but complicated Maxwell's equations. The electromagnetic field intensity, microwave power dissipation and the resulting thermal stress distribution in a concrete block heated with a typical industrial microwave heating system comprising a rectangular waveguide as the applicator were calculated. Results were compared with those obtained using the approximate Lambert's law formulation.

In chapter 7, the fundamentals of microwave-assisted RCA beneficiation technique proposed in this study used to remove the adhering mortar from RCA particles were explained. A preliminary experimental study was conducted to investigate the capability of microwave heating to remove the adhering mortar of RCA. In addition, to investigate the feasibility of using this method on a larger-scale, a pilot industrial microwave–assisted

beneficiation system was simulated. To consider the effect of the adhering mortar's water content, two different moisture conditions were considered.

Once the capability of microwaves to remove the concrete surface layer and to remove the adhering mortar from RCA was confirmed through the numerical and experimental studies conducted in chapters 5 to 7, the effort was focused on finding a suitable temperature measurement technique to be used in controlling these processes as well as to verify the numerical results. Since, the thermal stresses and pore pressure that develop in concrete are a function of the temperature and its gradient, monitoring the temperature in the concrete interior can be used as a process control tool to predict the removal thickness and to estimate the microwave power dissipation pattern in the microwave heated concrete and RCA. Thermocouples are the most commonly used temperature measurement sensors. However, because they are metallic in nature, such thermocouples are not immune to electromagnetic interference and may be inaccurate when deployed in a microwave field. Optical fiber sensors are well-known to be virtually immune to effects of electromagnetic fields. Because of their glass-based nature, optical fibers do not interact with the electromagnetic field and hence are expected to be accurate in the presence of microwaves. In chapter 8, the accuracy of thermocouples and Fiber Bragg Grating (FBG) optical fiber sensors for measuring the concrete temperature during microwave heating was investigated. In order to verify accuracy, both FBG sensors and thermocouple measurements were compared to the results obtained through a numerical modeling as well as the measurements taken using an infrared thermo-tracer camera.

One of the most important steps to commercialize the two microwave-assisted methods introduced in chapter 5 to 8 is to design an efficient, safe and economical

industrial system that can be eventually incorporated in an actual RCA production facility. Hence, in chapter 9, the various stages of design, assembly, and installation of a pilot microwave heating system installed at the NUS structural laboratory were presented.

In the first phase of the studies reported in chapter 10, the effects of the adhering mortar content of RCA on various properties of RCA including the water absorption and bulk specific gravity density were investigated experimentally. In addition, the effects of particle size, number of crushing stages, and strength of the parent concrete on the adhering mortar content of RCA were examined.

Once the relationship between the properties of RCA and the adhering mortar content was investigated in the first phase, the second phase studies were targeted at comparing the efficacy of various beneficiation methods to improve the properties of concrete by reducing the adhering mortar content. The focus was placed on investigating the efficacy of the microwave-assisted beneficiation technique on a larger scale by using the pilot microwave heating system fabricated during the current study. Moreover, the improvements in the RCA properties achieved using microwave–assisted RCA beneficiation were compared to that achieved using acid pre-soaking and conventional heating beneficiation methods. The efficacy of various RCA beneficiation methods was examined by comparing the bulk specific gravity, water absorption and the mortar content of RCA before and after beneficiation.

11.2 Conclusions

Results of the numerical and experimental studies presented in this thesis showed that microwave technology can be used to significantly improve the quality of the coarse recycled concrete aggregates. Microwave heating can be incorporated into conventional

recycling at two stages. First, microwave decontamination may be used to reduce the amount of the contaminants present in demolition debris prior to demolition and extraction for feeding into the recycling process. Second, microwave-assisted beneficiation can be used to reduce the amount of adhering mortar present on crushed RCA particles and thereby increase quality and yield. The findings and conclusions of the present study may be summarized as follows:

1. An easy-to-use analytical formulation based on the Lambert's law modified to account for the reflections at the incident surface as well as for the incident microwave power distribution mode was developed and used to simulate the thermal stresses and pore pressure developed in concrete when subject to microwaves. The accuracy of this method was verified using a more accurate but complicated simulation method based on Maxwell's equations. Hence, Lambert's law can be confidently used as a satisfactory approximation to simplify analytical modeling of the microwave heating process in concrete. Results of the numerical simulation also showed that:

- Microwave heating of the concrete surface at high microwave powers and frequencies may be used to remove a layer of the concrete surface by developing a localized field of high thermal stresses and pore pressure. The spalling depth of the concrete surface layer and the time for spalling to occur are inversely proportional to the microwave frequency.

- Drenching of the concrete surface with copious amount of water may be used to increase the efficiency of the microwave decontamination process, as considerably higher stresses in a thinner surface layer may be generated.

- The microwave decontamination process is significantly affected by concrete dielectric properties. The dielectric properties of concrete vary significantly with the concrete water content.

- The presence of reinforcing bars in concrete will generally lead to a higher temperature rise in the concrete surface layer. The effect of reinforcing bars on the microwave decontamination process decreases with a decrease in the microwave penetration depth. The microwave penetration depth appears to decrease with an increase in microwave frequency or water content of the concrete.

2. The results of the numerical and experimental studies confirmed that microwave heating may be effectively used to remove cementitious mortar adhering to RCA particles through developing high temperature gradients and thus high thermal stresses, especially at the interfacial zone.

3. The amount of the thermal stresses developed in the adhering mortar and interfacial transition zone increase significantly as the water content of the adhering mortar increases. Hence, saturating the RCA particles prior to exposure to microwaves can significantly increase the yield and quality of the RCA produced.

4. Bare FBG fibers can accurately measure concrete temperature when heated by microwaves and thus may be used as a reliable process control tool in applications such as microwave decontamination of concrete and microwave assisted RCA beneficiation.

5. Thermocouples are significantly affected by electromagnetic interference and mostly overestimate the actual temperature of the concrete. Moreover, the commercially-

packaged off-the-shelf FBG sensors currently used for strain and temperature measurements of concrete in normal environments cannot be used in the presence of strong microwave fields.

6. The temperatures measured using the FBG sensors and infrared camera verified the accuracy of the numerical simulations.

7. A 10 kW pilot microwave heating system that can be used for both microwave surface decontamination and microwave-assisted RCA beneficiation was designed and installed in the NUS structural laboratory. The capability of microwave heating to remove the adhering mortar content in a larger scale was confirmed using this system.

8. The water absorption and bulk specific gravity of RCA seemed to vary proportionally with the amount of the adhering mortar present on RCA particles. A higher amount of the adhering mortar generally leads to a higher water absorption and lower bulk specific gravity of RCA.

9. Amount of the adhering mortar present on RCA particles vary significantly with the RCA particle size and number of crushing stages used to produce RCA.

10. Microwave-assisted RCA beneficiation may improve the quality and yield of RCA by reducing the adhering mortar content. The improvements achieved through the microwave assisted beneficiation seemed to be considerably higher that through conventional heating and acid pre-soaking methods.

11.3 Future Work Recommendations

The future work of this study may be concentrated in the following areas:

1- Designing a mobile microwave decontamination system that can be safely deployed at demolition sites to remove the non-concrete impurities before demolition.

2- Measurement of the dielectric properties of concrete and mortar and investigating their variation with temperature, water content and mix proportion to enhance the accuracy of numerical simulations.

3- Experimental tests on the properties of concrete made using the RCA treated with different beneficiation techniques to investigate the effects on the short term and long term properties.

4- To investigate the possibility of using different combinations of the RCA beneficiation methods described in this thesis such as "microwave heating and rubbing".

5- Cost analysis of different beneficiation methods.

References

Albin, S. (1998), "Enhanced Temperature Sensitivity using Coated Fiber Bragg Grating.", SPIE **3483**.

Alexander Watson and St. Albans (1965), "Methods of Cracking Structures and Apparatus for Cracking Structures", United States Patent **3430021**

Ayappa, K. G., H. T. Davis, et al. (1991), "Microwave heating: An evaluation of power formulations", Chemical Engineering Science **64**(4): 1005-1016.

Ayers, K. W. (1998), "Feasibility of Recycling Contaminated Concrete", Environmental Engineering, Vanderbilt University. **PhD thesis**.

B. Degamber, G. F. F. (2003), "Fiber Optic Sensors for Noncontact Process Monitoring in a Microwave Environment", Journal of Applied Polymer Science **89**: 3868–3873.

B. Schmaup, M. M., and J. Ernst (1995), "A fiber-optic sensor for microwave field measurements", Rev. Sci. Instrum. **66**(8): 4031-4033.

Barringer, S., E. A. Davis, et al. (1995), "Microwave heating temperature profiles for thin slabs compared to Maxwell and Lambert's law predictions", Journal of Food Science **60**(5): 1137-1142.

Basak, T. (2004), "Analysis of Microwave Propagation for Multilayered Material Processing: Lambert's Law versus Exact Solution", Research notes, Department of chemical engineering, Indian institute of technology, Madras.

Bazant Z. P. and N. L.J. (1972), "Nonlinear water diffusion in non-saturated concrete", Materiaux et constructions **5**(25): 3-20.

Bazant, Z. P. and M. F. Kaplan (1996), "Concrete at high temperatures: material properties and mathematical models", Harlow, Essex : Longman Group.

Bazant, Z. P. and W. Thonguthai (1978), "Pore pressure and drying of concrete at high temperature", J. Eng. Mech. Div., Am. Soc. Civ. Eng **104**(5): 1059-1079.

Berkoff, A. D. K. a. T. A. (1992), "Fiber Optic Bragg Grating Differential Temperature Sensor", Photonics Technology Letters, IEEE.

Blast Technology Pte. Ltd., "Shot Blasting", Viewed 20 January, 2010. <http://www.gritblasters.co.uk>

BS 8500-2, Concrete. "Complementary British Standard to BS EN 206-1. Specification for constituent materials and concrete". 2006, BSI

BS EN 12620:2002+A1:2008. "Aggregates for concrete", 2008, BSI

Budelmann. H. and Dora. B. (1999), "Beton in Stoffkreislauf (Concrete in the Material Cycle)", Arconis 4, **Nr. 1**: S.10-13.

Chi-Sun, P. and C. Dixon (2007), "Effects of contaminants on the properties of concrete paving blocks prepared with recycled concrete aggregates", Construction & Building Materials **21**(1): 164-75.

Christopher K.Y. Leung and Thanakorn Pheeraphan (1995), "Very high early strength of microwave cured concrete", Cement and Concrete Research **25**(1): 136-146.

Christopher K.Y. Leung and Thanakorn Pheeraphan (1997), "Determination of optimal process for microwave curing of concrete", Cement and Concrete Research **27**(3): 463-472.

Chuan Wang, Z. Z., Zhichun Zhang, Jinping Ou (2006), "Early-age monitoring of cement structures using FBG sensors", Smart Structures and Materials **6167**.

Chulhun Seo and T. Kim (1999), "Temperature sensing with different coated metals on fiber Bragg grating sensors", Microwave Opt Technol Lett **21**: 162-165.

Cold Jet LLC, "Dry Ice Blasting", Viewed 12 December, 2009, <http://www.coldjet.com.au>

Concrete Knowledge Center (2007), "Aggregates for Concrete", American Concrete Institute. Technical note **E1-071**

Constantine A. Balanis (1989), "Advanced engineering electromagnetic", John Wiley & Sons.

David P. Lindroth, Roger J. Morrell, et al. (1991), "Microwave Assisted Hard Rock Cutting", United States Patent **5003144**

De Juan, M. S. and P. A. Gutierrez (2009), "Study on the influence of attached mortar content on the properties of recycled concrete aggregate", Construction and Building Materials **23**(2): 872-877.

De Vries. J (1996), "Concrete Recycled: Crushed Concrete as Aggregate", Proceedings of the International Conference: Concrete for Environment Enhancement and Protection, Dundee Scotland.

Dhir, R., K. Paine, et al. (2004), "Recycling construction and demolition wastes in concrete", Concrete (London) **38**(3): 25-28.

Dickerson. K.S., M.J. Wilson-Nichols, et al. (1995), "Contaminated Concrete: Occurrence and Emerging Technologies for DOE Decontamination", DOE-ORO-2034, Oak Ridge: US Department of Energy, National Laboratory, Oak Ridge.

DOE (1994), "Decommissioning Handbook (DOE/EM-0142P)", Washington DC: US Department of Energy, Office of Environmental Restoration.

DOE (1997), "The 2006 Plan", Washington DC: US Department of Energy

Elwood JM (1999), "A critical review of epidemiological studies of radiofrequency exposure and human cancers", Environ Health Perspect (Suppl 1): 155-168.

EnviroCentre, C. D., National Green Specification (2005), "Demolition: Implementing Best Practice", Waste and Resources Action Programme.

Fleischer, W. and M. Ruby (1998), "Recycled aggregates from Old Concrete Highway Pavements", Proceedings of International Symposium-Sustainable Construction:Use of Recycled Concrete Aggregate, London.

G. Meltz, W.W. Morey, et al. (1989), "Formation of Bragg gratings in optical fibers by a transverse holographic method", optics letters **14**(15): 823-825.

Goangseup Zi. and Z. P. Bažant (2003), "Decontamination of radionuclides from concrete by microwave heating. II: Computations", *J.Eng Mech.* **129**(7): 785-792.

Grubl, P. and A. Nealen (1998), "Construction of an Office Building using Concrete made from Recycled Demolition Material", Proceedings of International Symposium-Sustainable Construction: Use of Recycled Concrete Aggregate, London

Haase, R. and J. Dahm (1998), "Baustoffkreislauf am besonderen Beispiel von Beton in norddeutschen Raum (Material Recycling with Specific Example of Concrete Recycling in North Germany)", Zeitschrift Beton (Concrete Journal).

Hansen, T. C. and E. Boegh (1985), "Elasticity and drying shrinkage of recycled aggregate concrete", ACI Material **82**(5): 648-652.

Hansen, T. C. and H. Narud (1983), "Strength of recycled concrete made from crushed concrete coarse aggregate", Concrete International: Design and Construction **5**(1): 79-83.

Hemanth Satish (2005), "Exploring microwave assisted rock breakage for possible space mining applications", Department of Mechanical Engineering. Montreal, Canada, McGill. , **Thesis, Master of Engineering**.

Hill K.O (1997), "Fiber Bragg Grating Technology Fundamentals and Overview", Journal of Light wave Technology **15**(8): 1263-1276.

Homand-Etienne and R. Houper (1989), "Thermally induced micro-cracking in granites: characterization and analysis", <u>Int J Rock Mech Min Sci Geomech Abst</u> **26**(2): 125-134.

Shanghai Zenith Impact Crusher Pte. Ltd., "Impact Crusher", Viewed 6 February, 2010. < <u>http://www.impact-crushers.com/Impact-Crusher.html</u> >

Shanghai Shibang Machinery Co., Ltd., "Jaw crusher", Viewed 20 March, 2010, < <u>http://www.sbmchina.com/products/stone_crusher3.html</u>>

J. B. Hasted and M. A. Shah (1964), "Microwave absorption by water in building materials", <u>BRIT. J. APPL. PHYS</u> **15**.

J. B. Hasted, Susan P. Lovell, et al. (1964), "Discontinuity in temperature variation of microwave dielectric properties of absorbed water", <u>BRIT. J. APPL. PHYS</u> **15**.

Jaehoon Jung, Hui Nam, et al. (1998), "Fiber Bragg grating temperature sensor with controllable high sensitivity", <u>Proceedings of WEE5</u>.

Jean C. C. Silva, Cicero Martelli, et al. (2004), "Temperature effects in concrete structures measured with fiber Bragg grating", <u>Second European Workshop on Optical Fibre Sensors</u> **5502**.

Kou, S. and C. S. Poon (2006), "Compressive strength, pore size distribution and chloride-ion penetration of recycled aggregate concrete incorporating class-F fly ash", <u>Journal Wuhan University of Technology, Materials Science Edition</u> **21**(4): 130-136.

Lagos, L. E., W. Li, et al. (1995), "Heat transfer within a concrete slab with a finite microwave heating source", <u>Int. J. Heat Mass Transfer</u> **38**(5): 887-897.

Li J. (2004), "Study on mechanical behavior of recycled aggregate concrete". <u>Shanghai, Tongji University</u>. **Thesis, Master of Engineering**.

Li W and Ebadian M A (1994), "Heat and mass transfer in a contaminated porous concrete slab with variable dielectric properties", <u>Int. J. Heat Mass Transfer</u> **37**(6): 1013-1027.

Li, X. (2008), "Recycling and reuse of waste concrete in China. Part I. Material behaviour of recycled aggregate concrete", <u>Resources, Conservation and Recycling</u> **53**(1-2): 36-44.

Li. W., M. A. Ebadian, et al. (1993), "Heat transfer within a concrete slab applying the microwave decontamination process", <u>J. Heat Transfer</u> **115**: 42-50.

M. H. Maher, K. Tabrizi, et al. (1996), "Fiber Bragg Gratings for Civil Engineering Applications." <u>Proceedings of SPIE</u> **2682**.

Mary McSheny, Cohn Fitzpatrick, et al. (2004), "Investigation and development of a fiber optic temperature sensor for monitoring liquid temperature in a high power microwave environment", <u>Second European Workshop on Optical Fibre Sensors</u> **5502**.

Murilo A. Romero, A. C. Jr., et al. (1997), "A fiber-optic Bragg grating temperature sensor for high voltage transmission lines", <u>IEEE Proceedings (</u>34-38).

N. Lagakos, J.A. Bucaro, et al. (1981), "Temperature-induced optical phase shifts in fibers", <u>Appl Opt</u> **22**: 478-483.

Nagataki, S., A. Gokce, et al. (2004), "Assessment of recycling process induced damage sensitivity of recycled concrete aggregates", <u>Cement and Concrete Research</u> **34**(6): 965-971.

Nykvist, W. E. and R. V. Decareau (1976), "Microwave meat roasting", <u>Journal of Microwave Power</u> **11**: 3-24.

Ohlsson, T. and N. Bengtsson (1971), "Microwave heating profiles in foods-a comparison between heating experiments and computer simulation", <u>Microwave Energy Applications Newsletter.</u> **6**(3-8).

Pennisi C.P.A., Leija L., et al. (2002), "Fiber optic temperature sensor for use in experimental microwave hyperthermia", <u>Sensors, 2002. Proceedings of IEEE</u>.

Phadungsak Rattanadecho, Nattawut Suwannapum, et al. (2008), "Development of compressive strength of cement paste under accelerated curing by using a continuous microwave thermal processor", <u>Materials Science and Engineering</u> **427**: 299-307.

Piotr Kisala, Elzbieta Paw1ik, et al. (2004), "Fiber Bragg grating sensors for temperature measurement", <u>Lightguides and their Applications II</u> **5576**.

Poon, C.-S. and D. Chan (2007), "The use of recycled aggregate in concrete in Hong Kong", <u>Resources, Conservation and Recycling</u> **50**(3): 293-305.

Poon, C. S., S. C. Kou, et al. (2002), "Use of recycled aggregates in molded concrete bricks and blocks", <u>Construction and Building Materials</u> **16**(5): 281-289.

Puschner, H. A. (1965), "Apparatus for heating material by means of microwave device", <u>United States Patent</u> **4003554**.

Rei R.C., Prauznitz J. M., et al. (1987), "The properties of gases and liquids", 4th edition, <u>McGraw Hill, New York</u>.

Rhim, H. C. and O. Buyukozturk (1998), "Electromagnetic Properties of Concrete at Microwave Frequency Range", J. ACI Material **95**: 262-271.

The International Union of Laboratories and Experts in Construction Materials, Systems and Structures (Rilem), (1994), "Specification for Concrete with Recycled Aggregates".

RUHL and MARCUS (1997), "Water absorption of recycled demolition rubbish", Darmstadt Concrete **12**.

S.K. Ramesh and K. C. wong (1999), "Design and fabrication of a Fiber Bragg Grating temperature sensor", Proceedings of SPIE **3620**.

Santamarina, J. C. (1989), "Rock excavation with microwaves: a literature review", Found Eng Curr Pronc Pract**:** 459-473.

Scott A. Wade, Kenneth T. V. Grattan, et al. (2004), "Incorporation of Fiber-Optic sensors in concrete specimens: testing and evaluation", IEEE Sensors Journal **4**(1): 127-134.

The National Surface Treatment Center, United States of America, "Sponge Blasting", Viewed 22 March 2010, <http://www.nstcenter.com/writeup.aspx?title=Abrasive%20Blasting&page=TechResourcesAbrasiveBlasting.html>

Shayan, A. and A. Xu, (2003) "Performance and Properties of Structural Concrete made with Recycled Concrete Aggregate" ACI Materials Journal, **100(**5): p. 371-380.

StatLink, "Singapore Trade Statistics", Viewed 20 March, 2010, <https://statlink.iesingapore.gov.sg>

Stuchly S. S. and H. M. A. K. (1972), "Physical parameters in microwave heating processes", Journal of Microwave Power **7**: 117-137.

Tabsh, S. W. and A. S. Abdelfatah (2009), "Influence of recycled concrete aggregates on strength properties of concrete", Construction and Building Materials **23**(2): 1163-1167.

Tam V. W. Y., Tam C. M., et al. (2007), "Removal of cement mortar remains from recycled aggregate using pre-soaking approaches", Resources, Conservation and Recycling **50**(1): 82-101.

Taoukis, P., E. A. Davis, et al. (1987), "Mathematical modeling of microwave thawing by the modified isotherm migration method", Journal of Food Science **52**: 455-463.

Temperature Sensors, "Thermocouples (TCs)", Viewed 7 June, 2008, < http://www.temperatures.com/tcs.html>

V.N. Protopopov, V.I. Karpova, et al. (2000), "Temperature sensor based on fiber Bragg grating", Proceedings of SPIE **4083**.

W.K. Fung (2005), The Use of Recycled Concrete in Construction. Department of Civil Engineering. Hong Kong, University of Hong Kong. **Thesis, Ph.D**.

Watson, A. (1968), "Breaking of concrete", Microwave power engineering, E. C. Okress **2**.

Advance Manufacturing Laboratory, "Water Jet Drill", Viewed 7 December, 2009, The University of New South Wales, Sydney, Australia, School of Mechanical and Manufacturing Engineering, < http://www.mech.unsw.edu.au/content/labs_compu ting/Abrasive_Jet.cfm?ss=5>

White, T. L., Foster, D., Jr., Wilson, C. T., and Schaich, C. R. (1995), "Phase II microwave concrete decontamination results", *ORNL Rep. No. DE-AC05-84OR21400*, Oak Ridge National Laboratory, Oak Ridge, Tenn.

White, T. L., Grubb, R.G., Pugh L.P., Foster, D. Jr., Box, W.D. (1992), "Removal of Contaminated Concrete Surface by Microwave Heating - Phase 1 Results", Proceedings of 18th American Nuclear Society Symposium on Waste Management, Tucson, Arizona.

Y. Kiwamoto, H. Ae, et al. (1997), "Thermographic temperature determination of gray materials with an infrared camera in different environments", Rev. Sci. Instrum **68**(6).

Yage Zhan, Haiwen Cai, et al. (2004,. "Fiber Bragg grating temperature sensor with enhanced sensitivity", Optical Fibers and Passive Components **5279**.

Yage Zhan, Shiqing Xiang, et al. (2005), "Fiber Bragg grating sensor for the measurement of elevated temperature." Advanced Sensor Systems and Applications II **5634**.

Yoda, K., M. Harada, et al. (2003), "Field application and advantage of concrete recycled in-situ recycling systems", London, E14 4JD, United Kingdom, Thomas Telford Services Ltd.

Yonezawa, T., Y. Kamiyama, et al. (2001), "A study on a technology for producing high quality recycled coarse aggregate", Zairyo/Journal of the Society of Materials Science, Japan **50**(8): 835-842.

Yong Wang, Swee Chuan Tjin, et al. (2001), "Measurement of temperature profile of concrete structures using embedded fiber Bragg grating sensors and thermocouples", Proceedings of SPIE **4235**: 288-297.

Yong Wang, Swee Chuan Tjin, et al. (2001), "Monitoring of concrete curing process with embedded fiber Bragg gratings", Fiber Optic Sensor Technology II **4204**: 23-30.

Yonglin Huang, Jie Li, et al. (2003), "Temperature compensation package for fiber Bragg gratings", Microwave and Optical Technology Letters **39**(1).

Yung Bin Lin, Jenn Chuan Chern, et al. (2004), "The utilization of fiber Bragg grating sensors to monitor high performance concrete at elevated temperature", Smart Mater. Struct. **13**: 784–790.

Zdeněk P. Bažant and G. Zi (2003), "Decontamination of radionuclides from concrete by microwave heating. I: Theory", *J.Eng Mech.* **129**(7): 777-784.

APPENDIX A: Mix Proportions and Mechanical Properties of Concrete

Table A.1 Properties of Coarse and Fine Natural Aggregates

Property	Value
Dry Rodded Unit Weight of Coarse Aggregates (kg/m^3)	1676
Water Absorption of Coarse Aggregates (%)	0.74
Water Absorption of Sand (%)	0.21
Fineness Modulus of Sand	2.57
Maximum Aggregate Size (mm)	19
Bulk Specific Gravity (OD) of Coarse Aggregates (gr/cm^3)	2.533
Bulk Specific Gravity (SSD) of Coarse Aggregates (gr/cm^3)	2.546

Table A.2 Mix Proportion of Various Concrete Grades Cast in the Laboratory

Mix Proportion	Concrete Grade		
	C30	C60	C90
W/C	0.69	0.45	0.26
cement content (Kg)	282	375	480
water (Kg)	195	167	125
Fine agg. (Kg)	804	736	758
Coarse agg. (Kg)	1072	1072	1072

Table A.3 Mechanical Properties of Various Concrete Grades Cast in the Laboratory

Concrete Grade	Compressive Strength		Flexural Strength (28 day)
	7 day	28 day	
C30	25	31	5
C60	46	59	5.9
C90	74	92	6.4